

**Cranfield Institute of Technology
Silsoe College**

**Department of Agricultural and Environmental
Engineering**

**A Thesis Submitted for the Degree of
Doctor of Philosophy**

Academic year 1992/93

Richard Earl

**THE DEVELOPMENT OF TECHNIQUES OF ASSESSING SOIL
COMPACTABILITY**

Supervisor: Professor G Spoor

Presented: June 1993

ProQuest Number: 10820946

All rights reserved

INFORMATION TO ALL USERS

The quality of this reproduction is dependent upon the quality of the copy submitted.

In the unlikely event that the author did not send a complete manuscript and there are missing pages, these will be noted. Also, if material had to be removed, a note will indicate the deletion.



ProQuest 10820946

Published by ProQuest LLC (2018). Copyright of the Dissertation is held by Cranfield University.

All rights reserved.

This work is protected against unauthorized copying under Title 17, United States Code
Microform Edition © ProQuest LLC.

ProQuest LLC.
789 East Eisenhower Parkway
P.O. Box 1346
Ann Arbor, MI 48106 – 1346

Abstract

The recent decline in farming profits has prompted an urgent need to increase efficiency, either by increasing outputs or reducing the cost of inputs. Soil compaction can influence adversely all stages of crop development, and hence yield, and is expensive to ameliorate in terms of time taken and power required. Minimum cultivation or direct drill crop establishment systems can reduce inputs, however, they are very susceptible to compaction from the previous season.

There is a need to develop a greater understanding of the compactive nature of soil, and hence trafficability and workability, in relation to the selection of appropriate machinery to carry out agricultural operations. A study of research on soil compaction revealed that the majority of work to date has been carried out using disturbed soil samples in laboratory situations. The aim of this project is to develop techniques and models, based on field data, for assessing the susceptibility of soils to compaction by agricultural machinery. Work, conducted during this study, was carried out in the field in a range of soils, crops and climatic conditions. The study was approached by dividing the project into two sections:-

(1) Prediction of trafficability and workability on a go/no-go basis.

Soil water suction (h), soil moisture deficit (SMD) and cone penetration resistance were monitored at six field sites, under grass and an arable crop, covering a range of agricultural situations commonly found in central and eastern England.

Strong correlations were found to occur between both h and SMD and:-

- (a) a qualitative assessment of soil condition, and
- (b) cone penetration resistance.

These data formed the basis of models for predicting trafficability and workability at a given site on a particular day, and at any 5km square in England and Wales as an aid to business planning.

- (2) Assessment of the compactive nature of soil during loading.

A methodology was developed which provides a measure of the susceptibility of soil to damage if land is trafficked when in an unsuitable condition. It is based on results of plate sinkage tests, in conjunction with those from confined compression tests, performed in the field using tractor-mounted equipment. Soil behaviour during compression was found to be governed by three phases:-

- (a) compaction with uniform lateral stress,
- (b) compaction with increasing lateral stress, and
- (c) displacement of soil laterally.

Mathematical models are presented for predicting, for a given load and soil, the deformation phase and extent of disturbance likely to occur.

The prediction models developed during this study provide a new approach to the selection of, and assessment of damage by, agricultural machinery.

Acknowledgements

The author is grateful to Prof G Spoor, Prof A J Thomasson and Dr D L O Smith for their encouragement, assistance and constructive criticism.

Grateful thanks are also due to my wife for her continuous support throughout this project.

Table of Contents

	Page
Abstract	ii
Acknowledgements	iv
Table of Contents	v
List of Figures	ix
List of Tables	xviii
List of Plates	xxi
List of Symbols	xxii
1. Introduction and review of literature	1
1.1 Overall objective	1
1.2 Background	1
1.2.1 Trafficability and Workability	3
1.2.2 Soil compaction and displacement	6
1.3 Objectives	8
1.4 The Thesis structure	9
2. Soil water suction and soil strength	10
2.1 Qualitative relationship between soil water suction and trafficability and workability	14
2.2 Quantitative relationship between soil water suction and cone penetration resistance	26
2.2.1 The Cuckney soil series	27
2.2.2 The Wick soil series	31
2.2.3 The Upton soil series	34
2.2.4 The Whimple soil series	37
2.2.5 The Evesham soil series	39
2.2.6 The Denchworth soil series	41
2.3 Discussion	44
2.4 Conclusions	58
3. Soil moisture deficit and soil strength	60
3.1 Quantitative relationship between soil moisture deficit and cone penetration resistance	61
3.1.1 The Cuckney Soil Series	65

	Page
3.1.2 The Wick soil series	69
3.1.3 The Upton soil series	70
3.1.4 The Whimble soil series	72
3.1.5 The Evesham soil series	73
3.1.6 The Denchworth soil series	75
3.2 Discussion	76
3.2.1 Prediction of trafficability and workability at a given site	77
3.2.2 Prediction of trafficability and workability for business planning	81
3.3 Conclusions	85
4. The Development of tractor-mounted test equipment	87
4.1 Preliminary design of the equipment	90
4.1.1 Design of the confining cylinder	93
4.1.1.1 Determination of the angle of soil-metal friction	96
4.1.1.2 The influence of the coefficient of earth pressure at rest (K_0) on the design criteria of the confining cylinder	105
4.1.1.3 The influence of adhesion (C_α) on the stress distribution in a soil sample during a confined compression test	106
4.1.2 Design of the sampler assembly and confined compression equipment	110
4.1.2.1 Confining cylinder specifications	113
4.1.2.2 Selection of strain gauges for the confining cylinder	113
4.1.3 Calibration of the confining cylinder	117
4.1.3.1 Hoop stress calibration	120
4.1.3.2 Axial load calibration	123
4.1.4 Calibration of the 100kN load cell	126
4.1.5 Calibration of the linear variable displacement transducer (LVDT)	127
4.2 Field testing	129
4.2.1 Soil sampling procedure	129
4.2.2 Confined compression test	135
4.2.3 Plate sinkage test	139
4.3 Data collection procedure	140

	Page
5. Quantification of the compactive nature of soil (part I)	142
5.1 Initial field trials	143
5.1.1 The Confined compression test	146
5.1.2 The plate sinkage test	150
5.2 Assessing soil compaction and compactability	155
5.2.1 Classification of initial soil condition	155
5.2.2 Classification of soil deformation under loading	162
5.2.2.1 Confined compression test data	168
5.2.2.2 Plate sinkage test data	169
5.2.2.3 Determination of compaction point position	169
5.2.2.4 Radial stress	174
5.2.2.5 Prediction of the extent of soil disturbance below a sinkage plate	180
6. Quantification of the compactive nature of soil (part II)	212
6.1 Field work	212
6.2 Results	218
6.2.1 Classification results for initial soil condition	218
6.2.2 Results for soil behaviour under load	219
6.2.2.1 Results for the Evesham soil series	221
6.2.2.2 Results for the Bearsted soil series	224
5.4.2.3 Results from the soil damage prediction procedures	227
6.3 Discussion	231
6.3.1 The Evesham soil series	231
6.3.2 The Bearsted soil series	240
6.3.3 The interaction of sinkage plate diameter and load on extent of disturbance	243
6.4 Summary	250
7. Overall discussion, summary and conclusions	255
7.1 Predicting trafficability and workability	256
7.1.1 Prediction at a given site on a particular day	256

	Page
7.1.2 Prediction of the number of machinery work-days for a particular site	257
7.1.2.1 Comparison of trafficability and workability predictions with those from LANDIS	261
7.2 Assessing the compactive nature of soil during loading	267
7.3 Comparison of trafficability/workability prediction and compactability/strength assessment results	268
7.3.1 Soil water suction and compactability strength assessment	268
7.3.2 Strength prediction from soil moisture deficit and compactability/strength assessment	273
7.4 Summary, conclusions and recommendations	276
7.4.1 Summary	276
7.4.2 Detailed conclusions	278
7.4.3 Overall conclusion	279
References	280
Appendix 1	290
Appendix 2	326
Appendix 3	332
Appendix 4	335
Appendix 5	336
Appendix 6	340

List of Figures

	Page
2.1 Cuckney site diagram.	17
2.2 Wick site diagram.	18
2.3 Upton site diagram.	19
2.4 Whimble site diagram.	20
2.5 Evesham site diagram.	21
2.6 Denchworth site diagram.	22
2.7 The linear relationship between soil water suction (h) and resistance to cone penetration (RP) for a loamy sand - Cuckney series topsoil under grass (bulk density 1.45Mg/m^3) and wheat (1.44Mg/m^3).	28
2.8 The hyperbolic relationship between soil water suction (h) and resistance to cone penetration (RP) for a loamy sand - Cuckney series topsoil under grass (bulk density 1.45Mg/m^3) and wheat (1.44Mg/m^3).	30
2.9 The linear relationship between soil water suction (h) and resistance to cone penetration (RP) for a sandy loam soil - Wick series topsoil under grass (bulk density 1.50Mg/m^3) and wheat (1.34Mg/m^3).	32
2.10 The hyperbolic relationship between soil water suction (h) and resistance to cone penetration (RP) for a sandy loam soil - Wick topsoil under grass (bulk density 1.50Mg/m^3) and wheat (1.34Mg/m^3).	33
2.11 The linear relationship between soil water suction (h) and resistance to cone penetration (RP) for a clay loam soil - Upton series topsoil under grass (bulk density 1.06Mg/m^3) and wheat (0.89Mg/m^3).	34

	Page
2.12 The hyperbolic relationship between soil water suction (h) and resistance to cone penetration (RP) for a clay loam soil - Upton series topsoil under grass (bulk density 1.06Mg/m^3) and wheat (0.89Mg/m^3).	36
2.13 The linear relationship between soil water suction (h) and resistance to cone penetration (RP) for a loamy soil - Whimble series topsoil under grass (bulk density 1.54Mg/m^3) and wheat (1.47Mg/m^3).	37
2.14 The hyperbolic relationship between soil water suction (h) and resistance to cone penetration (RP) for a loamy soil - Whimble series topsoil under grass (bulk density 1.54Mg/m^3) and wheat (1.47Mg/m^3).	38
2.15 The linear relationship between soil water suction (h) and resistance to cone penetration (RP) for a clay soil - Evesham series topsoil under grass (bulk density 0.88Mg/m^3) and wheat (0.98Mg/m^3).	39
2.16 The hyperbolic relationship between soil water suction (h) and resistance to cone penetration (RP) for a clay soil - Evesham series topsoil under grass (bulk density 0.88Mg/m^3) and wheat (0.98Mg/m^3).	40
2.17 The linear relationship between soil water suction (h) and resistance to cone penetration (RP) for a clay soil - Denchworth series topsoil under grass (bulk density 1.02Mg/m^3) and wheat (0.91Mg/m^3).	42
2.18 The hyperbolic relationship between soil water suction (h) and resistance to cone penetration (RP) for a clay soil - Denchworth series topsoil under grass (bulk density 1.02Mg/m^3) and wheat (0.91Mg/m^3).	43
2.19 The soil moisture retention curves for the six soil series under both grass and wheat.	45

	Page
3.1 The variation in both resistance to cone penetration (RP) at 50 and 150mm depth, and soil moisture deficit for a 1500mm deep profile (SMD1500), over the 1987 - 1988 growing season for a loamy sand soil under grass - Cuckney series.	62
3.2 The variation in both resistance to cone penetration (RP) at 50 and 150mm depth, and soil moisture deficit for a 1500mm deep profile (SMD1500) over the 1987 - 1988 growing season for a clay soil under grass - Evesham series.	64
3.3 The relationship between resistance to cone penetration (RP) at 50mm depth and soil moisture deficit in the top 1500mm of the soil profile (SMD1500) for a loamy sand soil - Cuckney series topsoil under grass (bulk density 1.45Mg/m^3) and wheat (1.44Mg/m^3).	65
3.4 The relationship between resistance to cone penetration (RP) at 50 & 150mm depth and soil moisture deficit in the top 200mm of soil (SMD200) for a loamy sand soil - Cuckney series topsoil under grass (bulk density 1.45Mg/m^3) and wheat (1.44Mg/m^3).	67
3.5 The relationship between resistance to cone penetration (RP) at 50 and 150mm depth and soil moisture deficit of the top 200mm of soil (SMD200) for a sandy loam soil - Wick series topsoil under grass (bulk density 1.50Mg/m^3) and wheat (1.34Mg/m^3).	69
3.6 The relationship between resistance to cone penetration (RP) at 50 and 150mm depth and soil moisture deficit of the top 200mm of soil (SMD200) for a clay loam soil - Upton series topsoil under grass (bulk density 1.06Mg/m^3) and wheat (0.89Mg/m^3).	71
3.7 The relationship between resistance to cone penetration (RP) and soil moisture deficit of the top 200mm of soil (SMD200) for a clay loam soil - Whimple series topsoil under grass (bulk density 1.54Mg/m^3) and wheat (1.47Mg/m^3).	72

	Page
3.8 The relationship between resistance to cone penetration (RP) at 50 and 150mm depth and soil moisture deficit in the top 200mm of soil (SMD200) for a clay soil - Evesham series topsoil under grass (bulk density 0.88Mg/m^3) and wheat (0.98Mg/m^3).	74
3.9 The relationship between resistance to cone penetration (RP) at 50 and 150mm depth and soil moisture deficit in the top 200mm of soil (SMD200) for a clay soil - Denchworth series topsoil under grass (bulk density 1.02Mg/m^3) and wheat (0.91Mg/m^3).	75
3.10 The variation in the soil moisture deficit in the top 200mm of soil (SMD200), under winter wheat, during the 1987 - 1988 growing season for a sandy loam soil - Wick series.	79
3.11 The variation in 'wet quartile' potential soil moisture deficit (PSMD) for 15 years of data (1961 - 1975) from a weather station close to the Wick site.	82
4.1 Equipment for taking soil samples.	90
4.2 Equipment for carrying out confined compression tests.	91
4.3 Equipment for carrying out plate sinkage tests.	91
4.4 The relationship between tangential resistance per unit area, adhesion, normal stress and angle of soil-metal friction.	97
4.5 Apparatus for the determination of adhesion and the angle of soil-metal friction.	98
4.6 Modified apparatus for the determination of adhesion and the angle of soil-metal friction.	100
4.7 Average tangential sliding resistance per unit area (Γ') against average normal stress (σ) for a brass sledge on both Cottenham and Evesham soil series with and without Polyox resin.	102
4.8 Suggested curve for average tangential sliding resistance per unit area (Γ') against average normal stress (σ).	104

	Page
4.9 Graph of the ratio of stress at the sample centre to stress at the pistons (σ_m/σ_p) against stress at the pistons (σ_p) during a confined compression test.	108
4.10 Engineering drawing of sampling/compression equipment.	111
4.11 Lower piston and base plate.	112
4.12 Side elevation of Deutz Intrac 2004 tractor.	115
4.13 The brass confining cylinder.	117
4.14 The Wheatstone bridge circuit for the confining cylinder strain gauges.	118
4.15 Confining cylinder calibration curve for the hoop bridge circuit under increasing internal pressure (four replicates).	123
4.16 The Wheatstone bridge circuit for the axially mounted strain gauges.	124
4.17 Confining cylinder calibration curve for the axial bridge circuit under increasing axial load (four replicates).	125
4.18 Calibration curve for the 100KN load cell	126
4.19 Base plate and piston assembly used during confined compression tests.	135
5.1 Soil water suction down the soil profile - Evesham series site.	144
5.2 The relationship between axial stress (σ_A) and axial strain (ϵ_A) for a clay soil - Evesham series topsoil under grass (bulk density 1.05Mg/m^3).	146
5.3 The expected loading curve from a confined compression test.	147
5.4 The effect of unloading and reloading during a confined compression test.	148
5.5 Soil sample deformation after a confined compression test.	149
5.6 Schematic diagram of plate sinkage test.	150

	Page
5.7 The relationship between axial stress (σ_A) and axial sinkage (R) during a plate sinkage test at 50mm depth on a clay soil - Evesham series top soil.	151
5.8 Plate sinkage test analysis, Bernstein (1913).	153
5.9 Typical stress-sinkage relationship obtained from a plate sinkage test.	154
5.10 Typical curves generated from confined compression and plate sinkage tests.	158
5.11 The deformation mode of soil in various initial conditions.	161
5.12 The modes of soil deformation during a plate sinkage test.	163
5.13 Critical state diagram representing one-dimensional compression.	165
5.14 The overlaying of confined compression test results onto plate sinkage test results to determine the position of the Compaction Point (CP).	167
5.15 Schematic diagram of confined compression test results.	168
5.16 Schematic diagram of results from a plate sinkage test.	169
5.17 Confined compression and plate sinkage test results for a clay soil - Evesham series at 50mm depth under grass.	172
5.18 Confined compression and plate sinkage test results for a sandy loam soil - Bearsted series at 50mm depth under grass.	173
5.19 Typical form of graph of radial stress against axial stress for soil under compression.	174
5.20 Typical form of graph of coefficient of earth pressure at rest against axial stress.	176
5.21 The interpretation of typical stress-sinkage and K_0 graphs to assess the compactability of field soils.	178

	Page
5.22 Failure mechanisms during plate sinkage tests.	181
5.23 Diagram illustrating phase (1) failure below a sinkage plate.	183
5.24 Simplification of relationship between radial stress (σ_R) against axial stress (σ_A) during a plate sinkage test.	186
5.25 Schematic diagram of phase (2) deformation below a sinkage plate.	188
5.26 The assumed relationship between axial stress (σ_{Ap}) and distance below sinkage plate (X).	189
5.27 The assumed relationship between axial stress (σ_{Aw}) and distance below a sinkage plate (X).	190
5.28 Diagram of the failure pattern assumed to occur below a sinkage plate during phase (3) deformation.	193
5.29 Diagram illustrating the effect of sinkage depth on lateral disturbance below a sinkage plate.	194
5.30 Diagram illustrating soil disturbance below a sinkage plate.	195
5.31 Diagram of forces acting on soil surrounding a sinkage plate.	197
5.32 Force diagram (RHS only) for the failure zone under a sinkage plate at maximum phase (2) sinkage.	199
5.33 Diagram to illustrate computation of A_d , W_1 and l_2 .	201
5.34 Diagram illustrating the computation of soil weight W_2 .	202
5.35 Diagram illustrating the computation of moment due to cohesion for soil failure below a sinkage plate.	203
5.36 Diagram illustrating the determination of F_2 .	204

	Page
5.37 Diagram illustrating the determination of the point of application of passive pressure l_1 below a sinkage plate.	207
5.38 Diagram illustrating the computation of disturbed distance β .	208
5.39 Diagram illustrating prediction of the extent of soil disturbance resulting during a plate sinkage test.	210
6.1 Site plan for the Bearsted soil series.	214
6.2 Plan view of plateaus and positioning of the soil tests.	216
6.3 Soil water suction profiles for the four trial plots on the test days.	217
6.4 Stress-sinkage, σ_R and K_o curves for the Evesham series grass plot at 50mm depth.	221
6.5 Stress-sinkage, σ_R and K_o curves for the Bearsted series grass plot at 50mm depth.	225
6.6 Summary of prediction results for three loads applied to a range of soil profiles.	229
6.7 The relationship between dry bulk density and gravimetric moisture content obtained from a Proctor compaction test on clay soil - Evesham series topsoil.	233
6.8 Static compaction curves for a silty clay. (1) 13.8MPa static stress. (2) 6.9MPa static stress (3) 3.4MPa static stress. (4) 1.4MPa static stress. (From Turnbull,1950).	235
6.9 The relationship between load and dry bulk density for a silty clay loam.	236
6.10 Hypothetical relationship between axial stress (σ_A) and sinkage depth (R) for a clay soil at various moisture contents.	237
6.11 Hypothetical relationship between degree of saturation (S) and sinkage depth at the CP (R_{CP}) for the Evesham soil series.	238

	Page
6.12 The relationship between degree of saturation (S) and sinkage depth at the CP (R_{CP}) for the Evesham series.	239
6.13 The relationship between dry bulk density and gravimetric moisture content obtained from a Proctor compaction test on a clay soil - Bearsted series subsoil.	242
6.14 Prediction of extent of vertical and lateral disturbance resulting from increasing stress on a sinkage plate.	244
6.15 Prediction of the effect of reducing plate diameter, for a given load, on extent of soil disturbance.	246
6.16 Comparison of the extent of soil disturbance below a sinkage plate due to increasing load with that due to decreasing plate diameter.	248
7.2 Typical form of SMD200 - RP curves.	275
2.1A Cuckney soil series	326
2.2A Wick soil series	326
2.3A Upton soil series	327
2.4A Whimble soil series	327
2.5A Evesham soil series	328
2.6A Denchworth soil series	328

List of Tables

	Page
2.1 The six soil series under investigation.	13
2.2 Critical soil water suction limits (cm water) for trafficability and workability.	24
2.3 Summary of linear RP - h relationships for six soil series.	46
2.4 Summary of hyperbolic RP - h relationships for six soil series.	47
2.5 Soil strength RP (MPa) corresponding to critical soil water suction limits for trafficability and workability.	48
2.6 Data concerning the change in resistance to cone penetration (RP) with time, during periods of low rainfall, for the three midland sites.	52
2.7 Data concerning the change in resistance to cone penetration (RP) with time, during periods of low rainfall, for the three southern sites.	54
2.8 The ranking of the six soil series under investigation in terms of rate of increase in soil strength during periods of low rainfall.	56
3.1 Critical SMD200 limits (mm) for trafficability and workability.	78
3.2 Critical SMD1500 limits (mm) for trafficability and workability.	83
4.1 Average stress exerted on soil by various operations.	89
4.2 Results from soil-metal friction tests for brass on Cottenham and Evesham soil series.	103
4.3 The influence of coefficient of earth pressure at rest (K_0) on the design criteria of the confining cylinder.	105
5.1 The relationship between soil packing density and field properties.	157

	Page
5.2 The magnitude and combination of various parameters to which soil in a given condition can be attributed	179
6.1 Initial soil parameters for the two field sites.	218
6.2 Initial characterisation of the field sites.	219
6.3 Confined compression (CC) and plate sinkage (PS) test results for the Evesham and Bearsted soil series under grass and arable crops.	220
6.4 Soil deformation behaviour parameters for the Evesham soil series.	222
6.5 Degree of saturation (S) at the compaction point (CP) for the Evesham soil series.	223
6.6 Soil deformation behaviour parameters for the Bearsted soil series.	226
6.7 Description of scenarios in Figure 6.6.	228
6.8 Rated soil deformation behaviour parameters for the Evesham soil series.	232
6.9 Rated soil deformation behaviour parameters for the Bearsted soil series.	241
7.1 Regression equations for estimating critical limits for trafficability and workability from soil properties.	260
7.2 The ten most dominant arable soil in England and Wales.	261
7.3 5km squares selected for comparative work.	262
7.4 Predictions of the number of trafficable and workable days.	264
7.5 Soil condition prediction for the Wick soil series under wheat over the 1987-88 growing season.	266
7.6 Soil water suction (h) in the Evesham and Bearsted soil series profiles on sampling days.	269

	Page
7.7 Trafficability and workability predictions for the Evesham and Bearsted soil series on sampling days.	270
7.8 Comparisons of trafficability and workability predictions with compactability and strength assessments for the Evesham and Bearsted soil series on sampling days.	271
7.9 Predicted resistance to cone penetration (RP) for the Evesham and Bearsted soil series on sampling days.	272
7.10 Initial modulus (m_i) and predicted resistance to cone penetration (RP) for the Evesham and Bearsted soil series on sampling days.	273
7.11 Critical SMD200 limits for the Evesham and Cuckney soil series, and trafficability/workability assessment for the Evesham and Bearsted soil series on sampling days.	274
2.1A The number of workable days.	329
2.2A The number of trafficable days.	330
2.3A Julian days on which >5mm of rain fell during the preceding 24hrs or >10mm fell during the preceding 48hrs.	331
3.1A Calibration results for the neutron probe (top 20cm of the soil profile).	333
3.2A Calibration equations for the neutron probe.	334
5.1A Soil assessment for workability and trafficability.	337
5.2A Soil weightings applied to field capacity data for estimating machinery work days.	338

List of Plates

	Page
4.1 Calibration of the confining cylinder for hoop stress.	121
4.2 The load cell, LVDT and datum frame in operation during a plate sinkage test.	128
4.3 The Deutz Intrac tractor adapted to accomodate soil assessment equipment.	129
4.4 Assembly and lubrication of the sampling cylinder.	130
4.5 The sampling cylinder attached to the rear hydraulic ram on the tractor.	131
4.6 The sampling cylinder during sampling.	132
4.7 Trimming the ends of the soil sample within the confining tube.	134
4.8 A confined compression test.	137
4.9 Extruding the soil sample.	138
4.10 A plate sinkage test.	139
5.1 Section through two plate sinkage tests.	182

List of Symbols

A	Constant for the logistic regression equation.
a	Maximum axial stress during phase (1) deformation (kPa).
A ₁	Cross sectional area of piston ₂ for plate sinkage or confined compression test (mm ²).
A ₂	Wall area of half the confined compression cylinder (mm ²).
B	Constant for the logistic regression equation.
b	Radial stress during phase (1) deformation (kPa).
b	Plate diameter (mm).
C	Clay content (%).
C	Constant for the logistic regression equation.
C	Constant in linear regression equation for data from plate sinkage and confined compression test (kPa).
c	Cohesion (kPa).
cA	Cohesive force on lower slip-plane (kN).
Ca	Air capacity (%).
CC	Confined compression test.
CLAY	Clay content by weight (%).
Com	Failure due to compaction.
CP	Compaction point.
CSL	Critical state line.
C _α	Adhesion (kPa).
D	Diameter of plate sinkage and confined compression test pistons (mm).
DB	Bulk density (kg/m ³).

Db	Bulk density (kg/m^3).
Dis	Failure due to soil displacement.
DVM	Digital volt meter.
d	Diameter of confining cylinder (mm).
E	Young's modulus (GPa).
e	Void ratio.
F	Variance ratio.
F_2	Resultant of normal and frictional forces along upper slip-plane.
F_f	Passive force (kN).
F_p	Passive pressure (kPa).
h	Height of soil sample during a confined compression test (mm).
h	Soil water suction (mm of water).
hc_1	Critical soil water suction limit for workability (cm of water).
hc_2	Critical soil water suction limit for trafficability (cm of water).
I	Current (amps).
K	Soil parameter used in the Bernstein plate sinkage theory.
K_o	Coefficient of earth pressure at rest.
K_c, K_ϕ	Soil parameters for the Bekker plate sinkage theory.
Ld	Packing density (kg/m^3).
LVDT	Linear variable displacement transducer.
M	Constant for the logistic regression equation.
m_{CP}	Compaction modulus (kPa/mm).
m_i	Initial gradient of stress-strain curve (MPa/mm).

MTD	Number of machinery trafficable days.
MWD	Number of machinery workable days.
n	Exponent in the Bernstein plate sinkage theory.
n	Porosity (%).
OC	Organic carbon content (%).
P	Pressure (kPa).
p	Stress component in the critical state model (kPa).
PS	Plate sinkage test.
PSMD	Potential soil moisture deficit (mm of water).
q	Stress component in the critical state model (kPa).
R	Sinkage depth or reduction in height of soil sample (mm).
Ro	Electrical resistance of strain gauge (Ω).
r_0	Length of soil cone face below a sinkage plate (mm).
r_1	Radius of logarithmic spiral during phase (2) deformation (mm).
r_2	Radius of logarithmic spiral during phase (3) deformation (mm).
R^2	Coefficient of determination.
RP	Resistance to cone penetration (MPa).
RP_{ULT}	Asymptotic maximum value of resistance to cone penetration (MPa).
R_{ULT}	Asymptotic maximum value of sinkage derived from a confined compression test (mm).
RP0	Resistance to cone penetration at zero soil water suction (MPa).
R_T	Electrical resistance due to change in temperature (Ω).
S	Degree of saturation (%).

SAND	Sand content by weight (%).
SMD	Soil moisture deficit (mm of water).
SMD1500	Soil moisture deficit for a 1500mm deep soil profile (mm of water).
SMD200	Soil moisture deficit for a 200mm deep soil profile (mm of water).
t	Wall thickness of confining cylinder (mm).
V	Voltage (volts).
W_1	Soil weight on lower slip-plane (kN).
W_2	Soil weight on Upper slip-plane (kN).
w	Angle of r_1 from r_0 (radians).
X	Vertical extent of disturbance below a sinkage plate (mm).
β_1	Extent of maximum lateral disturbance during phase (2) deformation (mm).
β_2	Extent of maximum lateral disturbance during phase (3) deformation (mm).
γ	Bulk unit weight (kN/m^3).
δ	Angle of soil-metal friction ($^\circ$).
ϵ_A	Axial strain of confining cylinder.
ϵ_H	Hoop strain of confining cylinder.
$\theta^v(0.05)$	Retained water capacity (%).
σ_1	Major principal stress (kPa).
σ_3	Minor principal stress (kPa).
σ_A	Axial stress (kPa).
σ_{Ap}	Axial stress generated as a result of plate pressure (kPa).
σ_{Aw}	Axial stress generated as a result of soil weight (kPa).
$\sigma_{A(2)}$	Axial stress during phase (2) deformation (kPa).

$\sigma_{A(3)}$	Axial stress during phase (2) deformation (kPa).
σ_b	Mean normal stress at the bottom of the soil sample in a confined compression test (kPa).
σ_{CP}	Axial stress at the compaction point (kPa).
σ_h	Mean horizontal stress in the soil sample in a confined compression test (kPa).
σ_H	Hoop stress in confining cylinder (kPa).
σ_m	Mean normal stress at the centre of the sample in a confined compression test (kPa).
σ_N	Normal stress (kPa).
σ_p	Mean normal stress at the ends of the sample in a confined compression test (kPa).
σ_R	Radial stress (kPa).
σ_t	Mean normal stress at the top of the soil sample in a confined compression test (kPa).
σ_v	Mean vertical stress in half the soil sample in a confined compression test (kPa).
Γ'	Mean shear stress (kPa).
μ	Poisson's ratio.
ϕ	Angle of shearing resistance ($^{\circ}$).

CHAPTER 1

INTRODUCTION AND REVIEW OF LITERATURE

1.1 Overall objective

To develop techniques and models for assessing the susceptibility of soils to compaction by agricultural machinery.

1.2 Background

Compaction of soil has become a problem of world wide concern because of a steady increase in the size of agricultural equipment. Since 1948, the average tractor weight has increased from 2.7t to 6.8t today, (Gupta and Allmaras, 1987).

Compaction by wheeled traffic has often been found to influence adversely all stages of crop growth, responses being particularly marked in the early phases of establishment, (Soane et al, 1982).

The use of dual rear wheels, or steel tracks, can significantly reduce soil strain, compared with single rear wheels, and hence compaction (Kinney et al, 1992). A limited amount of surface compaction in the vicinity of planted seeds is considered beneficial because it promotes better soil-seed contact and rapid germination, and reduces the rate at which soil dries, (Bicki and Siemens, 1991). There are, however, conflicting reports as to the actual effects of compaction on yield, (Chancellor, 1977; Swan et al, 1987). Voorhees (1987), for example, reports that the relative change in soya bean and wheat yield, due to inter-row wheel traffic, is a function of growing season precipitation. If precipitation was low, yields were increased by inter-row compaction and vice versa. Soane (1985) states that for each crop, soil and season there is an optimum level of compaction for maximum crop yield. The optimum packing state of the soil in arable situations is often a compromise as the requirements for traction and mobility are quite different from those for infiltration and root propagation, (Shafer et al, 1990). Hakansson (1988, 1990) found during extensive trials that for different types of mineral soil, maximum crop yield was achieved with the same degree of compaction.

Generally, a given degree of shallow compaction will be detrimental under wet climatic regimes but of no consequence, or even beneficial, under dry climatic regimes.

Although compaction may either reduce or increase crop establishment, growth and yield depending on complex interactions between the crop, soil type and weather conditions, there is increasing evidence of widespread harmful effects of traffic by modern agricultural vehicles, (Soane, 1982).

The mechanical condition of soil, in the context of agricultural field operations, can be considered from two quite different perspectives:-

- (1) can the soil be trafficked or worked at depth without causing significant damage through compaction and smear, termed trafficability and workability respectively, and

- (2) if agricultural operations are carried out when the soil is in an unsuitable condition, what is the extent of the damage, or potential damage, to the soil that may result. Damage could arise from either a process of air expulsion during loading with resultant increase in bulk density or deformation due to soil movement with minimal reduction in soil volume, termed compaction and deformation respectively.

As yet, in agricultural research, standardised and widely accepted procedures for measuring these parameters do not exist (Koolen, 1987).

1.2.1 TRAFFICABILITY AND WORKABILITY

When a farmer assesses his land prior to carrying out operations with agricultural machinery, it is difficult to quantify exactly how he might integrate the information available to him when making his decision. An experienced farmer will generally know his land well enough to make informed decisions regarding the condition of the

soil. If, however, circumstances were to change, for example, a new machine, additional land, a different crop, or the installation of land drainage then this could affect his ability to assess the situation.

Van Wijk and Buitendijk (1988) developed a methodology for predicting workability of arable soils based on soil water suction data at 5cm depth. Soil damage as a result of compaction, however, often extends far below the top soil. Hakansson (1985) reported compaction, as a result of a 10t load, persisting below the plough layer for 7 to 8 years. It would be desirable to extend Van Wijk and Buitendijk's methodology to take account of soil water suction at depths greater than 5cm. Simalenga and Have (1992) based their workability model on 95% of the field capacity moisture content, however, the depth at which soil moisture sampling was carried out is not clear.

Collas (1987) introduced a technique for assessing trafficability based on cone penetration resistance. He found that critical values of penetration resistance were very similar for a range of soil types.

Godwin et al (1991) assessed soil strength and trafficability using a 2kg drop cone penetrometer and established linear relationships between cone penetration and soil moisture content.

There is a need for the development of reliable techniques for quantifying whether soil, in a given field situation, can be trafficked or worked without causing significant damage to it. Laboratory tests on disturbed soil samples are not appropriate for this purpose.

Investigations are required to establish suitable parameters for assessing trafficability and workability:-

- (a) at a given site on a particular day,
- (b) during the season as an aid to business planning.

Soil strength can be assessed either directly, for example using the cone penetrometer, or indirectly using parameters which affect, or are affected by soil strength. Suitable parameters must be quick and simple to determine or be readily available from data banks. From a review of current literature, the following may be appropriate and warrant further investigation:-

- (a) soil water suction,
- (b) soil moisture content or deficit,
- (c) resistance to cone penetration.

A trafficability or workability assessment methodology, developed from these parameters, must be applicable to a wide range of soil types.

1.2.2 SOIL COMPACTION AND DISPLACEMENT

Over the past three decades a considerable amount of research has been carried out into the mechanics of soil deformation. Bradford and Gupta (1986) point out that structural and foundation engineering deals with the consolidation of soils in relation to the construction of dams, buildings, roadbeds and embankments. This information is of limited use to agronomists and soil scientists for three reasons:-

- (1) the loads from agricultural equipment are normally smaller than those of superstructures such as buildings and dams,
- (2) most compression tests reported in foundation engineering literature are conducted on saturated soils, while agricultural soils are mostly unsaturated when field operations are carried out, and
- (3) the compressibility of unsaturated soils with various degrees of structural development differs considerably from that of dense, massive-structured, subsurface layers.

Data in the literature on the compressibility of agricultural soils are limited.

One of the more obvious outcomes of trafficking a field which is in an unsuitable condition is the development of wheel ruts. The ability of soils to support or fail under an applied static surface load is clearly related to their behaviour during the passage of a wheel, (Soane, 1981a). Bernstein (1913) and Bekker (1960) investigated the relationship between load and sinkage using plate sinkage tests.

Although these tests can provide useful in-situ data on the strength of field soils there are two drawbacks associated with them:-

- (a) the contact area and loading of tractor tyres are now so great that it is impracticable to use equivalent plate sizes and loads, and
- (b) the tests do not provide information on the type and extent of the deformation processes occurring below the plate.

There is a clear need to examine ways of addressing these drawbacks, possibly by mounting the equipment on a tractor and performing other tests alongside the sinkage tests to generate additional information on the compactive nature of the soil below the plate.

Koolen (1974), Larson and Gupta (1980), Larson et al (1980) and Seig (1985) used confined compression tests to assess soil compactability. Their tests, however, were carried out on air dried and sieved soil which may display very different compression characteristics to the original structured field soil. In addition, the sample diameters used were approximately 50mm.

Data from confined compression tests could be used to complement those obtained from plate sinkage tests. Equipment is required, however, which is capable of testing a representatively large sample of field soil, preferably in the field at the time when the plate sinkage tests are carried out.

1.3 Objectives

Overall objective:-

To develop techniques and models for assessing the susceptibility of soils to compaction by agricultural machinery.

To achieve the overall objective, the following detailed objectives were identified:-

- (1) To investigate the relationship between the strength of a range of field soils, under grass and cereals, and:-
 - (a) soil water suction, and
 - (b) soil moisture deficit.
- (2) To design and build tractor-mounted compression equipment for quantifying the compactive nature of soil.
- (3) To analyse and interpret data generated by the tractor-mounted compression equipment to develop a methodology for quantifying the compactability of field soils.
- (4) To compare trafficability and workability predictions based on findings from objective (1) with compactability and strength assessments based on objectives (2) and (3).

1.4 The Thesis structure

The nature of this study is such that the main body of the Thesis is divided into five discrete Chapters (2 to 6) entitled:-

- (2) Soil water suction and soil strength,
- (3) Soil moisture deficit and soil strength,
- (4) Development of tractor-mounted test equipment,
- (5) Quantification of the compactive nature of soil (part I), and
- (6) Quantification of the compactive nature of soil (part II).

CHAPTER 2

SOIL WATER SUCTION AND SOIL STRENGTH

Introduction

The review of literature, Chapter 1, highlighted a need for the development of techniques and models for predicting soil strength in the field. In Chapter 2, the relationship between soil water suction and soil strength is studied with a view to using soil water suction as a parameter in soil strength prediction models.

The two main factors contributing to soil strength are cohesion and friction.

Cohesion is the bonding between two particles or aggregates due to various particle-dependent forces and, more importantly, to the force from water tension. Water adheres to the surface of soil particles and cohesion occurs between adjacent water molecules and therefore the presence of water under negative pressure (suction) acts as a binding force.

Friction is the resistance experienced by soil particles when sliding over each other. It generally increases with increasing grain irregularity (Dumbleton and West, 1970) and with an increase in the number of particle contacts per unit volume. An increase in soil bulk density will generally result in an increase in soil friction (Godwin, 1974).

The relative contribution of both cohesion and intergranular friction to soil strength varies with percentage clay content. At clay contents less than approximately 10 to 15%, cohesion is only important over a very limited range of soil moisture contents and interparticle friction is dominant. At clay contents in the range 15 to 35%, both cohesion and intergranular friction are important and at clay contents of above about 35%, cohesion is the dominant component of soil strength, particularly under moist or wet conditions.

Cohesive forces are dependent on soil moisture suction rather than soil moisture content. Work by Lewis and Ross (1955), Dumbleton and West (1970) and Towner (1983) has confirmed that in a situation of moisture equilibrium in a structureless, unconsolidated, clay soil, the suction of the soil water is equivalent to the soil strength (when both are expressed in the same units). This is also demonstrated by the results of Davies (1985) who worked with a clay soil having a shear strength (vane measurement) of 16 - 25kPa at a suction of 2.5kPa. An increase in soil water suction of 2.5kPa resulted in a very similar increase in shear strength (2 - 3kPa).

The dependence, to varying degrees, of soil strength on cohesion has already been discussed, as has the effect of soil water suction on cohesion. It is therefore valid to investigate the relationship

between soil water suction and soil strength in the field. To do this, six field sites were selected and instrumented, covering a range of agricultural situations commonly found in central and eastern England. The main soil characteristics of the sites are given in Table 2.1.

Table 2.1 The six soils under investigation

Location	Soil series characteristics	Topsoil characteristics	Subsoil characteristics	Soil water regime
Gleadthorpe EHF, Cuckney Nottinghamshire	Slightly pebbly loamy sand	Slightly pebbly loamy sand	Brown slightly pebbly or loamy sand passing to reddish soft sandstone	Well drained. Subsoil rarely wet.
Lockington, Leicestershire	Slightly pebbly sandy loam	Slightly pebbly sandy loam	Brown slightly pebbly sandy loam with occasional moderately and very pebbly bands, passing to loamy medium sand	Well drained. Subsoil rarely wet.
Streatley, Bedfordshire	Slightly stony clay loam	Slightly stony clay loam	Very chalky brown clay loam passing to weathered chalk	Well drained. Subsoil rarely wet.
Southwell, Nottinghamshire	Slightly stony clay loam	Slightly stony clay loam	Slightly stony, slightly mottled brown clay loam over reddish brown slightly mottled clay	Slight seasonal water-logging. Upper parts of the soil are intermittently wet during winter and early spring.
Silsoe, Bedfordshire	Stoneless clay	Stoneless clay	Stoneless slightly mottled olive clay over mottled grey clay	Slight seasonal water-logging. Upper parts of the soil are intermittently wet during winter and early spring.
Faringdon, Oxfordshire	Stoneless clay	Stoneless clay	Stoneless mottled grey clay	Seasonally waterlogged. Topsoil wet for most of the winter and early spring.

2.1 Qualitative relationship between soil water suction and trafficability and workability.

The first part of the study involved a qualitative assessment of the field sites to determine whether the land was:-

- (a) untrafficable,
- (b) trafficable but not workable,
- (c) trafficable and workable.

This assessment was then related to soil water suction measured directly by tensiometers at 50 and 150mm depth down the soil profile. This exercise was carried out on a fortnightly basis from October 1987 to December 1989.

The assessments were based on an examination of the land in a similar manner to that which a farmer might make when deciding whether or not to carry out a field operation. When a farmer assesses soil strength, it is often in the absence of any vehicle or machinery. It is difficult to quantify exactly how a farmer might integrate the information available to him when forming an opinion however, certain aspects of the procedure dominate his final decision. These are:-

- (1) Amount of sinkage and smear experienced whilst walking on the land.
- (2) Ease with which a walking stick can be pushed into the soil, ie. a crude penetrometer assessment.

- (3) The tendency of soil to stick to boots, ie. a measure of adhesion.
- (4) The mode of failure of clods squeezed by hand, ie. plastic deformation or brittle failure?
- (5) Visual appearance of the soil surface, ie. wet or dry?
- (6) Knowledge of antecedent conditions, ie. how wet the upper soil profile might be.

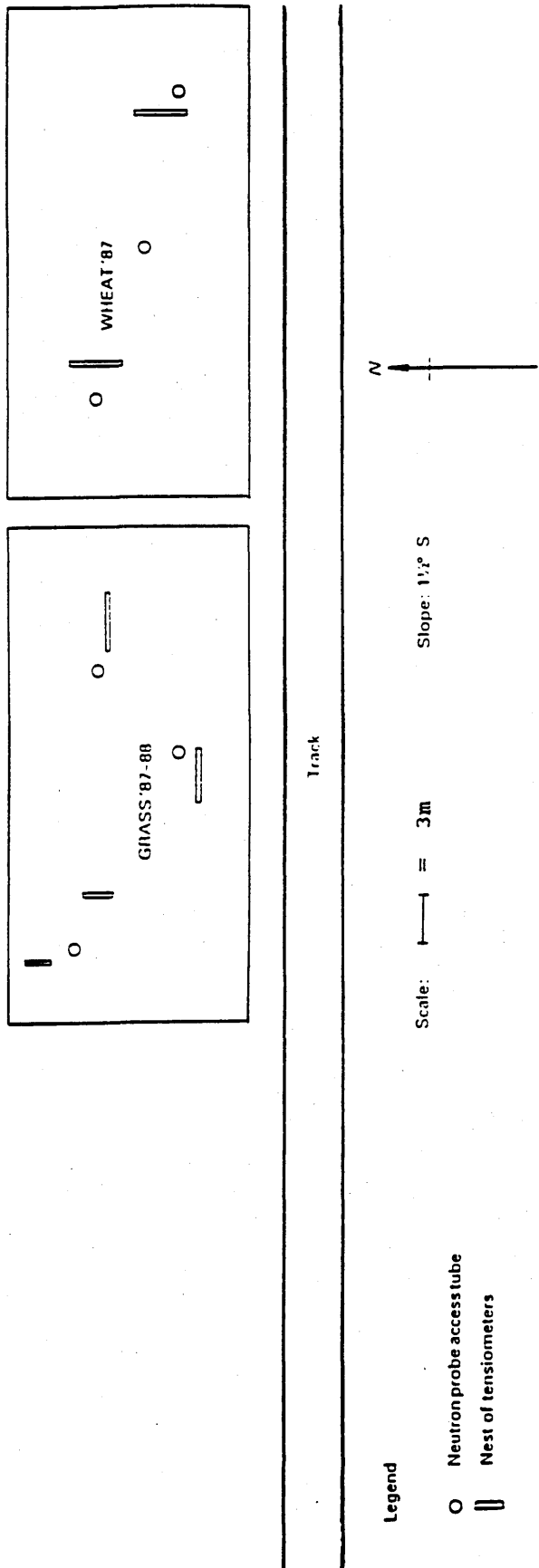
Few farmers dig holes when assessing soil strength - most of the assessment is concerned with soil surface conditions.

Paul and de Vries (1979) consider that 20% wheel slip can be used as a critical value for traction efficiency, but the assessment for trafficability in this study was necessarily qualitative. The definition for trafficable, used in this present study, was that, in the opinion of the assessor, a soil could be driven over by a conventional wheeled tractor of around 70kW without undue sinkage, slippage or adhesion of soil to the tyres.

The definition of workable was that, in the opinion of the assessor, ploughing or seedbed preparation could be carried out without the soil undergoing excessive damage through smearing and compaction.

The field assessments were carried out at the six sites under two crops - ley grassland and winter wheat. The plots were subjected to normal agronomic practices. Four silage cuts per year were taken from the grass plots. Site plans for all six soil series are given in Figures 2.1 to 2.6.

Figure 2.1 Cuckney Site Diagram



Legend

- Neutron probe access tube
- ▯ Nests of tensiometers

Scale: 1:1 = 3m

Slope: 1:1 S



Wick Site Diagram

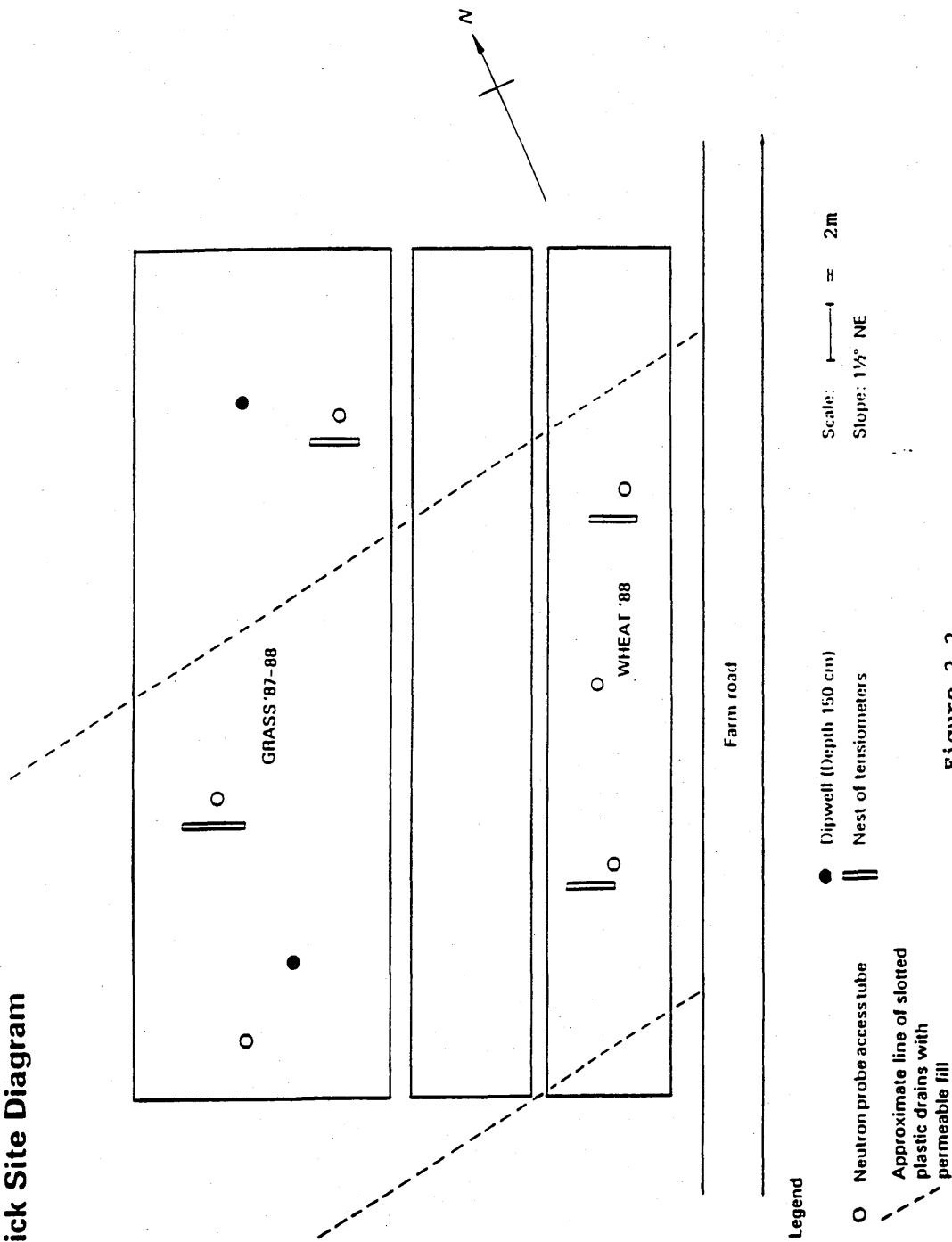
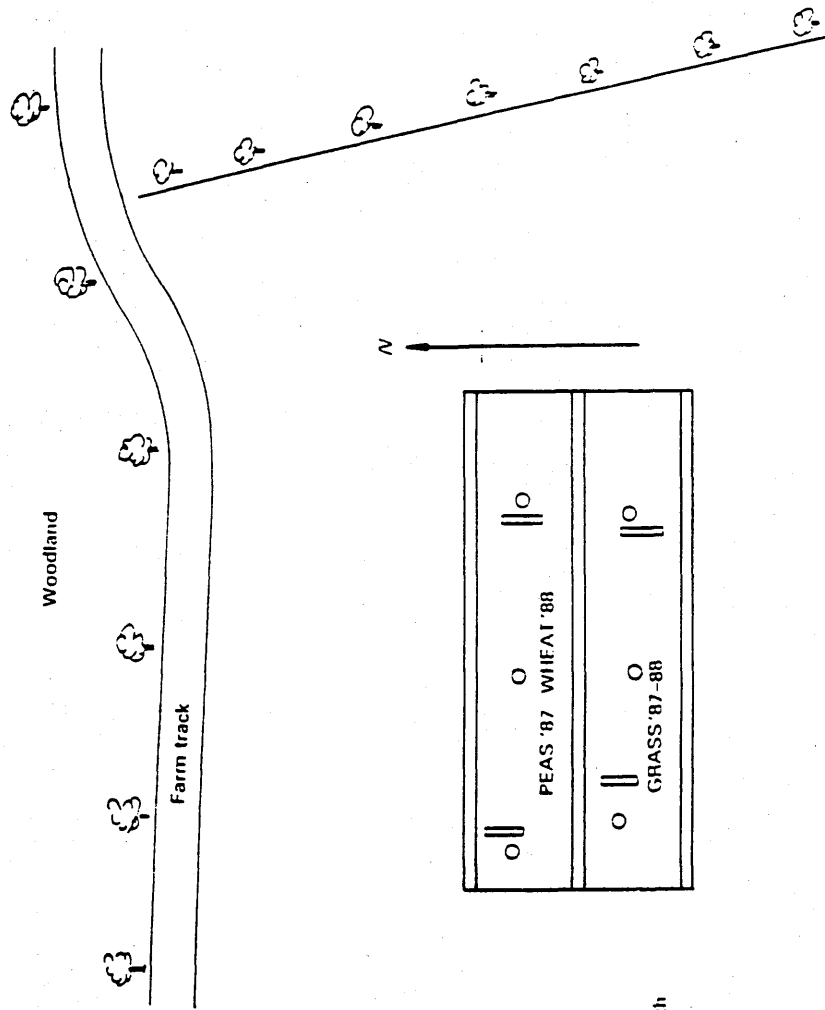


Figure 2.2

Upton Site Diagram



 PEAS '87 WHEAT '88	
 GRASS '87-88	

Path/Discard
2 x Drill Width

Legend

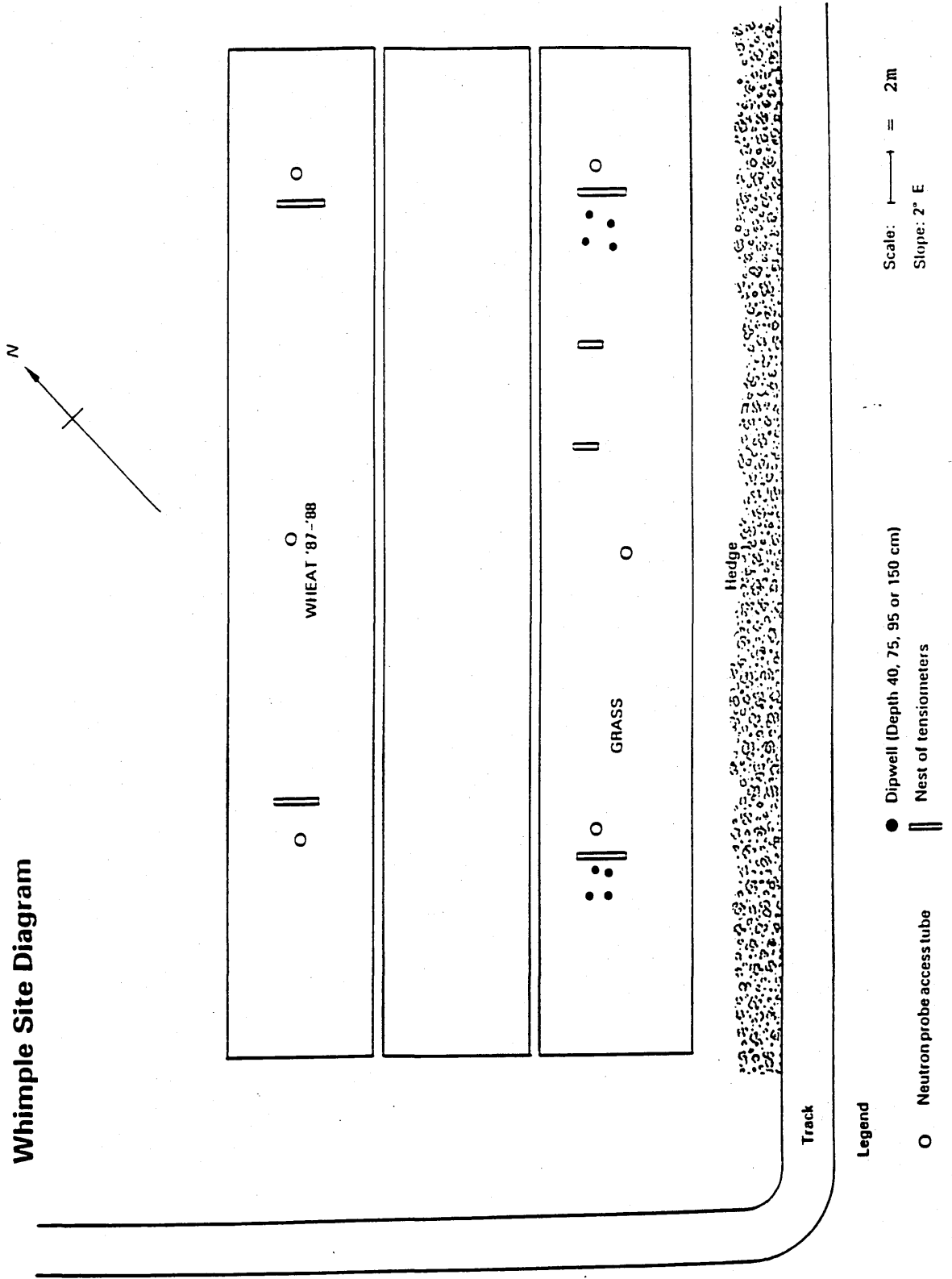
- Neutron probe access tube
- Nest of tensiometers

Scale: = 5m Slope: 2 1/2° SE

Figure 2.3

Figure 2.4

Whimble Site Diagram



Legend

- Dipwell (Depth 40, 75, 95 or 150 cm)
- Neutron probe access tube
- || Nest of tensiometers

Scale: 1 unit = 2m
Slope: 2° E

Evesham Site Diagram

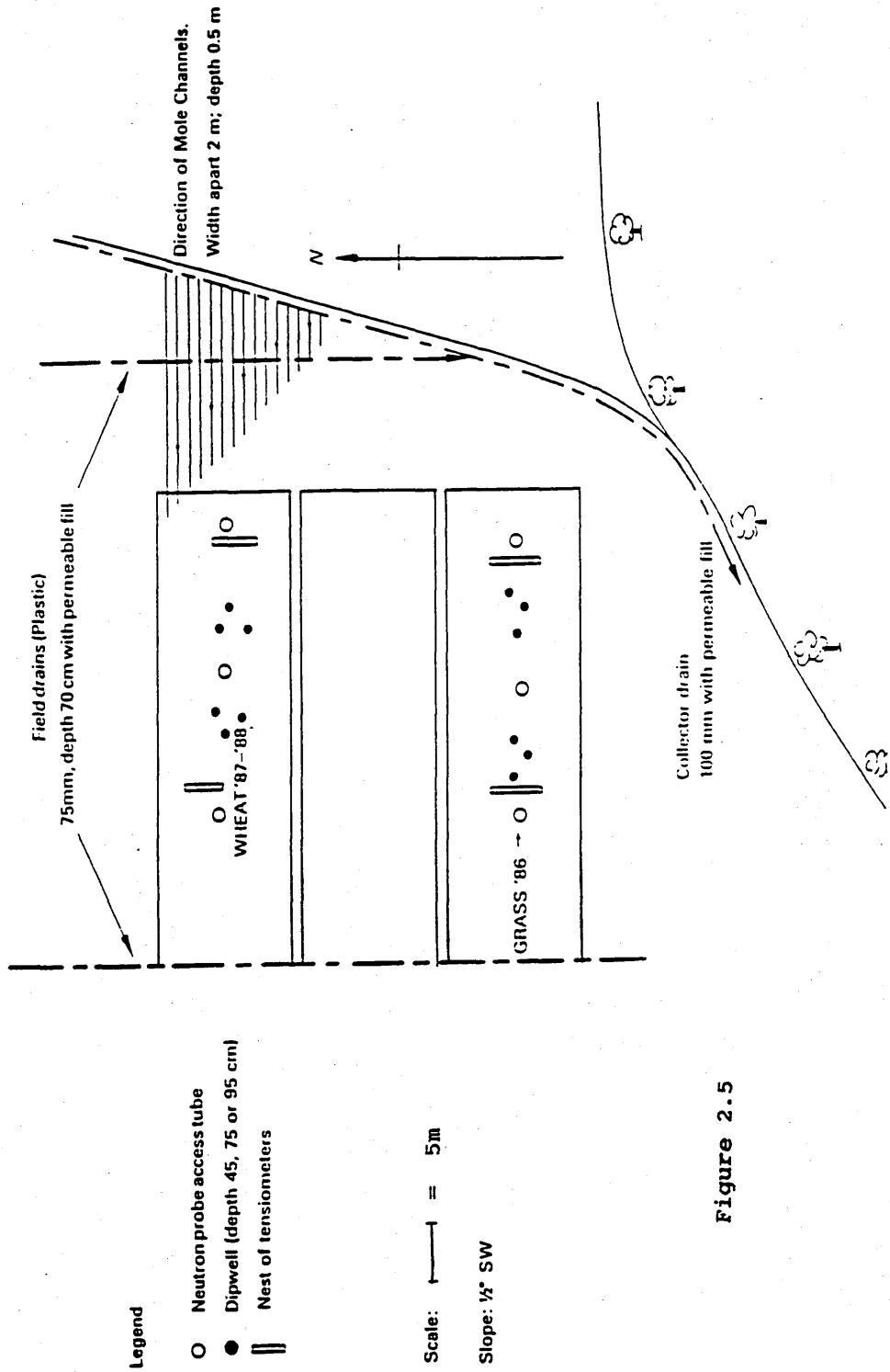
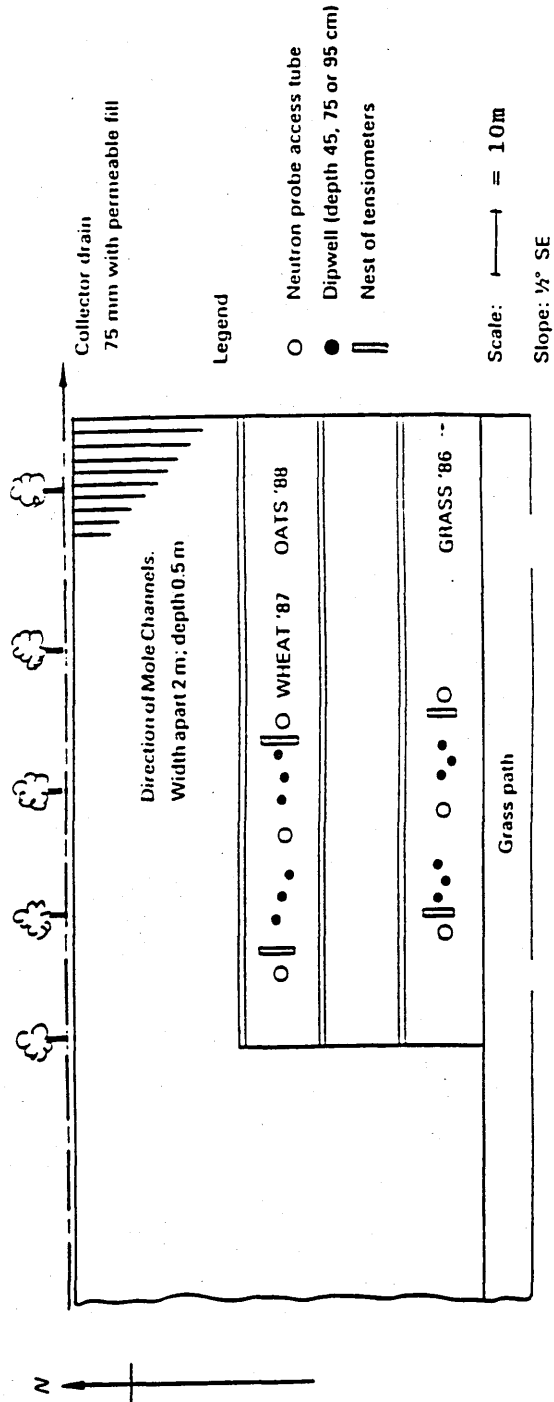


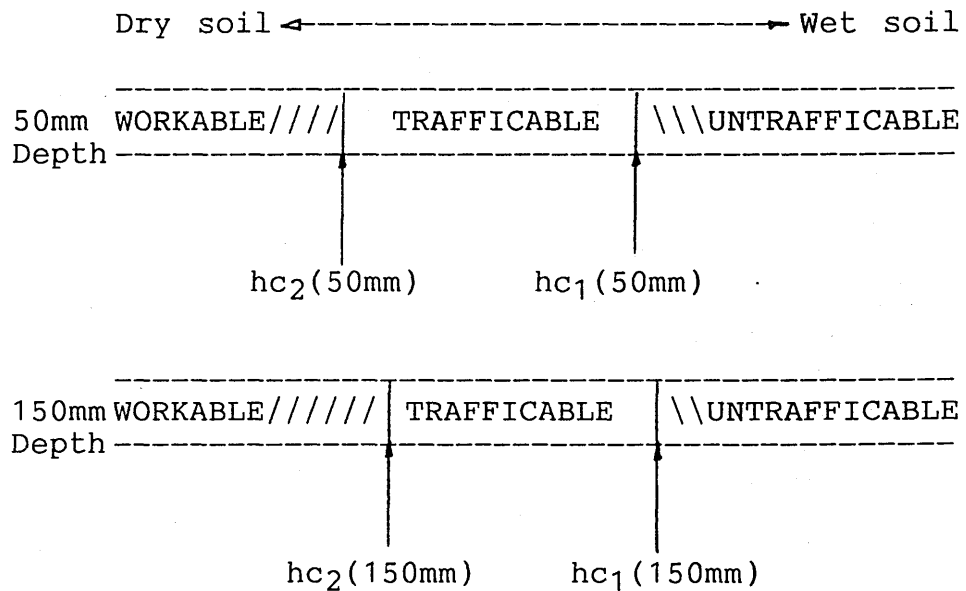
Figure 2.5

Figure 2.6 Denchworth Site Diagram



Previous work (Collas, 1987) concluded that trafficability prediction was difficult on days when more than 5mm of rain had fallen during the preceding 24 hours. An additional criterion, introduced for this study, was that assessments would not be made if more than 10mm of rain had fallen during the preceding 48 hours. This was introduced to guard against a situation arising whereby the soil surface appears very wet but, due to very low hydraulic conductivities at some of the sites, appreciable soil water suctions still persist at depths of only 100 to 150mm at the time of monitoring.

Trafficability assessments in conjunction with soil water suction data from the fifteen month investigation were analysed and critical soil water suction limits (defined below) derived for each plot at depths of 50 and 150mm.



Where:-

$hc_1(50mm)$ = critical soil water suction limit for trafficability at 50mm depth.

$hc_2(50\text{mm})$ = critical soil water suction limit for workability at 50mm depth.

$hc_1(150\text{mm})$ = critical soil water suction limit for trafficability at 150mm depth.

$hc_2(150\text{mm})$ = critical soil water suction limit for workability at 150mm depth.

The results for each site are given in Table 2.2 and are similar to values derived from a study in the Netherlands (Van Wijk and Feddes, 1986). The differences in critical suction between the grass and the wheat plots can be explained in the main by differences in soil bulk density.

Table 2.2 Critical soil water suction limits (cm of water) for trafficability and workability

Soil series	Depth (mm)	Trafficability		Workability	
		Grass	Wheat	Grass	Wheat
Cuckney	50	5	5	35	30
	150	5	5	30	25
Wick	50	30	35	45	35
	150	40	30	50	35
Upton	50	25	35	45	45
	150	30	25	45	35
Whimble	50	25	40	50	100
	150	25	30	30	35
Evesham	50	50	30	70	55
	150	25	20	40	10
Denchworth	50	25	40	100	100
	150	30	25	130	140

Similar results were obtained by Paul and de Vries (1979) who found that the critical suction for trafficking in a silty clay loam topsoil was 35cm of water under grassland and 27cm under cultivation. Wheel slip was minimised and ruts deeper than 50mm were avoided by trafficking only at suctions in excess of these.

The critical soil water suction limits presented in this study, Table 2.2, have been expressed in such a way so as to allow simultaneous measurements of soil water suction at both 50 and 150mm depth to be used to predict the trafficability status of a given soil. For example, if the suctions at 50 and 150mm depth were 120 and 28cm of water respectively on a given day at the Wick wheat plot, then from Table 2.2 the prediction would be one of "not trafficable". If the respective suctions were 80 and 32cm of water, then the prediction would be one of "trafficable but not workable". This would suggest that a farmer could apply fertilizer to the soil surface, but could not carry out any cultivation work without risking unacceptable damage to his land.

The critical soil water suction limit for trafficability on the Cuckney series is 5cm of water. This implies that a tractor could be driven over the land almost all year round without unduly damaging the soil, whereas the limits for the Wick and Upton series imply that more regard to the soil moisture status is necessary before one can embark on any field operation.

The critical soil water suction limits for trafficability on the heavier soils such as the Whimple, Evesham and Denchworth series are relatively low, particularly for the permanent grass plots. This is probably due to higher soil density under grass, but also to the

associated root mass effect, allowing tractors to be driven on relatively wet clayey soils.

2.2 Quantitative relationship between soil water suction and cone penetration resistance.

The derivation of the critical soil water suction limits (Table 2.2) was based on qualitative assessments of the soil. In general, farmers know their land well enough to make reasonably accurate assessments of the trafficability/workability status of the soil on a potential work-day. However, if circumstances on the farm were to change, for example a new crop, different machinery or additional land, or, a seasonal prediction is needed, the farmer may not be quite so well placed to make reliable assessments. Thus a quantitative procedure is desirable.

A second study was carried out alongside the critical soil water suction work, the aim being to establish what relationship, if any, exists between cone penetration resistance and soil water suction. If a strong relationship does exist, this information could be used to quantify the procedure described earlier, providing a further in situ assessment of the influence of moisture status on soil mechanical properties.

A cone penetrometer measures the resistance of soil to the penetration of a standardised cone. The penetration resistance depends on friction and cohesion, but theoretical analysis of the process has so far been impossible, except under some well defined conditions. Nevertheless, field results appear to simulate the tyre -

soil interaction well enough to provide an indication of soil bearing strength and likely vehicular mobility.

On the twelve experimental plots (wheat and grass plots at each of the six sites) cone penetration resistance was measured using a Bush Recording Soil Penetrometer (Anderson et al., 1980) fitted with a stainless steel cone of 20.27mm diameter and 30^o included angle.

Measurements of cone penetration resistance and soil water suction were made simultaneously at depths of 50 and 150mm on a fortnightly basis throughout one growing season. A 'W' shape was paced out over a given plot and 10 penetrations were recorded. These were then averaged and converted from kgf to MPa. Where less than 7 random penetrations were possible due to stoniness and/or soil strength, those readings were discarded.

2.2.1 THE CUCKNEY SOIL SERIES

A detailed description of the soil profile is given in Appendix 1. The top soil is a slightly stony loamy sand of moderately low soil and ped strength and extends to a depth of around 350 to 400mm.

The cone penetration/moisture suction results for the Cuckney topsoil were initially subjected to linear regression analysis and are shown in Figure 2.7.

A significant increase in topsoil strength, of about 2MPa/1000cm of water suction, is seen as the arable site dries out over the growing season. The intercepts of the plotted lines, ie penetration resistance at zero soil water suction (RP0) occur at around 0.35MPa. Data points around RP0 generally occurred during the early part of the growing season when the root mass effect on cone penetration resistance would be small.

Plant roots can modify soil strength by mechanically reinforcing the soil fabric (Adams et al, 1985). On the permanent grass plot, the binding effect of the grass roots can be clearly seen, the grass plot having higher strength at all soil water suctions despite being at a similar bulk density to the arable plot. The gradient of the regression line is approximately twice that of the arable plot (3.8MPa/1000cm of water suction).

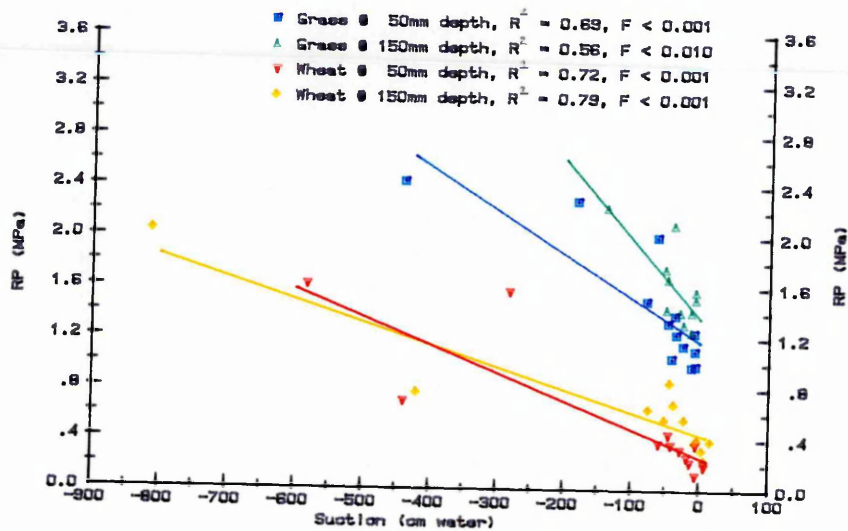
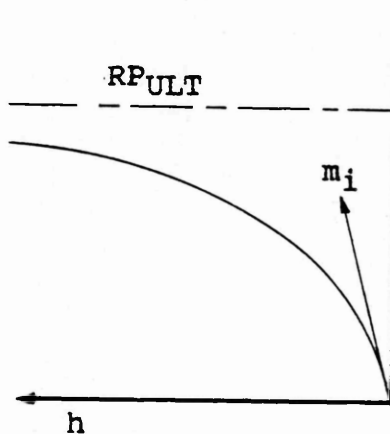


Figure 2.7 The linear relationship between soil water suction (h) and resistance to cone penetration (RP) for a loamy sand - Cuckney series topsoil under grass (bulk density 1.45Mg/m^3) and wheat (1.44Mg/m^3)

As the grass plot began to dry out in the spring, the rate of increase in soil strength was such that it was soon out of the working range of the cone penetrometer and therefore a good correlation at 150mm depth was difficult to obtain without reducing the cone size which could have affected the continuity of the results.

Although values of R^2 (coefficient of determination) are in the range 0.56 to 0.79, see Figure 2.7, the general path of the data points appears to be curved with a rapid increase in soil strength occurring as the soil begins to dry out when suction is low. The rate of increase in strength tails off as suction increases above 75 - 100cm of water. Steinhardt and Trafford (1974) and Gossage (1977) observed similar trends.

To improve the regression, the data were approximated to a hyperbola of the form:-



$$RP = \frac{h}{\frac{1}{m_i} + \frac{h}{RP_{ULT}}} \quad [1]$$

where:-

- RP = resistance to cone penetration
- h = soil water suction
- m_i = initial gradient
- RP_{ULT} = the asymptotic maximum value of RP

Rearranging equation [1] results in:-

$$\frac{h}{RP} = (h/RP_{ULT}) + (1/m_j) \quad [2]$$

which is linear with variables $\frac{h}{RP}$ and h .

The Cuckney results, subjected to hyperbolic analysis, are plotted in Figure 2.8.

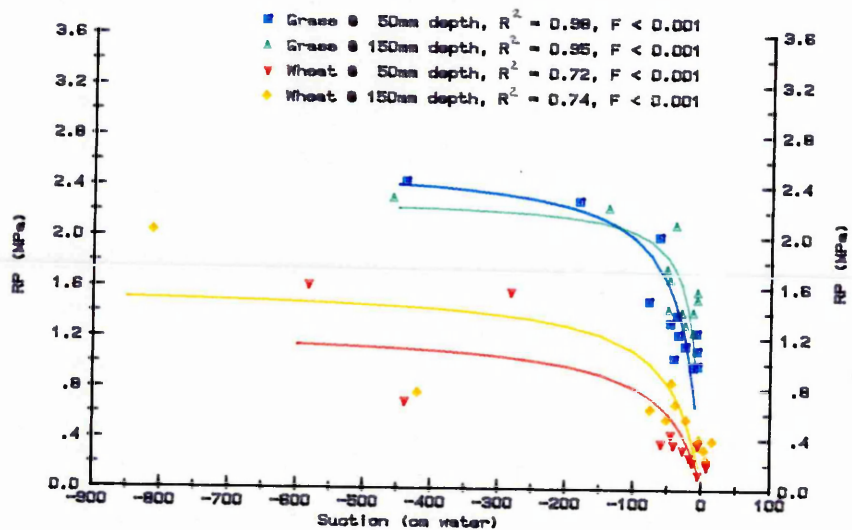


Figure 2.8 The hyperbolic relationship between soil water suction (h) and resistance to cone penetration (RP) for a loamy sand - Cuckney series topsoil under grass (bulk density 1.45Mg/m^3) and wheat (1.44Mg/m^3)

Value of R^2 of 0.72 to 0.98 were obtained using hyperbolic regression analysis. The 'F' values (variance ratio) achieved indicate that the relationships are highly significant.

As the soil begins to dry out and soil water suction (h) increases, the initial increase in RP is rapid, especially under grass. As h exceeds -50 to -100cm, further increases in h result in a much more modest increase in soil strength.

Greater strength is observed under grass than under wheat at all times during the season, despite the two plots being of similar bulk density. The strength difference is mainly due to the greater root mass effect under grass.

2.2.2 THE WICK SOIL SERIES

A detailed description of the soil profile is given in Appendix 1. The topsoil is a medium sandy loam of moderately low soil and ped strength and extends to a depth of around 250mm.

The linear regression analysis results for the Wick topsoil (50 & 150mm) are shown in Figure 2.9. The regression lines for the penetration resistance at 50 and 150mm depth, under both grass and wheat, all have similar slopes with an average increase in soil strength on drying of approximately 2.1MPa/1000cm of water suction. Soil strength under grass was generally greater than that under wheat throughout the growing season. This was probably partly due to differences in bulk density between the plots, but also

to the greater binding effect of the grass roots. On both plots, soil strength was greater at a depth of 150mm than at 50mm all through the year.

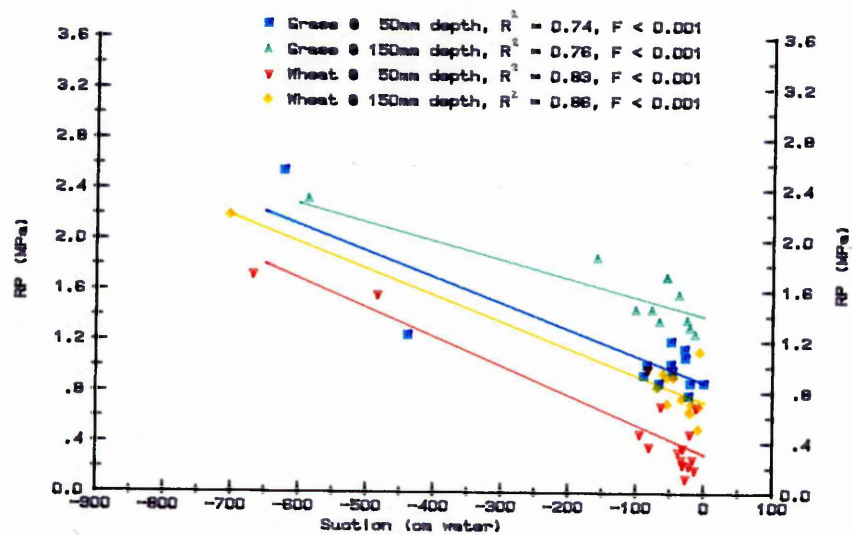


Figure 2.9 The linear relationship between soil water suction (h) and resistance to cone penetration (RP) for a sandy loam soil - Wick series topsoil under grass (bulk density 1.50Mg/m^3) and wheat (1.34Mg/m^3).

Despite obtaining reasonably high linear correlation coefficients, see Figure 2.8, soil strength for the Wick series, like that of the Cuckney series, appears to increase more rapidly as the soil dries when suction is low than when suction exceeds -100cm.

Figure 2.10 shows the Wick results with hyperbolic curves drawn through them.

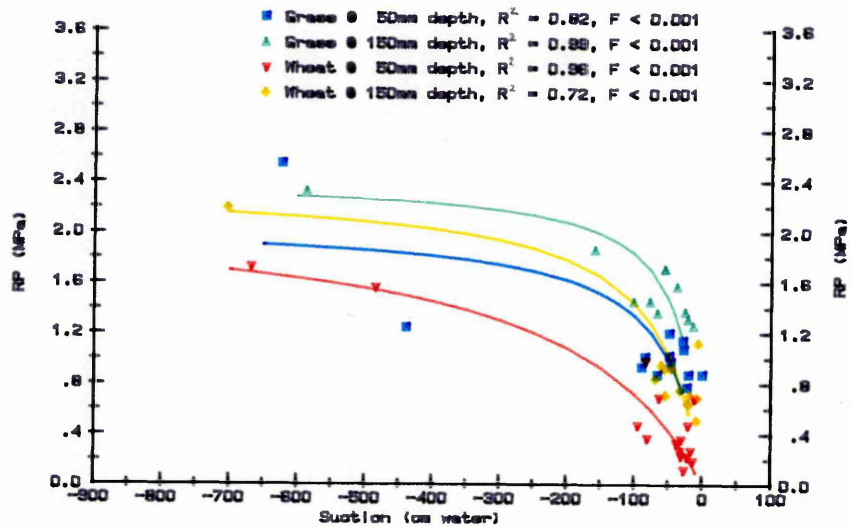


Figure 2.10 The hyperbolic relationship between soil water suction (h) and resistance to cone penetration (RP) for a sandy loam soil - Wick topsoil under grass (bulk density 1.50Mg/m^3) and wheat (1.34Mg/m^3).

Hyperbolic regression of the RP - h data improved on the R^2 values, see Figure 2.10, and levels of significance achieved when using linear regression analysis. The curves follow a similar path to those of the Cuckney series, however, the initial rate of strength increase, especially under grass, is lower. The soil strength at 150mm depth is greater than that at 50mm, under both grass and wheat, throughout the season.

2.2.3 THE UPTON SOIL SERIES

A detailed description of the soil profile is given in appendix 1. The topsoil is a slightly stony clay loam of moderately low soil strength and extends to a depth of around 250mm. Below 250mm, the soil consists almost entirely of chalk stones. It was not possible to push the penetrometer down as far as 350mm depth at any time during the growing season. The results for the Upton topsoil (50 & 150mm) are shown in Figure 2.11.

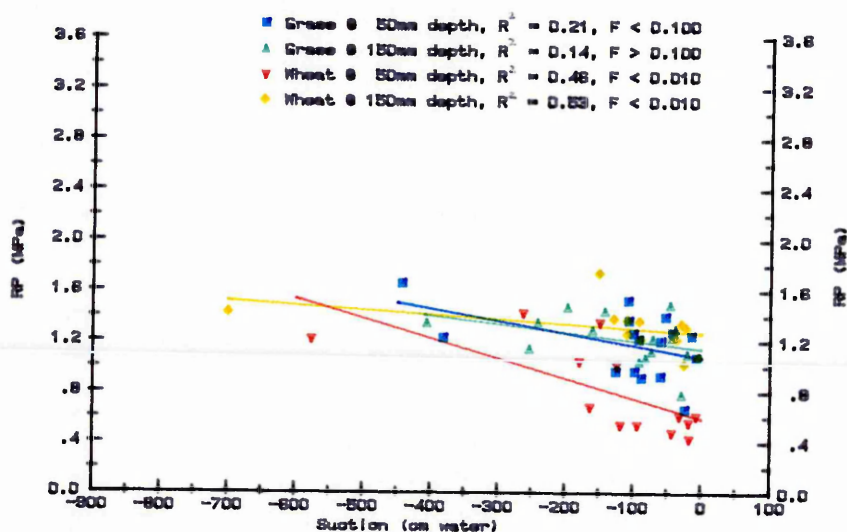


Figure 2.11 The linear relationship between soil water suction (h) and resistance to cone penetration (RP) for a clay loam soil - Upton series topsoil under grass (bulk density 1.06Mg/m^3) and wheat (0.89Mg/m^3)

The graph illustrates the relatively poor linear relationship which exists between cone penetration resistance and soil water suction for this soil. The scatter of data points is probably due, in the main,

to the cone penetrometer sampling a relatively small area as compared to that of the much larger chalk lumps, which are distributed fairly extensively throughout the topsoil. The effect of this is to produce very erratic readings, resulting in low linear correlation coefficients.

Certain trends can be picked out from the graphs. For both plots, the increase in soil strength on drying appears to be much greater at 50mm depth, (1.0 to 1.6MPa/1000cm of water suction), than at 150mm depth, (0.3 to 0.6MPa/1000cm of water suction. In general, soil strength at low suctions is high for this soil series and so the relatively low increase in strength on drying would not be seriously limiting for traffic.

The data for the Upton series appears to follow a hyperbolic type relationship, but the trend is not as obvious as those for the coarser textured Cuckney and Wick series. Figure 12 shows the results for the Upton series with hyperbolic curves drawn through them.

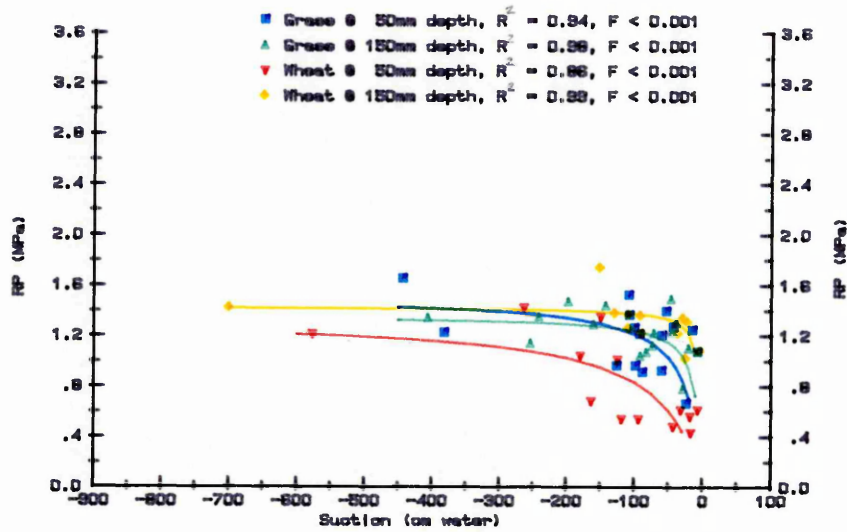


Figure 2.12 The hyperbolic relationship between soil water suction (h) and resistance to cone penetration (RP) for a clay loam soil - Upton series topsoil under grass (bulk density 1.06Mg/m^3) and wheat (0.89Mg/m^3)

The coefficient of determination (R^2) values obtained for the hyperbolic curves, (see Figure 2.12), were much greater than those from the linear regression analysis. The curves for both plots (grass and wheat) have a very similar form, with the exception of the wheat at 50mm depth, where the increase in soil strength with increasing moisture suction is more gradual.

2.2.4 THE WHIMPLE SOIL SERIES

A detailed description of the soil profile is given in Appendix 1. The topsoil is a clay loam of moderately low soil and ped strength and extends to a depth of around 320mm.

Figure 2.13 shows results for the Whimple topsoil (50 & 150mm).

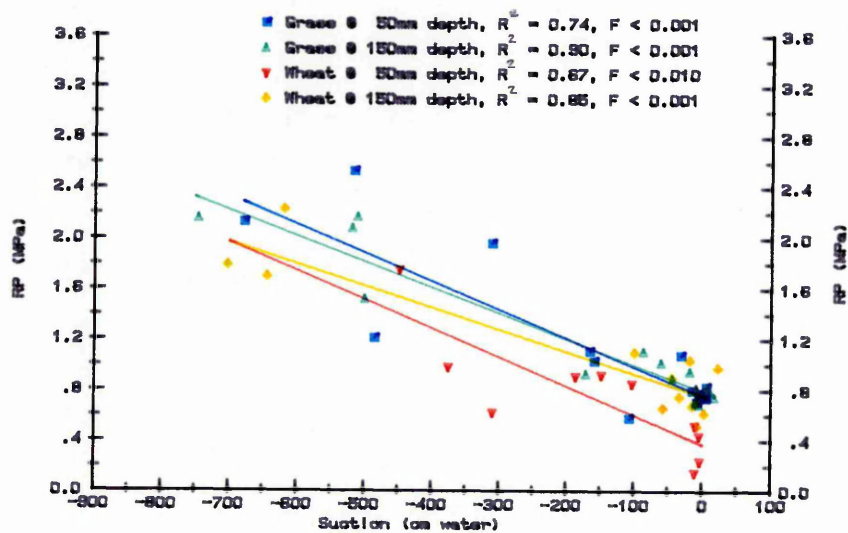


Figure 2.13 The linear relationship between soil water suction (h) and resistance to cone penetration (RP) for a loamy soil - Whimple series topsoil under grass (bulk density 1.54Mg/m^3) and wheat (1.47Mg/m^3).

The regression lines for penetration resistance at 50 and 150mm depth under both grass and wheat are similar with an average increase in strength on drying of $2\text{MPa}/1000\text{cm}$ of water suction.

The topsoil under grass has greater resistance to penetration than at equivalent depths under wheat, probably partly due to higher bulk density under grass (the grass plot was closer to the field headland) and partly due to the binding effect of the roots. The data were analysed using hyperbolic regression analysis and the results are presented in Figure 2.14.

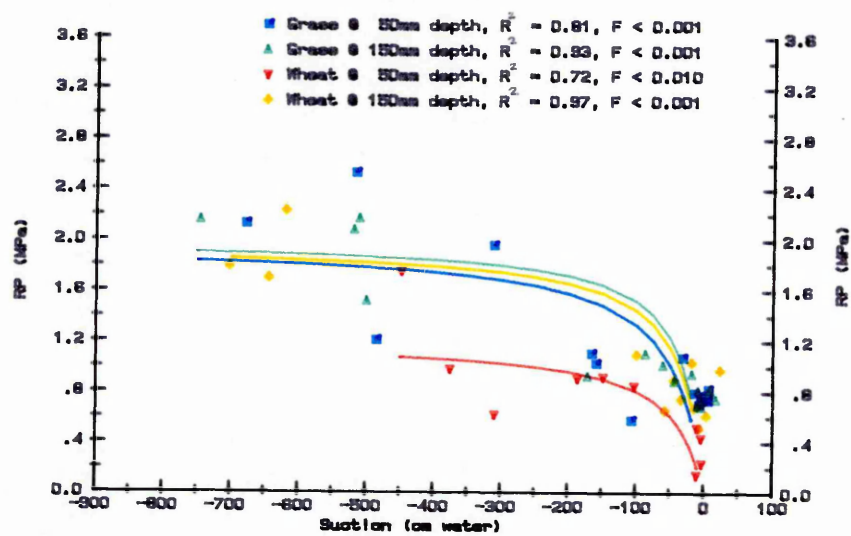


Figure 2.14 The hyperbolic relationship between soil water suction (h) and resistance to cone penetration (RP) for a loamy soil - Whimpe series topsoil under grass (bulk density 1.54Mg/m^3) and wheat (1.47Mg/m^3).

The hyperbolic regression analysis results again provided a better fit, with higher R^2 values (see Figures 2.13 and 2.14). The regression lines for penetration resistance at 50 and 150mm depth under grass, and at 150mm depth under wheat all have a similar form with a rapid increase in strength with increasing suction over a suction range 0 to -100cm of water. The rate of subsequent strength increase, at suctions greater than -100cm (more negative), is very much slower with the curves tending towards an asymptote of

2MPa. At 50mm under wheat, soil strength tends towards a lower plateau of 1.2MPa due mainly to a lower bulk density.

2.2.5 THE EVESHAM SOIL SERIES

A detailed description of the soil profile is given in Appendix 1. The topsoil is a stoneless clay of moderately low strength and extends to a depth of about 250mm. Figure 2.15 shows results for the Evesham series Topsoil.

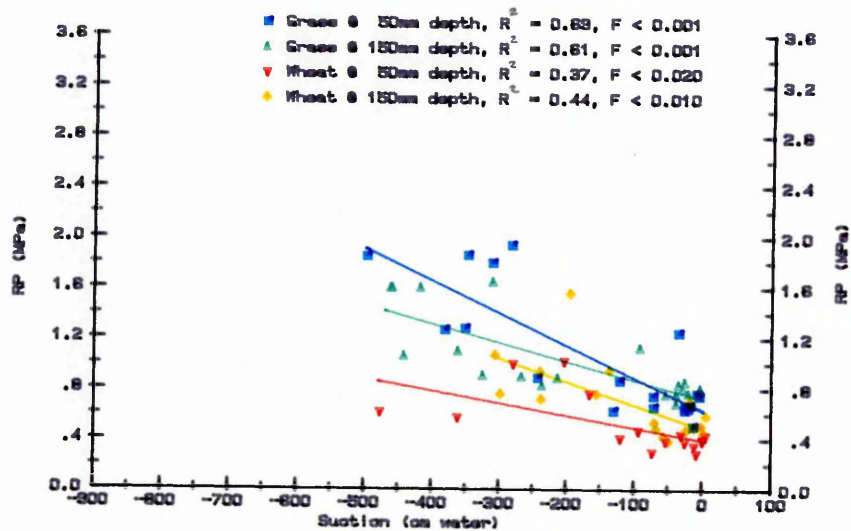


Figure 2.15 The linear relationship between soil water suction (h) and resistance to cone penetration (RP) for a clay soil - Evesham series topsoil under grass (bulk density 0.88Mg/m^3) and wheat (0.98Mg/m^3).

The soil strength - suction characteristics of the two plots are very different at 50mm depth, but become more similar at 150mm. At

50mm depth, the increase in strength is much greater under grass (2.6MPa/1000cm of water suction) than under wheat (1.0MPa/1000cm of water suction). This is probably due, in the main, to the binding effect of the grass roots as the wheat plot had a slightly higher bulk density at that depth.

The strength of the grass plot at 50mm depth remained greater than that of the wheat plot, at the same depth, throughout the growing season.

The data were also analysed using hyperbolic regression and these were found to be more appropriate than straight lines for this soil series. A higher level of significance was attained and R^2 values were improved (see Figure 2.16).

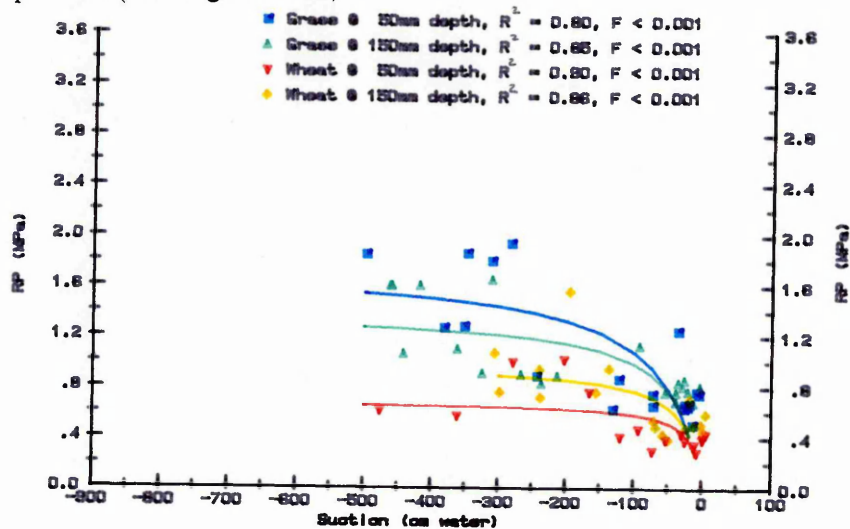


Figure 2.16 The hyperbolic relationship between soil water suction (h) and resistance to cone penetration (RP) for a clay soil - Evesham series topsoil under grass (bulk density 0.88Mg/m^3) and wheat (0.98Mg/m^3).

At soil water suctions greater (ie. more negative) than -300cm of water, soil strength at 50mm depth under wheat is very much lower than that at 150mm depth and those at both 50 and 150mm depth under grass. This was also observed at the other six sites. Conversely, strength at 50mm depth under grass was higher than that at 150mm depth and those under wheat at both 50 and 150mm depth, despite higher bulk density under wheat. This suggests that crop type could have a significant bearing on the trafficability of a soil at a given bulk density and suction, and must be accounted for in any prediction model.

2.2.6 THE DENCHWORTH SOIL SERIES

A detailed description of the soil profile is given in Appendix 1. The topsoil is a non-calcareous clay and extends to a depth of around 250mm.

Figure 2.17 shows the results for the Denchworth topsoil subjected to linear regression analysis.

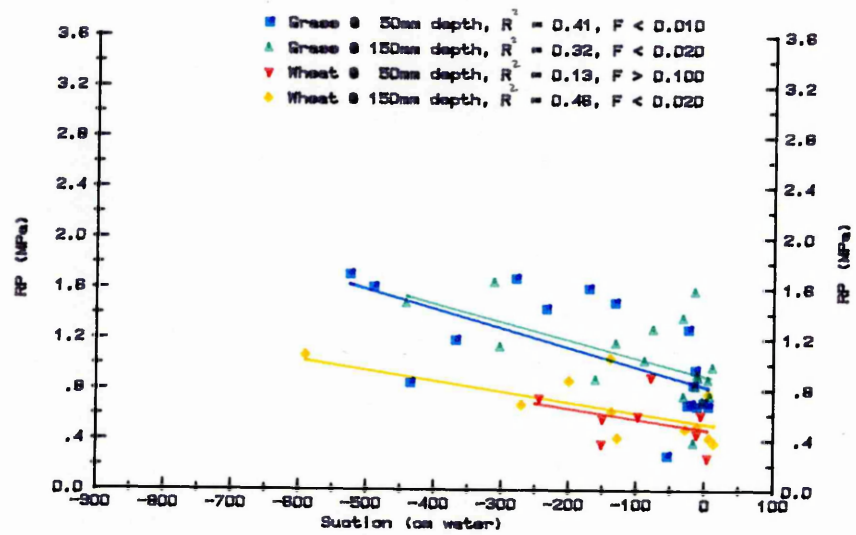


Figure 2.17 The linear relationship between soil water suction (h) and resistance to cone penetration (RP) for a clay soil - Denchworth series topsoil under grass (bulk density 1.02Mg/m^3) and wheat (0.91Mg/m^3).

These relationships are statistically significant, with the exception of the wheat plot at 50mm depth, however R^2 values are low ranging from 0.13 to 0.46 (see Figure 2.16). Very much better relationships were obtained using hyperbolic regression analysis and these are shown in Figure 2.18.

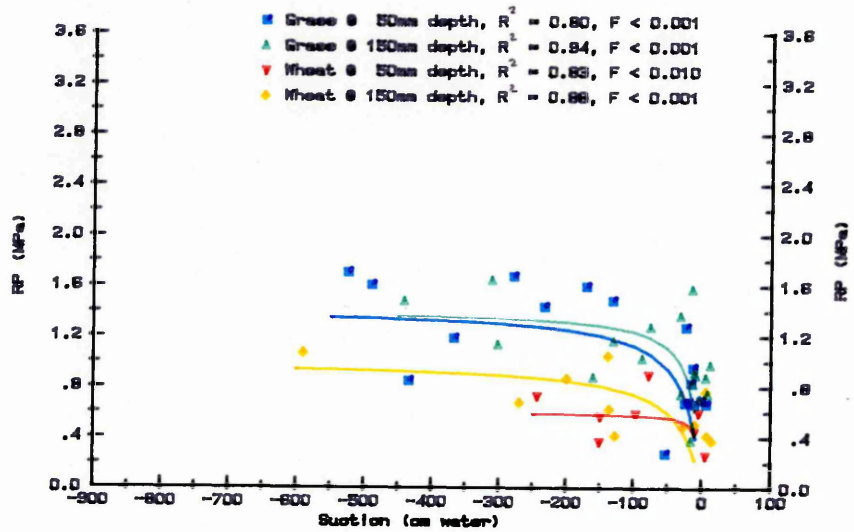


Figure 2.18 The hyperbolic relationship between soil water suction (h) and resistance to cone penetration (RP) for a clay soil - Denchworth series topsoil under grass (bulk density 1.02Mg/m^3) and wheat (0.91Mg/m^3).

The RP - h characteristics for the Denchworth soil series are similar to those of the Evesham series with a greater soil strength increase under grass than wheat at low suctions (0 to -100cm of water). As suction increases (becomes more negative), strength under grass tends towards an asymptotic value of 1.4MPa which is significantly higher than that under wheat viz. 0.6 and 1.0MPa at depths of 50 and 150mm respectively.

2.3 Discussion

If a cone penetrometer is pushed through a soil profile when the soil is close to saturation, ($h = 0$) individual peds deform. As soil dries ($h = 50$ to 100cm suction) and ped strength exceeds the penetration force, then peds will tend to move relative to each other during cone penetration rather than deforming individually. This increases the resistance to cone penetration considerably. As the soil dries further still, the situation is little changed, with peds moving relative to each other, resulting in little increase in strength with increase in soil water suction, and hence the shape of $RP - h$ curves approximates to a hyperbola.

At low suctions, the rate of increase in strength with increasing soil water suction is much greater, and the transition more abrupt, for coarse textured soils and this is reflected in the moist part of their moisture retention curves. Three replicate soil samples were taken from the topsoil of each plot and were analysed using sand suction tables to determine the moisture retention curve - see Figure 2.19.

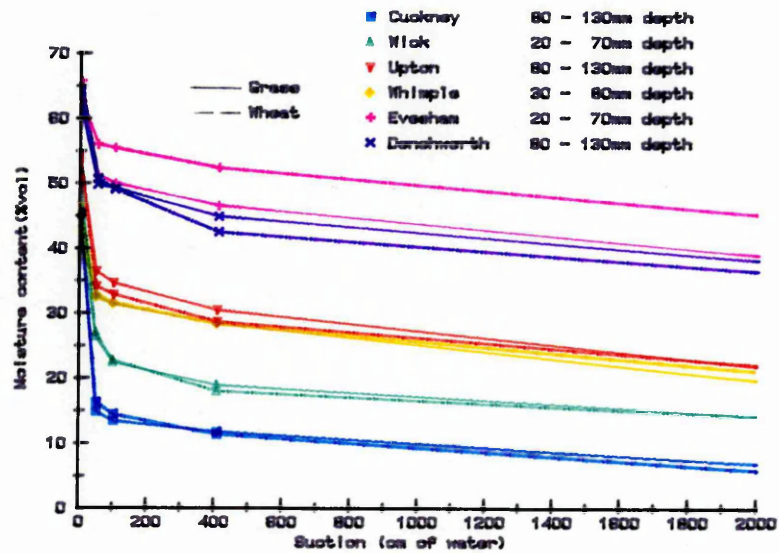


Figure 2.19 The soil moisture retention curves for the six soil series under both grass and wheat.

For the coarse textured soil series, moisture content drops off fairly rapidly between suctions of zero (saturation) and 100cm of water, whereas for finer textured series, the decrease in moisture content is more gradual. It is over this range of suction (0 - 100cm) that the fine textured series experience a very rapid increase in strength with increasing suction. Further increase in strength, at suctions in excess of 100cm, is much more gradual.

Regression equations, both linear and hyperbolic, have been derived for the twelve field sites and are presented in tables 2.3 and 2.4.

Table 2.3 Summary of linear RP - h relationships for six soil series.

Soil series	Crop	Depth (mm)	Gradient (MPa/cm)	Intercept (MPa)	R ²	F
Cuckney	Grass	50	-0.003444	1.1704	0.69	<0.001
		150	-0.006256	1.3625	0.56	<0.010
	Wheat	50	-0.002188	0.2610	0.72	<0.001
		150	-0.001750	0.4407	0.79	<0.001
Wick	Grass	50	-0.002063	0.8711	0.74	<0.001
		150	-0.001640	1.4009	0.76	<0.001
	Wheat	50	-0.002297	0.3107	0.83	<0.001
		150	-0.002094	0.7241	0.861	<0.001
Upton	Grass	50	-0.000949	1.0678	0.21	<0.100
		150	-0.000645	1.1439	0.14	<0.100
	Wheat	50	-0.001551	0.5926	0.46	<0.010
		150	-0.000357	1.2656	0.53	<0.010
Whimble	Grass	50	-0.002244	0.7595	0.86	<0.001
		150	-0.002035	0.7992	0.95	<0.001
	Wheat	50	-0.002269	0.3744	0.82	<0.001
		150	-0.001731	0.7605	0.92	<0.001
Evesham	Grass	50	-0.002555	0.6347	0.83	<0.001
		150	-0.001475	0.7289	0.78	<0.001
	Wheat	50	-0.000955	0.3996	0.61	<0.020
		150	-0.001823	0.4970	0.66	<0.010
Denchworth	Grass	150	-0.001419	0.9115	0.56	<0.010
		350	-0.000769	0.8950	0.55	<0.020
	Wheat	150	-0.000950	0.5358	0.68	<0.100
		350	-0.000814	0.8414	0.79	<0.020

Where R² = Coefficient of determination
 F = Variance ratio.

Table 2.4 Summary of hyperbolic RP - h relationships for six soil series.

Soil series	Crop	Depth (mm)	Asymptotic maximum RP (MPa)	Initial tangent gradient (MPa/cm H ₂ O)	R ²	F
Cuckney	Grass	50	2.56	-0.090	0.98	<0.001
		150	2.29	-0.187	0.95	<0.001
	Wheat	50	1.24	-0.023	0.72	<0.001
		150	1.59	-0.036	0.74	<0.001
Wick	Grass	50	2.05	-0.038	0.82	<0.001
		150	2.40	-0.077	0.99	<0.001
	Wheat	50	2.19	-0.011	0.72	<0.001
		150	2.34	-0.037	0.96	<0.001
Upton	Grass	50	1.49	-0.064	0.94	<0.001
		150	1.35	-0.157	0.98	<0.001
	Wheat	50	1.33	-0.022	0.86	<0.001
		150	1.42	-0.417	0.99	<0.001
Whimble	Grass	50	1.95	-0.042	0.81	<0.001
		150	1.98	-0.067	0.93	<0.001
	Wheat	50	1.18	-0.026	0.72	<0.010
		150	1.95	-0.057	0.97	<0.001
Evesham	Grass	50	1.73	-0.029	0.80	<0.001
		150	1.37	-0.036	0.85	<0.001
	Wheat	50	0.68	-0.045	0.90	<0.001
		150	0.97	-0.039	0.86	<0.001
Denchworth	Grass	50	1.41	-0.057	0.80	<0.001
		150	1.41	-0.110	0.94	<0.001
	Wheat	50	0.60	-0.163	0.83	<0.010
		150	0.99	-0.031	0.88	<0.001

Where R² = Coefficient of determination
 F = Variance ratio.

In Table 2.2, critical soil water suction limits for both trafficability and workability are given, the derivation of which was based on an assessment of the land in a similar manner to that which a farmer

might make when deciding whether or not to carry out a field operation.

The resistance to cone penetration (RP) corresponding to the critical suction limits has been calculated using the linear and hyperbolic relationships of Tables 2.3 & 2.4 and are presented in Table 2.5 below.

Table 2.5 Soil strength RP (MPa) corresponding to critical soil water suction limits for trafficability and workability

Soil series	Depth (mm)	Trafficability		Workability	
		Grass	Wheat	Grass	Wheat
Cuckney	50	0.38	0.10	1.41	0.44
	150	0.67	0.16	1.63	0.57
Wick	50	0.75	0.32	0.94	0.32
	150	1.35	0.76	1.48	0.85
Upton	50	0.77	0.49	0.98	0.57
	150	1.05	1.25	1.13	1.29
Whimble	50	0.69	0.55	1.01	0.81
	150	0.91	0.91	1.00	0.99
Evesham	50	0.78	0.45	0.92	0.53
	150	0.54	0.43	0.69	0.28
Denchworth	50	0.71	0.55	1.13	0.58
	150	0.98	0.43	1.28	0.81

In general, the RP values, corresponding to critical suction limits, are fairly uniform regardless of soil series.

It would appear that the workable limit for the Cuckney series grass plot at 50mm depth is high, as the corresponding RP is 1.41MPa, which is somewhat higher than those for the other sites. The grass plot was considered to be trafficable on a day when the soil suction (h) was -7cm of water at both 50 and 150mm depth, and workable when h was -35cm of water at 50mm depth and -30cm at 150mm depth. No assessment data is available on days when h was between these values and so the critical workable limit was set on the safe side at -35 and -30cm for depths of 50 and 150mm respectively. However the true limits are likely to occur at lower suctions, for example -20cm of water corresponding to RP values of 1.1 and 1.4MPa respectively.

The RP values corresponding to the critical soil water suction limits for workability for the Cuckney wheat plot are low to average when compared with those of the other sites. However, despite this, they may be a little on the high side for this sandy soil as the upper horizon comprises 5% clay and 10% silt and so the risk of soil damage through smearing is minimal. More realistic limits might be -10 and -15cm suction, corresponding to RP values of 0.19 and 0.40MPa at 50 and 150mm depth respectively.

Figures 2.1A to 2.6A, Appendix 2, show graphs of the variation in resistance to cone penetration (RP) over the growing season for the six soil series under investigation.

The RP values corresponding to critical soil water suction limits for trafficability (dashed line) and workability (solid line) have been

superimposed on Figures 2.1A to 2.6A and the number of trafficable and workable days, during the spring and autumn periods, determined. The results from this analysis are given in Tables 2.1A and 2.2A, Appendix 2.

The southern sites (Upton, Evesham and Denchworth) were monitored over the whole of 1988, whereas monitoring of the midland sites (Cuckney, Wick and Whimple) commenced in the autumn of 1987 and continued through to the summer of 1988.

Days where >5mm and >10mm of rain had fallen during the preceding 24 and 48 hours respectively were assumed to be untrafficable, even if high suctions persisted at depth, (see Appendix 2). The number of days conforming to the above criteria was subtracted from the trafficability/workability periods to give a measure of the number of days on which the sites were trafficable and workable during the autumn and spring periods.

In general, the number of workable/trafficable days decreases as soil texture moves from sand to clay. The Cuckney site (loamy sand) was trafficable virtually throughout the autumn of 1987 and the spring of 1988. In contrast, very few workable days occurred for the Evesham and Denchworth series during the spring of 1988 indicating that these soils are poorly suited to spring sown crops under the climatic conditions which prevailed in 1988. Ample spring workable days occurred for the Wick, Upton and Whimple series and spring crops were common in fields near to each of the sites.

The shape of the RP - h curves for all six series are such that soil strength increases rapidly with increasing soil suction at low suctions, but the rate of increase is reduced as soil suction increases further. It would be valuable to gain some idea of the rate of increase in soil strength with time during periods of low rainfall. This could influence a farmer's decision on whether to carry out field operations in marginal conditions or, by waiting a day or so, could a rapid increase in soil strength on his particular soil series be expected, provided that little rain was anticipated.

To obtain an indication of the rate at which soil strength increases with time and to make comparisons between the six soil series, the RP data were analysed in terms of daily rate of change of RP during a drying period. However, because of the climatic differences between the midland and southern sites, it was not possible to find a period between consecutive site visits when approximately the same amount of rain had fallen over the six sites, when the crops were at a similar growth stage. Separate comparisons have, however, been made between the three sites in the midlands and also between the three southern sites.

THE MIDLAND SITES

Table 2.6 shows the RP - time data for the three midland sites.

Table 2.6 Data concerning the change in resistance to cone penetration (RP) with time, during periods of low rainfall, for the three midland sites.

Soil series	Monitoring period	Total rain (mm)	Average daily rain (mm/day)	Rain during two days preceding 2nd site visit (mm)		Crop	Depth (mm)	Change in RP (MPa)	Rate of change in RP (MPa/day)
Cuckney	04/5/88-26/5/88	11.9	0.5	1.6, 3.3	Grass	50	1.33	0.060	
						150	-	-	
Wick	03/5/88-25/5/88	14.5	0.7	1.1, 2.8	Grass	50	1.40	0.064	
						150	0.46	0.021	
Whimble	06/5/88-25/5/88	7.9	0.4	0.4, 4.0	Grass	50	1.33	0.070	
						150	0.70	0.037	
					Wheat	50	1.81	0.095	
					Wheat	150	1.11	0.058	

The monitoring period was during May when average daily rainfall, on all three sites, was between 0.4 and 0.7mm/day and antecedent rainfall for the two days before the second site visits was fairly similar.

The data shows an increase in soil strength, expressed in terms of 'rate of change of RP (MPa/day)'. The general trend is that the greatest rate of strength increase occurs on the Whimple series, followed by the Wick with the lowest rate of increase on the sandy Cuckney series. This trend is particularly apparent at 50mm depth for both the grass and the wheat plots. The average strength increase at 50mm depth is 0.083, 0.061 and 0.058MPa/day for the Whimple, Wick and Cuckney sites respectively.

THE SOUTHERN SITES

Table 2.7 shows RP - time data for the three southern sites.

Table 2.7 Data concerning the change in resistance to cone penetration (RP) with time, during periods of low rainfall, for the three southern sites.

Soil series	Monitoring period (mm)	Total rain (mm)	Average daily rain (mm/day)	Rain during		Crop	Depth (mm)	Change in RP (MPa)	Rate of change in RP (MPa/day)
				two days preceding 2nd site visit (mm)	2nd site visit (mm)				
Upton	23/3/88-02/4/88	9.1	0.9	0.0, 0.0	0.0, 0.0	Grass	50	0.30	0.030
							150	0.26	0.026
Evesham	11/5/88-25/5/88	14.0	1.0	0.0, 0.0	0.0, 0.0	Grass	50	0.41	0.029
							150	0.21	0.015
Denchworth	26/4/88-10/5/88	15.3	1.1	0.0, 0.0	0.0, 0.0	Grass	50	0.10	0.007
							150	0.34	0.024
						Wheat	50	0.36	0.026
						Wheat	150	0.26	0.019

The monitoring period for each of the three sites was 10 - 14 days and occurred between late March and late May when average daily rainfall was 0.9, 1.0 and 1.1mm/day for the Upton, Evesham and Denchworth sites, respectively and antecedent rainfall for the two days before the second site visit was zero.

In general, the strength increase is greatest at the Upton site under both grass and wheat at depths of 50 and 150mm. The Denchworth series appears to increase in strength at a greater rate than the Evesham, except at 50mm depth under grass.

THE MIDLAND AND SOUTHERN SITES

To rank the six sites in terms of the rate of increase in RP during periods of low rainfall, the data for the Upton series were compared with those of the Wick series. These two soils were chosen because the average daily rainfall on both sites was fairly similar during the chosen period of monitoring. No rain fell at the Upton site during the two days prior to the second site visit, whereas nearly 4mm fell at the Wick site. Despite this, in general, the rate of increase in RP was greater at the Wick site.

Although average daily rainfall at the Cuckney site was a little less than that at the Upton site, nearly 5mm of rain fell during the two days prior to the second Cuckney site visit. However, the rate of strength increase appears to be greater at the Cuckney site. This would suggest that the ranking of the six soil series, in terms of the rate of strength increase, is as shown in Table 2.8.

Table 2.8 The ranking of the six soil series under investigation in terms of rate of increase in soil strength during periods of low rainfall.

Soil series	Rank	Average daily increase in soil strength at 50mm depth (MPa/day)	Average daily increase in soil strength at 150mm depth (MPa/day)
Whimble	1	0.083	0.048
Wick	2	0.061	0.039
Cuckney	3	0.058	0.062
Upton	4	0.037	0.031
Denchworth	5	0.017	0.022
Evesham	6	0.020	0.016

The rate of increase in soil strength during dry periods will vary throughout the season, influenced, in the main, by crop evapotranspiration. At all six sites, the increase in strength was found to be fairly similar under both grass and wheat and so the figures for both crops have been averaged and are presented in Table 2.8. These figures have been included to give some idea of the magnitude of the daily increase in strength that might be expected during periods of low rainfall in the months of March to May.

Future work could be conducted to establish the rate of increase in soil strength, for representative soil series at a range of bulk densities, during periods of no rain in both the autumn and the

spring. These data, in conjunction with a local weather forecast, could be a valuable aid to farmers when deciding whether or not to carry out field operations in marginal conditions. An example of how this data might be used is given below.

The farmer at the Cuckney site wishes to drill his wheat. However, RP at 50 and 150mm depth is 0.20 and 0.30MPa respectively. From Table 2.2, RP values corresponding to critical soil water suction limits for workability are 0.44 and 0.57MPa at 50 and 150mm respectively.

From table 2.8, the rate of increase in soil strength in dry weather is 0.058 and 0.062MPa/day at 50 and 150mm respectively.

The number of dry days required for the field to become workable is calculated as follows:-

$$\text{@ 50mm depth, } 0.44 - 0.20 = 0.24 \text{ and } \frac{0.24}{0.058} = 4.1$$

$$\text{@ 150mm depth, } 0.57 - 0.30 = 0.27 \text{ and } \frac{0.27}{0.062} = 4.3$$

Therefore, just over four dry days would be required for the field to become workable.

This type of analysis, coupled with the weather forecast for the following week, could aid the farmer when deciding whether to carry out his field operations.

2.4 Conclusions

The results of this work suggest that a good correlation exists between resistance to cone penetration (RP) and soil water suction (h). Over the soil water suction range 0 to 900cm of water, this relationship is statistically significant, for six different soil series under both grass and wheat, if either a linear or a hyperbolic regression analysis is used. In general, however, higher values of R^2 were achieved using a hyperbolic relationship and this results in a better fit to the data in the suction range 0 to 900cm of water.

As soil water suction increases, soil strength appears to approach a constant value. This value is not only dependent on soil type and density, but also on crop characteristics. At soil water suctions less than 100cm of water, resistance to cone penetration at 50mm depth under wheat was generally found to be lower than that at 150mm depth. Conversely, RP at 50mm depth under grass was generally higher than that at 150mm and those at both 50 and 150mm depth in cereals despite bulk densities at some sites being higher under wheat than under grass.

This study has shown that it is possible to define critical soil water suction limits for predicting trafficability and workability of a wide range of soil types. However, because they are density dependent, these suction limits are likely to vary from season to season.

Further work is required in the following areas:-

- (1) Investigations into the influence of differences in bulk density on the relationship between resistance to cone penetration and soil water suction for a given soil series.
- (2) To establish figures for the rate of increase in soil strength, for representative soil series at a range of bulk densities and soil water suctions, during periods of zero rain.

CHAPTER 3

SOIL MOISTURE DEFICIT AND SOIL STRENGTH

Introduction

The use of soil water suction as a parameter for the prediction of soil strength has been discussed in Chapter 2. Soil strength, and its prediction, is studied further in this Chapter where the use of soil moisture deficit as a predictive parameter for strength is investigated.

The critical minimum soil water suction limits for both trafficability and workability have already been discussed and are presented in Table 2.2. They range from suctions of 5 to 40cm of water for trafficability and from 10 to 140cm for workability, the precise value depending upon soil type and cropping regime.

Soils are generally at a suction of less than 50cm of water for most of the winter period and are prone to waterlogging after heavy rainfall. For well drained soils, such as the Cuckney series, this waterlogging is temporary and the soils drain to a fairly stable suction of 30 - 60cm in a matter of hours. In slowly permeable soils, however, for example the Denchworth series, there is sustained waterlogging and topsoils remain at low suctions (<30cm of water) for much of the winter period. Only well-drained sandy soils will be at a suction higher than their critical trafficable and workable limits for a significant part of the winter period. Other soils will seldom be at this state and will not attain it until surplus water can be removed from the soil profile by evapotranspiration and drainage and a soil moisture deficit begins to build up.

To ascertain the strength of the relationship between soil moisture deficit and soil strength, a study was carried out to investigate the gain in soil strength relative to loss in soil moisture. The aim of the study was to establish whether soil moisture deficit (SMD) might be as suitable as, or a better parameter than, soil water suction (h) for predicting trafficability and workability since its value would be easier to determine.

3.1 Quantitative relationship between soil moisture deficit and cone penetration resistance.

On each of the twelve experimental plots, three access tubes were monitored with the Neutron Probe moisture meter, on a fortnightly basis, throughout the growing season. This information was averaged and converted to SMD, firstly for a 1.50m deep soil profile and then for 0.50m and 0.20m profiles. The calibration procedure for the neutron probe is given in Appendix 3.

Soil resistance to cone penetration (RP) was measured at 50 and 150mm depth with a Bush Recording Soil Penetrometer, (Anderson et al. 1980), fitted with a stainless steel cone of 20.27mm diameter and 30° included angle. Measurements of RP were made simultaneously with those of SMD.

Figure 3.1 shows the variation in resistance to cone penetration (RP) at 50 and 150mm depth, and SMD for a 1500mm deep soil profile (SMD1500), for the Cuckney series grass plot over the 1987 - 1988 growing season.

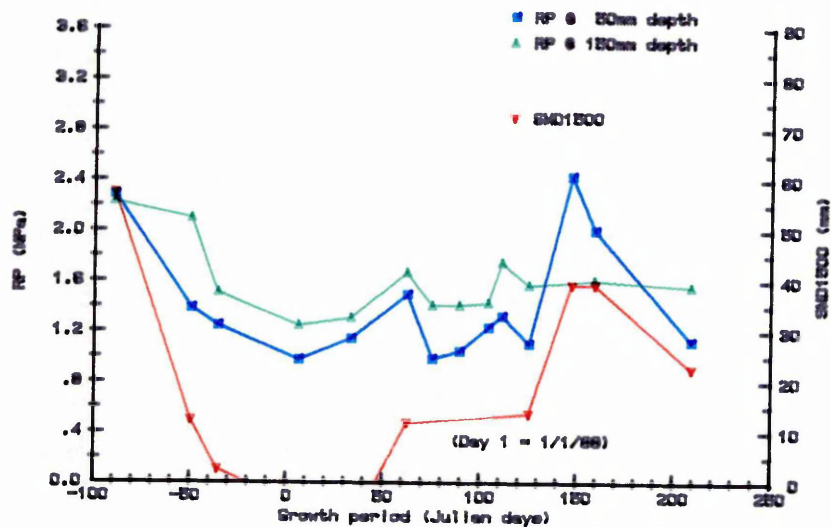


Figure 3.1 The variation in both resistance to cone penetration (RP) at 50 and 150mm depth, and soil moisture deficit for a 1500mm deep profile (SMD1500), over the 1987 - 1988 growing season for a loamy sand soil under grass - Cuckney series.

The shape of the SMD1500 graph follows that of RP at 50mm depth quite closely. The graphs show the reduction in soil moisture deficit and hence soil strength over the autumn period of 1st September to 31st December (day number -100 -> 0) down to minimum values during the winter months when the soil is around field capacity. The field capacity period persists through to March for this site, after which RP begins to rise as the soil dries out. The correlation between RP and SMD1500 is less obvious at 150mm depth.

The graphs suggest that a strong relationship may exist between RP at 50mm depth, and to a lesser extent RP at 150mm depth, and SMD for sandy soils.

Similar graphs were constructed for a heavy clay soil, the Evesham series, and are shown in Figure 3.2. A similar pattern to that observed for the sandy Cuckney series emerged. Again fluctuations in RP over the season being greater near the soil surface with a strong relationship between soil strength (RP) and SMD.

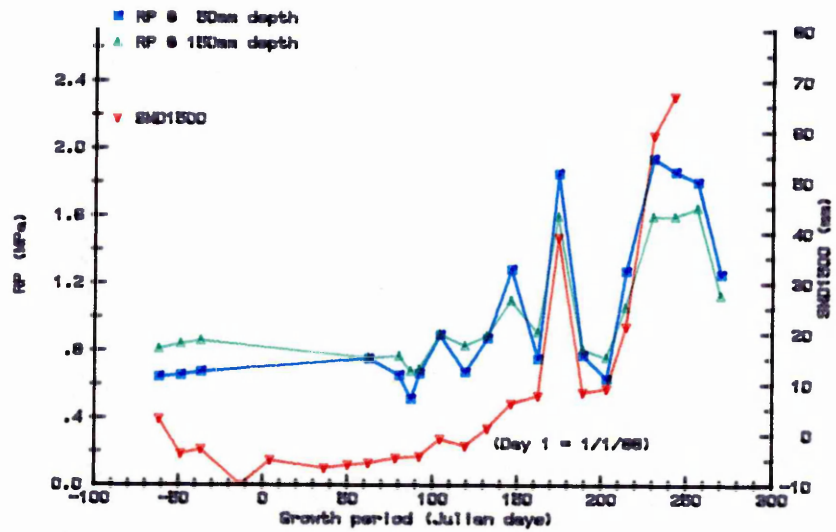


Figure 3.2 The variation in both resistance to cone penetration (RP) at 50 and 150mm depth, and soil moisture deficit for a 1500mm deep profile (SMD1500) over the 1987 - 1988 growing season for a clay soil under grass - Evesham series.

The relationship between RP and SMD, for six soil series, will now be considered.

3.1.1 THE CUCKNEY SOIL SERIES

Figure 3.3 shows the relationship between RP at 50mm depth and SMD1500 for the grass and wheat plots on the Cuckney series.

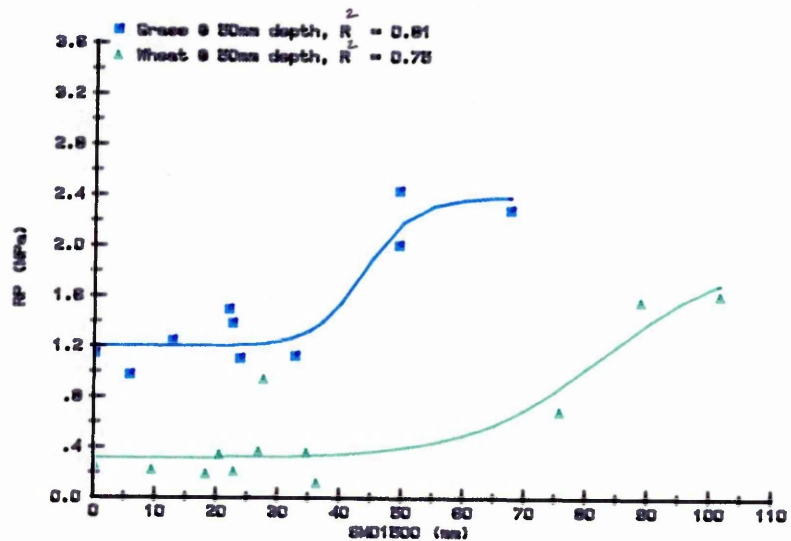
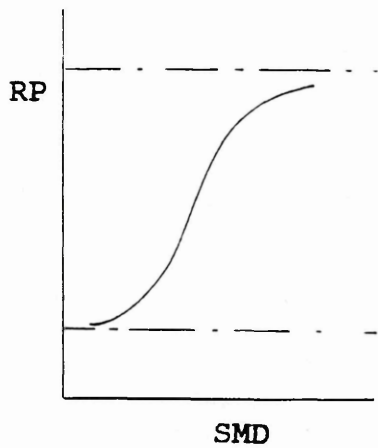


Figure 3.3 The relationship between resistance to cone penetration (RP) at 50mm depth and soil moisture deficit in the top 1500mm of the soil profile (SMD1500) for a loamy sand soil - Cuckney series topsoil under grass (bulk density 1.45Mg/m^3) and wheat (1.44Mg/cm^3).

The data were analysed using a logistic regression analysis as this produced curves which appear to give the most suitable fit. Details from the regression analysis are presented in Appendix 4.

The logistic curve is of the form:-



$$RP = A + \frac{C}{[1 + e^{-B(SMD-M)}]}$$

where RP = resistance to cone penetration.

A)
C)
B) = constants
M)

SMD = soil moisture deficit

The graphs suggest that a fairly strong relationship exists between RP and SMD1500.

The RP - SMD graphs were redrawn using SMD calculated for the top 500mm (SMD500) and the top 200mm (SMD200) of the soil profile to compare the relationships. In general, a better correlation was obtained using SMD200.

Figure 3.4 shows the relationships between RP, at 50 and 150mm depth, and SMD200 for the Cuckney soil series under both grass and wheat.

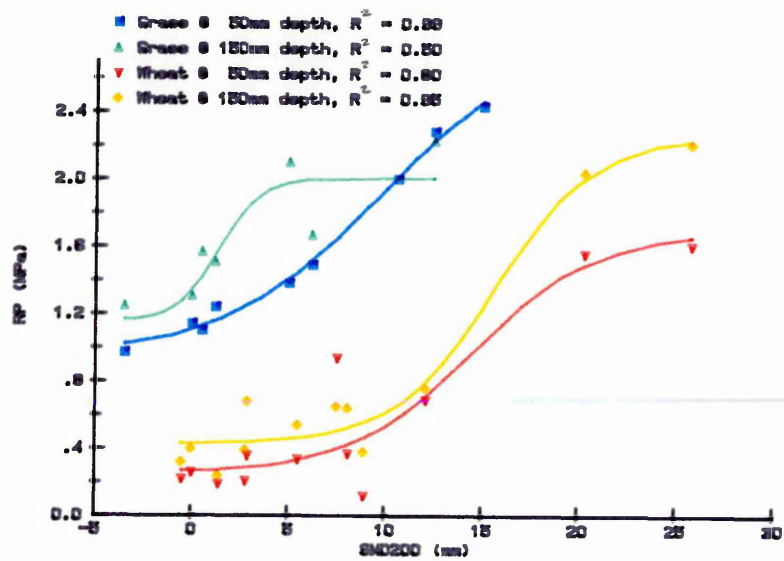


Figure 3.4 The relationship between resistance to cone penetration (RP) at 50 & 150mm depth and soil moisture deficit in the top 200mm of soil (SMD200) for a loamy sand soil - Cuckney series topsoil under grass (bulk density 1.45Mg/m^3) and wheat (1.44Mg/m^3).

The shape of the regression lines suggest that when the soil profile is near field capacity, the increase in strength with increasing SMD200 is relatively modest. The increase in strength, however,

accelerates as the soil dries until a point is reached where further increases in SMD200 have a reduced affect on soil strength.

As the season progressed, soil strength, particularly under grass, exceeded the working range of the penetrometer. The data appears to tend towards an asymptote - suggesting that once the soil dries to a certain deficit, further drying will result in little subsequent increase in soil strength.

Logistic regression analysis gives values, for the asymptotes, of 2.86 and 2.01MPa under grass at 50 and 150mm depth, and 1.69 and 2.27MPa under wheat at 50 and 150mm respectively. If more data had been available under grass at 150mm depth, the shape of the curve may have followed that at 50mm depth more closely and the resulting asymptote could have been nearer 3.0MPa. Further studies, using a penetrometer with a smaller cone, could provide useful information at the drier end of these relationships.

Under permanent grass, the contribution of the binding effect of the grass roots to soil strength can be clearly seen, the grass plot having higher RP than the arable plot at similar SMD200 values. RP under grass was higher than that under wheat throughout the entire growing season despite both being at similar bulk densities.

The coefficient of determination (R^2) value for the grass plot at 150mm depth is somewhat lower than that at 50mm and those of the arable plot due to a lack of data points. It was not possible to obtain more data points because soil strength at this depth soon exceeded the working range of the penetrometer as the soil profile dried.

3.1.2 THE WICK SOIL SERIES

Graphs of RP at 50 and 150mm depth were plotted against SMD1500 and a reasonably strong relationship was found. However, a better relationship was obtained between RP and SMD200 (see Figure 3.5) despite the data points covering only part of the logistic curve.

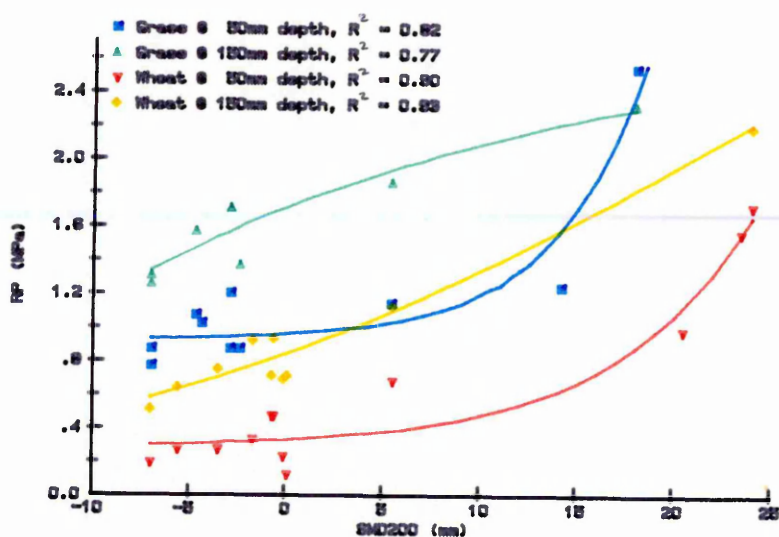


Figure 3.5 The relationship between resistance to cone penetration (RP) at 50 and 150mm depth and soil moisture deficit of the top 200mm of soil (SMD200) for a sandy loam soil - Wick series topsoil under grass (bulk density 1.50Mg/m^3) and wheat (1.34Mg/m^3).

Soil strength under grass was generally greater than that under wheat during the growing season - partly attributable to the wheat

plot starting at a lower bulk density following autumn cultivations, but also to the greater root mass effect under the permanent grass ley. Soil strength was greater at 150mm depth than at 50mm on both plots throughout the year.

The shape of the RP - SMD200 curve under grass at 150mm differs from that at 50mm and those under wheat. Strength was relatively high at low SMD200 (1.71MPa @ SMD = 0) and therefore as it increased in the spring, it was soon above the working range of the penetrometer. Eleven data points were recorded but the majority were taken over a very limited range of RP values which has affected the shape of the regression curve.

3.1.3 THE UPTON SOIL SERIES

Figure 3.6 shows the relationship between RP at 50 and 150mm depth and SMD200 for the grass and wheat plots on the Upton series.

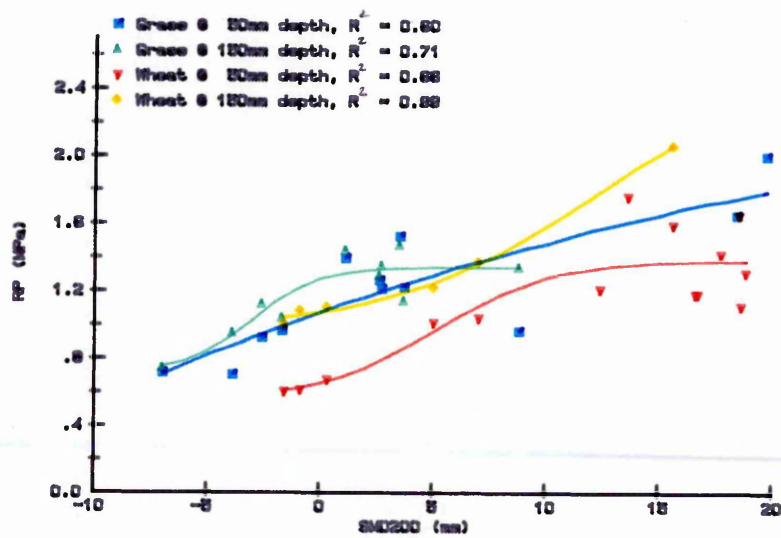


Figure 3.6 The relationship between resistance to cone penetration (RP) at 50 and 150mm depth and soil moisture deficit of the top 200mm of soil (SMD200) for a clay loam soil - Upton series topsoil under grass (bulk density 1.06Mg/m^3) and wheat (0.89Mg/m^3).

In general the relationship between RP and SMD200 is not as strong for this soil as it is for the Cuckney and Wick soil series. However, R^2 values under both grass and wheat at 50 and 150mm depth were between 0.60 and 0.99.

Soil strength at 50mm depth under both crops, when SMD200 = 0, was far higher than that at any of the other experimental sites, but subsequent strength increase with increasing soil moisture deficit was relatively modest.

3.1.4 THE WHIMPLE SOIL SERIES

Figure 3.7 shows the relationship between RP at 50 and 150mm depth and SMD200 for the grass and wheat plots on the Whimble series.

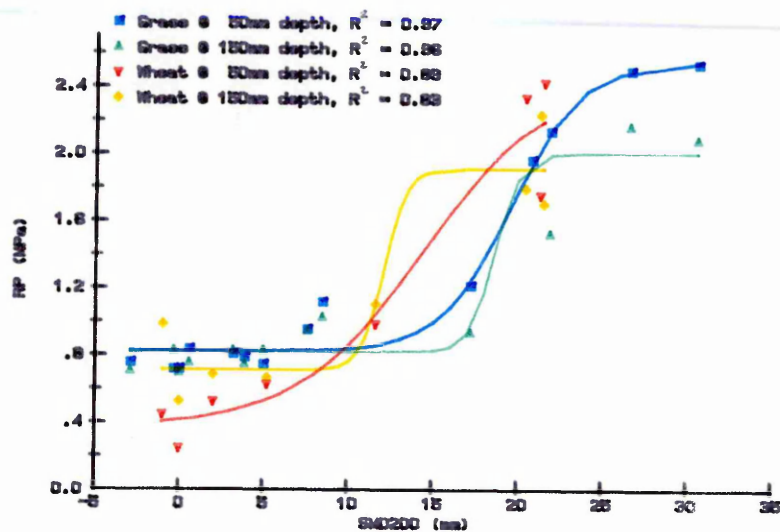


Figure 3.7 The relationship between resistance to cone penetration (RP) and soil moisture deficit of the top 200mm of soil (SMD200) for a clay loam soil - Whimble series topsoil under grass (bulk density 1.54Mg/m^3) and wheat (1.47Mg/m^3).

The relationship between RP and SMD200 is very strong for this soil series with R^2 values of 0.83 to 0.97.

As SMD200 increases from zero to around 10mm, soil strength remains fairly constant. However a further increase in SMD200 results in a very abrupt increase in strength with maximum values attained at around SMD200 = 15 to 20mm.

This could have implications for a farmer working with this soil series. If the soil is not workable when he wishes to carry out field operations, then by delaying his work, by a rain-free day or so, soil strength may increase sufficiently to allow him on the land. For other soil series, such as the Wick series, one or two rain-free days may result in very little change in soil strength.

3.1.5 THE EVESHAM SOIL SERIES

Figure 3.8 shows the relationship between RP at 50 and 150mm depth and SMD200 for the grass and wheat plots on the Evesham soil series.

The relationship between RP and SMD200, for this soil series, appears to be strong. The path of the regression curves under grass are very different to those under wheat. As the soil dries, the data completes its 'S' shape over a fairly narrow range of SMD200 (-5 to 30mm).

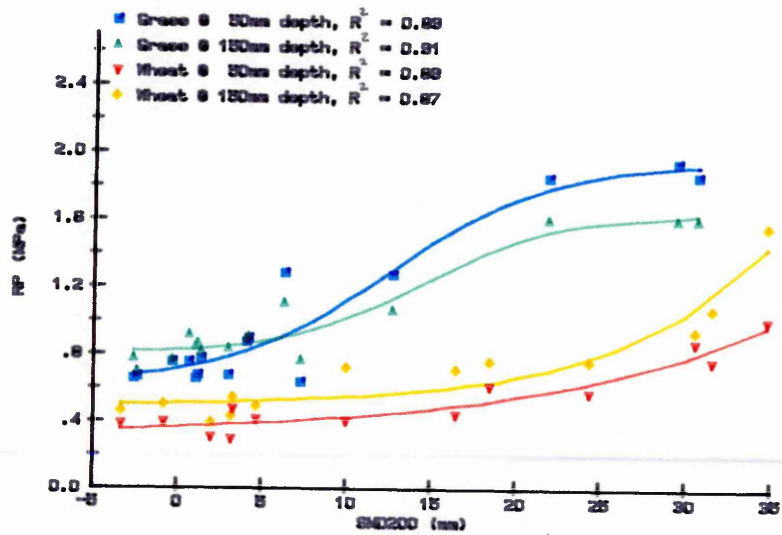


Figure 3.8 The relationship between resistance to cone penetration (RP) at 50 and 150mm depth and soil moisture deficit in the top 200mm of soil (SMD200) for a clay soil - Evesham series topsoil under grass (bulk density 0.88Mg/m^3) and wheat (0.98Mg/m^3).

Under wheat, soil strength at low soil moisture deficits is very much less than that under grass and the subsequent increase in strength, with increasing SMD200, is relatively gradual until deficits of around 25 to 30mm are reached. No further data are available at deficits greater than these and so the lower half only of the 'S' shape can be seen.

3.1.6 THE DENCHWORTH SOIL SERIES

Figure 3.9 shows the relationship between RP at 50 and 150mm depth and SMD200 for the grass and wheat plots on the Denchworth soil series.

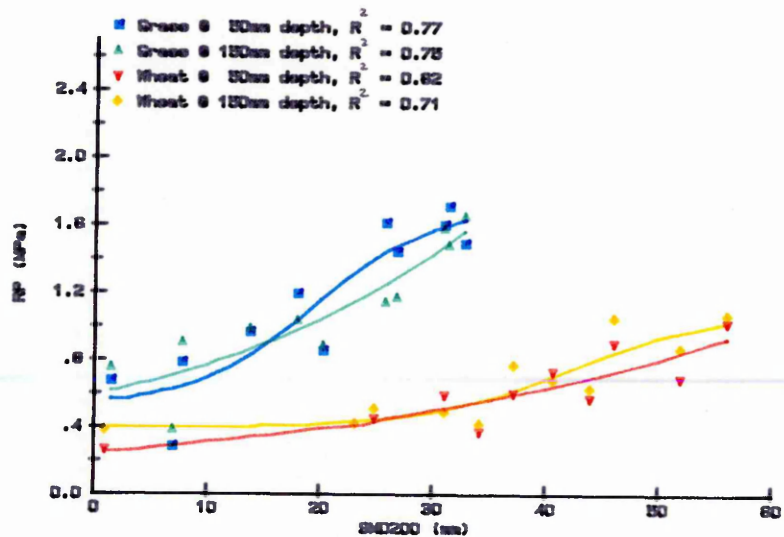


Figure 3.9 The relationship between resistance to cone penetration (RP) at 50 and 150mm depth and soil moisture deficit in the top 200mm of soil (SMD200) for a clay soil - Denchworth series topsoil under grass (bulk density 1.02Mg/m^3) and wheat (0.91Mg/m^3).

The RP - SMD200 characteristics for the Denchworth series are very similar to those of the Evesham series, with a very much more gradual increase in soil strength, with increasing SMD200, under wheat than under grass. Soil strength under grass was greater than that under wheat throughout the year - partly due to the root mass

effect, but also to reduced bulk density under the arable crop as a result of loosening during autumn cultivations.

On this weaker soil, data collection was possible at deficits in excess of 50mm under wheat and so the 'S' shape of the curve can be observed.

3.2 Discussion

The studies described in section 3.1 suggest that a reasonably strong relationship exists between resistance to cone penetration (RP) and soil moisture deficit (SMD), especially for heavy soils, where the penalties for working the land under poor conditions can be severe. In general, SMD for the top 200mm of the soil profile (SMD200) is better correlated with RP than either SMD for a 500 or 1500mm deep profile.

The logistic regression analyses results for the six soil series, under both grass and wheat, are given in Appendix 4. In most cases, the relationships between resistance to cone penetration (RP) and soil moisture deficit in the top 200mm of the profile (SMD200) are highly significant ($F < 0.01$) and in just under half - very highly significant ($F < 0.001$). The strength of these relationships could allow SMD to be used as a parameter for the prediction of trafficability and workability. However, it must be recognised that the RP - SMD relationships developed during this study are specific to given soil series under climatic conditions prevalent during the study period, at specific bulk densities. If bulk density were to

change significantly the following year, for example, through minimum cultivation, then the RP - SMD relationship may alter.

Further work is necessary to establish what effect differences in bulk density have on these relationships. It may be that each soil series under a given crop could be represented by a family of curves. Notwithstanding this, the RP - SMD relationships developed during this study will be used to develop trafficability and workability prediction models - but it is accepted that some data may need to be enhanced/updated at a later date in order to make the models generally applicable.

3.2.1 PREDICTION OF TRAFFICABILITY AND WORKABILITY AT A GIVEN SOIL SITE.

Critical SMD200 limits have been derived for both trafficability and workability for the twelve experimental plots under investigation and are presented in Table 3.1. They were defined using a similar methodology to that used for the derivation of critical soil water suction limits in Chapter 2.

Table 3.1. Critical SMD200 limits (mm) for trafficability and workability.

Soil series	Crop	Trafficable limit	Workable limit
Cuckney	grass	2	5
	wheat	5	8
Wick	grass	3	5
	wheat	3	8
Upton	grass	5	10
	wheat	5	13
Whimble	grass	5	8
	wheat	5	13
Evesham	grass	5	13
	wheat	8	13
Denchworth	grass	8	13
	wheat	10	20

These critical limits can be used, as illustrated in the following example, to estimate the number of machinery work days in a given season.

Figure 3.10 shows the variation in SMD200 for the Wick soil series, under winter wheat, during the 1987 - 1988 growing season.

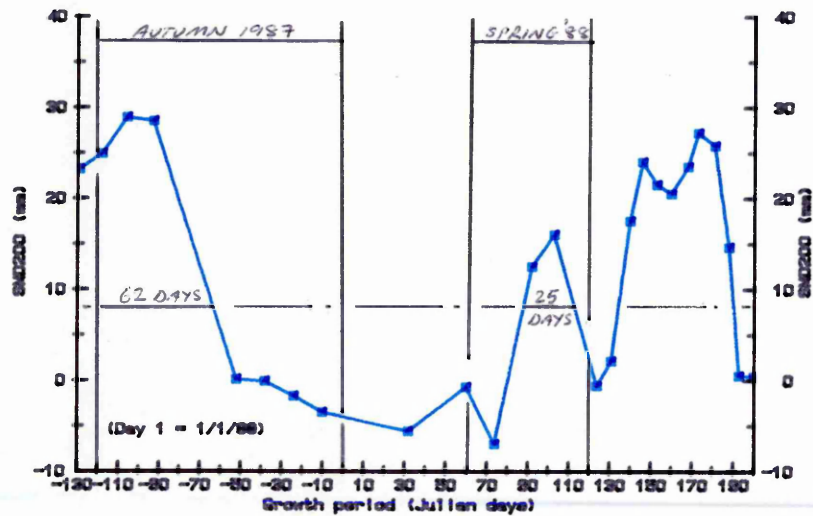


Figure 3.10 The variation in the soil moisture deficit in the top 200mm of soil (SMD200), under winter wheat, during the 1987 - 1988 growing season for a sandy loam soil - Wick series.

From Table 3.1, the critical SMD200 limit for workability for the Wick winter wheat plot is 8mm. If a line is drawn horizontally across figure 3.10 from SMD200 = 8mm, then it is possible to count the number of days where SMD200 is equal to, or greater than, 8mm during the autumn and spring periods. This figure can then be corrected to take account of the number of days during that period where >5mm and >10mm of rain had fallen during the preceding 24 and 48 hours respectively (see Table 2.3A, Appendix 2).

Autumn machinery work days:-

If the autumn cultivation period extends from 1st September to 31st December, then from figure 3.10 and Appendix 2, the number of workable days in autumn 1987 was:-

$$62 - 16 = 46.$$

Spring machinery work days:-

If the spring cultivation period extends from 1st March to 30th April, then from figure 3.10, the number of workable days in spring 1988 was:-

$$25 - 1 = 24.$$

The following procedure is suggested for predicting trafficability and workability, at a given site, during the autumn and spring periods.

A water balance model, similar to that used for irrigation scheduling, is run for the given site. SMD is calculated from data obtained from the neutron probe moisture meter. SMD200 is extrapolated for a week in advance, based on the previous week's data, and plotted on a graph against time. Corrections to that value are then made as the week progresses. If an approximate figure for SMD200 is known in advance, then predictions of trafficability and workability can be made by comparing the predicted SMD200 with the critical values, Table 3.1. This data could be used, in conjunction with local weather forecasts, to aid decisions on the timing of machinery operations.

3.2.2 PREDICTION OF TRAFFICABILITY AND WORKABILITY FOR BUSINESS PLANNING.

Average meteorological soil moisture deficit (SMD) data is readily available, for all parts of England and Wales, from a large number of weather stations. This SMD data could be used in the planning of agricultural production systems for determining the number and size of machinery and equipment required to complete necessary land work in the time available.

An example of the use of meteorological SMD data, for predicting workability, is given below:-

Figure 3.11 is a graph of the variation in 'wet quartile' potential soil moisture deficit (PSMD) against growing days, based on fifteen years of meteorological data (1961 - 1975) from a weather station close to the Wick series site. Wet quartile, rather than average or dry quartile data, was chosen for this example because 1987 - 1988 was considered to be quite a wet year for the Wick site location.

Average meteorological SMD data is more representative of SMD in the entire root zone rather than just the top 200mm - which was used for soil strength prediction purposes in section 3.2.1. Depth of the root zone under wheat is assumed to be 1.5m for the majority of the growing season and therefore, critical soil moisture deficit limits for a 1.5m profile will be used. These have been defined for the twelve experimental plots and are presented in Table 3.2.

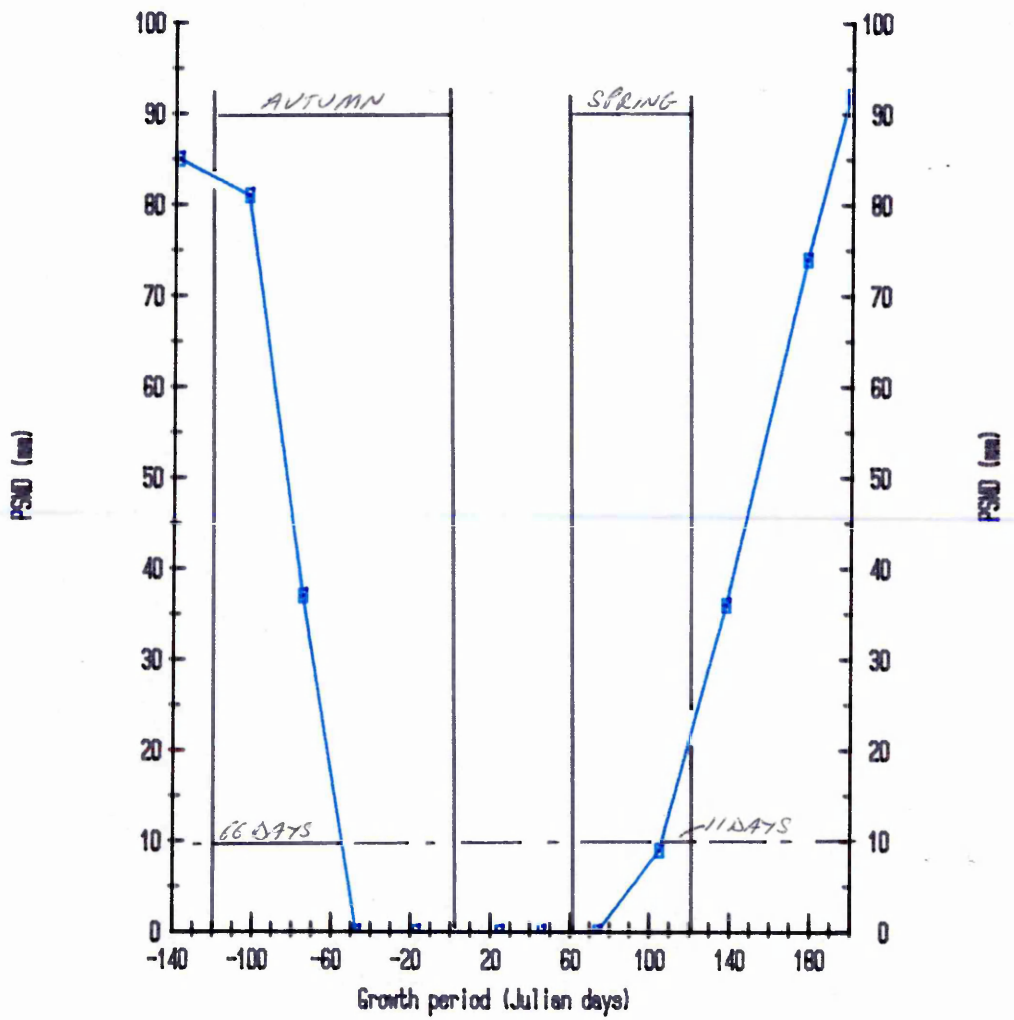


Figure 3.11

The variation in 'wet quartile' potential soil moisture deficit (PSMD) for 15 years of data (1961 - 1975) from a weather station close to the Wick site.

Table 3.2. Critical SMD1500 limits (mm) for trafficability and workability

Soil series	Crop	Trafficable limit	Workable limit
Cuckney	grass	5	10
	wheat	5	10
Wick	grass	15	25
	wheat	5	10
Upton	grass	15	25
	wheat	10	20
Whimble	grass	5	10
	wheat	5	15
Evesham	grass	5	15
	wheat	10	15
Denchworth	grass	10	15
	wheat	20	30

Assuming that potential SMD is similar to actual SMD for the first 50 to 60mm of deficit under wheat (Smith and Trafford, 1976), then the critical SMD1500 limit, from Table 3.2, can be superimposed onto figure 3.11 allowing a prediction to be made of the average number of workable and/or trafficable days during the autumn and spring periods.

This procedure has been carried out for the Wick site and the results are as follows:-

Autumn machinery work days:-

From 1st September to 31st December = 66

Spring machinery work days:-

From 1st March to 30th April = 11

Comparisons can be made between the results from this procedure and those from the more empirical Soil Survey procedure (Thomasson, 1982). For comparative purposes, the Soil Survey procedure has been applied to the Wick winter wheat plot - see Appendix 5. For the same site, the results from the Soil Survey's procedure were:-

70 Autumn machinery work days

10 Spring machinery work days

The estimates derived from the two procedures are in close agreement.

3.3 Conclusions

This work has shown that a reasonably strong relationship exists between resistance to cone penetration (RP) and soil moisture deficit (SMD). Better correlations, between RP and SMD, were achieved using SMD for the top 200mm of the profile (SMD200) than for the top 500 or 1500mm, however a strong relationship exists for all three.

R^2 values of 0.60 to 0.99 can be expected from the logistic regression analysis of RP - SMD200 data from a wide variety of soil types ranging from loamy sands to stoneless clays.

In most cases, the relationships are statistically highly or very highly significant.

The close relationship between soil moisture deficit and soil strength has been used to develop a model which can predict the number of days a given soil will be trafficable or workable during the year. The model requires average meteorological SMD data, preferably over 15 years, from a weather station where information is considered to be representative of that for the site under investigation, and also critical soil moisture deficit limits for the particular soil series.

Information derived from this model could be used in the planning of agricultural production systems in terms of the number and size of equipment required to complete necessary land work in the time available. For example, a farmer could use the model as an aid

when deciding whether to purchase one large tractor or two smaller ones.

Results obtained using the proposed model are in good agreement with those from the standard procedure used by the Soil Survey and Land Research Centre (SSLRC). The SSLRC procedure has been developed empirically over a number of years whereas the procedure proposed in this study is based on a mechanistic approach.

Soil moisture deficit (SMD) appears to be a useful parameter for soil strength prediction, however, there is one drawback associated with its use. The determination of SMD requires a knowledge of the volumetric moisture content, at field capacity, of the soil in question. This is particularly difficult to ascertain on swelling clay soils where, for example, volumetric moisture content after a wet autumn might be 50% but following a drier year may be only 30% due to less swelling.

This study has investigated the use of soil moisture deficit as a workability and trafficability prediction parameter, however, further research is required to establish what effect differences in dry bulk density have on the relationship between resistance to cone penetration and soil moisture deficit for a given soil series.

CHAPTER 4

THE DEVELOPMENT OF TRACTOR-MOUNTED TEST EQUIPMENT

Introduction

The techniques detailed in Chapters 2 and 3 have shown soil water suction and soil moisture deficit to be useful prediction parameters of soil strength for classification/ranking purposes. They cannot, however, be fine-tuned to predict the severity of damage likely to result from trafficking by different sized equipment. In particular, damage to the subsoil is expensive to ameliorate and so a more rigorous approach is required. This chapter is concerned with the development of tractor-mounted equipment for quantifying the compactive nature of a given soil. Analysis and discussion of data obtained using this equipment is given in Chapters 5 and 6.

Soil compaction is the process of air expulsion during loading with a resultant increase in the dry bulk density. Compactability is the ease with which a given soil compacts.

Koolen (1974) and Seig (1985) investigated ways of assessing soil compactability using a confined compression test.

The confined compression apparatus comprised a soil-filled rigid cylinder and piston. The piston gradually compressed the soil yielding information on the effect of increasing axial stress on a range of soil properties.

Koolen (1974) used the relationship between compaction pressure and void ratio as a measure of soil compactability.

The confined compression test could be a useful method of assessing compactability of field soils, especially if the equipment was enlarged, to accommodate more representative soil samples, and used for on-site assessment. If, however, the sample size were to be increased from Seig's 50mm diameter x 90mm length to say 150mm x 150mm, then considerable force would be required to carry out the test and hence the use of tractor-mounted equipment would be needed and was considered.

The proposed tractor-mounted confined compression equipment was developed so that it could be very easily adapted to carry out plate sinkage tests in addition to compression tests.

A plate sinkage test involves the loading of a plate placed either on the soil surface or on a soil plateau excavated at the depth of interest. Load and sinkage depth are monitored simultaneously. The load applied during a plate sinkage test must equal, or exceed, that expected during agricultural field operations. Typical static loads for various forms of trafficking are given in Table 4.1.

Table 4.1 Average stress exerted on soil by various operations.

Source of load	Stress (kPa)	Reference
LGP sprayer	41- 46	Smith (1985)
Human	50	Reeve & Earl (1989)
Bulldozer	50- 60	Manufactures brochure
Tractor	54- 95	Blackwell et al (1985) Paul & de Vries (1979)
2 axled trailer	93-104	Smith (1985)
1 axled trailer	99	Smith (1985)
Laden combine	105-150	Smith (1985)
Friesian cow	130	Scholefield & Hall (1986)
Large dumper	490	Bradshaw & chadwick (1980)
Earth scraper	685-785	Manufactures brochure

Source: Reeve and Earl (1989).

In a review of literature on compaction by agricultural vehicles, Soane et al (1982) concluded that an important attribute of the plate sinkage test is that a measure of soil deformation and strength properties of the soil can be established from the results. Caution should, however, be exercised in using the results to make field analogies with soil behaviour under running gear.

4.1 Preliminary design of the equipment

Preliminary designs of the equipment are shown in Figures 4.1, 4.2 and 4.3 below

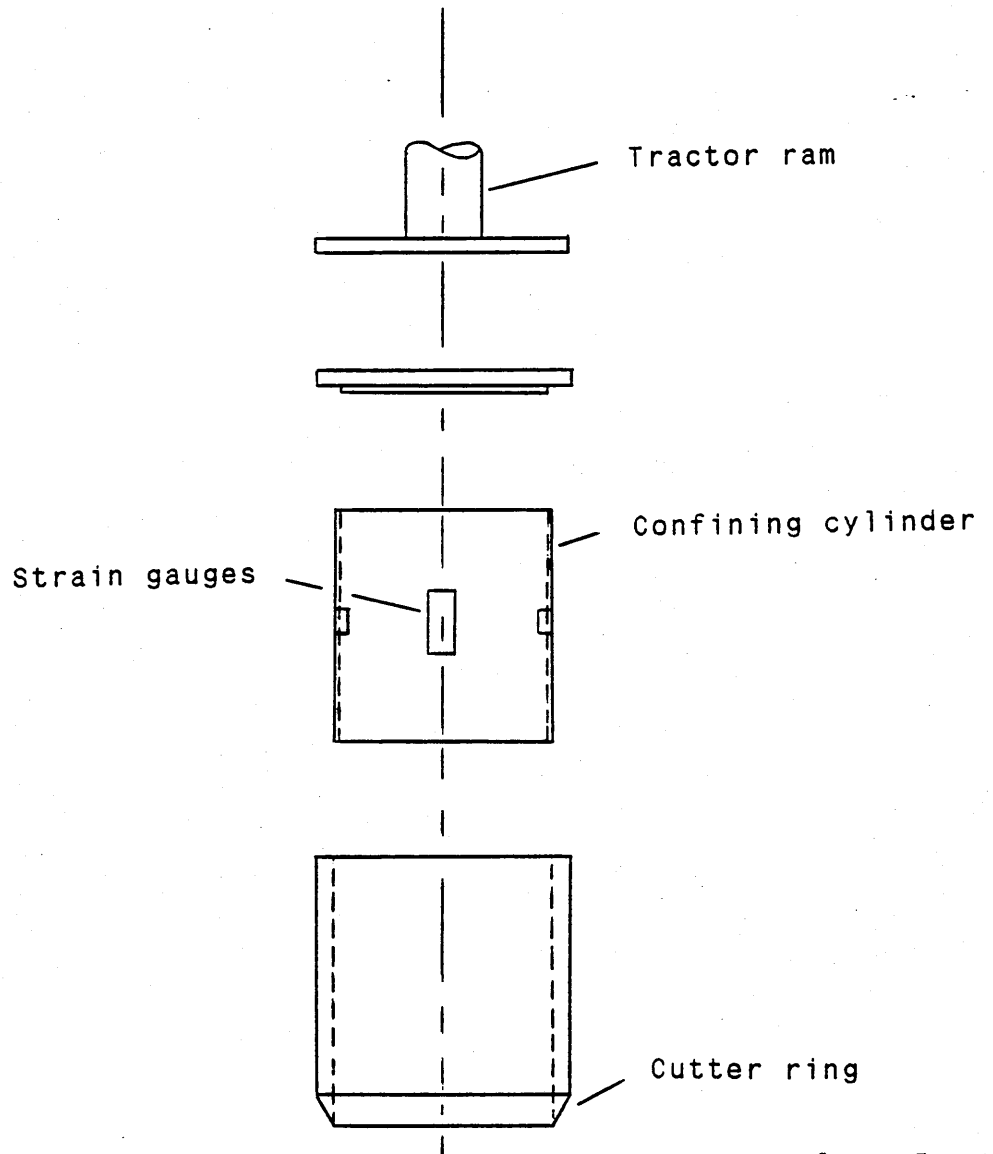


Figure 4.1 Equipment for taking soil samples.

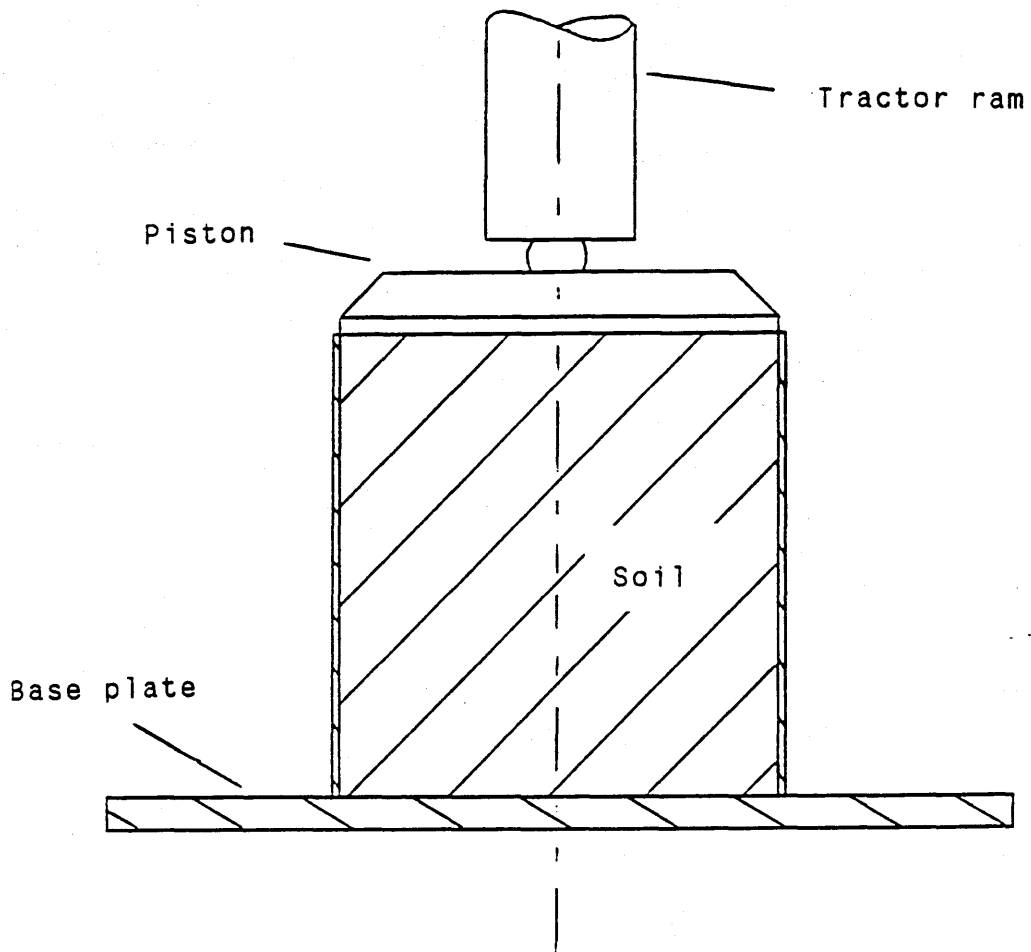


Figure 4.2 Equipment for carrying out confined compression tests.

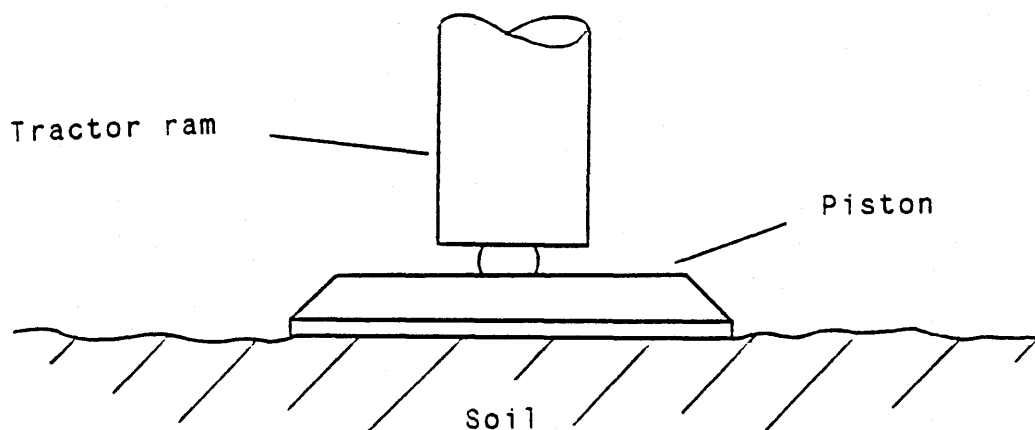


Figure 4.3 Equipment for carrying out plate sinkage tests.

The test equipment comprises a sampling cylinder, within which the confining cylinder is located. The confining cylinder is instrumented with strain gauges which monitor axial and radial stress during compression of soil within it. The same compression piston can be used for confined compression and plate sinkage tests.

The following field procedure was proposed:-

- 1) Sink the sampler assembly into the soil using a hydraulic ram mounted on a tractor.
- 2) Retrieve the assembly, extract the brass confining cylinder full of soil and trim the ends flush.
- 3) Place the confining cylinder on the steel base plate and zero the dial gauge.
- 4) Perform a confined compression test monitoring axial load, radial stress and deformation.
- 5) Extrude and bag up the soil sample for subsequent determination of initial and final moisture content and bulk density.

- 6) Perform a plate sinkage test and monitor axial load and sinkage depth.

4.1.1 DESIGN OF THE CONFINING CYLINDER

When designing the confining cylinder, certain attributes were considered important:-

- (1) Resistance to corrosion.
- (2) Sample size representative.
- (3) Minimal soil-wall friction and adhesion.

The equipment will be in contact with soil and water and so a brass cylinder was selected to reduce the risk of corrosion. A diameter of 150mm was considered desirable for a representative soil sample. This was a compromise because a smaller size might not include many peds, and a larger size would require considerable force to impart sufficient stress to the soil sample.

Selection of the cylinder height was a compromise between being large enough for the sample to be representative and generating unacceptable stress differences down the sample during compression due to adhesion and soil-metal friction.

Koolen and Kuipers (1983) suggest that the height to diameter ratio of the soil sample should be kept as low as possible during all stages of a confined compression test.

Koolen (1974) developed the following formula for calculating a suitable ratio:-

$$\frac{\sigma_b}{\sigma_t} = \frac{(D/h) - 2K \tan \delta}{(D/h) + 2K \tan \delta}$$

Where: σ_t = mean normal stress at the top of the soil sample

σ_b = mean normal stress at the bottom of the soil sample

D = inner diameter of the cylinder

h = actual height of the sample

δ = angle of soil-metal friction

K = σ_3/σ_1 in "ideal" confined compression test

σ_1 = major principal stress

σ_3 = minor principal stress

Koolen's formula was derived for apparatus with one piston. To reduce the resistance effect at the soil-metal interface, Koolen's apparatus was modified to accommodate two pistons - one at the top, the other replacing the base plate. This necessitated an amendment to the derivation of Koolen's equation follows:-

Let σ_m and $\sigma_p =$ mean normal stress at the cylinder centre and at the pistons, respectively

If the ratio $\sigma_m/\sigma_p \approx 1$, then the desired situation is nearly established.

The mean vertical stress σ_v in half the sample can be approximated as:-

$$\sigma_v = 1/2(\sigma_p + \sigma_m) \quad (1)$$

For an ideal compression test:-

$$\sigma_3 = K_0\sigma_1$$

where $K_0 =$ coefficient of earth pressure at rest

Koolen made the assumption that

$$\sigma_h = K_0\sigma_v \quad (2)$$

where σ_h is the mean horizontal stress

Combining (1) and (2):-

$$\sigma_h = 1/2K_0(\sigma_p + \sigma_m) \quad (3)$$

The mean shear stress acting on the cylinder wall can be expressed as:-

$$\Gamma' = \sigma_h \tan\delta$$

Combining this with (3) gives:-

$$\Gamma' = 1/2K_0(\sigma_p + \sigma_m)\tan\delta \quad (4)$$

Resolving forces vertically:-

$$\sigma_p A_1 = \sigma_m A_1 + \Gamma' A_2 \quad (5)$$

where $A_1 =$ cross sectional area of sample
 $= 1/4\pi D^2$

$A_2 =$ half cylinder wall area $= \pi Dh/2$

D = internal diameter of cylinder

h = sample height

substituting (4) in (5):-

$$\sigma_p 1/4\pi D^2 = \sigma_m 1/4\pi D^2 + 1/2K_o(\sigma_p + \sigma_m) \tan\delta \pi Dh/2$$

$$\sigma_p D = \sigma_m D + K_o h \sigma_p \tan\delta + K_o h \sigma_m \tan\delta$$

$$\sigma_p (D - K_o h \tan\delta) = \sigma_m (D + K_o h \tan\delta)$$

$$\frac{\sigma_m}{\sigma_p} = \frac{D/h - K_o \tan\delta}{D/h + K_o \tan\delta}$$

4.1.1.1 Determination of the angle of soil-metal friction.

Soil-metal friction, during confined compression tests, can affect the validity of results and so ways of reducing it were examined. Its influence on the design specification for the confining cylinder was such that it necessitated the determination of δ between brass and a range of soil types. The tangential resistance/unit area (Γ') can be expressed in terms of the following equation:-

$$\Gamma' = C_\alpha + \sigma \tan\delta$$

where Γ' = tangential resistance/unit area

C_α = adhesion

σ = normal stress

δ = angle of soil-metal friction

This relationship is shown graphically in Figure 4.4.

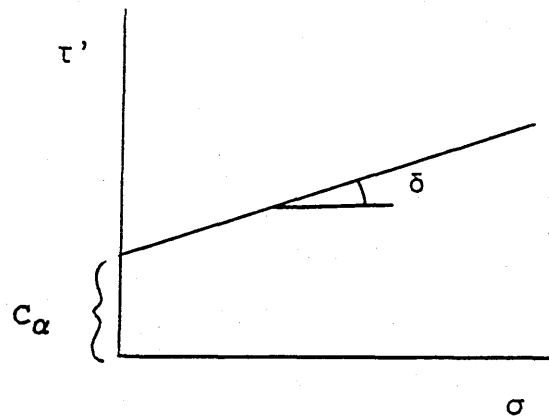


Figure 4.4 The relationship between tangential resistance per unit area, adhesion, normal stress and angle of soil-metal friction.

The value of δ is greatly influenced by the roughness of the metal surface, whereas c_α is influenced more by the moisture content of the soil.

Apparatus in the soil mechanics laboratory at Silsoe College was used to determine values for δ and c_α for a sandy and a clayey soil at various soil moisture contents. A schematic diagram of the apparatus is given in Figure 4.5.

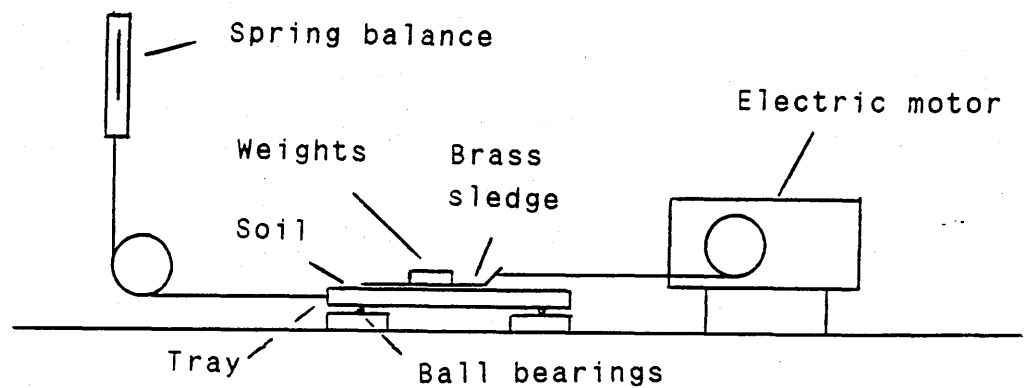


Figure 4.5 Apparatus for the determination of adhesion and the angle of soil-metal friction.

The following procedure was used:-

- (1) The tray was filled with an "undisturbed" slab of soil excavated from a profile pit in the field. Soil samples were taken to determine moisture content.
- (2) A brass sledge was placed on the soil surface and attached to the motor with a cord.

- (3) The sledge was winched across the soil surface using the electric motor and the spring balance reading recorded.
- (4) The procedure was repeated using a range of normal loads.
- (5) Graphs of average tangential sliding resistance/unit area against average normal stress were plotted.

Tests were repeated using grease as a lubricant to reduce the friction angle. The results obtained without grease implied negative values for adhesion at low normal loads necessitating a closer examination of the procedure and apparatus. Five sources of error were identified:-

- (1) Friction between the ball bearings and runners.
- (2) Friction in the pulley bearing.
- (3) The spring balance had a zero error.
- (4) Some weights, providing the normal load, did not weigh the value indicated on them.
- (5) The sliding bed was not level.

The apparatus was redesigned and is schematically represented in Figure 4.6.

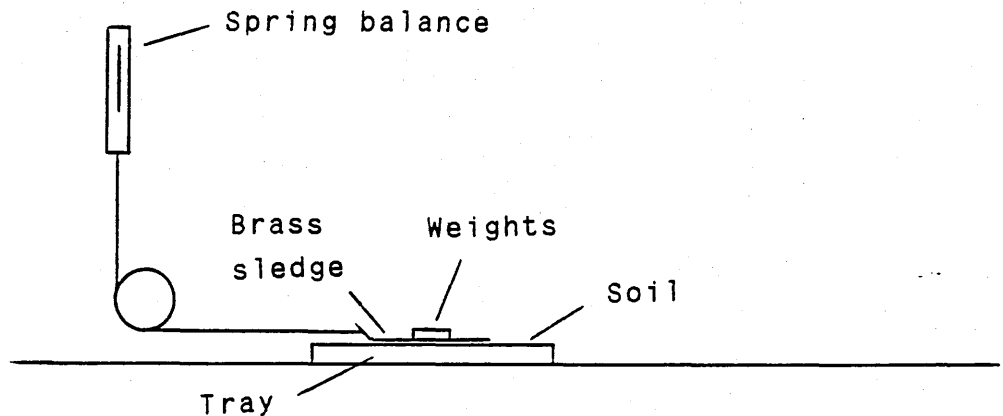


Figure 4.6 Modified apparatus for the determination of adhesion and the angle of soil-metal friction.

This configuration of the apparatus eliminated the effect of the ball bearing/runner friction. The pulley friction error was very much reduced by lubrication with a light machine oil. The bed was levelled and fixed to the bench and allowances were made for both the spring balance and weight errors.

Tests were carried out on topsoil from the Cottenham (sandy loam) and Evesham (stoneless clay) soil series. The tests were repeated using various different lubricants to assess their effect on the tangential resistance per unit area. The application of a grease lubricant to the brass sledge reduced δ but increased C_{α} . Viscous lubricants such as grease were considered in the first place because it was thought that they would be less susceptible to penetration by

soil particles/aggregates particularly in coarse textured soils. Further tests using P5 oil, which is very much less viscous than grease, were more promising, both δ and $C\alpha$ being reduced. Values for δ and $C\alpha$ were reduced further when Polyox resin was used to lubricate the sledge. This material is supplied in powder form and becomes a moderately viscous liquid when mixed with water. Figure 4.7 shows the average tangential sliding resistance/unit area plotted against average normal stress for both the Cottenham and Evesham soil series with and without Polyox resin.

The operating range of the apparatus was limited to normal stresses very much lower than those expected to be generated during a confined compression test. These results, therefore, allow a rather tentative conclusion that δ can be drastically reduced by lubrication with Polyox resin and that the value of δ may be independent of the soil texture. Values of 2 to 3⁰ for δ can be expected when Polyox is used.

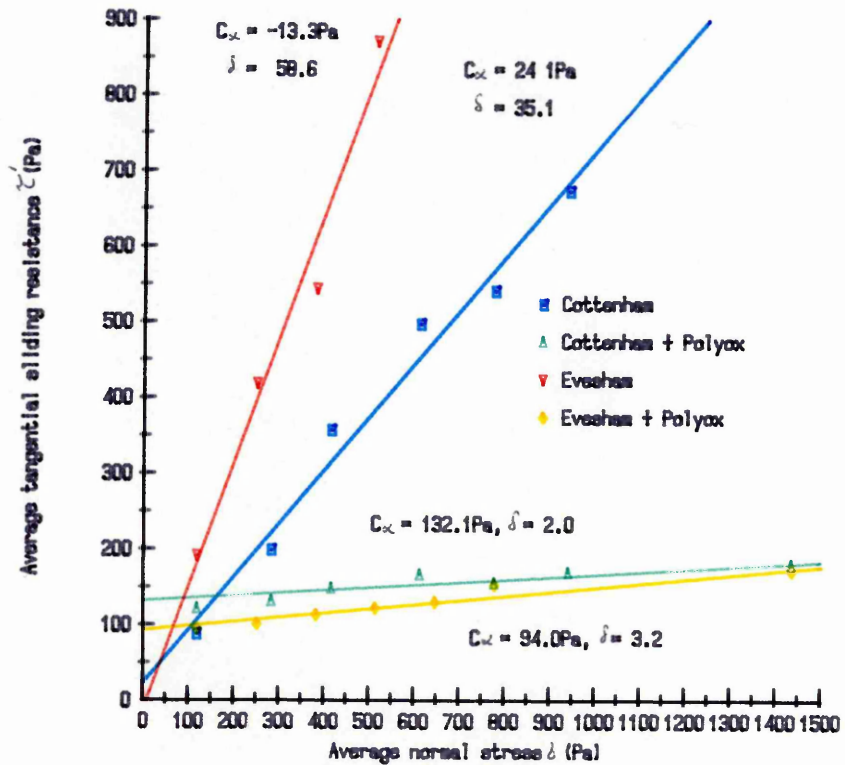


Figure 4.7 Average tangential sliding resistance per unit area (τ') against average normal stress (σ) for a brass sledge on both Cottenham and Evesham soil series with and without Polyox resin.

Results from all the tests are tabulated in Table 4.2.

Table 4.2 Results from soil-metal friction tests for brass on Cottenham and Evesham soil series.

Soil series	Lubricant	Gravimet. moisture content (%)	Angle of soil-metal friction	Adhesion (Pa)
Cottenham	-	12.7	34.9 ⁰	23.6
"	Grease	12.7	19.0 ⁰	148.5
"	P5 oil	12.7	9.7 ⁰	27.9
"	-	14.2	35.1 ⁰	24.1
"	Polyox	14.2	2.0 ⁰	31.4
Evesham	-	28.1	58.6 ⁰	-13.3
"	Polyox	28.1	3.2 ⁰	94.0

The results for the Cottenham soil series, without lubrication, concur with those of Godwin (1974). The Evesham results, without lubrication, show a small negative value for adhesion. Payne (1956) also experienced apparent negative adhesion when measuring soil-metal friction in the field. A possible explanation for this anomaly is that when the applied normal stress was small, the sledge was partially supported by pore water. As the normal stress increased, a critical point was exceeded permitting the excess normal stress to be carried by the soil itself and so the plotted line on the graph followed a different path as suggested in Figure 4.8.

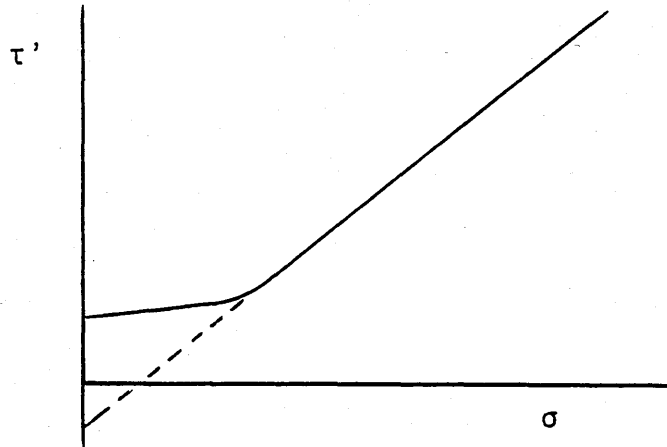


Figure 4.8 Suggested curve for average tangential sliding resistance per unit area (τ') against average normal stress (σ).

The soil-metal resistance test procedure used weights to provide easily definable normal loads. Caution must be exercised when making analogies between results obtained from a sledge test and those expected from pressing a cylinder into the soil. This is because the horizontal surface of soil in the sledge test may have different characteristics to those encountered by forcing a cylinder into the soil. The results, therefore, are taken merely as a guide for design purposes only.

- 4.1.1.2 The influence of the coefficient of earth pressure at rest (K_0) on the design criteria of the confining cylinder.

The coefficient of earth pressure at rest (K_0) appears in both the numerator and the denominator of Koolen's equation and therefore does not have much effect on the ratio σ_m/σ_p . Typical approximate values of K_0 are given in Table 4.3.

Table 4.3 Typical approximate values of K_0

Saturated sand	loose	0.50
	dense	0.35
Sandy clay		0.43
Normally consolidated clay		0.40-0.70
Lightly overconsolidated clay		0.80-1.20
Heavily overconsolidated clay		1.20-2.80
Remoulded clay		0.70
Boulder clay, compacted		0.56

Data from Koolen (1974)

From Table 4.3 values for K_0 range from 0.35 to 0.70 for normally consolidated soils and up to 3.00 for heavily overconsolidated soils.

Koolen's equation was used to calculate the ratio σ_m/σ_p using the following data:-

$$\delta = 3^\circ$$

$$K_o = 0.35 \text{ to } 3.00$$

$$D = 150\text{mm}$$

$$h = 150\text{mm}$$

These data gave values for σ_m/σ_p in the range 0.73 to 0.96 at the start of compression which were considered to be acceptable, particularly as the range of K_o values expected in the field (0.42 to 0.75) gave σ_m/σ_p ratios of 0.92 to 0.96.

4.1.1.3 The influence of adhesion (C_a) on the stress distribution in a soil sample during a confined compression test.

Koolen's equation for evaluating the ratio σ_m/σ_p takes no account of the effect of adhesion (C_a) at the soil-metal interface. To assess its influence, the equation was re-derived as follows:-

With reference to equation (3), section 4.1.1

$$\sigma_h = K_o/2(\sigma_p + \sigma_m) \quad (3)$$

The mean shear stress acting on the cylinder wall can be expressed as:-

$$\Gamma' = C_\alpha + \sigma_h \tan \delta$$

Combining this with (3):-

$$\Gamma' = C_\alpha + K_o/2(\sigma_p + \sigma_m) \tan \delta \quad (4)$$

Resolving forces vertically:-

$$\sigma_p A_1 = \sigma_m A_1 + \Gamma' A_2 \quad (5)$$

where A_1 = cross sectional area of sample

$$= 1/4\pi D^2$$

A_2 = half cylinder wall area = $\pi Dh/2$

D = internal diameter of cylinder

h = sample height

Substituting (4) in (5):-

$$\frac{\sigma_p D^2}{4} = \frac{\sigma_m D^2}{4} + \frac{C_\alpha Dh}{2} + \frac{K_o(\sigma_p + \sigma_m)Dhtan\delta}{2}$$

$$\sigma_p D = \sigma_m D + K_o \sigma_p h \tan \delta + K_o \sigma_m h \tan \delta + 2C_\alpha h$$

$$\frac{\sigma_m}{\sigma_p} = \frac{D/h - K_o \tan \delta}{D/h + K_o \tan \delta} - \frac{2C_\alpha}{\sigma_p (D/h + K_o \tan \delta)}$$

This modification to Koolen's equation, to take account of the influence of C_α , produces a very much more complicated solution requiring an iterative procedure.

Figure 4.9 shows the ratio σ_m/σ_p plotted against σ_p . The coordinates were calculated using the modified Koolen equation and the following data:-

$$D/h = 1$$

$$K_O = 0.5$$

$$\delta = 3^\circ, 6^\circ \text{ \& \ } 9^\circ$$

$$C\alpha = 150\text{Pa}$$

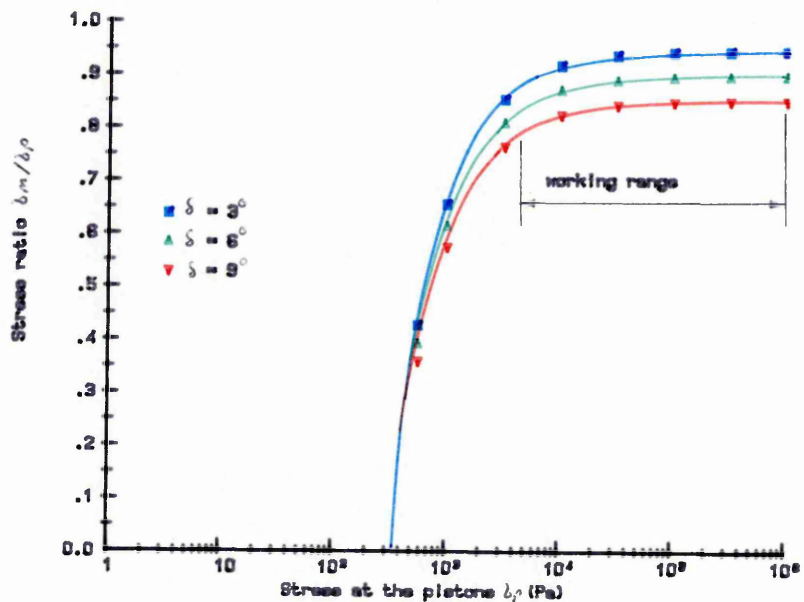


Figure 4.9 Graph of the ratio of stress at the sample centre to stress at the pistons (σ_m/σ_p) against stress at the pistons (σ_p) during a confined compression test.

From Figure 4.9, it can be seen that as σ_p increases, the ratio σ_m/σ_p increases, tending towards an asymptote equal to the value of the ratio when the effect of C_α is ignored. For σ_p less than 308.7Pa, the calculated ratio of σ_m/σ_p is below zero. This implies that the applied stress is not sufficient to overcome the limiting value of adhesion, in this case 150Pa, and, therefore, the soil is not stressed. In practice, piston stresses of below 2000Pa would not be significant during a confined compression test and therefore the minimum ratio of σ_m/σ_p that can be expected would be approximately 0.8 for the given situation. As compression commences, both the effect of C_α , and the sample height reduce, and hence σ_m/σ_p increases.

For a field soil, the following combination of parameters gives a "worst case" situation:-

$$\begin{aligned}K_o &= 0.75 \\ \sigma_p &= 2\text{kPa} \\ \delta &= 9^\circ \\ C_\alpha &= 150\text{Pa}\end{aligned}$$

From these data, σ_m/σ_p lies in the range 0.70 to 0.95 which is considered acceptable.

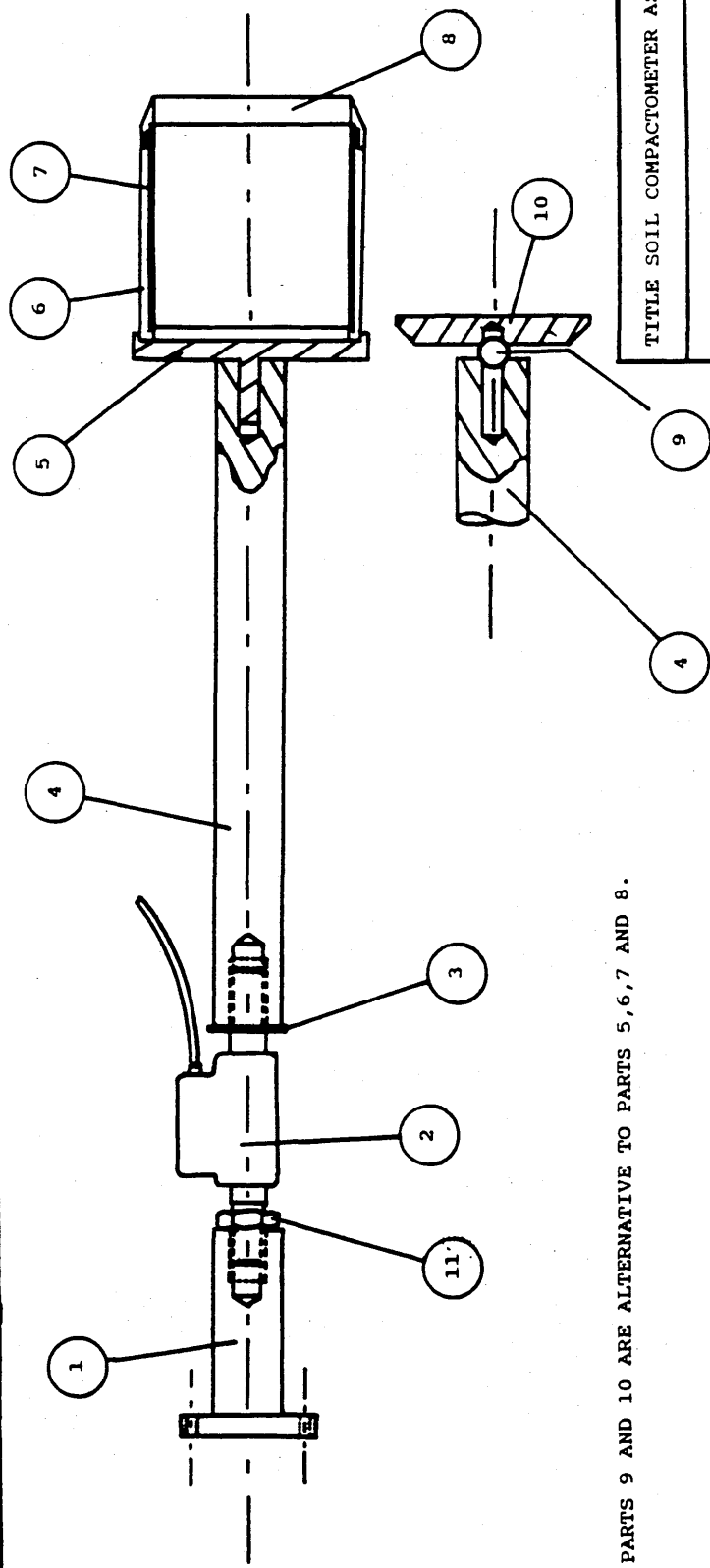
The final specification for the brass confining cylinder is given in section 4.1.2.1.

4.1.2 DESIGN OF THE SAMPLER ASSEMBLY AND CONFINED COMPRESSION EQUIPMENT.

Equipment was required which could be forced into soil to take a sample but causing as little disturbance to the sample as possible.

Figure 4.10 shows an engineering drawing of the sampling/compression equipment designed to bolt onto the rear end of a tractor. In addition, a lower piston and base plate were fabricated (see figure 4.11).

ITEM	DESCRIPTION	MATERIAL	No OFF	ITEM	DESCRIPTION	MATERIAL	No OFF
1	COUPLING	SEE DETAILED DRAWING	1	7	INNER CYLINDER	SEE DETAIL DRAWING	1
2	LOAD CELL	FOR REFERENCE	1	8	CUTTER RING	SEE DETAIL DRAWING	1
3	WASHER	STEEL (1" I/D)	2	9	STEEL BALL 18mm DIA	STEEL	1
4	DISC	SEE DETAIL DRAWING	1	10	PISTON	SEE DETAIL DRAWING	1
5	DISC	SEE DETAIL DRAWING	1	11	LOCKNUT	STEEL 1" BSF	1
6	OUTER CYLINDER	SEE DETAIL DRAWING	1				



PARTS 9 AND 10 ARE ALTERNATIVE TO PARTS 5, 6, 7 AND 8.

Figure 4.10

TITLE SOIL COMPACTOMETER ASSEMBLY	
MATL. SEE PARTS LIST	
SCALE 1:5	No. OFF 1
PART No. 12	

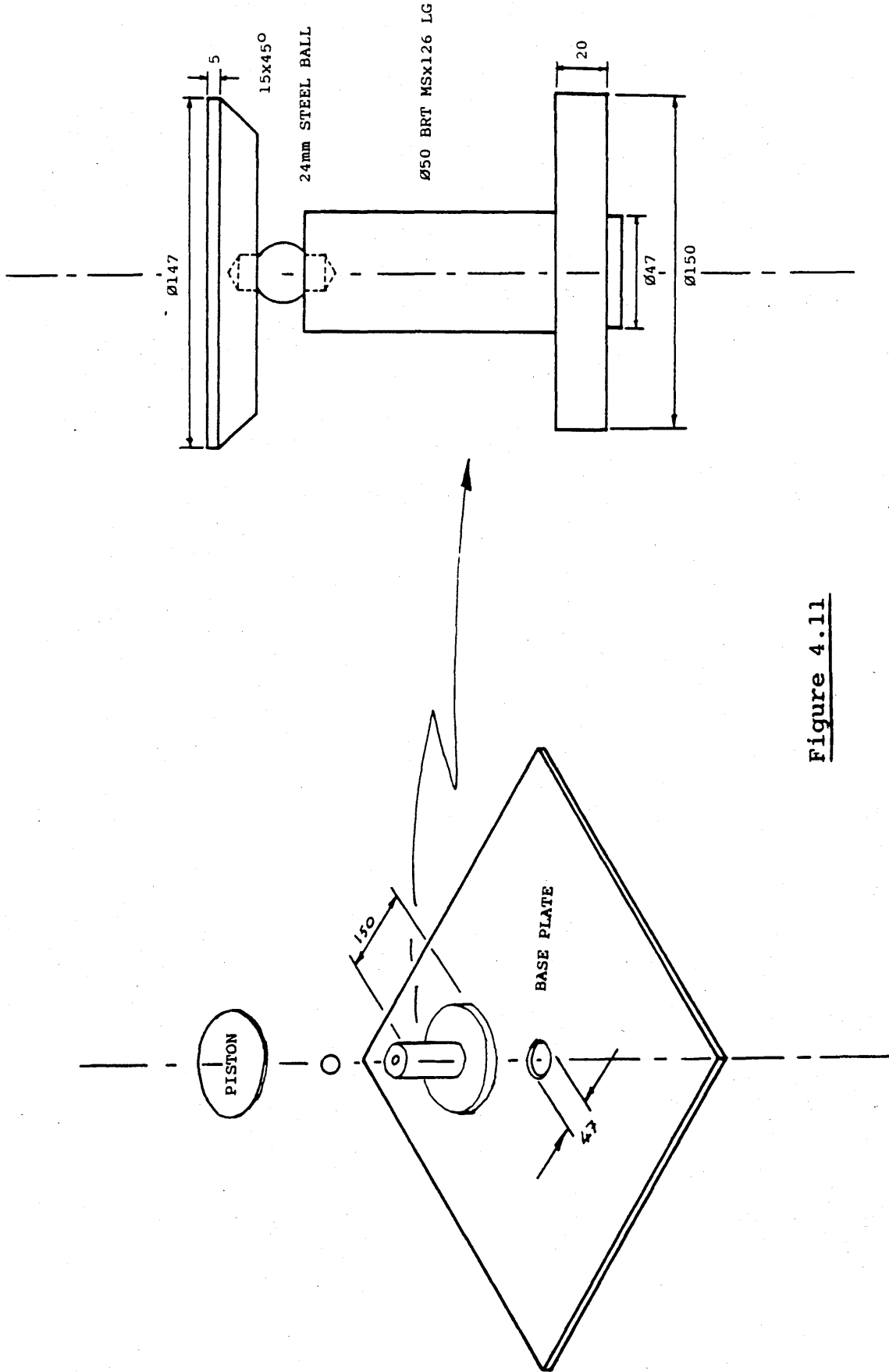


Figure 4.11

4.1.2.1 Confining cylinder specifications.

The brass confining cylinder was built to the following specifications:-

Material	-	Brass
Height (h)	-	150.0mm
Outside diameter	-	151.5mm
Inside diameter (D)	-	147.5mm
Initial D/h ratio	-	0.98

4.1.2.2 Selection of strain gauges for the confining cylinder.

Strain gauges were to be mounted on the external wall of the confining cylinder to monitor axial and radial stresses imparted by soil under compression within the cylinder

In order to select appropriate strain gauges for this application, it was necessary to calculate the maximum strain likely to be exerted by the confining cylinder on the gauges.

Maximum hoop and axial strains due to internal pressure can be calculated from the following:-

$$\begin{aligned}\text{Hoop stress, } \sigma_H &= PD/2t \\ \text{Hoop strain, } \varepsilon_H &= \sigma_H/E - \mu\sigma_A/E \\ \text{Axial stress, } \sigma_A &= PD/4t \\ \text{Axial strain, } \varepsilon_A &= \sigma_A/E - \mu\sigma_H/E\end{aligned}$$

Where:-

$$\begin{aligned}P &= \text{internal pressure} \\ d &= \text{diameter of cylinder} \\ t &= \text{wall thickness} \\ E &= \text{Young's modulus} \\ \mu &= \text{Poisson's ratio}\end{aligned}$$

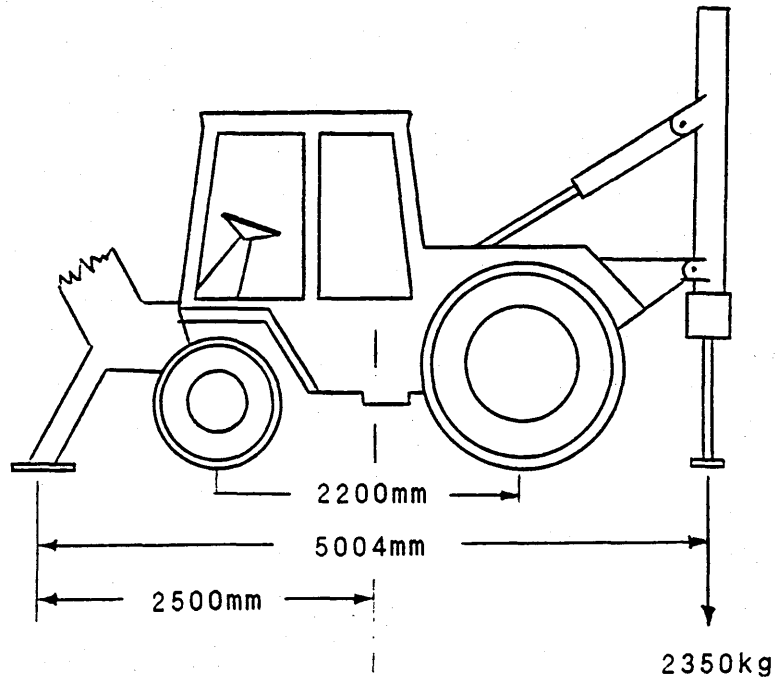
For the brass confining cylinder:-

$$\begin{aligned}\mu &= 0.33 \\ d &= 150\text{mm} \\ t &= 2\text{mm} \\ E &= 102\text{GPa}\end{aligned}$$

The maximum downward force available would be dependent upon the loading equipment used. A Deutz Intrac 2004 tractor was to be adapted to accommodate the developed equipment. A vertical ram

was fitted to the rear of the tractor which was taken to a local weighbridge to establish the maximum downward force available.

Figure 4.12 shows the results of the weighbridge test.



Maximum downward force of ram = 2350kg

For a piston diameter of 150mm:-

maximum piston stress $\sigma_p = 1.31\text{MPa}$

Figure 4.12 Side elevation of Deutz Intrac 2004 tractor.

A maximum downward force of 2350kg-f (23.05kN) was attainable, corresponding to a normal stress of 1.3MPa for a 150mm diameter piston/plate. From this test, it was assumed that the maximum

internal pressure could not exceed 1.3MPa. Limiting stresses and strains achievable are therefore as follows:-

$$\begin{aligned}\text{Max hoop stress} &= \frac{1.3 \times 10^6 \times 0.15}{2 \times 0.002} = 48.75 \text{MPa} \\ \text{Max axial stress} &= \frac{1.3 \times 10^6 \times 0.15}{4 \times 0.002} = 24.38 \text{MPa} \\ \text{Max hoop strain} &= \frac{48.75 \times 10^6}{102 \times 10^9} - \frac{0.33 \times 24.38 \times 10^6}{102 \times 10^9} \\ &= 0.04\% \\ \text{Max axial strain} &= \frac{24.38 \times 10^6}{102 \times 10^9} - \frac{0.33 \times 48.75 \times 10^6}{102 \times 10^9} \\ &= 0.008\%\end{aligned}$$

Strain gauges selected for use on the brass confining cylinder must be able, therefore, to accommodate strains of 0.04%. Specifications for the strain gauges chosen are given below:-

Gauge type	EA-06-240LZ-120
Resistance	120.0Ω ± 0.3%
Gauge factor @ 75°F	2.045 ± 0.5%
Temperature range	-100° to +350°F
Strain limits	5%

The maximum strains expected in the confining cylinder lie well within the operating range of the strain gauges.

4.1.3 Calibration of the confining cylinder

The confining cylinder comprises a brass cylinder with two pairs of strain gauges mounted on the outside - one pair axially mounted, the other circumferentially (see Figure 4.13).

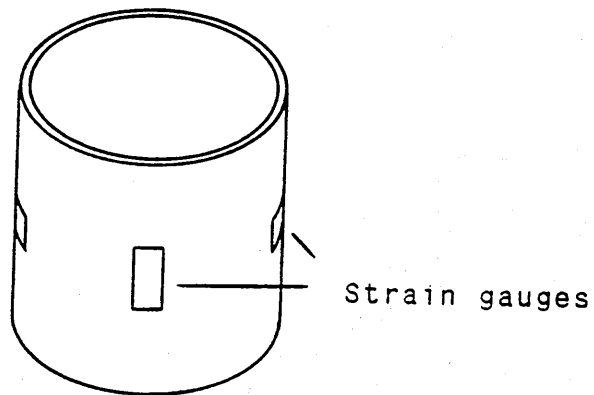


Figure 4.13 The brass confining cylinder.

Each pair of strain gauges is connected into a Wheatstone bridge circuit together with two dummy gauges which provide temperature compensation (see Figure 4.14).

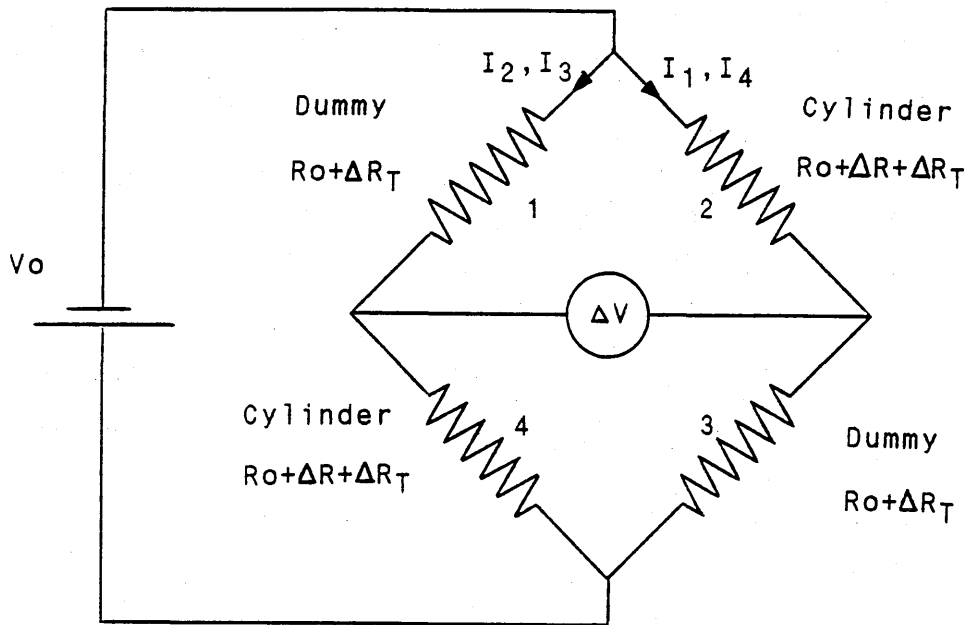


Figure 4.14 The Wheatstone bridge circuit for the confining cylinder strain gauges.

The derivation of equations for the Wheatstone bridge circuits are given below:-

- $R_o = 120\Omega$
- $\Delta R =$ change in resistance due to strain
- $\Delta R_T =$ change in resistance due to temperature

$$I_1, I_4 = \frac{V_0}{2R_0 + \Delta R + 2\Delta R_T}$$

$$I_2, I_3 = \frac{V_0}{2R_0 + \Delta R + 2\Delta R_T}$$

Voltage drop across gauge (1):-

$$\begin{aligned} V_1 &= \frac{V_0}{2R_0 + \Delta R + 2\Delta R_T} \times (R_0 + \Delta R_T) \\ &= \frac{V_0(R_0 + \Delta R_T)}{2R_0 + \Delta R + 2\Delta R_T} \end{aligned}$$

Voltage drop across gauge (2):-

$$\begin{aligned} V_2 &= \frac{V_0}{2R_0 + \Delta R + 2\Delta R_T} \times (R_0 + \Delta R + \Delta R_T) \\ &= \frac{V_0(R_0 + \Delta R + \Delta R_T)}{2R_0 + \Delta R + 2\Delta R_T} \end{aligned}$$

Measured change in voltage due to strain:-

$$\begin{aligned} \Delta V &= V_2 - V_1 \\ &= \frac{V_0 \times R}{2R_0 + \Delta R + 2\Delta R_T} \end{aligned}$$

But ΔR_T and ΔR are small compared to R_0 and are neglected:-

$$\Delta V = \frac{V_0 \Delta R}{2R_0}$$

$$\frac{\Delta V}{V_0} = \frac{\Delta R}{2R_0}$$

For a given change in resistance due to strain, the effect on the voltage output is doubled. This circuit is fully temperature compensated.

The confining cylinder was calibrated for hoop stress and axial load.

4.1.3.1 Hoop stress calibration.

A special test rig was designed and built to house the confining cylinder to enable a balloon to be inflated inside the cylinder - providing a known hoop stress equal to the inflation pressure.

The voltage supply was taken from the mains and converted to 12V d.c., corresponding to the voltage expected from a tractor battery. The output voltage from the bridge circuit was monitored by a digital volt meter (DVM) and the test rig connected to a compressor via an airline and pressure regulator.

Initially, pressure was monitored using a small pressure gauge mounted on the regulator. However, the resolution was insufficient and so a much larger Bourdon gauge was calibrated using a dead weight tester and incorporated into the calibration equipment.

Plate 4.1 shows the equipment used during the calibration procedure.

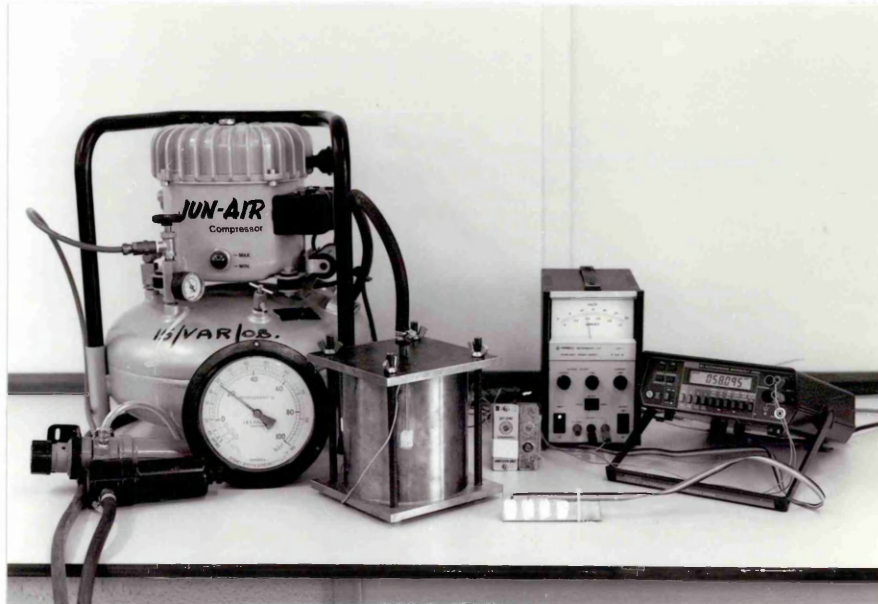


Plate 4.1 Calibration of the confining cylinder for hoop stress.

Balloons, and condoms, were found to be unsuitable for this application as they burst at relatively low pressures. Success was eventually achieved by sealing the cylinder to the top and bottom plates of the test-rig using plastic electrical insulating tape and pressurising with water. This allowed pressures of up to 6.5bar to be maintained.

Outputs were monitored using a Campbell Scientific data logger powered by internal batteries. This could be programmed to record up to eight different inputs simultaneously providing the potential to log hoop stress, axial load and axial strain in the field.

The confining cylinder was calibrated using internal pressure, the procedure being repeated a further three times. During calibration, the dummy strain gauges, mounted on a brass reference plate, were bonded to the confining cylinder using heat sink compound to ensure, as far as possible, that all gauges were at the same temperature. The relationship between hoop stress and output voltage from the bridge circuit is given in Figure 4.15.

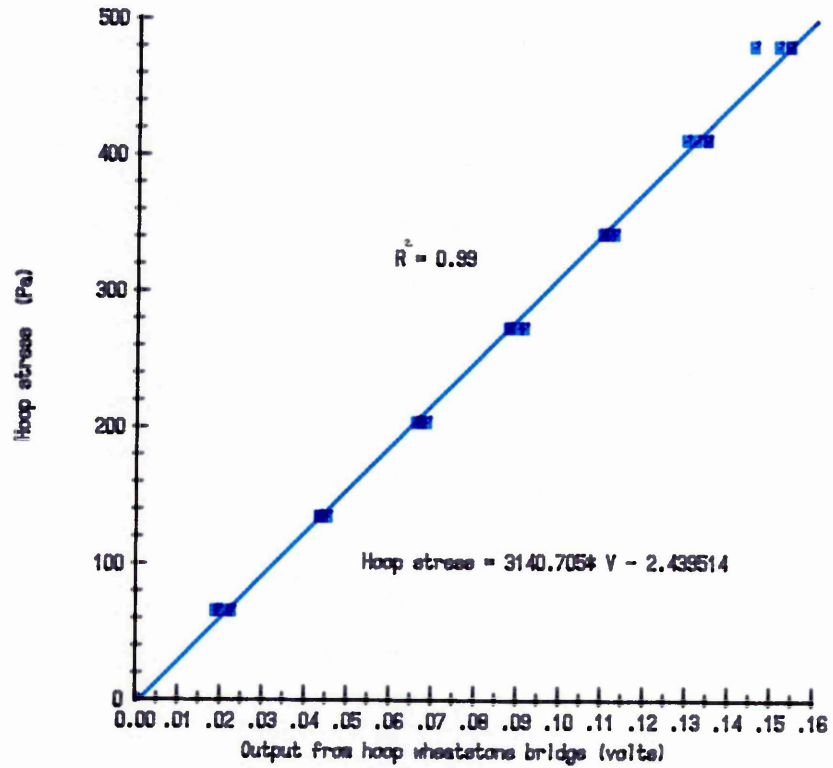


Figure 4.15 Confining cylinder calibration curve for the hoop bridge circuit under increasing internal pressure (four replicates).

4.1.3.2 Axial load calibration.

The two strain gauges axially mounted on the confining cylinder and two dummy gauges were connected into the following Wheatstone bridge circuit using the Campbell 21X data logger (see Figure 4.16).

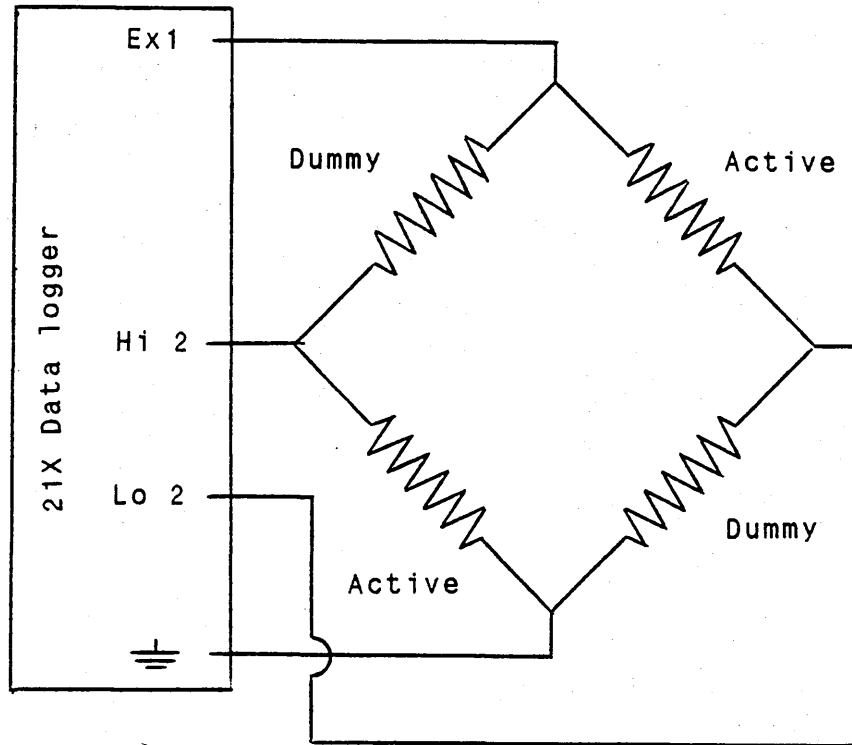


Figure 4.16 The Wheatstone bridge circuit for the axially mounted strain gauges.

An Instron 1122 universal tester was used to apply known axial loads to the confining cylinder. A 5kN load cell (ref. 2511 - 317) was selected and the full scale load dial was set at 1-50, 10 which gave a range of 1KN. The two dummy gauges were bonded to the cylinder using heat sink compound. The calibration procedure was carried out four times and the results are shown in figure 4.17.

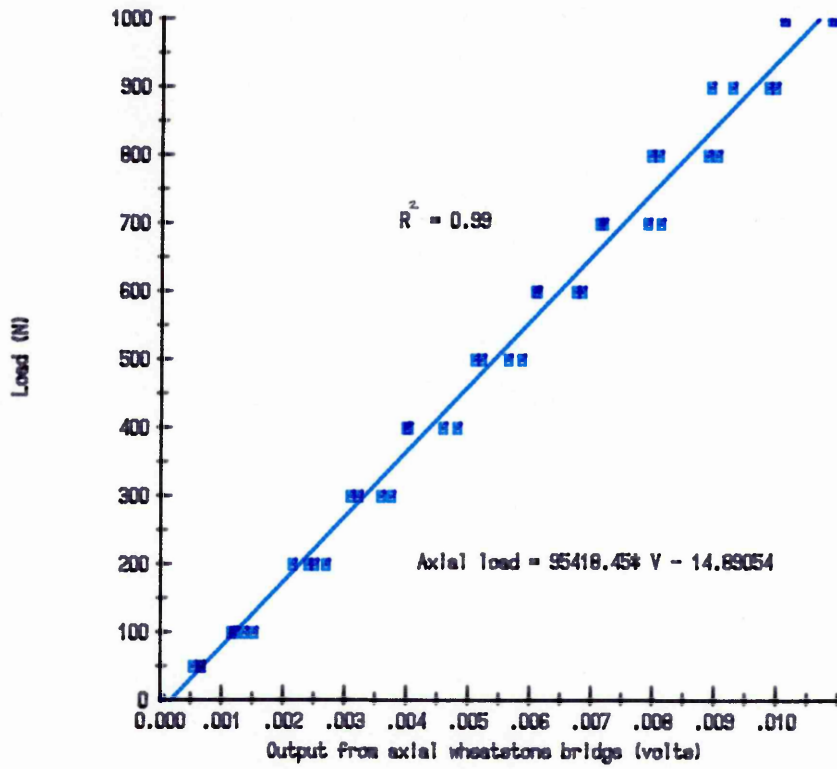


Figure 4.17 Confining cylinder calibration curve for the axial bridge circuit under increasing axial load (four replicates).

4.1.4 CALIBRATION OF THE 100kN LOAD CELL

The tractor mounted equipment was attached to the hydraulic ram on the rear of the tractor via a 100kN load cell which monitored the load applied during compression and sinkage tests. The load cell was connected to the 21X data logger and calibrated on an Avery universal testing machine. The results of the calibration are given in Figure 4.18.

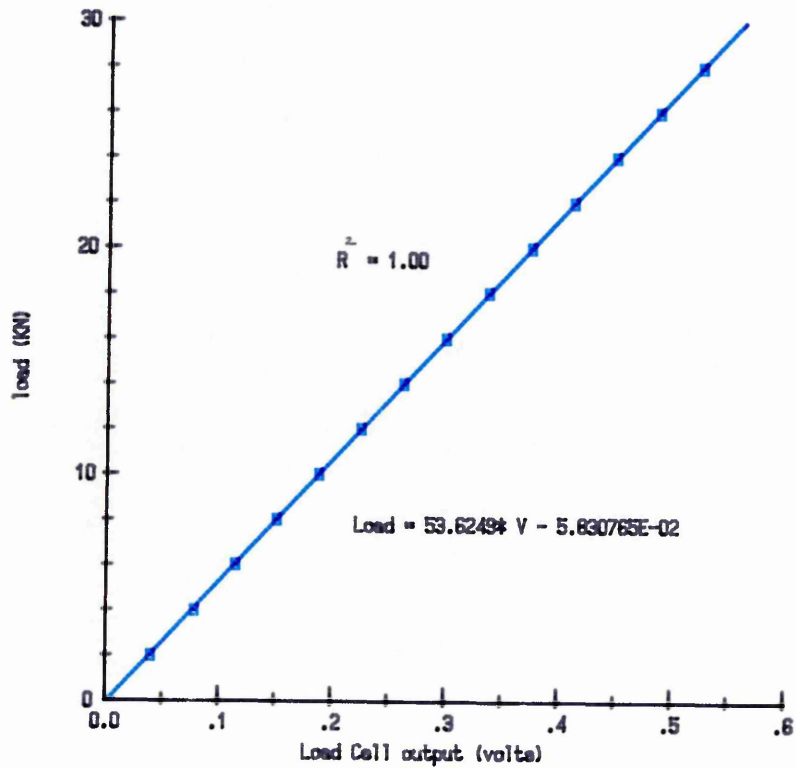


Figure 4.18 Calibration curve for the 100kN load cell

4.1.5 CALIBRATION OF THE LINEAR VARIABLE DISPLACEMENT TRANSDUCER (LVDT)

An LVDT was used to measure changes in soil sample height during compression tests, and changes in depth during plate sinkage tests. This was connected to the 21X data logger along with the bridge circuits and the load cell. The data logger was programmed to give the LVDT output in mm.

A frame was designed and built to act as a datum for the LVDT to ensure that readings would be independent of any tractor movement. Plate 4.2 shows the load cell, LVDT and datum frame in operation during a plate sinkage test.

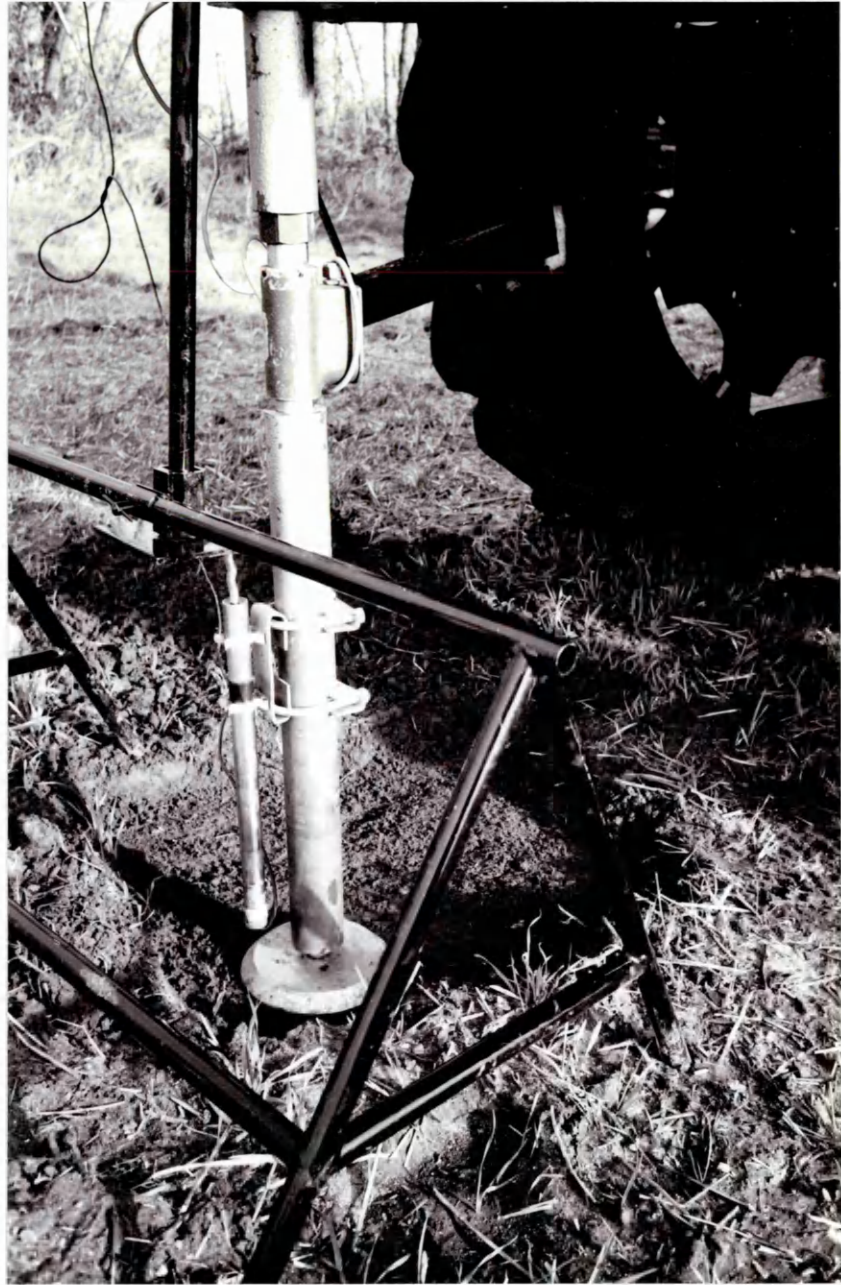


Plate 4.2 The load cell, LVDT and datum frame in operation during a plate sinkage test.

4.2 Field testing.

Field testing of the equipment was carried out on the Evesham soil series experimental plots.

4.2.1 SOIL SAMPLING PROCEDURE.

The soil sampling procedure was as follows:-

- (1) The tractor was reversed on to the plot and the ram moved to a vertical position (see Plate 4.3).



Plate 4.3 The Deutz Intrac tractor adapted to accommodate soil assessment equipment.

- (2) The soil sampling cylinder was assembled, lubricated on the inside with polyox resin and then pushed into the soil surface (see Plates 4.4 to 4.6).



Plate 4.4 Assembly and lubrication of the sampling cylinder.

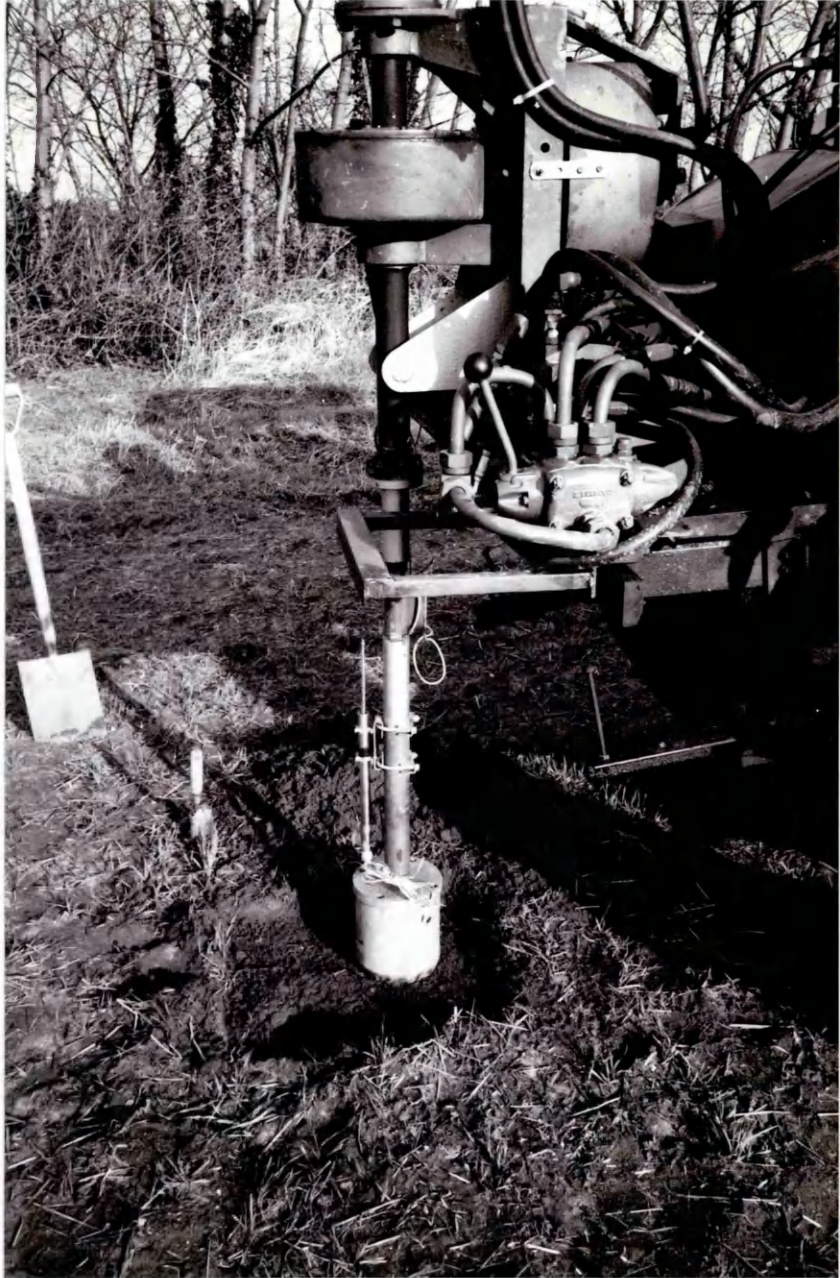


Plate 4.5 The sampling cylinder attached to the rear hydraulic ram on the tractor.

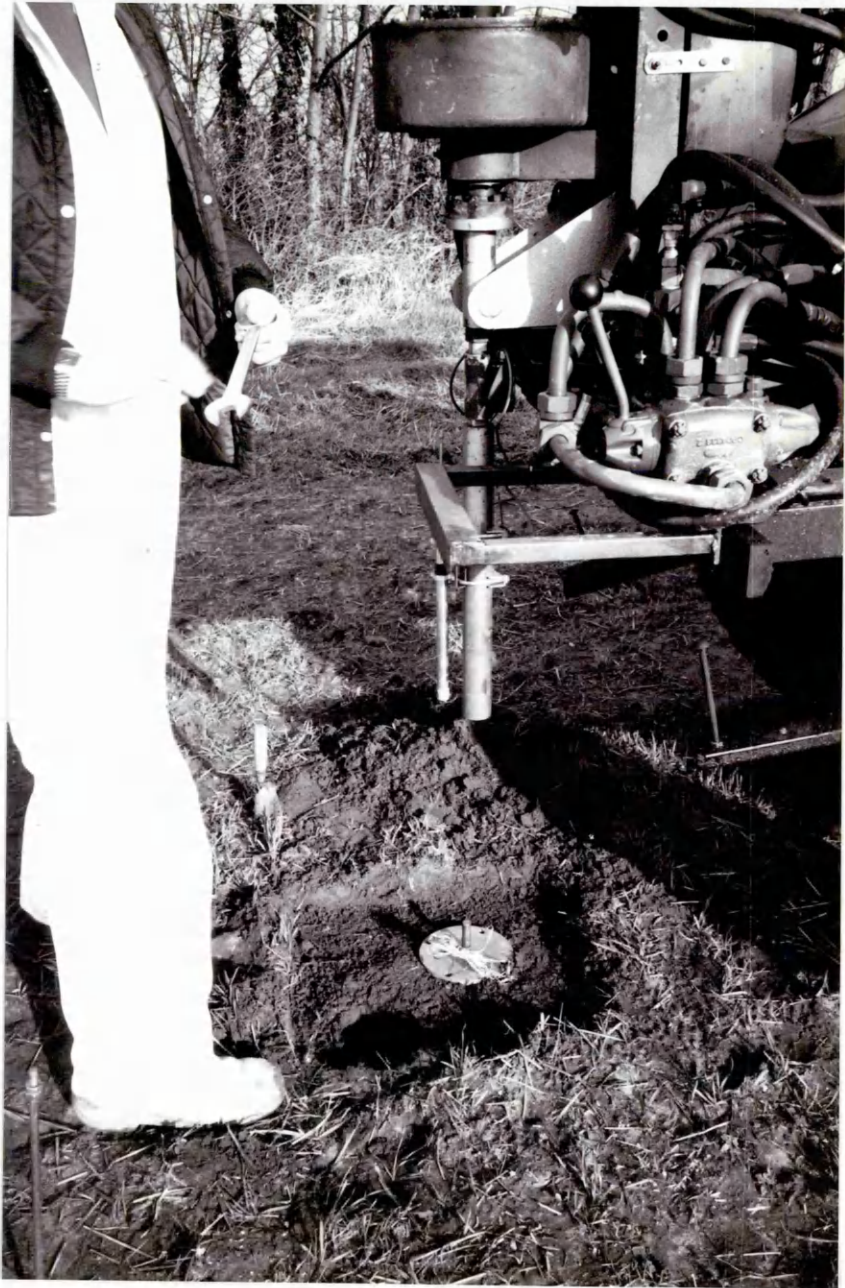


Plate 4.6 The sampling cylinder during sampling.

- (3) The difference between the height of the surrounding soil and that within the cylinder was noted during sampling to check that the soil sample was relatively uncompacted. The maximum load required during sampling was 6.7kN.
- (4) The sampling cylinder was retrieved from the soil and the confining cylinder extracted full of soil. Plate 4.7 shows the trimming of the ends.



Plate 4.7 Trimming the ends of the soil sample within the confining cylinder.

4.2.2 CONFINED COMPRESSION TEST

To carry out a confined compression test, a large aluminium base plate was placed on a layer of coarse sand and levelled. The confining cylinder was then positioned between the upper and lower pistons (see Figure 4.19).

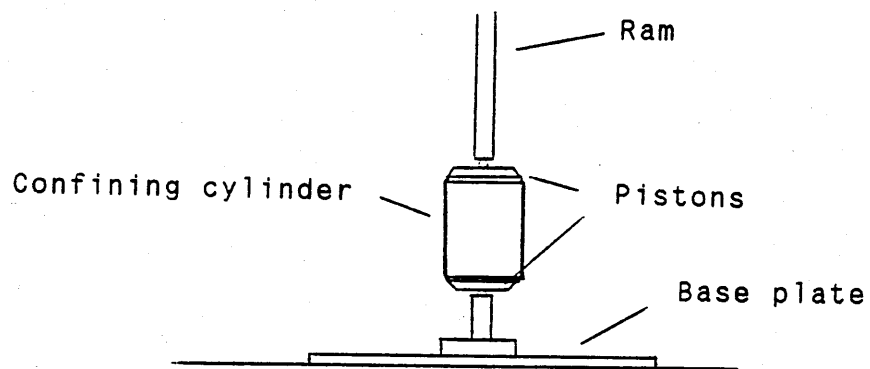


Figure 4.19 Base plate and piston assembly used during confined compression tests.

During initial tests, a maximum load of 500kg only was achievable before the confining cylinder slewed to one side. This problem was marginally improved by jacking up the front of the tractor until the rear ram leaned backwards to compensate for the forward rotation of the tractor about the front jacks during ram extension. The maximum load was still 700kg only - far short of the estimated

2000Kg required. Similar problems were also encountered during initial plate sinkage tests.

Following the problems encountered during the initial field trials, the confined compression equipment was redesigned. The main change concerned the base plate. This was securely fixed to the ram and suspended above the ground to form a compression cell. The advantages gained from this configuration were:-

- (1) The pistons were constrained to move along the direction of the applied force regardless of whether or not the tractor was level.
- (2) The area of damage to the soil surface was much reduced.

The modified design was built and fitted to the tractor. A soil sample was taken as before, and set up in the compression cell. A load of 2000kg was successfully applied to the sample. Plate 4.8 shows a soil sample under compression in the modified equipment.



Plate 4.8 A confined compression test.

An extruder was fabricated from a PVC cylinder and is shown in Plate 4.9 below.



Plate 4.9 Extruding the soil sample.

This allowed the tractor ram to be used to push the soil sample out of the confining cylinder and into a polythene bag for the determination of moisture content and bulk density.

4.2.3 PLATE SINKAGE TEST

A plate sinkage test is shown below in Plate 4.10.

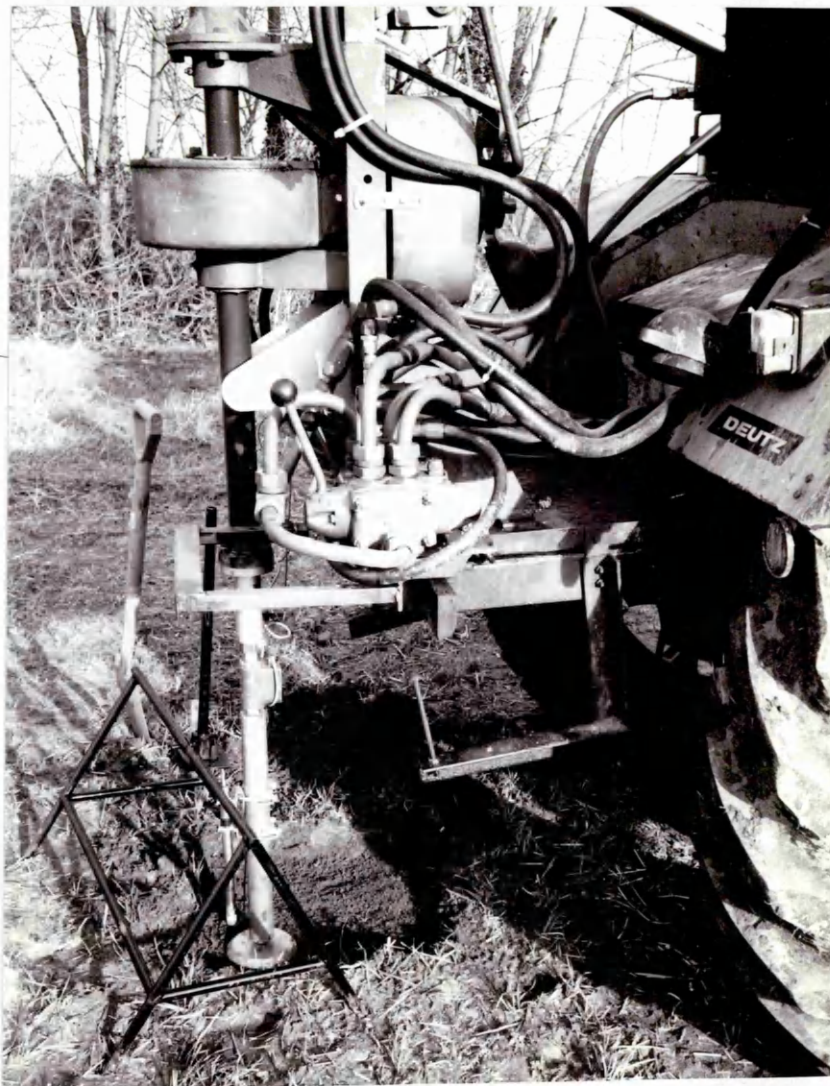


Plate 4.10 A plate sinkage test.

4.3 Data collection procedure

The data logger was programmed to monitor axial stress, radial stress and axial strain by keying in a sequence of numbers. The following sequence, representing seven different computer programmes, was used for this work:-

Programme sequence for the 21X data logger

Main programme table *1:-

*1,D5,91,21,1,86,2,91,21,0,6,1,1,1,1,5000,2,
95418,?,6,1,1,2,1,5000,3,3140D7,?,6,1,5,3,3,
5000,4,D55438C,?,6,1,1,4,4,5000,5,53D625C,?,
86,10,70,5,1.

Sub routine table *3:-

85,1,26,0,95,85,2,26,6,30,10,7,38,6,7,1,95.

The data logger requires programming each day the equipment is used. Keying the sequence by hand is both tedious and can lead to errors and so the programmes were put onto a microcomputer with a facility for automatically downloading them to the data logger. At the start of a field work day, the number sequence would be downloaded using a programme called TERM. The data logger would then be ready for data collection in the field. After field work, the data would be off-loaded into the microcomputer again using TERM.

The form of the data was such that it could not be used directly with standard data analysis packages and so a further programme, SPLIT, was used to modify the data layout for subsequent data analysis.

Field work was carried out using the equipment and the results and discussion are given in Chapters 5 and 6.

CHAPTER 5

QUANTIFICATION OF THE COMPACTIVE NATURE OF SOIL (PART I)

Introduction

This chapter is concerned with the development of a procedure for quantifying the compactive nature of soil based on the analysis and interpretation of data generated from the tractor-mounted compaction assessment equipment described in Chapter 4.

5.1 Initial field trials

Initial field trials were carried out on the Evesham soil series site near Silsoe to identify the most promising way forward for developing techniques to quantify soil compaction and to test field procedures - see Chapter 2 for a site description. Two nests of tensiometers were used to monitor the soil moisture status and Figure 5.1 shows mean soil water suction down the soil profile. Despite it being mid-winter, considerable tensions, in excess of 100cm of water, persisted between 50 and 750mm depth. The site could therefore be considered workable as the soil water suction was greater than the critical limit for that site (see Chapter 2).

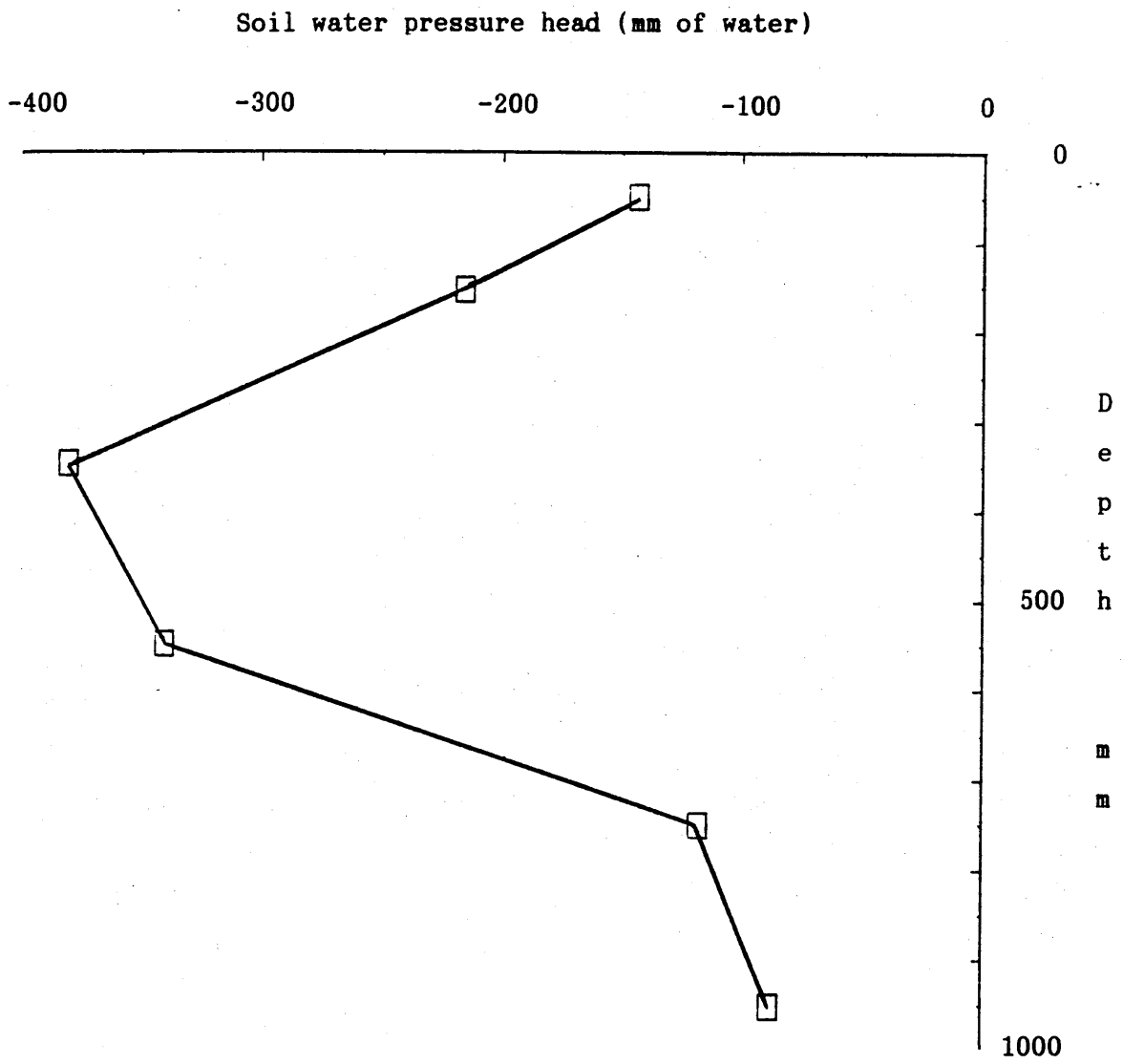
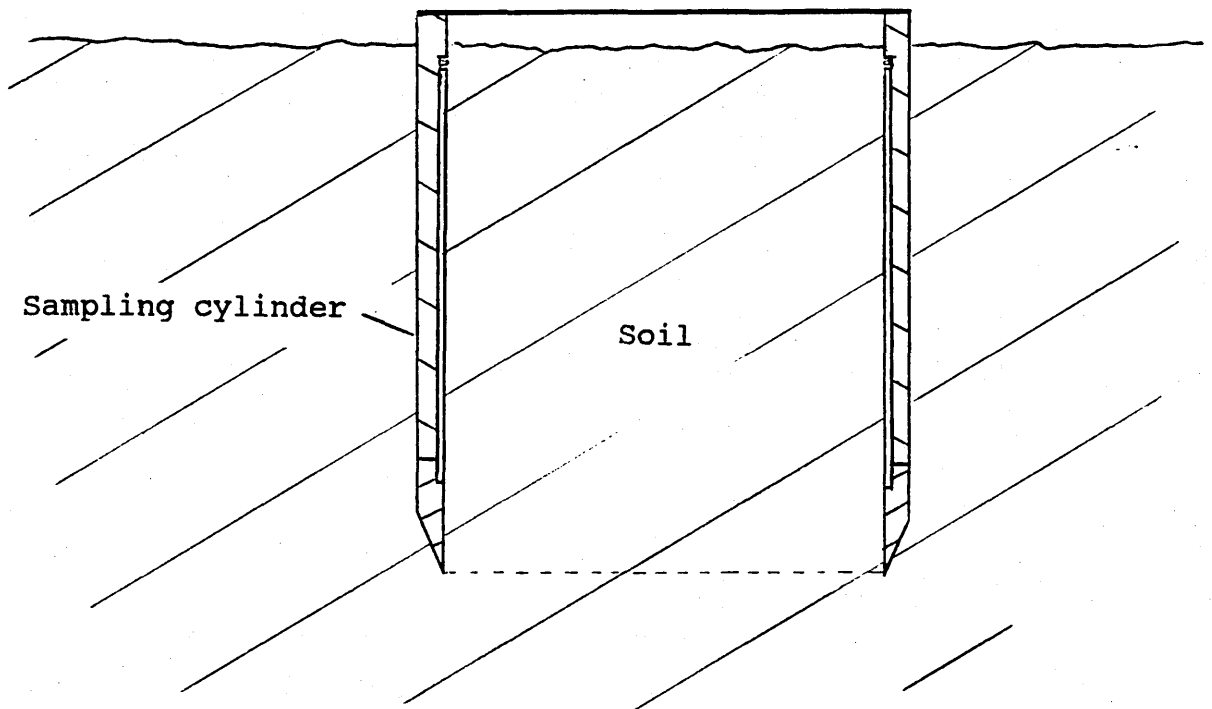


Figure 5.1 Soil water suction down the soil profile - Evesham series site.

The test procedures, described in Chapter 4, were carried out on the grass plot. Sample disturbance was minimal since after the sampling equipment had been forced into the soil, there was no perceptible height difference between the soil surface in the cylinder and that of the surrounding.



The ends of the sample were trimmed flush with the confining cylinder whilst preventing free movement of the soil core within the cylinder caused by the polyox lubricant.

5.1.1 THE CONFINED COMPRESSION TEST

During the confined compression test, the load was increased at approximately 0.5mm/s until the axial stress reached 650kPa - the maximum stress considered safe at that time. Readings were logged every half second and the results from one test are shown in Figure 5.2.

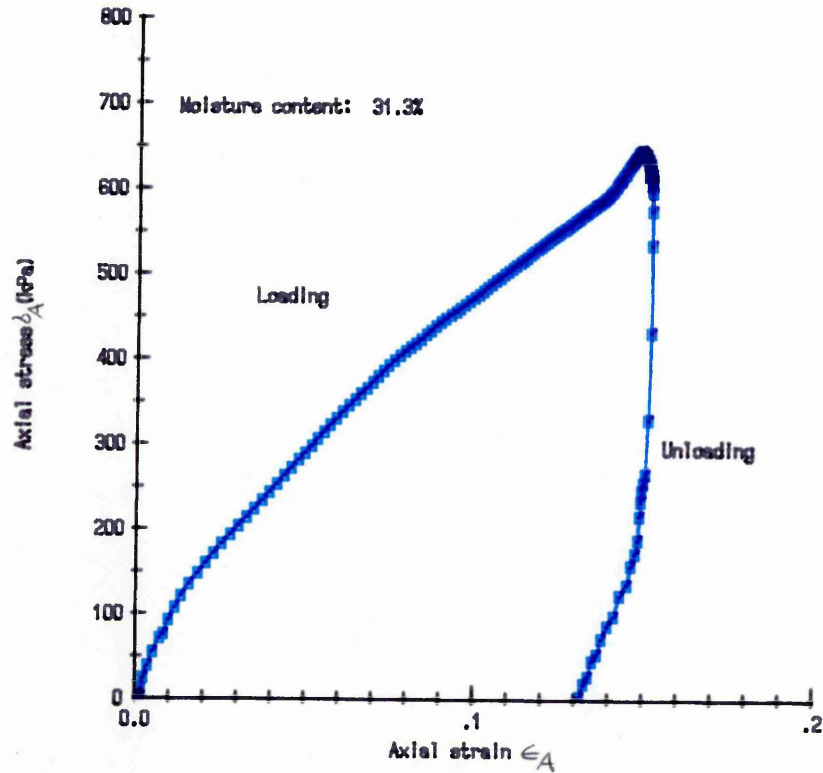


Figure 5.2 The relationship between axial stress (σ_A) and axial strain (ϵ_A) for a clay soil: Evesham series topsoil under grass (bulk density 1.05Mg/m³).

The shape of the loading curve shows some evidence of a reversed S - shape. Had the test continued to higher axial stresses the trend shown in Figure 5.3 would have been expected, with the curve tending towards an asymptote.

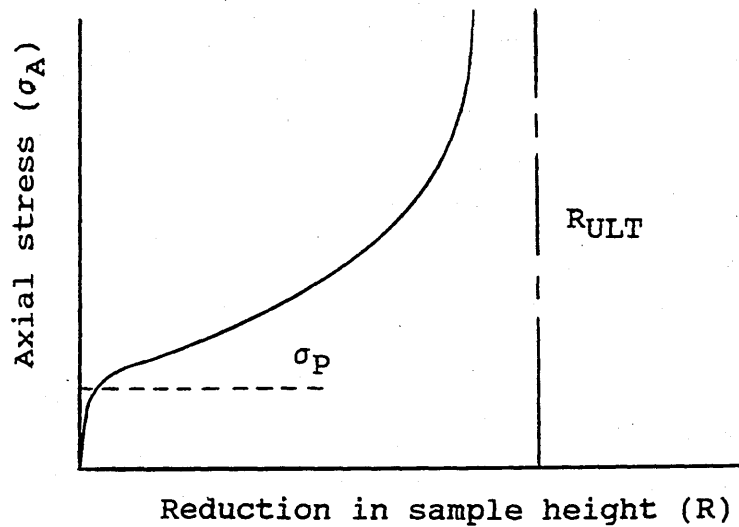


Figure 5.3 The expected loading curve from a confined compression test.

The initial gradient of the curve is a function of the initial soil strength. Figure 5.2 shows the results for a single loading and unloading operation. If the soil core had been reloaded the following characteristic, shown in Figure 5.4, would have been expected, Bradford and Gupta (1986).

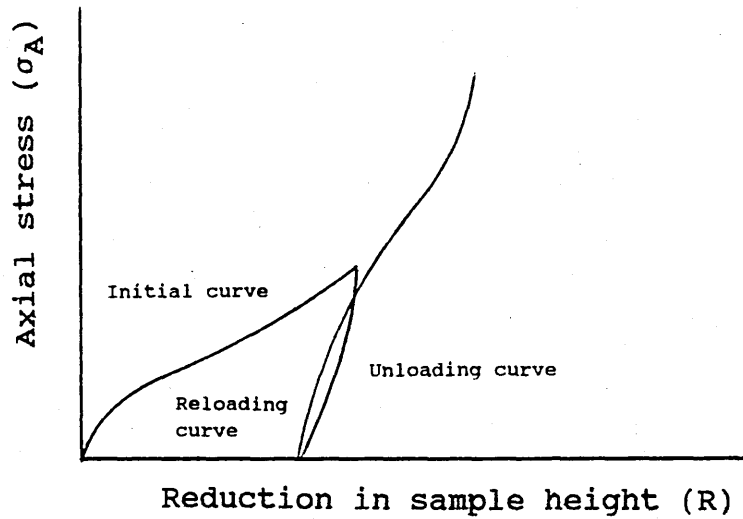


Figure 5.4 The effect of unloading and reloading during a confined compression test.

A small portion only of the strain is recovered during unloading since the strains that result from the sliding or fracturing of particles are largely irreversible. The recovery that does occur is caused by the elastic energy stored within individual particles as the soil is loaded (Lambe and Whitman, 1979). When the reloading stress exceeds the maximum applied during loading, the stress-strain curve follows approximately the path that it would have followed had there been no unloading. If the soil under test had been subjected to loading prior to the test, then any initial kink in the curve generated from the test could be used to estimate the level of the previous loading.

Following the initial test, the soil core was found to have compressed non-uniformly as illustrated in Figure 5.5 below.

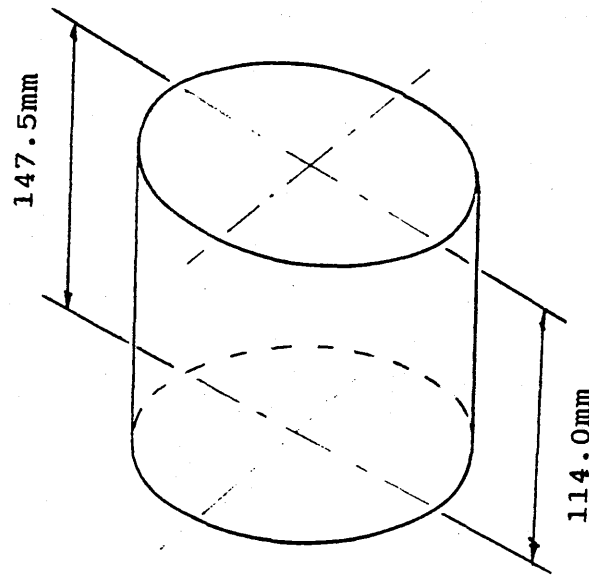


Figure 5.5 Soil sample deformation after a confined compression test.

This was most probably due to the Evesham soil series being a cracking clay soil with varying localised packing. The sample size could not be increased to limit this effect because of the practicalities of producing sufficient force to compress the sample. In all future work three replicate tests were carried out and strain measured at the central axis of the sample.

5.1.2 THE PLATE SINKAGE TEST

A plate sinkage test was carried out in close proximity (0.5m) to the confined compression test and at a similar deformation rate. A plateau (0.5 x 0.5m) was prepared at the depth of interest, in this case 50mm, to prevent surcharging from any soil heave around the plate, see Figure 5.6.

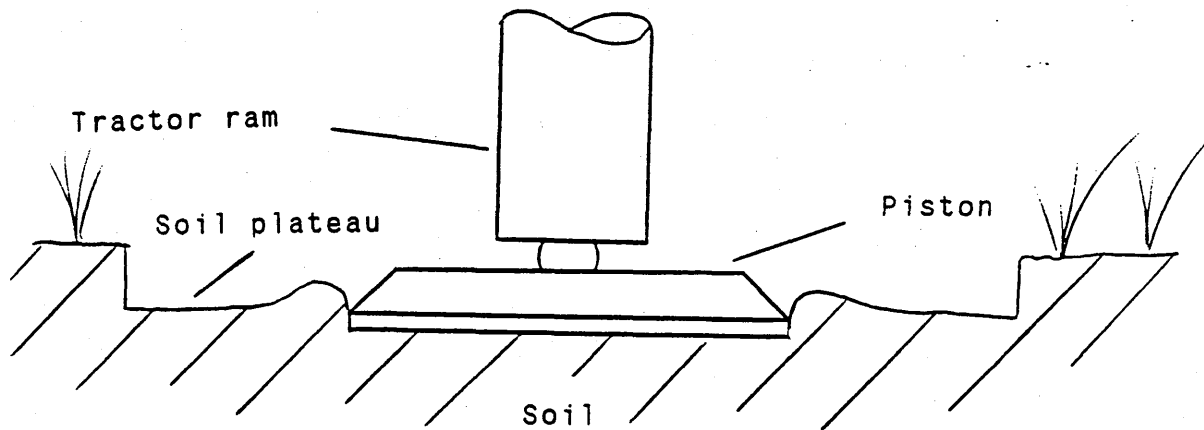


Figure 5.6 Schematic diagram of plate sinkage test.

Sample plate sinkage test results are presented in Figure 5.7 below showing the general shape of the curve to be a hyperbola which tends towards an asymptote at an ultimate stress σ_{ULT} .

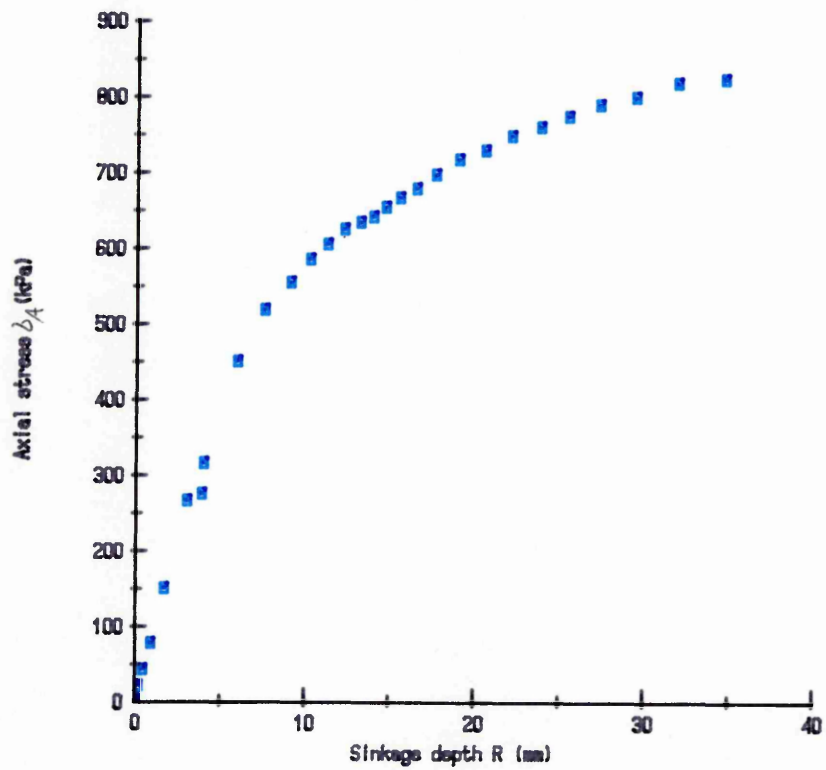


Figure 5.7 The relationship between axial stress (σ_A) and axial sinkage (R) during a plate sinkage test at 50mm depth on a clay soil: Evesham series top soil.

Bernstein (1913) suggested the following mathematical model to describe the curve:-

$$\sigma_A = K \cdot R^n \quad [1]$$

Where σ_A = axial stress

K = soil parameter

R = sinkage

n = exponent

Taking logarithms, equation [1] becomes:-

$$\log \sigma_A = n \log R + \log K$$

which is a straight line equation with slope n and intercept logK as shown in Figure 5.8.

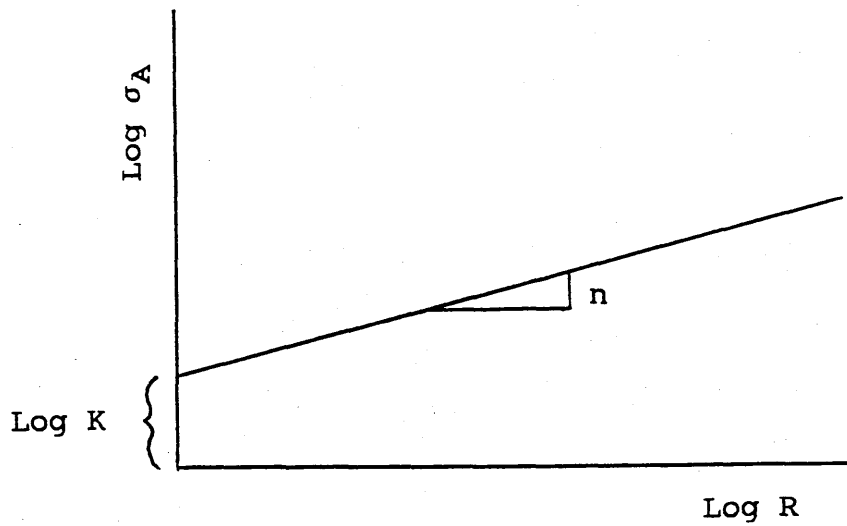


Figure 5.8 Plate sinkage test analysis, Bernstein (1913).

Bekker (1960) modified the Bernstein equation to:-

$$\sigma_A = (K_C/b + K\phi)z^n$$

where b is plate diameter and K_C , $K\phi$ and n are soil parameters determined from two tests with different plate diameters. According to Karafiath and Nowatzki (1978) the Bernstein and Bekker models are conceptually inadequate because the sinkage curve is generated from several different physical processes (see Figure 5.9). Initially, the sinkage process is governed by elastic deformation. This, however, very quickly changes to an elastic-plastic phase before passing to one of plastic failure.

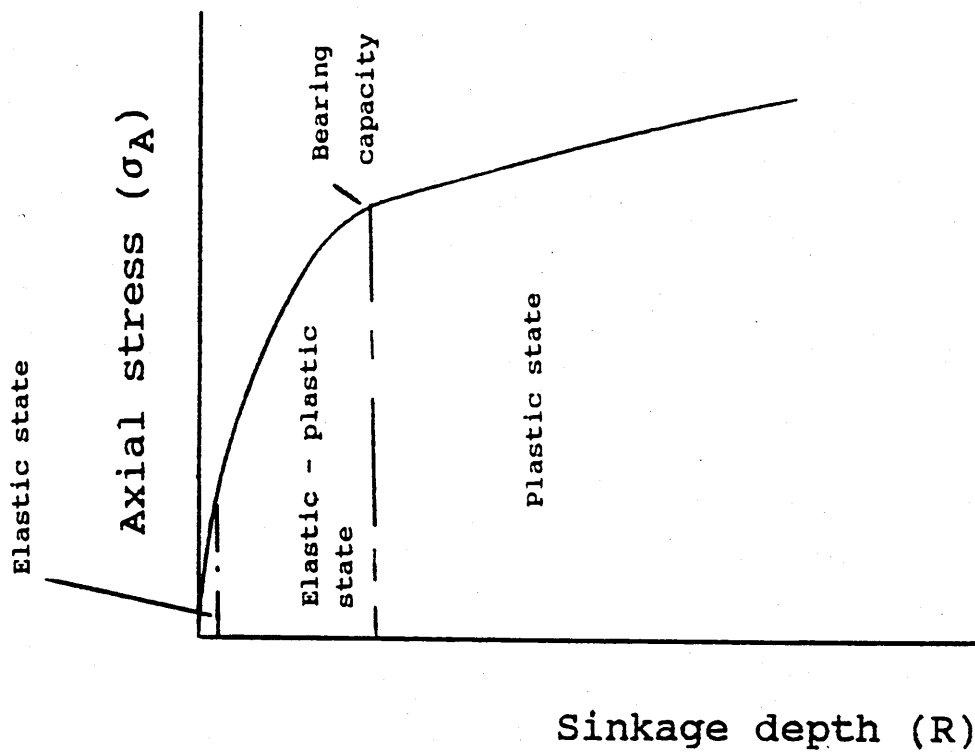


Figure 5.9 Typical stress-sinkage relationship obtained from a plate sinkage test.

5.2 Assessing soil compaction and compactability

When assessing a given soil in terms of compaction and compactability, it is necessary to firstly, describe the soil condition prior to testing, as the soil may have already sustained loading, and secondly, to test the soil's susceptibility to further loading.

5.2.1 CLASSIFICATION OF INITIAL SOIL CONDITION

Researchers have used a number of different parameters to describe the compactive nature of soil. Unfortunately, no single parameter fully describes a given situation. Porosity and void ratio are widely used:-

$$\text{Porosity (n)} = \frac{\text{volume of pores}}{\text{total volume}}$$

$$\text{Void ratio (e)} = \frac{\text{volume of pores}}{\text{volume of solids}}$$

These parameters, however, take no account of the proportion of water filled to air filled pores and, therefore, give no information on how much a partly saturated soil can be compressed before it approaches saturation and cannot be compacted further. This is particularly relevant for fine textured soils.

Air capacity gives some measure of the proportion of water filled to air filled pores.

$$\text{Air capacity (Ca)} = \frac{\text{volume of air}}{\text{total volume}}$$

A more appropriate parameter would be one which gives a measure of the volume of air or water in the soil as a percentage of the total pore volume ie the degree of saturation.

$$\text{Degree of (S) saturation} = \frac{\text{volume of water}}{\text{volume of pores}}$$

$$S = \frac{\text{weight of water}/1000}{\text{total vol} - \frac{\text{weight of dry soil}}{\text{particle density}}}$$

In addition to degree of saturation, it is necessary to describe the initial soil condition in terms of packing state and strength. Dry bulk density gives some insight into the packing state of soil. Soils of different textural classes, however, can have very different dry bulk densities but appear to be in similar packing states. For example, loose Evesham series may have a dry bulk density of 1.0Mg/m^3 , whereas that for loose Bearsted series could be as high as 1.4Mg/m^3 . For this reason, dry bulk density is a useful parameter for comparative work using the same soil, but not ideal for an absolute measure for compaction.

Renger (1970) carried out a statistical study which revealed that it is possible to assign a numerical value to compactness (packing

density) derived from dry bulk density (Db) and a correction for clay content (%C).

$$\text{Packing density (Ld)} = \text{Db} + (0.009 \times \%C)$$

Table 5.1 shows the relationship between soil packing density and field properties.

Table 5.1 The relationship between soil packing density and field properties.

<i>Packing density</i>		<i>Field properties</i> ¹
Low	g cm^{-3} < 1.40	Loose when moist if single grain; peds if present are fine or medium and easily displaced; weak ped and/or soil strength when moist (Table 8). (Rarely encountered in clay or sandy clay mineral soils.)
Medium	1.40-1.75	Neither strong nor loose consistence (Table 8); peds not easily displaced, but may be well formed; weakly developed fine or medium peds, or strongly developed coarse peds with many macropores and moderately firm ped strength.
High	> 1.75	Compact if single grain; peds are coarse (angular or prismatic) and structure is normally weakly developed; soils with strongly developed structure have very firm or strong ped strength (Table 8) and few macropores. (Rarely encountered in A horizons unless clay or clay loam.)

¹ Field properties modified after Benecke (1966).

From Soil Survey Field Handbook (1976)

The parameters considered so far for assessing soil in its initial condition prior to loading do not give a direct measure of strength. It is essential that a parameter is included which will give a measure of the resistance of the soil to deformation under stress. The confined compression and plate sinkage tests can give a useful measure of strength. When the results from the two tests are plotted on the same axis, the curves initially follow approximately similar linear paths - see Figure 5.10.

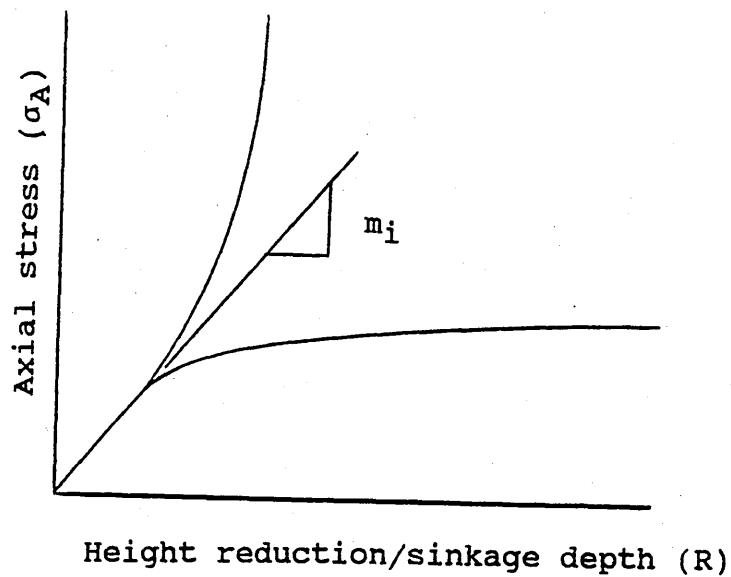


Figure 5.10 Typical curves generated from confined compression and plate sinkage tests.

The gradient of the lower portion of the curves, which will be referred to as the initial modulus (m_i), gives an indication of initial soil strength, viz. the greater the gradient, the stronger the soil.

The initial soil condition can be characterised in terms of:-

- (1) Packing state
- (2) Susceptibility to further damage through either compaction or displacement (Deformability).

An indication of packing state can be obtained directly from considering packing density (see Table 5.1). A measure of deformability is more difficult to ascertain as it depends on:-

- (a) soil strength: indicated by initial gradient of the stress-strain curves, and
- (b) degree of saturation: ie. how much air is left in the sample which is available for expulsion

If a soil has a high degree of saturation but a low initial modulus then the soil might be expected to readily deform under load. The mode of failure, however, would be predominantly one of soil displacement rather than compaction (see Figure 5.11a). If a soil has a low degree of saturation and a low initial modulus then it might be expected to deform readily, however, the mode of failure could be through either compaction or displacement depending on the ability of the surrounding soil to resist lateral movement of soil

(see Figure 5.11b). If a soil has a high degree of saturation and a high initial modulus, then the soil would be resistant to deformation. Any that did take place would initially occur through compaction, and then predominantly through displacement (see Figure 5.11c). Finally, if a soil has a low degree of saturation, but a high initial modulus, then it would be expected to resist deformation. The mode of any that did occur would depend on the confining strength of the surrounding soil (see Figure 5.11d).

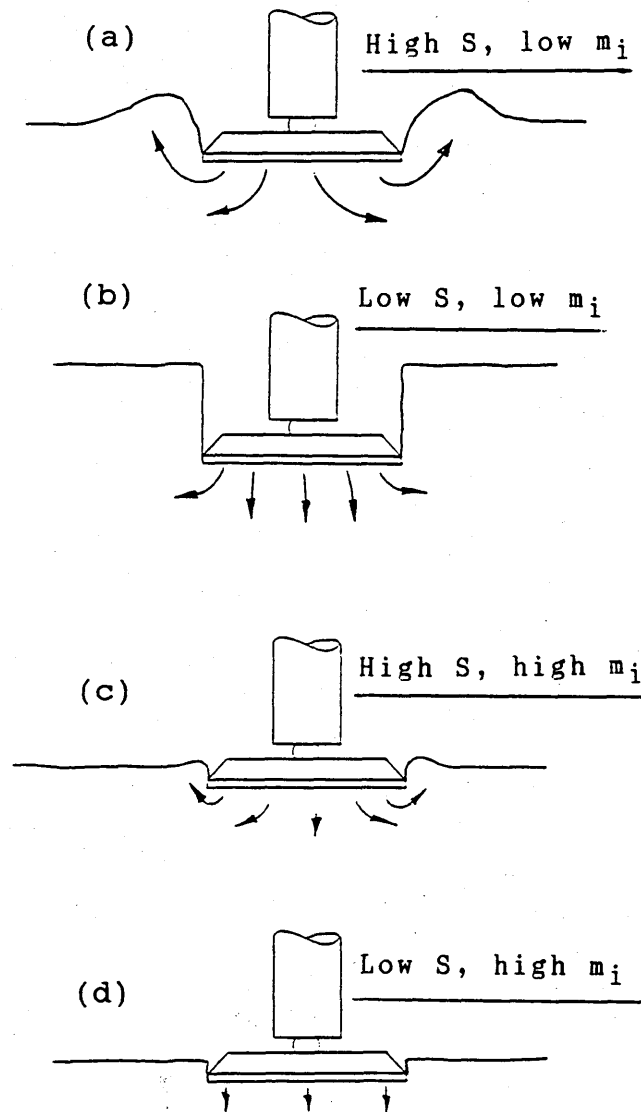


Figure 5.11 The deformation mode of soil in various initial conditions.

Based upon the initial results, for the purposes of this study, degree of saturation and initial gradient will be rated as follows:-

Degree of saturation (%)	Failure mode
<70	compaction or displacement
>70	displacement

Initial modulus (m_i) (kPa/mm)	Strength rating
<15	low
15 to 30	medium
>30	high

5.2.2 CLASSIFICATION OF SOIL DEFORMATION UNDER LOADING.

In this study, soil damage due to loading is divided into two components governed by two quite different processes:-

- (1) the process of air expulsion during loading with a resultant increase in dry bulk density which is termed compaction, and
- (2) deformation due to soil movement with minimal reduction in soil volume which is termed displacement.

During the initial stages of a plate sinkage test, the sinkage will be predominantly due to compaction under the plate. As the axial stress is increased and the plate continues to sink, a point will be reached when the deformation process will change and further sinkage will be predominantly due to lateral soil displacement (see Figure 5.12).

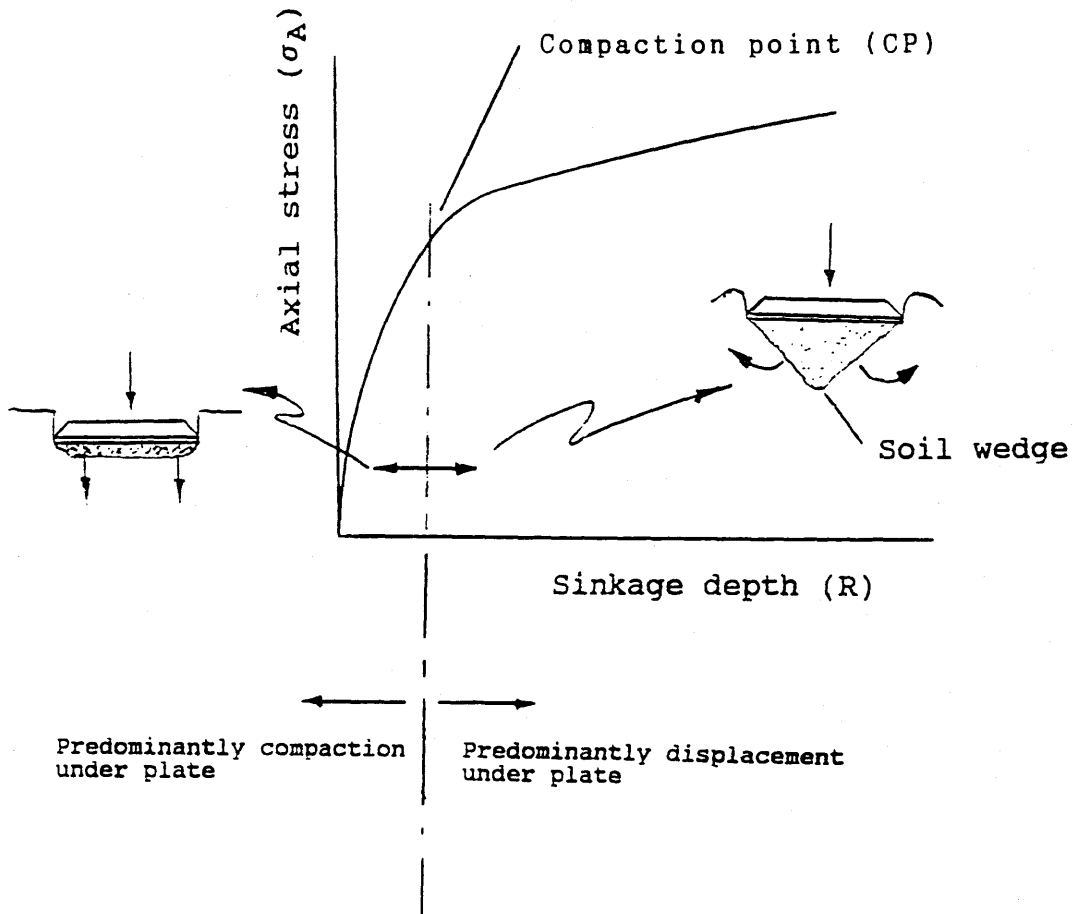


Figure 5.12 The modes of soil deformation during a plate sinkage test.

The point denoting the change in the process of deformation will be termed the Compaction Point (CP). The location of the CP can be ascertained with the aid of results from a confined compression test. In this latter test, soil placed in a rigid smooth-walled cylinder is subjected to one-dimensional compression. Hettiarachi (1992) explains the compression process in the following way:-

Using the subscripts h and v to denote vertical and horizontal directions respectively, the stresses (σ) and strains (ϵ) in this type of loading are:-

$$\sigma_h = K \cdot \sigma_v; \quad \epsilon_h = 0$$

If side-wall friction is assumed to be zero then σ_h and σ_v can be considered to be principal stresses. It can be shown that:-

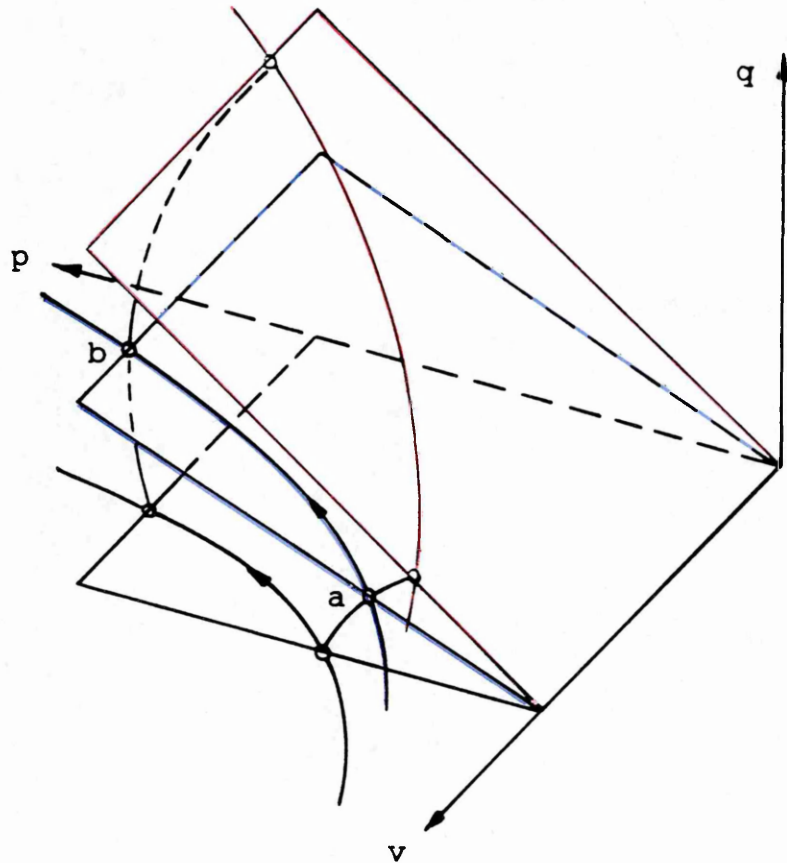
$$q = K \cdot p; \quad K = 3(1-K_0)/(1+2K_0)$$

where p and q are the stress components used in the critical state model and K_0 is the coefficient of earth pressure at rest:-

$$p = 1/3(\sigma_v + 2\sigma_h)$$

$$q = (\sigma_v - \sigma_h)$$

With reference to Figure 5.13, for one-dimensional compression, the stress path must follow a trace such as ab.



- Isotropic compression
- One-dimensional compression
- Critical state line

Figure 5.13 Critical state diagram representing one-dimensional compression.

Although the sample is subject to shear, it cannot reach critical state conditions as ab does not intersect the Critical State Line (CSL). The soil therefore cannot fail. Under these conditions, the boundary wedge, normally formed beneath sinkage plates when in compression, cannot occur and so provided that air is allowed to escape during compression, and the test is terminated before water is expelled, the reduction in soil volume can be considered to have occurred under conditions of pure compaction.

If the results from a confined compression test are superimposed onto those from a plate sinkage test, then the point at which the two curves diverge can be assumed to be the CP (see Figure 5.14).

The portion of the confined curve extending beyond the CP would not normally be achievable in the field through simple loading since lateral soil movement would occur reducing the confining stress.

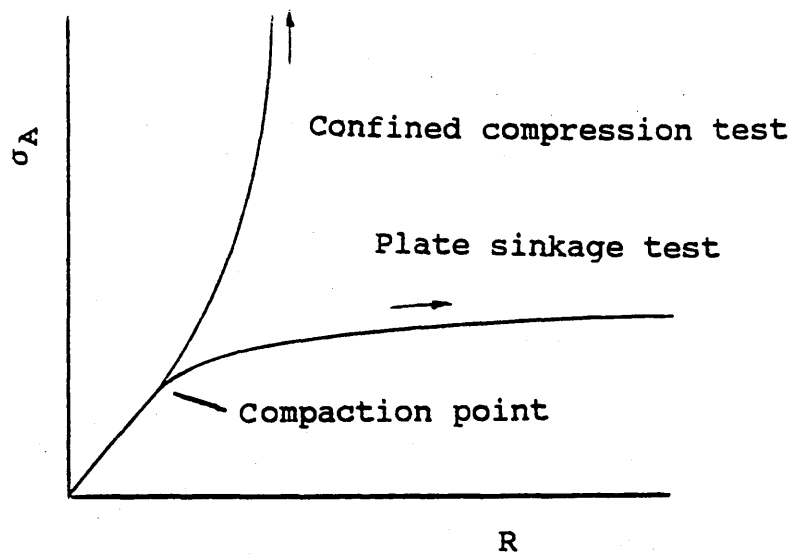


Figure 5.14 The overlaying of confined compression test results onto plate sinkage test results to determine the position of the Compaction Point (CP).

5.2.2.1 Confined compression test data.

Stress-sinkage relationships from confined compression tests are of the form shown below in Figure 5.15 and can be approximated by a hyperbola.

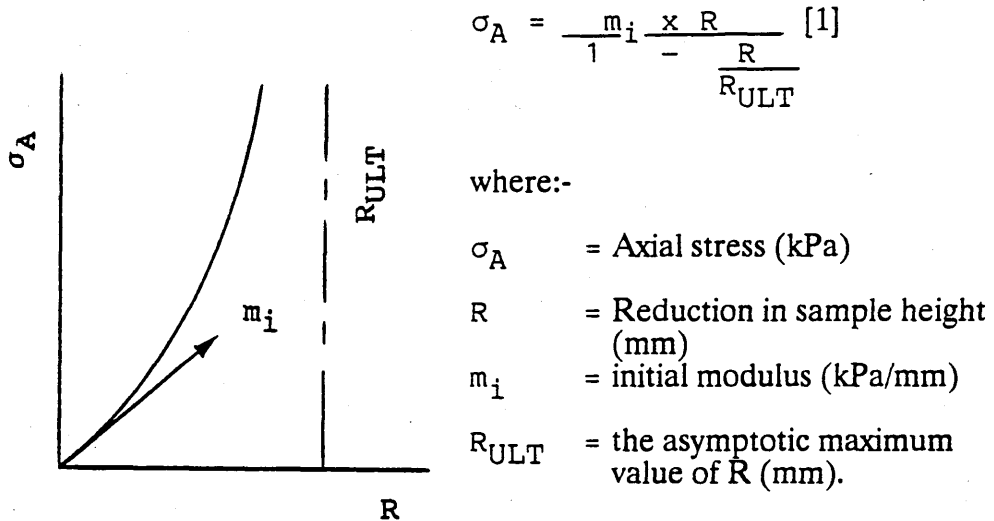


Figure 5.15 Schematic diagram of confined compression test results.

Rearranging equation [1]:-

$$\frac{\sigma_A}{R} = \frac{\sigma_A}{R_{ULT}} + m_i \quad [2]$$

which is linear with variables σ_A/R and σ_A ; m_i and $1/R_{ULT}$ are constants which can be evaluated using the least squares procedure to fit the best straight line to observed data.

5.2.2.2 Plate sinkage test data.

Stress-sinkage relationships from plate sinkage tests are of the form shown below in Figure 5.16 and can be approximated by a hyperbola:-

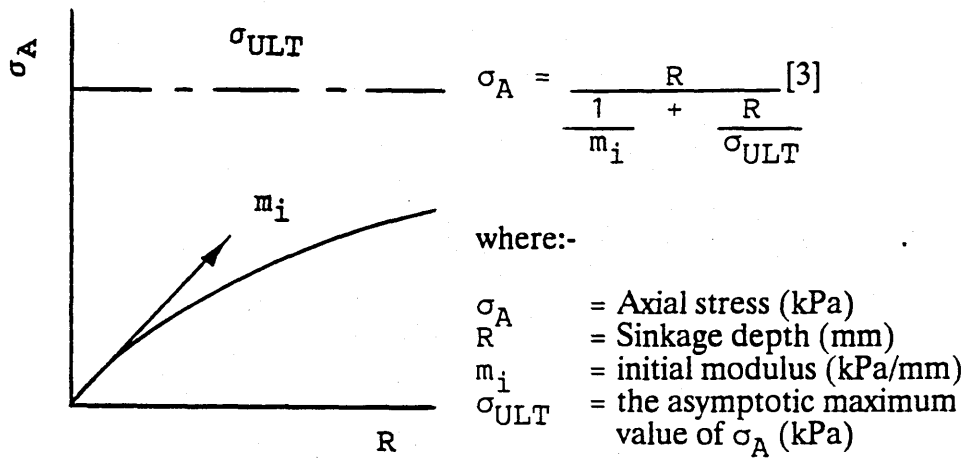


Figure 5.16 Schematic diagram of results from a plate sinkage test.

Rearranging equation [3] results in:-

$$\frac{R}{\sigma_A} = \frac{1}{\sigma_{ULT}} \cdot R + \frac{1}{m_i} \quad [4]$$

which is linear with variables R/σ_A and R ; m_i and $1/\sigma_{ULT}$ are constants which can be evaluated using the least squares procedure to fit the best straight line to observed data.

5.2.2.3 Determination of compaction point position.

The compaction point (CP) is defined as the point on the sinkage curve separating failure due predominantly to compaction from that due to soil displacement below a plate during a plate sinkage test. It is located using regression curves of data obtained from confined compression and plate sinkage tests.

The following procedure can be used to establish the coordinates of the CP for a given soil:-

- (1) Carry out both a confined compression test and a plate sinkage test, with three replicates, at the depth of interest.
- (2) Perform linear transformations on the test data to evaluate the hyperbolic regression parameters.
- (3) Plot the hyperbolic regression curves.
- (4) Calculate the coordinates of the intersection for the two curves.

At the intersection:-

$$\frac{m_i \cdot R}{1 - R \cdot \frac{1}{R_{ULT}}} = \frac{R}{1 + R \cdot \frac{1}{m_i \sigma_{ULT}}}$$

- (5) Examine the significance of the overlapped test data at the CP by performing a linear regression analysis of data between the origin and the CP.

Figures 5.17 and 5.18 show typical data plotted using this procedure. The data were generated from tests on the Evesham and Bearsted soil series grass plots at 50mm depth. The orientation of the axes has been reversed to comply with the analysis procedure proposed later in this Chapter.

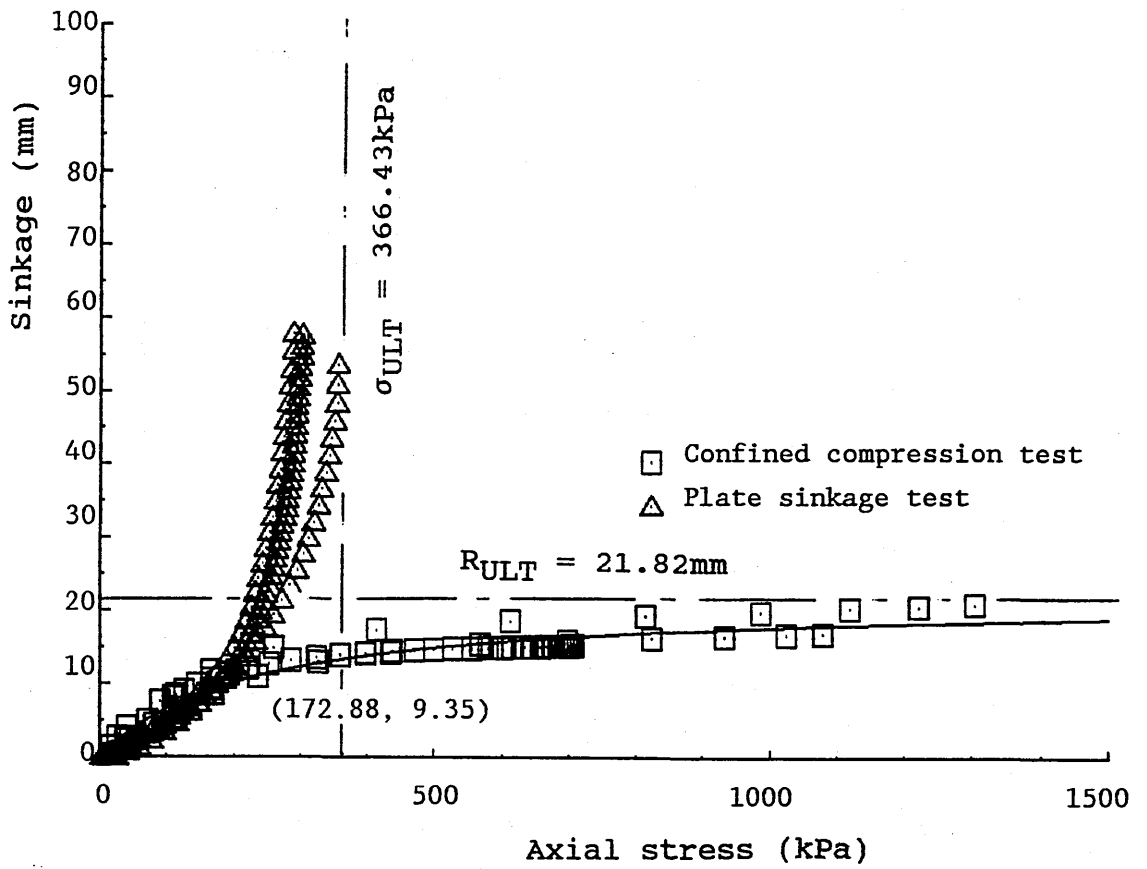


Figure 5.17 Confined compression and plate sinkage test results for a clay soil: Evesham series at 50mm depth under grass.

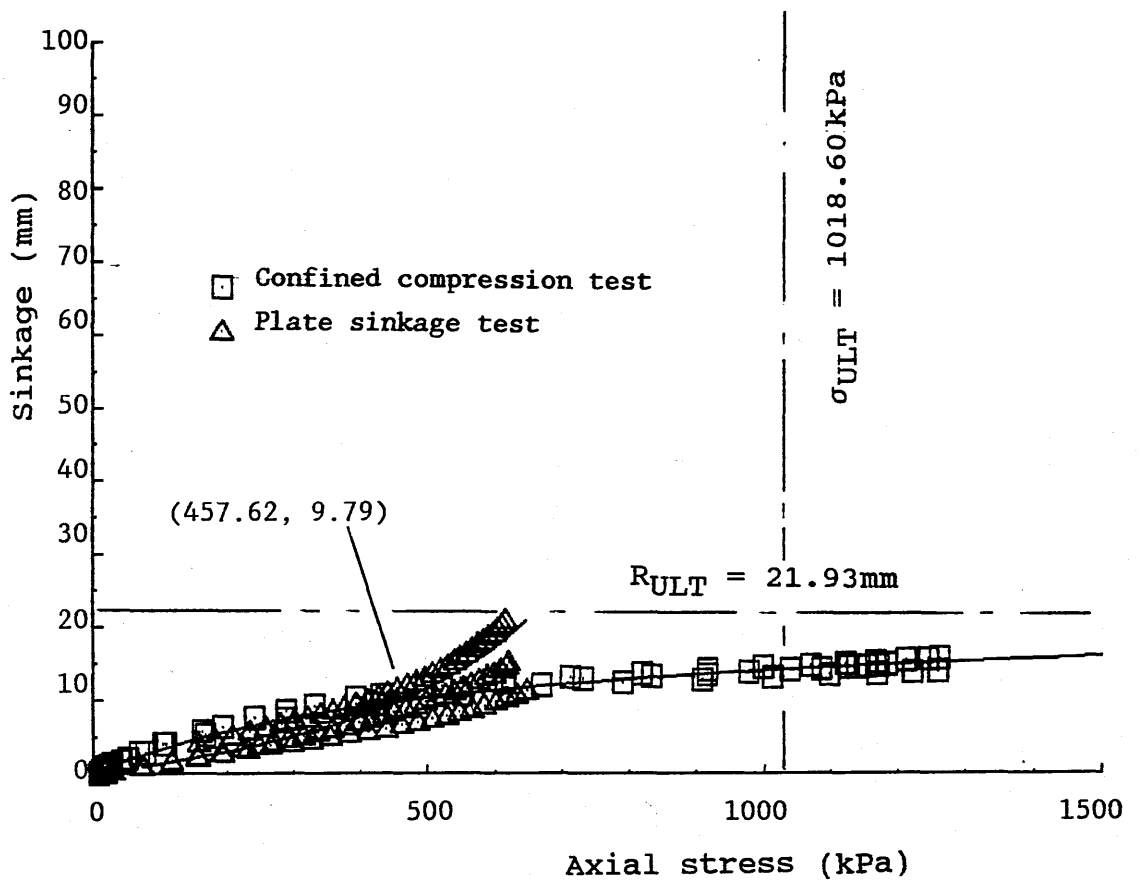


Figure 5.18 Confined compression and plate sinkage test results for a sandy loam soil: Bearsted series at 50mm depth under grass.

5.2.2.4 Radial stress

During deformation by pure compaction, little lateral stress is expected initially. Once the CP is approached, radial stress (σ_R) should start to increase as soil is pushed sideways by the newly formed soil wedge. The shape of a graph of radial stress against axial stress could therefore provide a valuable insight into the deformation characteristics of a particular soil during compression. A typical curve would be of the form shown in Figure 5.19.

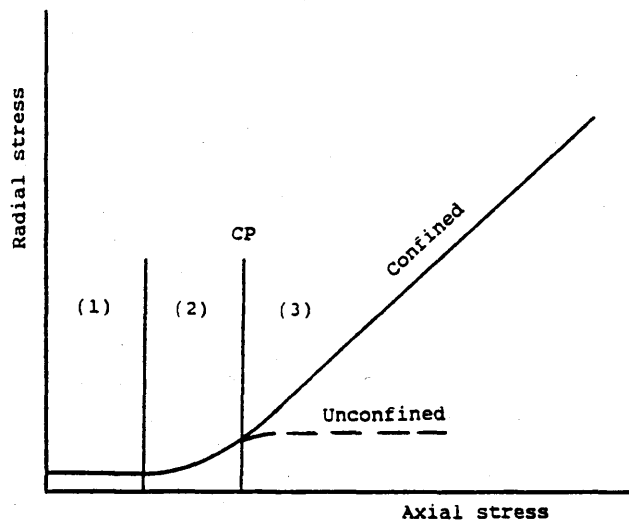
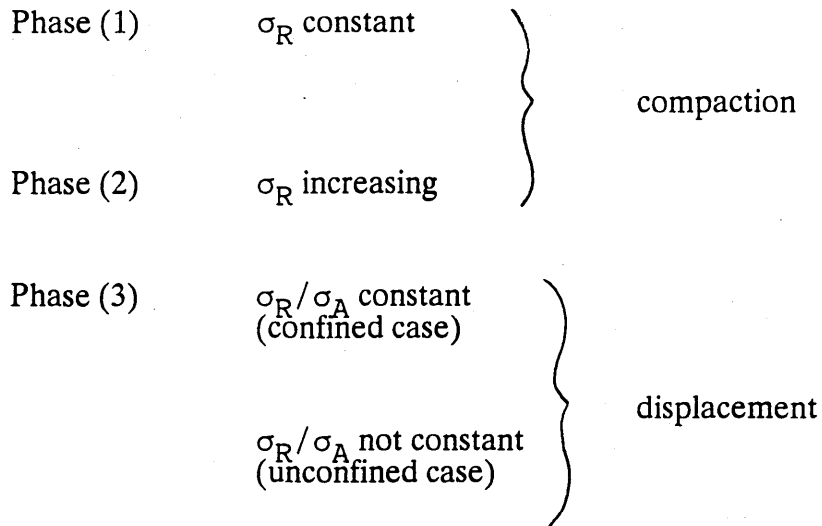


Figure 5.19 Typical form of graph of radial stress against axial stress for soil under compression.

From Figure 5.19, the compression process can be divided into three distinct phases:-



The same data can be presented in the form of a graph of coefficient of earth pressure at rest (K_0) against axial stress (σ_A) where:-

$$K_0 = \sigma_R/\sigma_A$$

The divisions between the three phases are very distinct when the data is expressed in this way (see Figure 5.20). During phase (1), ie. compaction with no increase in lateral stress, K_0 falls reaching a minimum at which point the mode of compaction changes from phase (1) to phase (2), ie. compaction with increasing lateral stress, and K_0 begins to increase. K_0 continues to increase until the CP is reached and phase (3) commences. The path of the curve in phase (3) depends on the nature of the test conditions. For confined compression test conditions, the curve will tend towards a relatively constant K_0 value, this, however, is not so for the plate sinkage case. It can be seen from the plate sinkage curves in Figures 5.17

and 5.18 that σ_A continues to increase once the CP is passed but tends towards an asymptote at σ_{ULT} . Assuming that the radial (lateral) stress cannot exceed the axial stress, ie. $K_0 < 1$, then σ_R cannot exceed σ_{ULT} and is likely to be significantly less. As the σ_A increases beyond σ_{ULT} during phase (3), then K_0 will decrease and probably begins decreasing at the CP before that stress level is reached (see Figure 5.20)

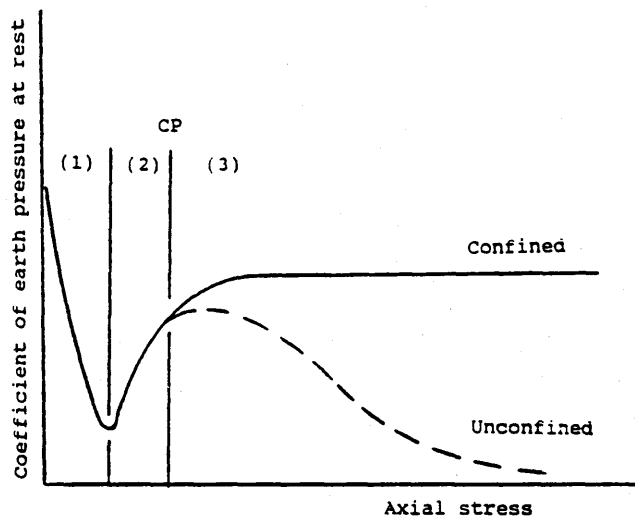


Figure 5.20 Typical form of graph of coefficient of earth pressure at rest against axial stress.

From Figure 5.20, once the CP is exceeded, K_0 results, obtained from confined compression tests, are not valid for sinkage situations in the field because the lateral stress generated would exceed the confining capability of the surrounding soil. The implications of this are that unless soil is saturated and rigidly confined, K_0 cannot be assumed to be constant as is commonly the case. This is also likely

to be the case for Poisson's ratio (μ). An indication of the variation in Poisson's ratio with increasing axial stress can be gained by assuming that elasticity theory applies to soils during loading. Poisson's ratio can be calculated from:-

$$\text{Poisson's ratio } \mu = \frac{K_o}{(1+K_o)}$$

The Poisson's ratio curve, therefore, is of a similar form to that of K_o , however, the values are somewhat lower. For plate sinkage situations, the path of K_o , or μ , with increasing axial stress will be dependent on the extent of each phase of compaction which takes place. Consequently, the K_o curve, in conjunction with a combined plate sinkage and confined compression stress-sinkage curve can yield a great deal of information regarding the way in which given soils deform under compression as illustrated in Figure 5.21.

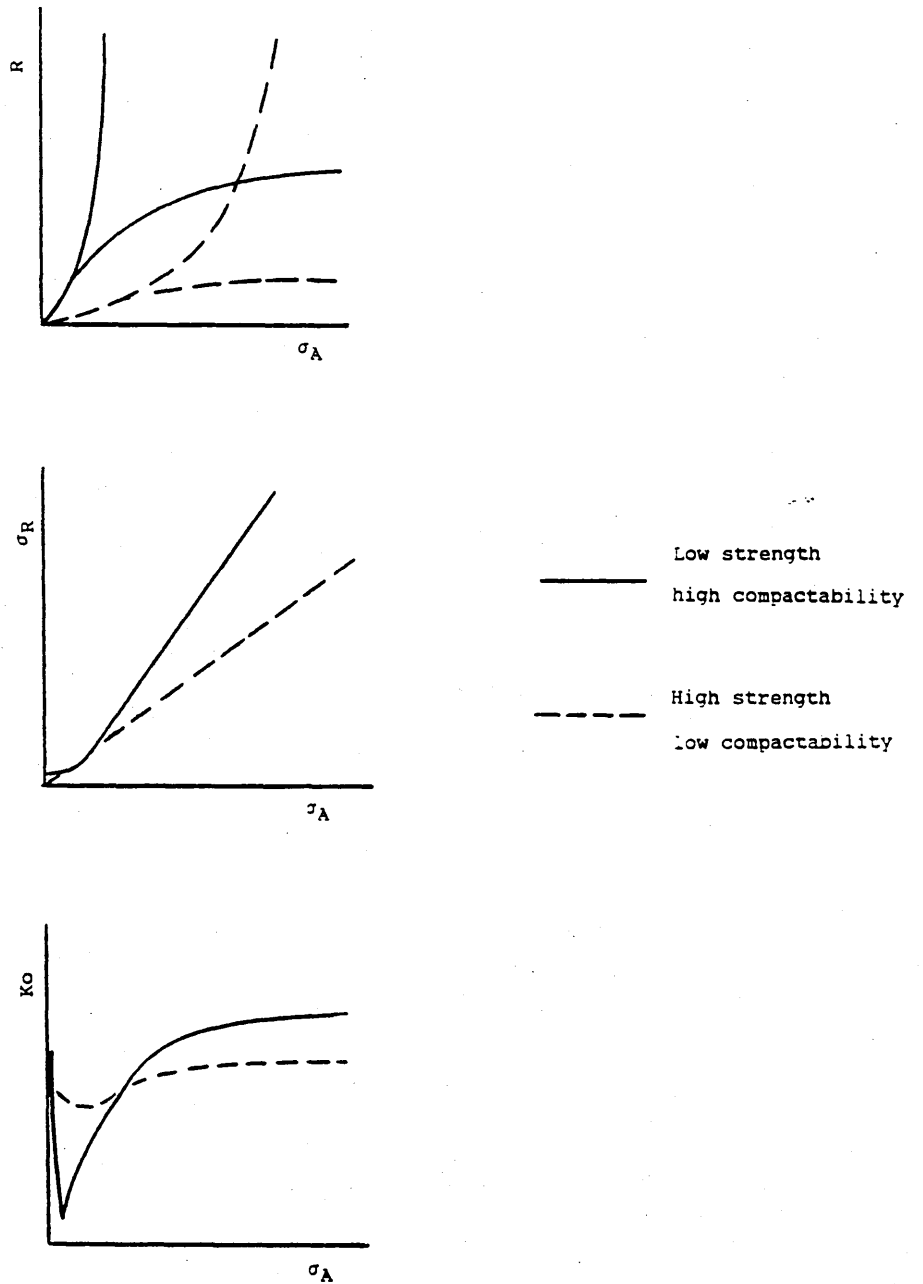


Figure 5.21 The interpretation of typical stress-sinkage and K_o graphs to assess the compactability of field soils.

From Figure 5.21, combinations and magnitudes of various parameters can be attributed to soil condition, in terms of compactability, in specific states. This, therefore, allows these parameters to be used, as shown in Table 5.2, to describe the soil deformation behaviour during compression. m_{CP} , defined as axial stress (σ_A)/sinkage (R) at the CP, is termed the compaction modulus and is a measure of soil compactability.

Table 5.2 The magnitude and combination of various parameters to which soil in given conditions can be attributed.

	σ_{ULT}	σ_{CP}	R_{CP}	m_{CP}	m_i	Ko dip	Final Ko
Compactable				LOW			
Non-compactable				HIGH			
Strong	HIGH				HIGH		LOW
Weak	LOW	LOW			LOW		HIGH
PHASE (1)						HIGH	
KEY	kPa	kPa	mm	kPa/mm			
LOW	<400	<200	<5	<5	<15	<.4	<.5
MEDIUM	400 to 700	200 to 350	5 to 15	5 to 15	15 to 30	.4 to .6	.50 to .75
HIGH	>700	>350	>15	>15	>30	>.6	>.75

5.2.2.5 Prediction of the extent of soil disturbance below a sinkage plate.

The trafficability and workability prediction procedures presented in Chapters 2 and 3, and that currently employed by the Soil Survey and Land Research Centre, are useful procedures for ranking soils in terms of available machinery workdays per year, however, they are general models and cannot be fine-tuned to predict the likely extent of damage resulting from loading by equipment of different sizes. Other workers, Erbach et al (1991) for example, have developed transducers to measure soil strain, however, the nature of these devices requires a certain degree of soil disturbance to take place during installing prior to loading.

Plate sinkage test data, combined with those from confined compression tests, can yield information regarding the amount of sinkage and mode of soil deformation for given loading situations. The analysis of data from these two tests can be extended to predict the extent of soil disturbance below the plate which is a function of soil type, packing state and moisture status. Soil deformation mode is governed by three phases, as discussed earlier in Section 5.2.2.4, and each will affect the extent of deformation differently. The failure mechanisms for the three phases are illustrated in Figure 5.22.

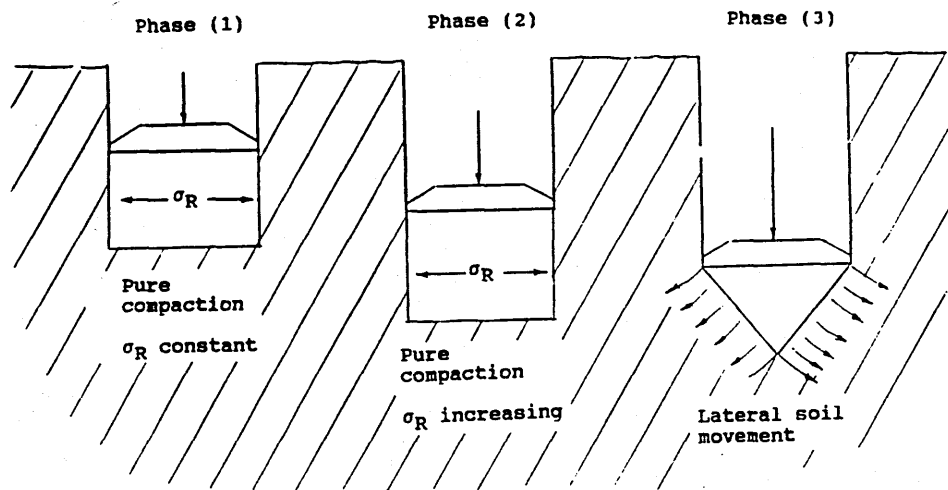


Figure 5.22 Failure mechanisms during plate sinkage tests.

Plate 5.1 shows the excavation following two plate sinkage tests performed on sandy loam soil in a soil bin. The soil was prepared in layers to facilitate observations of deformation below the plates. The overlay highlights the disturbed areas for:-

- (a) phase (3) deformation
- (b) phase (1)/(2) deformation

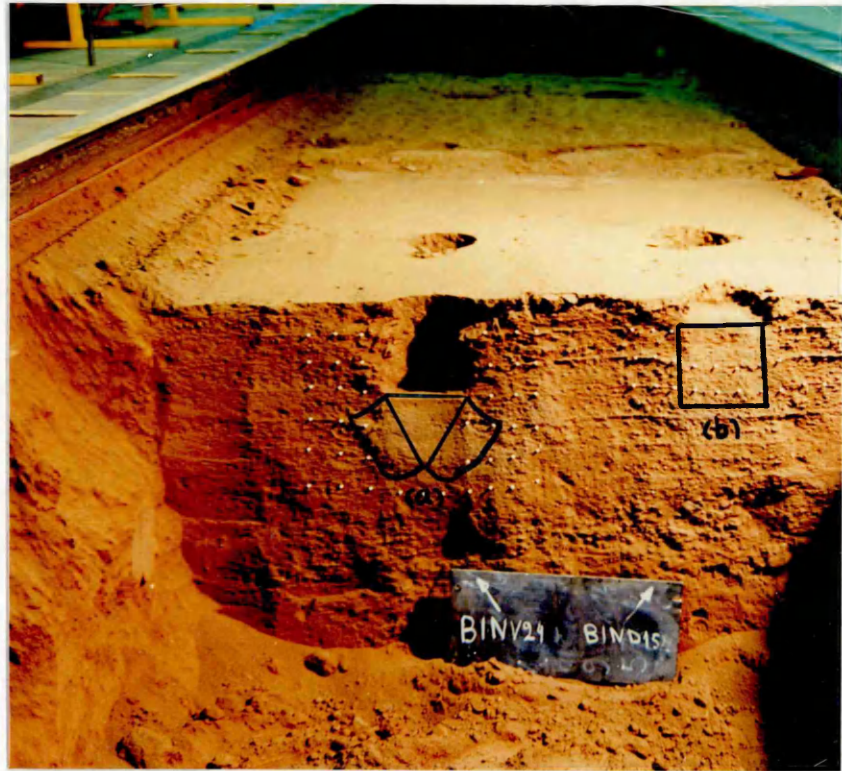


Plate 5.1 Section through two plate sinkage tests. Courtesy of A Alexandru.

Mathematical models for predicting the extent of soil disturbance below a sinkage plate, based on soil failure patterns observed in the soil bin, have been developed for each deformation phase and are presented separately in the following text.

Phase (1) deformation.

Consider the Phase (1) situation illustrated in Figure 5.23.

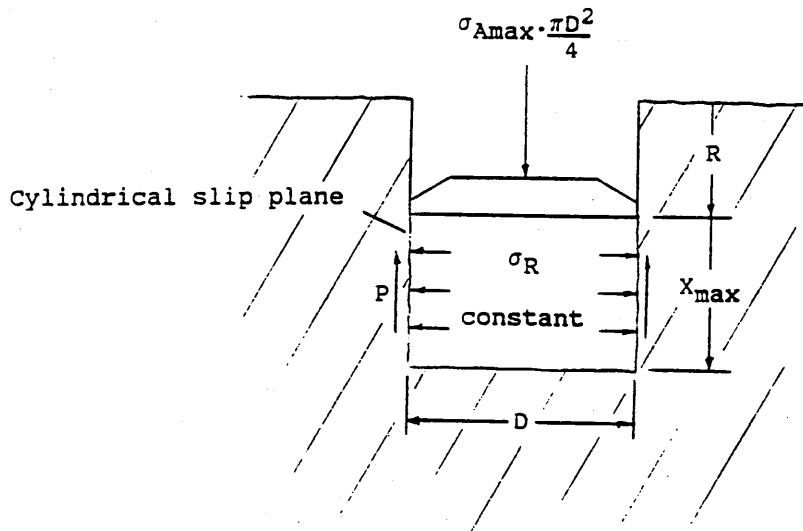


Figure 5.23 Diagram illustrating phase (1) failure below a sinkage plate.

From Coulomb, Shear stress $\Gamma = c + \sigma_R \tan \phi$ [1]

Where: c = cohesion (kPa)
 σ_R = radial stress (kPa)
 ϕ = angle of shearing resistance.

Radial stress remains constant during phase (1). Stress-strain curves for confined compression and plate sinkage tests follow similar paths during phase (1), and so the disturbed area can be assumed to be cylindrical. If equation [1] is multiplied throughout

by the area of the cylindrical slip plane, an expression is obtained for the total shear resistance P:-

$$P = \pi D X_{\max} (c + \sigma_R \tan \phi) \quad [2]$$

but total shear resistance P = force applied

$$P = (\sigma_{A\max} + \gamma(R + X_{\max})) \cdot \pi D^2 / 4 \quad [3]$$

where γ = bulk unit weight in kN/m^3

substituting [3] in [2] and rearranging:-

$$X_{\max} = \frac{D(\sigma_{A\max} + \gamma R)}{4(c + \sigma_R \tan \phi) - \gamma D}$$

Depth of disturbance from the soil surface:-

$$= \underline{\underline{R + X_{\max}}}$$

To predict the maximum dry bulk density (D_B) of the disturbed soil:-

$$\text{Initial } D_B = \frac{\text{mass of dry solids}}{\text{plate area} \cdot (R + X_{\max})} \quad [4]$$

$$\text{Average final } D_B = \frac{\text{mass of dry solids}}{\text{plate area} \cdot X_{\max}} \quad [5]$$

Substituting [4] in [5]:-

$$\text{Average final } D_B = \frac{\text{Initial } D_B (R + X_{\max})}{X_{\max}} \quad [6]$$

If dry bulk density is assumed to decrease linearly with X from a maximum at X=0 to the initial state at X=X_{max} then:-

$$\text{Average final } D_B = \frac{\text{Initial } D_B + D_{B\text{max}}}{2} \quad [7]$$

Substituting [6] in [7] and rearranging:-

$$D_{B\text{max}} = \frac{\text{Initial } D_B(2R + X_{\text{max}})}{X_{\text{max}}}$$

Phase (2) deformation.

During loading, the radial stress (σ_R) generated as a result of increasing axial stress (σ_A) follows the trend shown in Figure 5.19. If the shape of the curve is simplified as shown in Figure 5.24, it can be described mathematically provided that the maximum σ_A and σ_R during phase (1) are known.

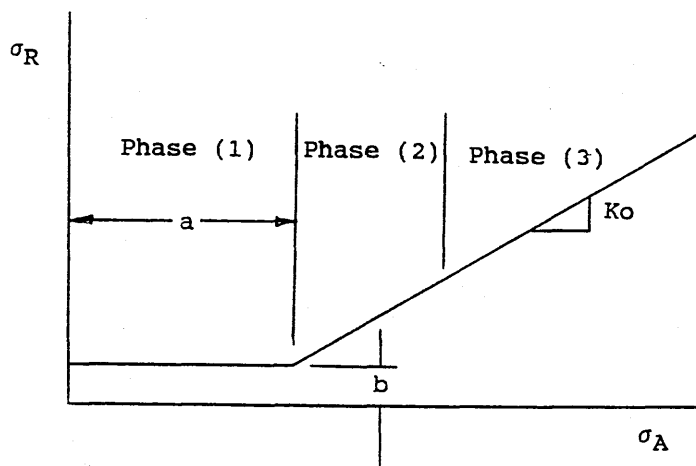


Figure 5.24 Simplification of relationship between radial stress (σ_R) against axial stress (σ_A) during a plate sinkage test.

During Phase (2) deformation, axial stress (σ_{Ap}), generated in the soil as a result of plate pressure, is assumed to be at a maximum immediately below the plate but tends towards zero at a point down the soil profile where soil remains undisturbed by the sinkage test. Conversely, axial stress due to soil weight (σ_{Aw}) is zero immediately below the plate and tends towards X_{max} at the limit of disturbance. Radial stress, therefore, may start in phase (2) of Figure 5.24, however, it will diminish with depth below the plate, reaching a constant minimum value b when axial stress no longer exceeds the maximum axial stress for phase (1), ie at $\sigma_A < a$. The two portions of Figure 5.24 can be described by:-

$$(1), \sigma_R = b \quad \text{For phase (1)}$$

$$(2), \sigma_R = b + K_o(\sigma_A - a) \quad \text{For phase (2)}$$

During phase (2), stress-strain curves for confined compression and plate sinkage tests coincide and so the disturbed zone below a sinkage plate can be assumed to be cylindrical and the situation illustrated in Figure 5.25 arises.

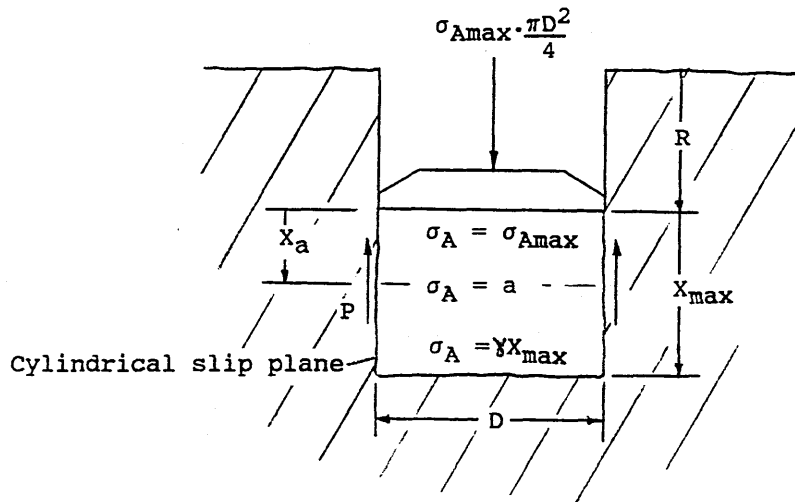


Figure 5.25 Schematic diagram of phase (2) deformation below a sinkage plate.

$$\text{Shear resistance } P = c.A + R.A \tan \phi$$

where A = cylindrical area

Integrating between 0 to X=X_a and X=X_a to X=X_{max}:-

$$P = \pi D \int_0^{X_a} \{c + \tan \phi [b + K_o(\sigma_A - a)]\} dx \text{ phase (2)}$$

$$+ \pi D \int_{X_a}^{X_{max}} \{c + b \tan \phi\} dx \text{ phase (1)} \quad [8]$$

To solve equation [8], an equation describing the decrease in σ_A with X is required. If σ_{Ap} is assumed to diminish linearly with X the relationship in Figure 5.26 is obtained.

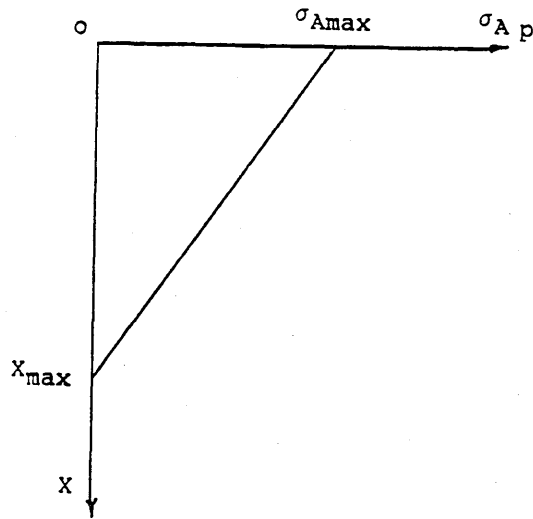


Figure 5.26 The assumed relationship between axial stress (σ_{Ap}) and distance below sinkage plate (X).

With reference to Figure 5.26, for a straight line:-

$$\sigma_{Ap} = \frac{-\sigma_{Amax} \cdot X + \sigma_{Amax} X_{max}}{X_{max}}$$

$$\sigma_{Ap} = \sigma_{Amax}(1 - X/X_{max}) \quad [9]$$

If σ_{Aw} is assumed to increase linearly with X the relationship illustrated in Figure 5.27 is obtained.

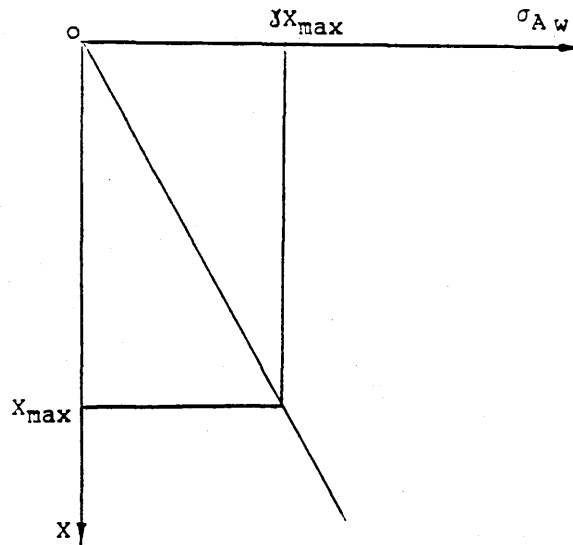


Figure 5.27 The assumed relationship between axial stress (σ_{Aw}) and distance below a sinkage plate (X).

With reference to Figure 5.27:-

$$\sigma_{Aw} = \gamma X \quad [10]$$

Total axial stress below a sinkage plate:-

$$\sigma_A = \sigma_{Ap} + \sigma_{Aw} \quad [11]$$

Substituting [9] and [10] in [11]:-

$$\sigma_A = \sigma_{Amax} \left(1 - \frac{X}{X_{max}}\right) + \gamma X \quad [12]$$

Substituting [12] in [8]:-

$$P = \int_0^{X_a} \pi D \{c + \tan\phi [b + K_o (X (\gamma - \frac{\sigma_{Amax}}{X_{max}}) + \sigma_{Amax} - a)]\} dx$$

$$+ \int_{X_a}^{X_{max}} \pi D \{c + b \tan\phi\} dx$$

Let $A = c + (b - a + K_o \cdot \sigma_{Amax}) \tan\phi$

Let $B = K_o \cdot (\gamma - \frac{\sigma_{Amax}}{X_{max}}) \tan\phi$

$$P = \int_0^{X_a} \pi D [A - Bx] dx + \int_{X_a}^{X_{max}} \pi D [c + b \tan\phi] dx$$

Integrating with respect to X:-

$$P/\pi D = X_a (A + BX_a / 2) + (c + b \tan\phi) (X_{max} - X_a) \quad [13]$$

From [12], if X_a occurs at a:-

$$a = X_a (\gamma - \frac{\sigma_{Amax}}{X_{max}}) + \sigma_{Amax} \quad \dots \quad X_a = \frac{a - \sigma_{Amax}}{\gamma - \frac{\sigma_{Amax}}{X_{max}}} \quad [14]$$

Substituting for A, B and [14] in [13]:-

$$P = \frac{(a - \sigma_{Amax})}{\gamma - \frac{\sigma_{Amax}}{X_{max}}} [c + (b - a + K_o \sigma_{Amax}) \tan\phi]$$

$$+ \frac{K_o (\gamma - \frac{\sigma_{Amax}}{X_{max}}) (a - \sigma_{Amax}) \cdot \tan\phi}{2}$$

$$+ (c + b \tan\phi) (X_{max} - \frac{(a - \sigma_{Amax})}{\gamma - \frac{\sigma_{Amax}}{X_{max}}}) \quad [15]$$

To solve equation [15], a value for the disturbed bulk unit weight is required. From equation [6], average disturbed bulk unit weight can be assumed to be:-

$$\gamma_{DIST} = \frac{\gamma(R + X_{max})}{X_{max}} \quad [16]$$

Substituting [16] in [15] and rearranging:-

$$\begin{aligned} \sigma_{Amax} = & \frac{4X_{max}(a - \sigma_{Amax})}{D(\gamma(R + X_{max}) - \sigma_{Amax})} [c + (b - a + K_0\sigma_{Amax})\tan\phi] \\ & + \frac{K_0(\gamma(R + X_{max}) - \sigma_{Amax})(a - \sigma_{Amax})\tan\phi}{2\gamma(R + X_{max}) - \sigma_{Amax}} \\ & + \frac{4X_{max}(c + b\tan\phi)}{D} \left(1 - \frac{a - \sigma_{Amax}}{\gamma(R + X_{max}) - \sigma_{Amax}}\right) \quad [17] \end{aligned}$$

Depth of disturbance from the soil surface:-

$$= \underline{\underline{R + X_{max}}}$$

Equation [17] can be solved iteratively to predict X_{max} and hence depth of disturbance from the soil surface. These calculations are lengthy but could be readily solved using computers.

Phase (3) deformation.

During phase (3) deformation, the confining stress of the soil surrounding the sinkage plate is exceeded allowing soil below the plate to deform laterally, compacting/deforming the surrounding soil. Prandtl (1920 & 1921), Terzaghi (1943) and Meyerhof (1951 & 1961) proposed that the failure pattern in close proximity to foundations can be approximated by a logarithmic spiral. If this is assumed to apply to soil deformation below a sinkage plate during phase (3), then the situation illustrated in Figure 5.28 arises.

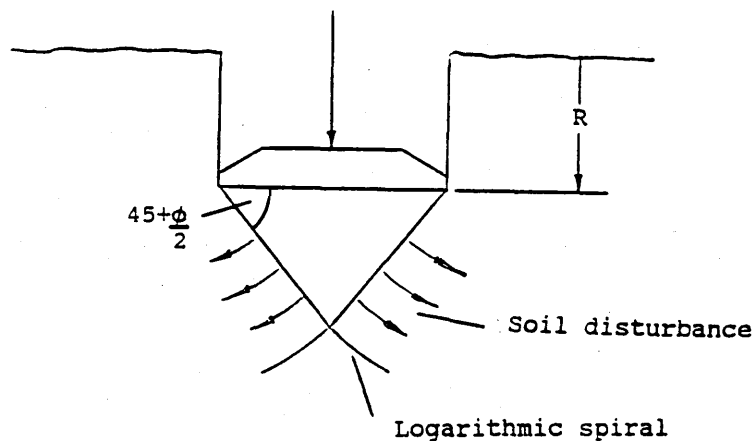


Figure 5.28 Diagram of the failure pattern assumed to occur below a sinkage plate during phase (3) deformation.

A stable cone of soil forms under the plate causing lateral displacement and compaction of soil. The potential failure plane,

approximated by a logarithmic spiral, can be described by the following equation:-

$$r_1 = r_0 e^{w \tan \phi}$$

where: r_1 = radius
 r_0 = length of cone face
 w = angle (in radians) of r_1 from r_0
 ϕ = angle of shearing resistance

During phase (3) deformation, the extent of lateral disturbance depends, not only on soil mechanical factors but also, on the depth of sinkage, see Figure 5.29.

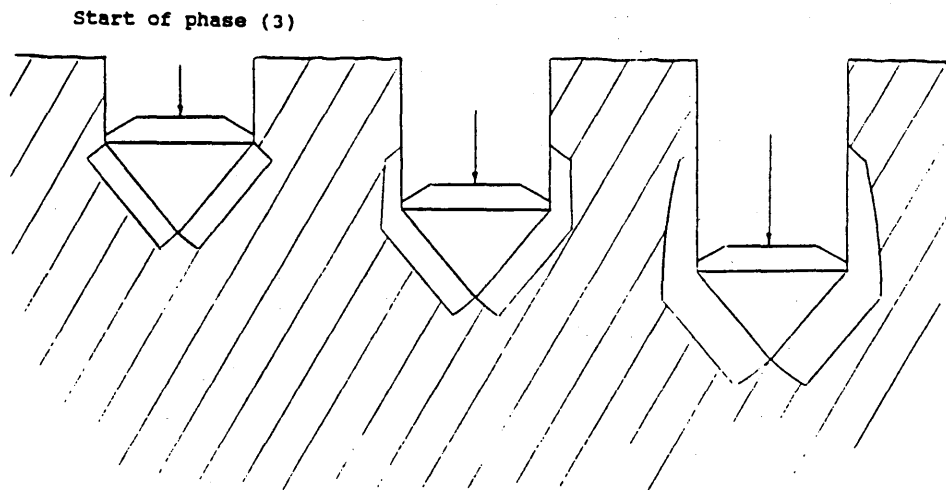


Figure 5.29 Diagram illustrating the effect of sinkage depth on lateral disturbance below a sinkage plate.

The failure patterns in Figure 5.29 are complex to analyse. The extent of lateral disturbance relative to the plate centre lies in the range $D/2$ to some maximum value dependent on depth of sinkage (R) and resistance to shear along the slip planes.

The following procedure was used to develop mathematical expressions for predicting the extent of disturbance during phase (3) deformation.

Determination of extent of soil disturbance.

With reference to Figure 5.30(a), as deformation passes from phase (2) to (3), soil is assumed to be disturbed laterally a distance β_1 along the slip plane.

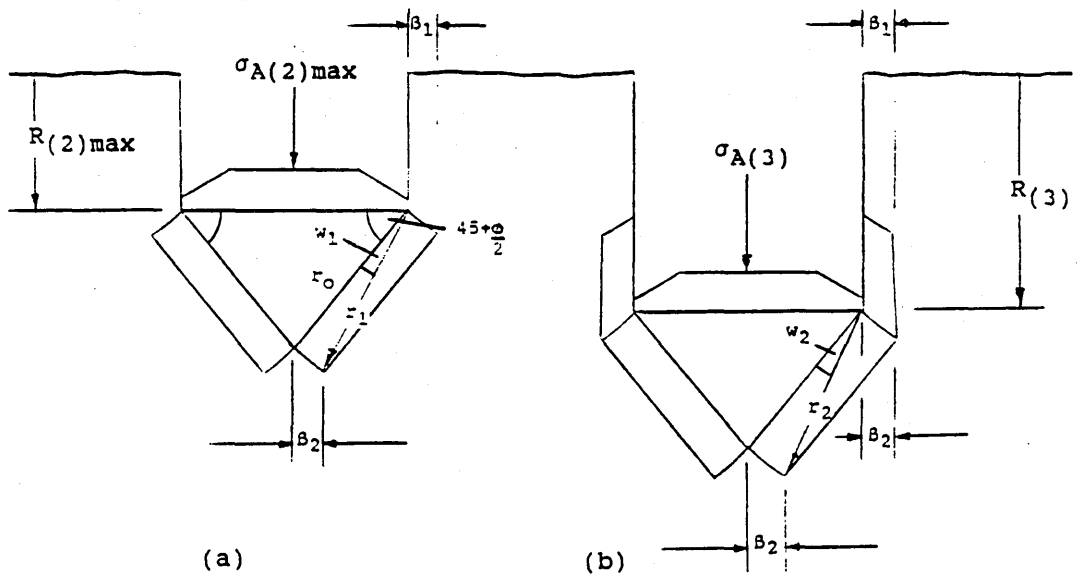


Figure 5.30 Diagram illustrating soil disturbance below a sinkage plate.

As load is increased and the plate sinks below $R_{(2)\max}$, lateral disturbance is increased further to β_2 .

A mathematical expression can be developed for phase (3) deformation by balancing the moment of forces about the pole of the logarithmic spiral. Components of the final expression, considered separately in the following text, are:-

Passive force due to the applied load	(F_f)
Soil weight on lower slip-plane	(W_1)
Soil weight on upper slip-plane	(W_2)
Cohesive force along lower slip-plane	(cA)
Resultant of normal and frictional forces along upper slip-plane	(F_2)

Determination of passive force F_f

With reference to Figure 5.31, the disturbed soil surrounding the soil cone is subject to passive earth pressure F_p .

The proportion and direction of σ_A resulting in passive pressure is governed by the cohesion c and the resultant F_p of the normal and frictional stresses along ab .

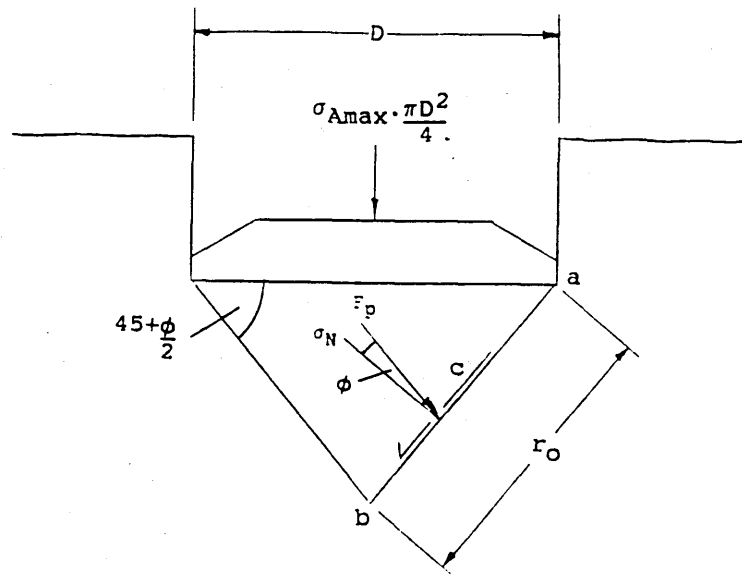


Figure 5.31 Diagram of forces acting on soil surrounding a sinkage plate.

From Coulomb:-

$$\begin{aligned} \text{Shear stress } \Gamma &= c + \sigma_N \tan \phi \\ &= c + F_p \end{aligned}$$

$$F_p = \sigma_N \tan \phi$$

F_p can be expressed in terms of force F_f by multiplying F_p by the cone area:-

$$F_f = F_p \cdot \text{area} = \sigma_N \tan \phi \cdot \text{cone area} \quad [18]$$

From a vector diagram of forces:-

The diagram consists of two parts. The top part shows a downward vertical force vector labeled $\frac{\sigma_{Amax} \cdot \pi D^2}{4}$. From its base, a vector labeled N extends downwards and to the right. A right-angled triangle is formed with the vertical force as the hypotenuse and N as one side. The angle between the vertical force and N is $45 + \frac{\phi}{2}$. The top part of the diagram is associated with the equation $N = \frac{\pi D^2 \sigma_A \cos(45 + \phi/2)}{4}$. The bottom part shows a right-angled triangle with a vertical side labeled N and a horizontal side labeled T . The hypotenuse is labeled $\frac{\sigma_{Amax} \cdot \pi D^2}{4}$. The angle between the vertical side N and the hypotenuse is $45 - \frac{\phi}{2}$. The angle between the horizontal side T and the hypotenuse is $45 + \frac{\phi}{2}$. The bottom part of the diagram is associated with the equation $\sigma_N = \frac{N}{\text{cone area}} = \frac{\pi D^2 \sigma_A \cos(45 + \phi/2)}{4 \cdot \text{cone area}}$ [19].

Substituting [19] in [18]

$$F_f = \frac{\pi D^2 \sigma_A \cos(45 + \phi/2) \tan \phi}{4} \quad [20]$$

Location of slip planes

Consider the force diagram, Figure 5.32, for the failure zone to the right of the plate centre line when sinkage is at a maximum for phase (2).

The forces acting on obdegh are:-

- W_1 = weight of soil on lower slip-plane
- W_2 = weight of soil on upper slip-plane
- F_1 = resultant of normal and frictional forces along bd
- F_2 = resultant of normal and frictional forces along oe
- F_f = passive earth force
- $c.A_1$ = resultant of the cohesive force along bd
- $c.A_2$ = resultant of the cohesive force along oe
- $c.A_w$ = the cohesion along ob

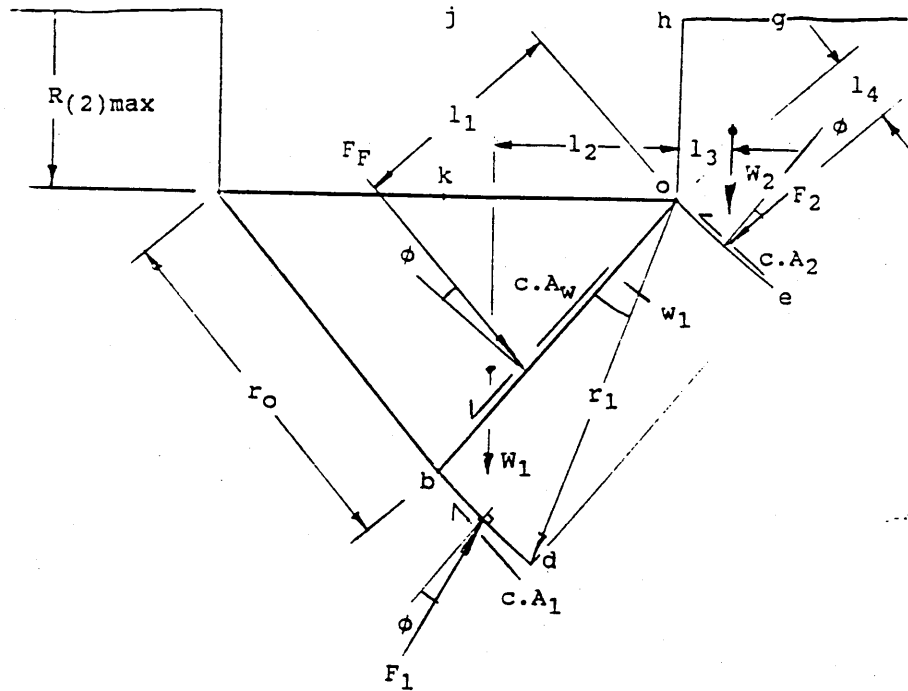


Figure 5.32 Force diagram (RHS only) for the failure zone under a sinkage plate at maximum phase (2) sinkage.

The pole of the logarithmic spiral is located at o . Every radius of the spiral makes an angle ϕ with the normal to the spiral at the point where it intersects the curve and so F_1 also makes an angle ϕ with the normal and lies in the direction of o .

Determination of moment about the pole

With reference to Figure 5.32, equilibrium of moments requires that the sum of moments about the pole o is zero.

The direction of F_1 , and c along ob , pass through o and therefore have no moment about o . The moment due to cohesion along oe can likewise be assumed to be zero.

Taking moments about o :-

$$F_f \cdot l_1 = -W_1 \cdot l_2 + W_2 \cdot l_3 + M_c + F_2 \cdot l_4 \quad [21]$$

where M_c is the moment due to cohesion along bd

Determination of weight W_1 :-

With reference to Figure 5.33, weight W_1 can be assumed to comprise weight of soil in $bdej$ at the undisturbed bulk density because soil from area $ohjk$ has been compacted and moved vertically downwards, but still contributes to W_1 .

Assume $W_1 = \text{initial bulk unit weight} \times \text{shaded area } A_d$

$$W_1 = \beta(R + R_d) \quad \text{but:-}$$

$$R_d = r_3 \cos(45 - (\phi/2) - w_1/2) \quad \text{where } w_1 = (180/\pi) \ln(r_1/r_o) \cot \phi$$

$$\text{and } r_3 = r_o e^{(w_1/2) \tan \phi} = r_o e^{(1/2) \ln(r_1/r_o)}$$

$$\therefore W_1 = \beta \{ R$$

$$+ r_o e^{(1/2) \ln(r_1/r_o)} \cdot \cos(45 - (\phi/2) - (180/2\pi) \ln(r_1/r_o) \cot \phi) \} \quad [22]$$

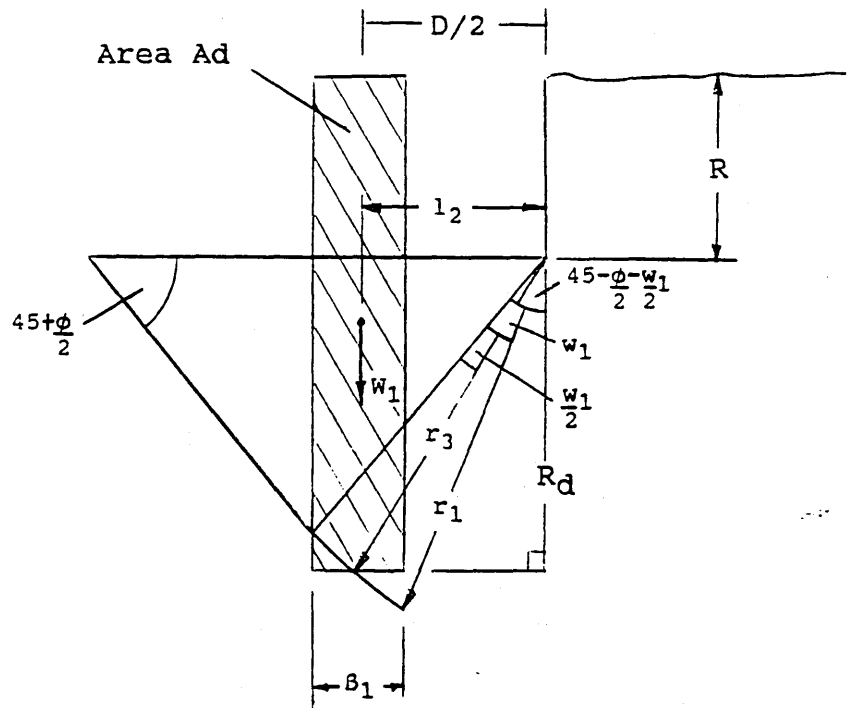


Figure 5.33 Diagram to illustrate computation of A_d , W_1 and l_2 .

Determination of l_2 :-

With reference to Figure 5.33:-

$$l_2 = -\left(\frac{D}{2} - \frac{\beta}{2}\right) = -\frac{(D - \beta)}{2}$$

[23]

Determination W_2 :-

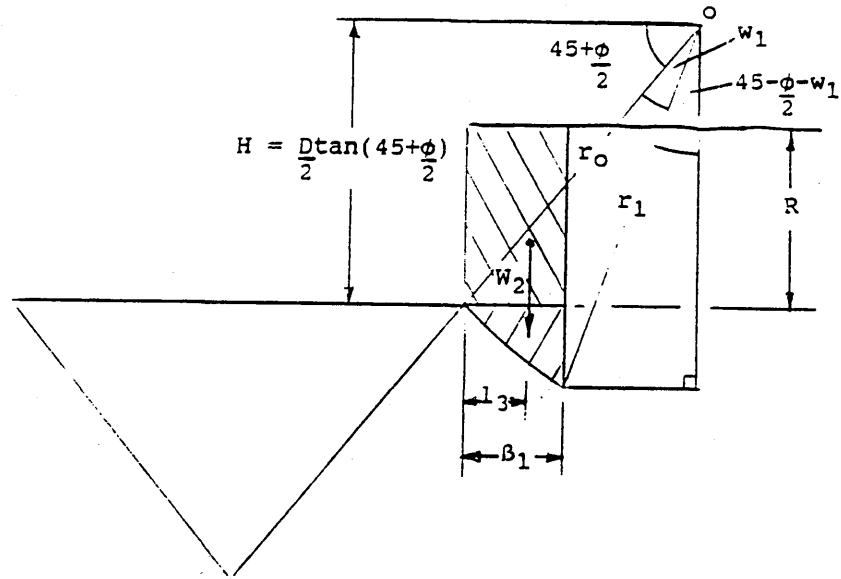


Figure 5.34 Diagram illustrating the computation of soil weight W_2 .

With reference to Figure 5.34:-

Assume the shaded area above the slip-plane comprises a rectangle and a triangle.

$$\begin{aligned}
 W_2 &= \gamma \beta R + \beta/2 [(D/2)\tan(45+\phi/2) - r_1 \cos(45-(\phi/2)-w_1)] \\
 &= \gamma \beta [R + (D/4)\tan(45+\phi/2) - (r_1/2)\cos(45-(\phi/2) - (180/\pi)\ln(r_1/r_0)\cot\phi)] \quad [24]
 \end{aligned}$$

Determination of I_3 :-

With reference to Figure 5.34:-

Assume $I_3 = \beta/2$ for the rectangle, and

$$I_3 = 2\beta/3 \text{ for the triangle.} \quad [25]$$

Determination of cohesion along slip plane bd:-

The shearing force on an elemental length Δs is $c \cdot \Delta s$, see Figure 5.35.

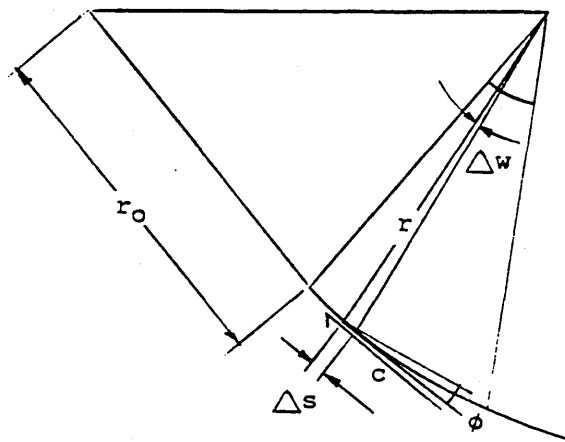


Figure 5.35

Diagram illustrating the computation of moment due to cohesion for soil failure below a sinkage plate.

Moment about o:-

$$\Delta M_C = r.c.\Delta s.\cos\phi$$

$$\text{but } \Delta s.\cos\phi = r.\Delta\theta$$

$$\Delta M_C = cr^2 \Delta\theta$$

Integrating for all values of w from 0 to w_1 to derive an expression for the total cohesion along bd:-

$$M_C = \int_0^{w_1} \Delta M_C = \int_0^{w_1} cr^2 d\theta \quad \text{where } r = r_0 e^{w \tan\phi}$$

$$M_C = c \int_0^{w_1} r_0^2 e^{2w \tan\phi} d\theta = \frac{c[r_0^2 e^{2w \tan\phi}]}{2 \tan\phi} \Big|_0^{w_1}$$

$$M_C = \frac{c}{2 \tan\phi} (r_1^2 - r_0^2) \quad [26]$$

Determination of F_2 :-

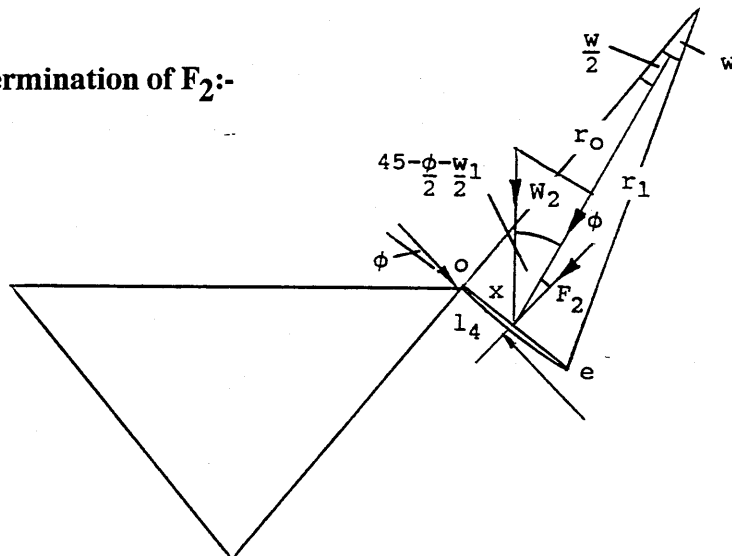


Figure 5.36 Diagram illustrating the determination of F_2 .

With reference to Figure 5.36:-

$$\begin{aligned} F_2 &= N \tan \phi \\ &= W_2 \cos(45 - (\phi/2) - (90/\pi)w_1) \tan \phi \\ &= W_2 \cos(45 - (\phi/2) - (90/\pi) \ln(r_1/r_0) \cot \phi) \tan \phi [27] \end{aligned}$$

Determination of l_4 :-

With reference to Figure 5.36, Assume F_2 acts halfway along cord oe .

$$\begin{aligned} x &= r_0 \sin[90w_1/\pi] \\ l_4 &= r_0 \sin[90w_1/\pi] \cos \phi \\ &= r_0 \sin[(90/\pi) \ln(r_1/r_2) \cot \phi] \cos \phi \quad [28] \end{aligned}$$

Determination of l_1 :-

Determination of the point of application of F_p is complex and therefore assumptions concerning its position are required to simplify the analysis. Terzaghi (1943) developed a technique for solving passive earth pressure of cohesive soils on walls.

This involved the resolving of the pressure into two parts:-

- (1) that due to soil weight alone which acts at a point $2/3$ down the wall, and
- (2) that due to cohesion and any surcharge which acts halfway down the wall.

Terzaghi (1943) points out that the subdivision of passive pressure into two parts is strictly correct only when the back of the wall is vertical and perfectly smooth. For all other conditions the procedure is approximate. If the point of application of F_p is assumed to lie in the range $1/2$ to $2/3$ down the wedge face, r_1 can be determined by following an iterative procedure. In practice, the use of one or the other positionings makes little difference to the prediction of r_1 . With reference to Figure 5.37, a range within which l_1 lies can be determined.

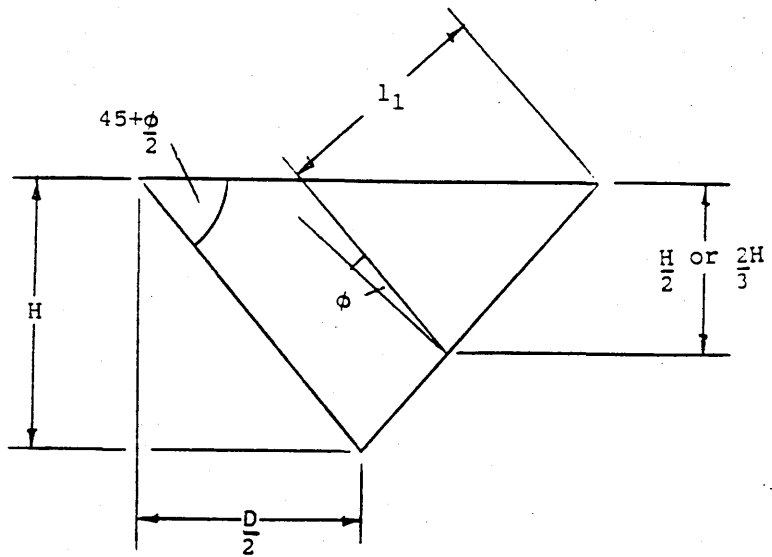


Figure 5.37 Diagram illustrating the determination of the point of application of passive pressure l_1 below a sinkage plate.

$$l_1 = \frac{(H/2) \text{ to } (2H/3) \cdot \cos\phi}{\sin(45+\phi/2)}$$

But $H = (D/2)\tan(45+\phi/2)$ and therefore

$$l_1 = (D/4)\operatorname{cosec}(45+\phi/2)\cos\phi \text{ to } (D/3)\operatorname{cosec}(45+\phi/2)\cos\phi \quad [29]$$

Determination of disturbed distance β :-

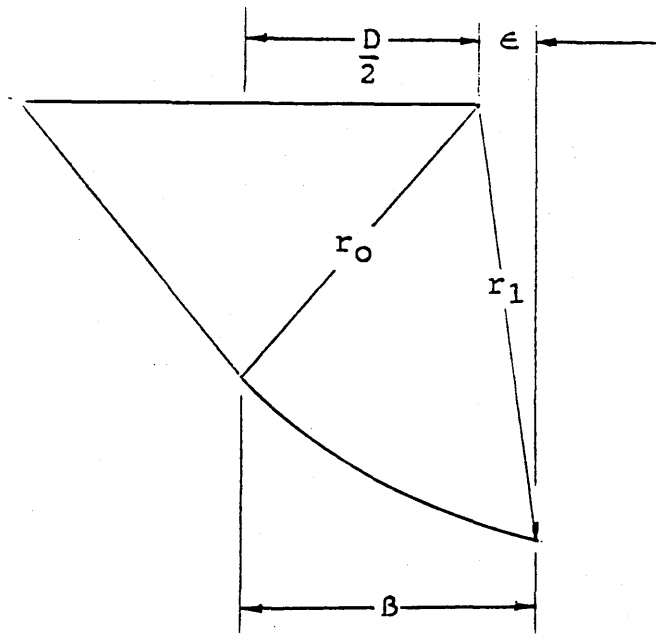


Figure 5.38 Diagram illustrating the computation of disturbed distance β .

With reference to Figure 5.38.

$$\beta = \frac{D}{2} + \epsilon$$

$$\beta = \frac{D}{2} + r_1 \cos\left(180 - \left(45 + \frac{\phi}{2} - w_1\right)\right)$$

but $r_1 = r_0 e^{w_1 \tan \phi}$, $\therefore w_1 = \ln \left[\frac{r_1}{r_0} \right] \cot \phi$

$$\beta = \frac{D}{2} + r_1 \cos\left(135 - \frac{\phi}{2} - \frac{180}{\pi} \ln \left[\frac{r_1}{r_0} \right] \cot \phi\right) \quad [30]$$

Derivation of general equation

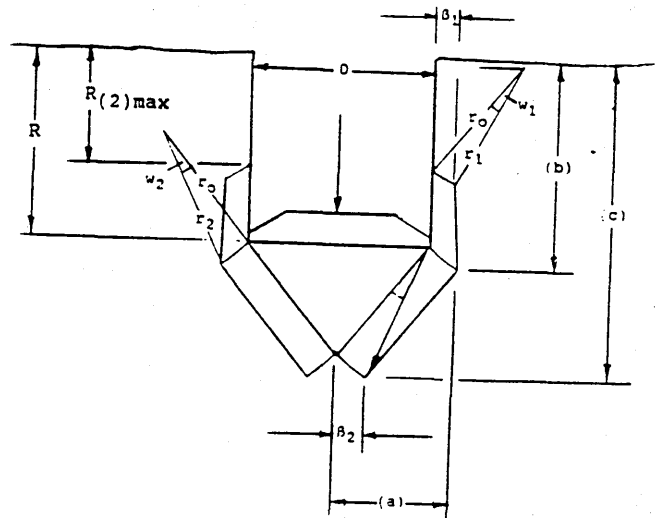
Substituting [20], [22], [23], [24], [25], [26], [27], and [28] in [21]:-

$$\begin{aligned}
 & \frac{\pi D^2 \sigma_A \cos(45+\phi) \tan\phi \cdot l_1}{4} = \\
 & - \gamma \beta \left\{ R + r_0 e^{(1/2) \ln(r_1/r_0)} \cdot \cos\left(45 - \frac{\phi}{2} - \frac{180}{2\pi} \ln \left[\frac{r_1}{r_0} \right] \cdot \cot\phi \right) \right\} \frac{(D-\beta)}{2} \\
 & + \frac{c}{2 \tan\phi} (r_1^2 - r_0^2) \\
 & + \gamma \beta^2 \left[\frac{R}{2} + \frac{D \tan(45+\phi)}{6} - \frac{r_1}{3} \cos\left(45 - \frac{\phi}{2} - \frac{180}{\pi} \ln \left[\frac{r_1}{r_0} \right] \cdot \cot\phi \right) \right] \\
 & + \gamma \beta \left[R + \frac{D \tan(45+\phi)}{4} - \frac{r_1}{2} \cos\left(45 - \frac{\phi}{2} - \frac{180}{\pi} \ln \left[\frac{r_1}{r_0} \right] \cdot \cot\phi \right) \right] \\
 & \cdot \cos\left(45 - \frac{\phi}{2} - \frac{90}{\pi} \ln \frac{r_1}{r_0} \cdot \cot\phi \right) r_0 \sin\left(\frac{90}{\pi} \ln \left[\frac{r_1}{r_0} \right] \cdot \cot\phi \right) \sin\phi \quad [31]
 \end{aligned}$$

By substituting for l_1 , equation [29], and β , equation [30], in equation [31], r_1 can be determined at the phase (2) threshold. r_2 can be determined using the same equation by substituting new values for σ_A and R .

β_1 and β_2 can be evaluated by substituting values for r_1 and r_2 respectively in equation [30].

β_1 and β_2 , in conjunction with a scale drawing, can be used to predict the extent of soil disturbance resulting from plate sinkage tests, see Figure 5.39.



- (a) Maximum extent of lateral disturbance.
- (b) Depth at which (a) occurs from soil surface.
- (c) Maximum extent of vertical disturbance.
- (β_2) Location of (c) from the plate centre line.

Figure 5.39 Diagram illustrating prediction of the extent of soil disturbance resulting during a plate sinkage test.

With reference to Figure 5.39, the dimensions (a), (b) and (c) can be determined using trigonometry:-

$$(a) = \frac{D}{2} + \beta_2$$

$$(b) = R + r_2 \cos\left(45 - \frac{\phi}{2} - \frac{180}{\pi} \ln \left[\frac{r_2}{r_0} \right] \cdot \cot \phi\right) -$$

$$r_0 \cos\left(45 - \frac{\phi}{2}\right)$$

$$(c) = (b) + r_0 \cos\left(45 - \frac{\phi}{2}\right)$$

Worked examples using the prediction theory for phases (1), (2) and (3) are presented in Appendix 6.

CHAPTER SIX

QUANTIFICATION OF THE COMPACTIVE NATURE OF SOIL (PART II)

Introduction

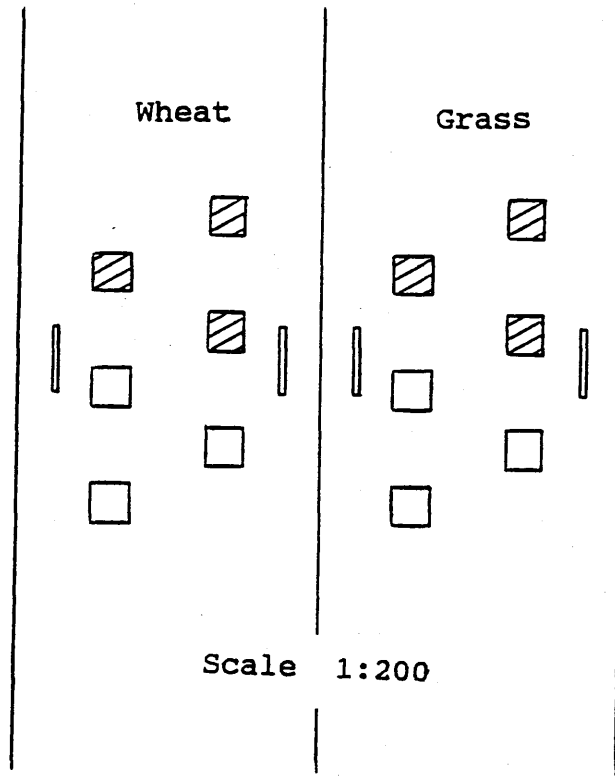
Techniques for quantifying the compactive nature of soil have been described in Chapter 5. In Chapter 6, the application of these techniques, to two soil types, is described including field work and prediction of the extent of soil disturbance resulting from loading. Results from a sensitivity analysis applied to the prediction model are also presented to examine the implications of varying the area and magnitude of applied loads on soil disturbance.

6.1 Field work

Soil physical and mechanical properties are generally dependent on the soil moisture status. Resources did not allow tests at a wide range of soil moisture contents and hence it was decided to carry out field work on two soil types in a reference state. Field capacity

was chosen as the reference state because water is able to drain readily over a short period of time as the soil profile moves from a state of saturation to field capacity. Once field capacity is reached, further increase in soil strength, through evapotranspiration, will be slow particularly in the subsoil.

Field trials were carried out on the Evesham soil series, under grass and oats, and the Bearsted series under grass and winter wheat to test the proposed compaction and compactability assessment procedures. The Evesham site was the same site studied in Chapters 2 and 3. The Bearsted site is located in Sandpit Field, Silsoe College Farm, and a site plan is given in Figure 6.1. The topsoil extends to a depth of approximately 300 to 350mm and is described as a slightly stony sandy loam (11% clay, 33% silt) of moderately weak soil and ped strength (Verma and Bradley, 1988). Two nests of septum tensiometers were installed at depths of 50, 150, 350, 550, 750, and 950mm.






-  Soil plateau - 50mm deep
-  Soil plateau - 300mm deep
-  Nest of tensiometers

Figure 6.1 Site plan for the Bearsted soil series.

Field work involved:-

- (1) monitoring the tensiometers
- (2) performing confined compression tests: three replicates at both 50 to 200mm and 300 to 450mm depth, and
- (3) performing plate sinkage tests: three replicates at both 50 and 300mm depth.

Three plateaus of 1m^2 were excavated at 50 and 300mm depth on the grass and arable plots at both sites giving a total of 24 plateaus. Confined compression and plate sinkage tests were carried out on each plateau (see Figure 6.2).

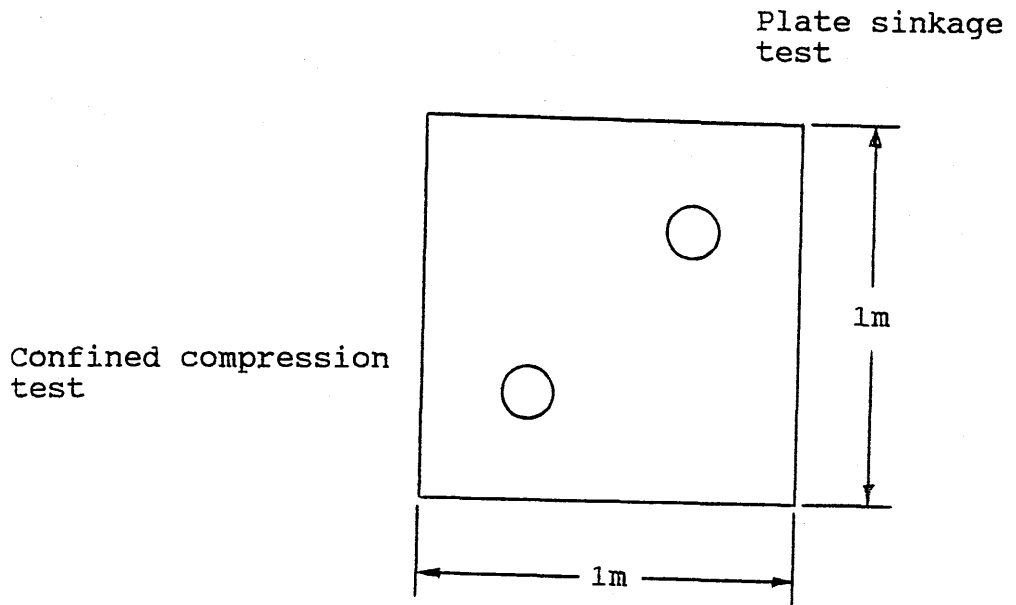


Figure 6.2 Plan view of plateaus and positioning of the soil tests.

Field work was carried out in January 1990 on days when no rain had fallen for 48 hours following heavy rain and the soil profiles could be considered to be at field capacity. Data from the two nests of tensiometers were averaged for each plot and the soil water suction profiles are shown in Figure 6.3.

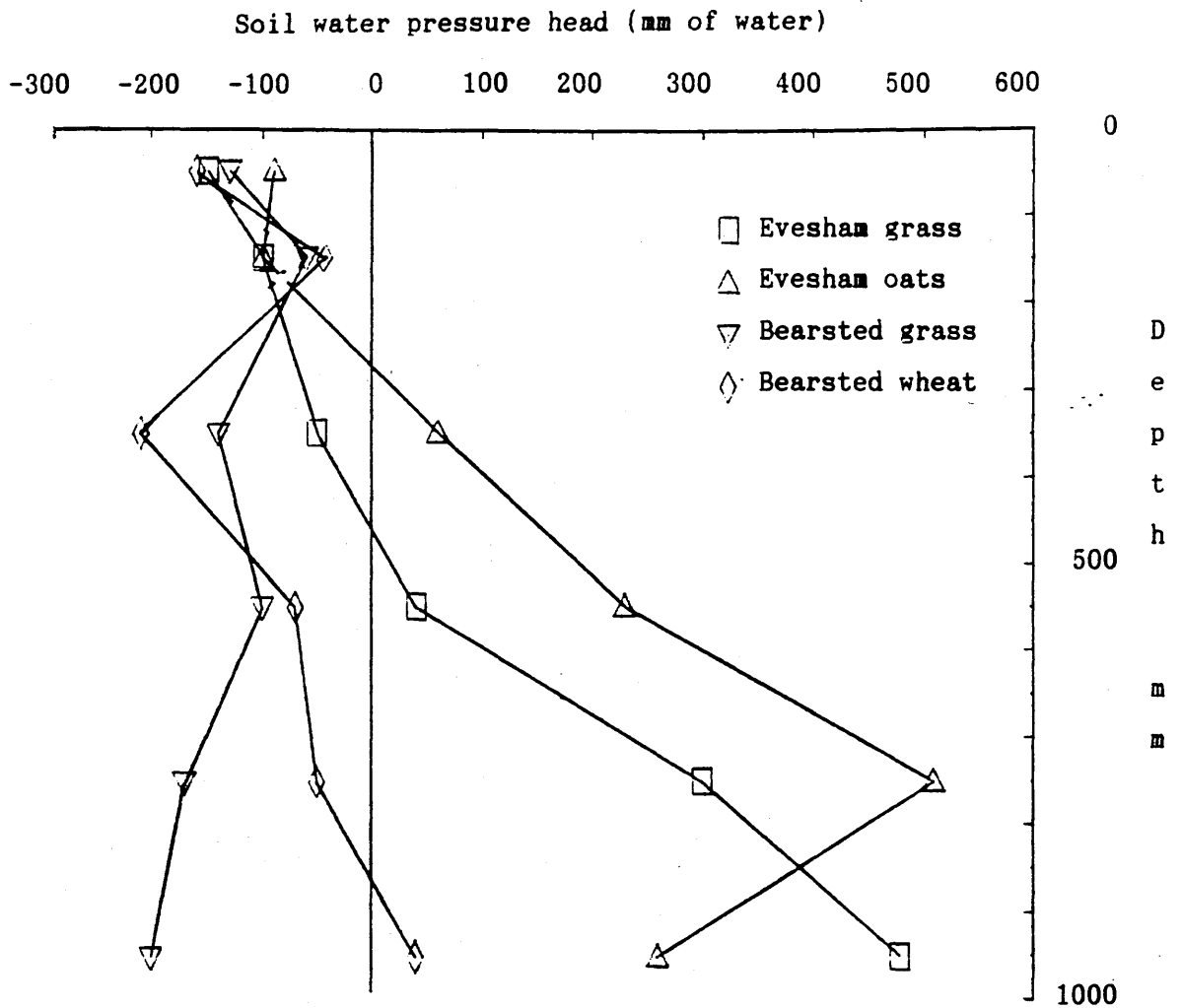


Figure 6.3 Soil water suction profiles for the four trial plots on the test days.

Low suctions (<200mm of water) occurred for all plots on the test days. A water table depth of 300 to 450mm existed in the Evesham plots despite 48 hours drainage taking place following saturation. This would suggest that the deeper soil cores, taken for the confined compression test, would be close to saturation, rather than field capacity, and therefore not very compactable.

6.2 Results.

6.2.1 CLASSIFICATION RESULTS FOR INITIAL SOIL CONDITION.

The dry bulk density, soil water pressure, degree of saturation, packing density and initial modulus for soils at both field sites are given in Table 6.1.

Table 6.1 Initial soil parameters for the two field sites.

Plot	Depth (mm)	Db (kg/m ³)	h (mm)	S (%)	Ld (kg/m ³)	mi (MN/m ³)
Evesham	50-200	1045	-125	78.7	1675	16.5
Grass	300-450	1186	+15	75.7	1807	16.6
Evesham	50-200	884	-95	63.7	1514	4.5
Oats	300-450	1152	+80	81.6	1773	24.0
Bearsted	50-200	1612	-95	69.7	1711	51.2
Grass	300-450	1522	-120	35.6	1585	33.5
Bearsted	50-200	1468	-110	67.1	1567	13.3
Wheat	300-450	1533	-155	41.2	1596	20.0

The soil parameters for the eight plots under investigation, presented in Table 6.1, have been analysed in terms of packing state and deformability and the results are given in Table 6.2.

Table 6.2 Initial characterisation of the field sites

Soil series	Crop	Depth (mm)	Packing state	Strength rating	Failure mode
Evesham	Grass	50	Med 4	Med 6	Dis
		300	High 1	Med 5	Dis
	Oats	50	Med 8	Low 8	Com or Dis
		300	High 2	Med 3	Dis
Bearsted	Grass	50	Med 3	High 1	Com or Dis
		300	Med 6	High 2	Com or Dis
	Wheat	50	Med 7	Low 7	Com or Dis
		300	Med 5	Med 4	Com or Dis

NB Com = compaction, Dis = displacement.

From Table 6.2, The soils can be ranked in terms of initial packing state and strength. For example, the Evesham series grass plot at 300mm depth has a high packing density, possibly due, in part, to past cultivation practices, but also as a result of a dry summer the previous year preventing the soil from swelling to its full potential. Soil strength is classed as medium and the suggested mode of subsequent failure is predominantly one of displacement. For the Bearsted soil series, degree of saturation (S) may not be a good prediction parameter for the mode of failure because the soil is freely draining and S rarely exceeds 70%.

6.2.2 RESULTS FOR SOIL BEHAVIOUR UNDER LOAD

Results from the four plots at 50 and 300mm depth are presented in Table 6.3.

Table 6.3 Confined compression (CC) and plate sinkage (PS) test results for Evesham and Bearsted soil series under grass and arable crops.

Soil series	Crop	Depth (mm)	Test	m_i (kPa/mm)	R_{ULT} (mm)	σ_{ULT} (kPa)	C (kPa)	n	R^2	F	σ_{CP} (kPa)	R_{CP} (mm)
Evesham	Grass	50	CC	10.55939	21.82	-	-	61	0.95	<0.001		
			PS	34.98911	-	366.43	-	142	0.97	<0.001	(172.88, 9.35)	
			CC/PS	16.48835	-	-	11.16208	167	0.91	<0.001		
Evesham	Grass	300	CC	8.13452	18.24	-	-	44	0.90	<0.001		
			PS	34.37600	-	392.66	-	110	0.92	<0.001	(184.31, 10.11)	
			CC/PS	16.58743	-	-	16.40559	35	0.72	<0.001		
Evesham	Oats	50	CC	3.67153	27.34	-	-	38	0.94	<0.001		
			PS	8.49254	-	246.11	-	98	0.88	<0.001	(67.82, 11.02)	
			CC/PS	4.53858	-	-	12.75294	32	0.68	<0.001		
Evesham	Oats	300	CC	20.47751	18.83	-	-	34	0.97	<0.001		
			PS	129.32110	-	268.72	-	63	0.82	<0.001	(203.69, 6.51)	
			CC/PS	24.03659	-	-	33.57636	27	0.74	<0.001		
Bearsted	Grass	50	CC	25.86402	21.93	-	-	67	0.91	<0.001		
			PS	84.86413	-	1018.60	-	87	0.69	<0.001	(457.62, 9.79)	
			CC/PS	51.23044	-	-	2.33014	83	0.82	<0.001		
Bearsted	Grass	300	CC	38.73725	22.37	-	-	40	0.77	<0.001		
			PS	58.53000	-	742.62	-	134	0.96	<0.001	(160.24, 3.49)	
			CC/PS	33.45579	-	-	0.66380	19	0.44	<0.010		
Bearsted	Wheat	50	CC	11.05677	25.20	-	-	55	0.89	<0.001		
			PS	18.44186	-	404.40	-	75	0.97	<0.001	(86.54, 5.97)	
			CC/PS	13.32411	-	-	-3.93932	28	0.65	<0.001		
Bearsted	Wheat	300	CC	14.44654	36.65	-	-	64	0.70	<0.001		
			PS	83.83112	-	524.04	-	214	0.91	<0.001	(370.53, 15.09)	
			CC/PS	19.97024	-	-	67.36414	68	0.62	<0.001		

From Table 6.3, it can be seen that the hyperbolic regression curves selected for the two tests provide a close approximation of the path of the data with coefficient of determination (R^2) values of up to 0.97 and variance ratio (F) values <0.001.

6.2.2.1 Results for the Evesham soil series

Results for the Evesham series grass plot at 50mm depth are presented, in graphical form, in Figure 6.4

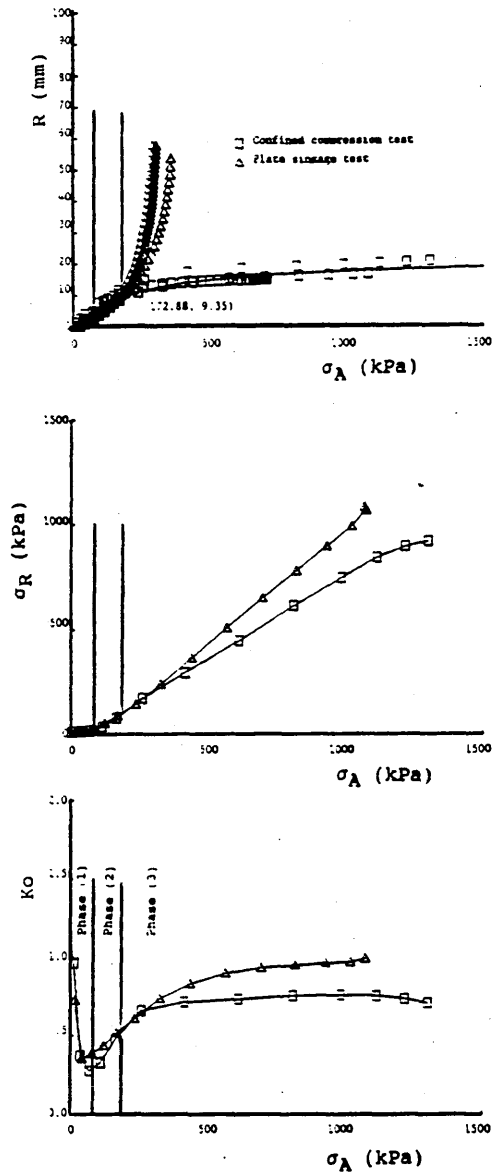


Figure 6.4 Stress-sinkage, σ_R and K_0 curves for the Evesham series grass plot at 50mm depth.

From Figure 6.4, as compression commenced, and axial stress increased from 0 to 70kPa, the first 2.5mm of sinkage occurred through compaction with no increase in lateral stress, ie. phase (1). From 70 to 172kPa, the lateral stress increased, however the mode of deformation was still that of compaction ie. phase (2). The compaction point was encountered at 172kPa and the deformation mode changed to displacement directly under the plate ie. phase(3). With reference to the plate sinkage test, as sinkage continued to increase in phase (3), the axial stress tended towards a relatively low asymptote of 366kPa and had the test continued to this stress level, the plate would have continued to sink for no further increase in axial stress until σ_{ULT} increased further down the soil profile due to overburden on the deforming soil.

Tests were carried out under both grass and oats at 50 and 300mm depth and the data from these tests are presented in Table 6.4.

Table 6.4 Soil deformation behaviour parameters for the Evesham soil series.

Crop	Depth mm	σ_{ULT} kPa	σ_{CP} kPa	RCP mm	mCP kPa/mm	m _i kPa/mm	Phase (1)		Ko dip	Phase (2)		Final Ko
							kPa	mm		kPa	mm	
Grass	50	366	172.9	9.4	18.5	16.5	0-70	0-2.5	0.55	70-172	2.5- 9.4	0.80
	300	393	184.3	10.1	18.2	16.6	0-30	0-1.0	0.05	30-184	1.0-10.1	0.99
Oats	50	246	67.8	11.0	3.6	4.5	0-60	0-9.3	0.85	60- 68	9.3-11.0	0.88
	300	269	203.7	6.5	31.3	24.0	0-20	0-0.2	0.37	20-204	0.2- 6.5	0.95

The degree of saturation values, calculated at the compaction point (CP), are presented in Table 6.5.

Table 6.5 Degree of saturation (S) at the compaction point (CP) for the Evesham soil series.

Crop	Depth (mm)	Initial S (%)	S @ CP (%)	Initial D _B (kg/m ³)
Grass	50	78.7	87.4	1045
	300	75.7	91.5	1186
Oats	50	63.7	71.3	884
	300	81.6	88.0	1152

For three of the four treatments, the degree of saturation at the CP lies between 88.0 and 91.5%. The exception to this is the topsoil under oats which was markedly less dense than the other treatments, following autumn cultivations. The greater percentage of air within the soil at this depth and the more compactable soil surrounding the plate resulted in a lower degree of saturation at the CP (71.3%). Also, for the three other treatments, the axial stress at the CP lies between 170 and 205kPa, whereas that for the topsoil under oats is less than 70kPa. The ultimate axial stress for this treatment, derived from the regression equation, is also low for this treatment compared to the other three.

These data suggest that if dry bulk density and degree of saturation are low for a given clay soil, then the CP will occur at a low axial stress despite there being a relatively high soil air content available for expulsion. Displacement, rather than compaction, dominates the mode of deformation under the plate because soil is moved sideways into readily compactable surrounding soil. The resulting ultimate axial stress, ie the stress at which the plate will continue to sink, will be low.

The data from Table 6.5 suggests that for a given clay soil, soil samples of uniform bulk density will attain similar degrees of saturation (S) at the CP. Further work is required to examine the significance of variations in the initial value of S on that at the CP for uniform dry bulk density, as this could be a function of the percentage of trapped air and soil strength.

6.2.2.2 Results for the Bearsted soil series.

The Bearsted soil series under both grass and wheat was assessed using the same procedures applied to the Evesham series in Section 6.2.2.1. The results for the topsoil under grass are presented, in graphical form, in Figure 6.5.

From Figure 6.5, compaction takes place initially with no increase in lateral stress ie. phase(1). As the axial stress approaches 80kPa, the soil continues to compact, however, phase (2) is reached and lateral stress begins to increase. The mode of deformation changes from compaction to displacement at 457.6kPa (the CP). As axial stress is increased further, the sinkage curve tends towards an asymptote in excess of 1MPa.

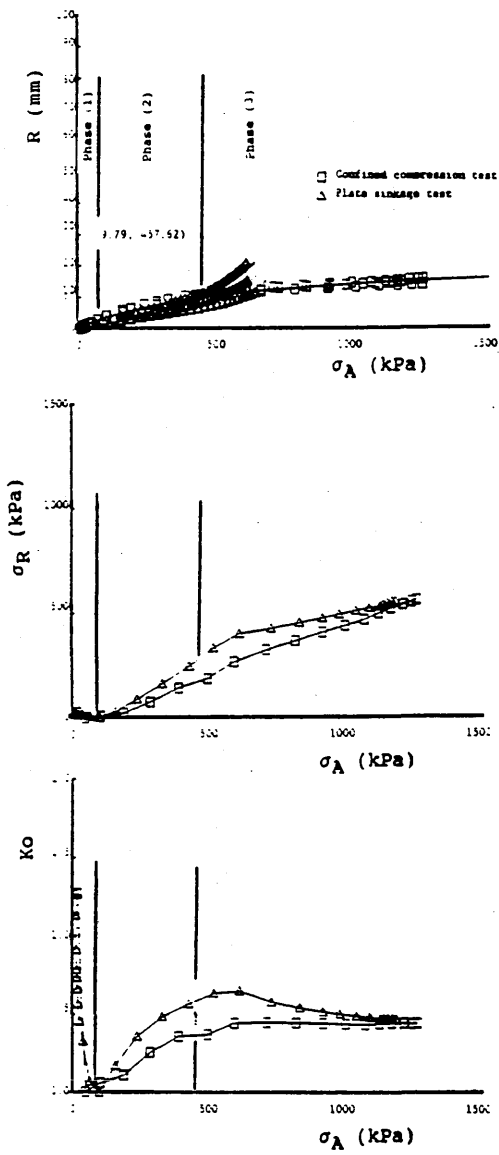


Figure 6.5 Stress-sinkage, σ_R and K_0 curves for the Bearsted series grass plot at 50mm depth.

The K_o curve shows clearly a dip which represents the point at which phase (1) compaction changes to phase (2). In phase (3), the curve tends towards a constant value (final K_o) of around 0.5; somewhat lower than that for the Evesham series topsoil under grass. The Bearsted series is a freely draining sandy soil and so intergranular moisture is unlikely to transmit a significant proportion of the axial stress laterally, even at field capacity, and hence the final K_o is low.

The final K_o , generated from a confined compression test, would not be achievable in the field for plate sinkage conditions because once the CP is exceeded, the surrounding soil can no longer completely confine the lateral stresses generated under the sinkage plate.

The results for the Bearsted soil series are presented in Table 6.6

Table 6.6 Soil deformation behaviour parameters for the Bearsted soil series.

Crop	Depth mm	σ_{ULT}	σ_{CP}	R_{CP}	m_{CP}	m_i kPa/mm	Phase (1)		Ko dip	Phase (2)		Final K_o
		kPa	kPa	mm	kPa/mm		kPa	mm		kPa	mm	
Grass	50	1019	457.6	9.8	46.7	51.2	0.80	0.1.0	0.50	80-458	1.0- 9.8	0.50
	300	743	160.2	3.5	45.9	33.5	0.00	0.0.0	0.00	00-160	0.0- 3.5	0.70
Oats	50	404	86.5	6.0	14.5	13.3	0.75	0.5.0	0.40	75- 87	5.0- 6.0	0.60
	300	524	370.5	15.1	24.6	20.0	0.55	0.0.7	0.50	55-371	0.7-15.1	0.70

6.2.2.3 Results from the soil damage prediction procedures.

Prediction theory, developed in Section 5.2.2.5, has been applied to a range of different scenarios to assess the effect of soil type, strength, compactability and load on extent of disturbance. Three loads have been applied to each scenario. These were based on the average vertical stress expected from:-

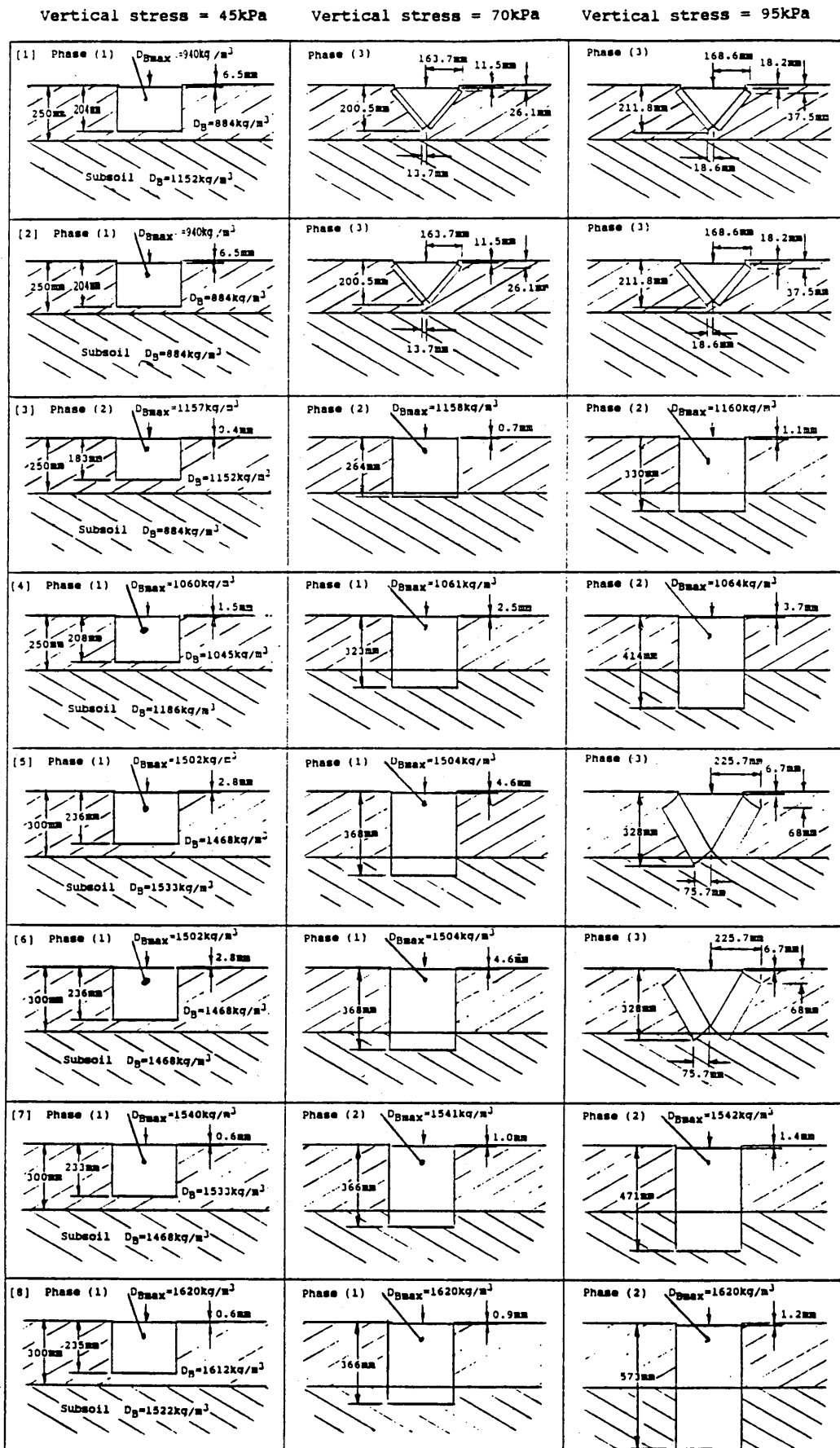
- (1) A low ground pressure sprayer - 45kPa
- (2) A 60kW tractor - 70 kPa
- (3) A 100kW tractor - 95 kPa

Details of these scenarios are given in Table 6.7 and the results are presented in Figure 6.6.

Table 6.7 Description of scenarios in Figure 6.6.

Scenario	Soil series	Crop	Strength	Compact-ability	Dry bulk density (kg/m ³)
1 Topsoil Subsoil	Evesham	Oats	Low Medium	High Low	884 1152
2 Topsoil Topsoil	Evesham	Oats	Low Low	High High	884 884
3 Subsoil topsoil	Evesham	Oats	Medium Low	Low High	1152 884
4 Topsoil Subsoil	Evesham	Grass	Low/med Low/med	Low Low	1045 1186
5 Topsoil Subsoil	Bearsted	Wheat	Low Medium	Medium Low	1468 1533
6 Topsoil Topsoil	Bearsted	Wheat	Low Low	Medium Medium	1468 1468
7 Subsoil Topsoil	Bearsted	Wheat	Medium Low	Low Medium	1533 1468
8 Topsoil Subsoil	Bearsted	Grass	High High	Low Low	1612 1522

Figure 6.6 Summary of prediction results for three loads applied to a range of soil profiles



For a vertical stress of 45kPa, soil deformation in all scenarios, with the exception of [3], is phase (1) - ie pure compaction with no increase in lateral stress. Any soil disturbance that occurs is wholly contained within the topsoil. The extent of vertical disturbance is greater in sandy loam than in clay but at lower intensity (less sinkage and increase in dry bulk density). In general, sinkage is very low (0.4 to 6.5mm).

If vertical stress is increased to 70kPa, the highly compactable/low strength soils are subjected to phase (3) deformation, however, disturbance is still confined to the topsoil. Soils of medium and high strength experience phase (2) and (1) deformation respectively. Disturbance from both phases (1) and (2) extends into the subsoil. There is little increase in dry bulk density as stress increases from 45 to 70kPa.

If vertical stress is increased further to 95kPa, soil deformation is either phase (3) (soils of low strength) or phase (2) (medium or high strength)- ie either compaction with increasing lateral stress or lateral displacement of soil. For phase (3) deformation, the vertical extent of disturbance is less than that for phase (2) due to a change in failure mechanism, however, lateral disturbance extends beyond the plate diameter.

6.3 Discussion

6.3.1 THE EVESHAM SOIL SERIES

From Table 6.4, it can be seen that both the topsoil and subsoil under grass, and the arable subsoil all compacted in a similar manner characterised by a very brief phase (1) with the majority of compaction occurring during phase (2).

The arable topsoil, however, was at a lower initial dry bulk density than the other three treatments following autumn cultivations and, as a consequence, the degree of saturation was also significantly lower (see Table 6.1). The soil was therefore more compactable with the majority of compaction occurring during phase (1) and hence a large K_0 dip is observed. This is also reflected in the initial and compaction moduli which were both comparatively low. The CP occurs at relatively low axial stress because soil below the sinkage plate can readily move laterally because the confining stress of the surrounding soil is low.

The results for the subsoils under both grass and oats are very similar except the sinkage due to compaction under oats is somewhat less than that under grass. This can be explained by a difference in the initial degree of saturation (75.7% under grass and 81.6% under oats). The dry bulk densities for each were similar as was the degree of saturation at the CP (91.5 and 88.0% respectively) and so it can be concluded that there was less air in the soil under oats available for expulsion during compression.

The results from Table 6.4 have been rated in terms of magnitude ie. high, medium or low according to Table 5.2 and are presented in Table 6.8.

Table 6.8 Rated soil deformation behaviour parameters for the Evesham soil series.

Crop	Depth	σ_{ULT}	σ_{CP}	RCP	mCP	m_i	Ko dip	Final Ko
Grass	50mm	L	L	M	H	M	M	H
	300mm	L	L	M	H	M	L	H
Oats	50mm	L	L	M	L	L	H	H
	300mm	L	M	M	H	M	L	H

From Table 6.8, the condition of the Evesham soil series, at the time of assessment, can be described in the following manner:-

Under grass at both 50 and 300mm depth:-

Low to medium strength, low compactability.

Under oats at 50mm depth:-

Low strength, high compactability.

Under oats at 300mm depth:-

Medium strength, low compactability.

The results for the two topsoils show a significant dip in the K_0 curve indicating that compaction below the sinkage plate takes place initially with little lateral stress and hence lateral compaction.

According to Lambe (1951), the moisture content at the time of compaction is critical in determining the final density for fine grained soils. Figure 6.7 shows a curve generated from a Proctor compaction test on a sample of Evesham series topsoil.

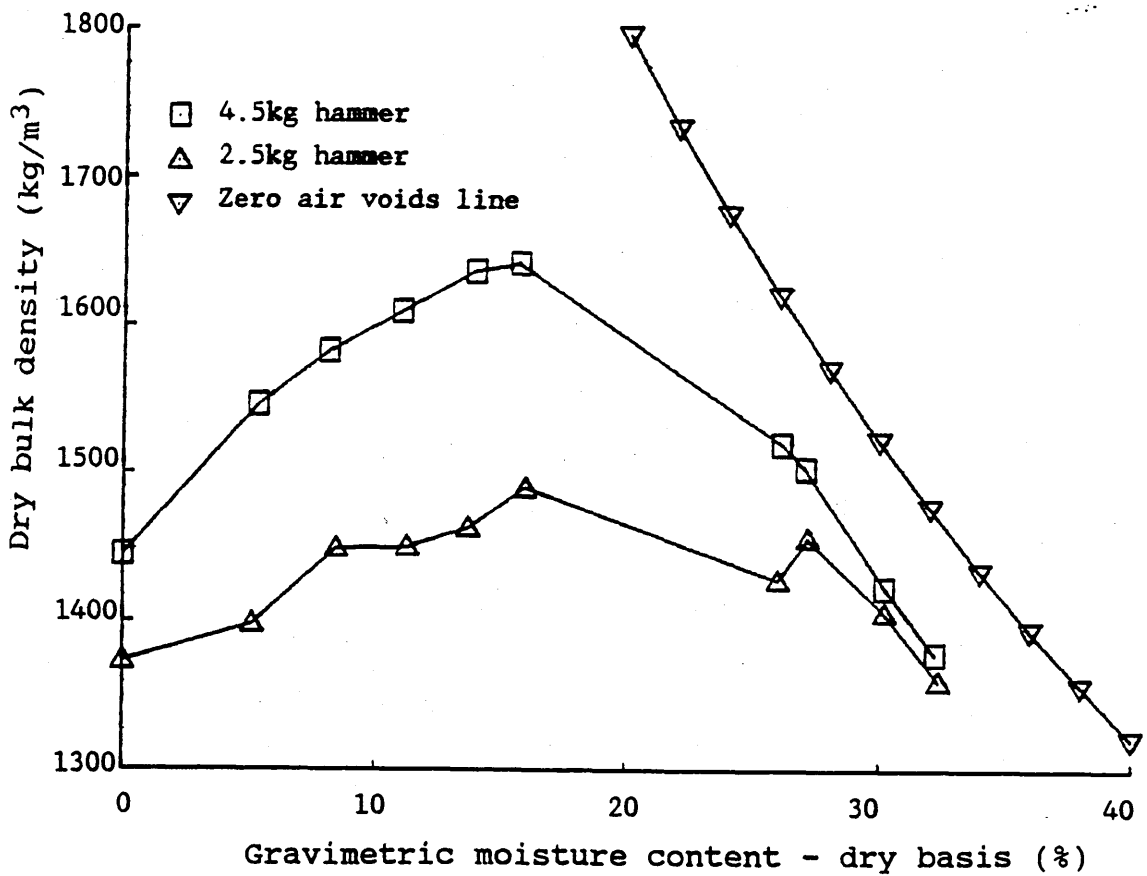


Figure 6.7 The relationship between dry bulk density and gravimetric moisture content obtained from a Proctor compaction test on clay soil: Evesham series topsoil.

Maximum dry bulk density is achieved at an optimum moisture content for a given soil under a particular intensity of load. Lambe's hypothesis for this effect is that as the soil moisture is increased, soil air is expelled. The soil particles absorb water until a surface film is formed which permits the soil particles to slide over each other more easily under load, i.e. effective stress, soil water tension and hence friction reduces. Since film thickness is negligible compared to the particle diameter of coarse grained soils, this effect is not as pronounced for sands as for clays. If the soil moisture content is increased further still, the entrapped air remains essentially constant and the water has the opposite effect, i.e. it occupies pore space which could be filled with soil particles on the application of load.

During a plate sinkage test, the compactive effort is not constant but increases as soil resists deformation. Raghaven and Ohu (1985) found that Proctor test blows of 5, 15 and 25, with a 2.5kg hammer, were equivalent to static pressures of 175, 404 and 618kPa respectively. The general shape of the compaction curves could therefore apply to results from plate sinkage tests.

Figure 6.8 shows a family of curves generated using various static loads, (from Turnbull, 1950).

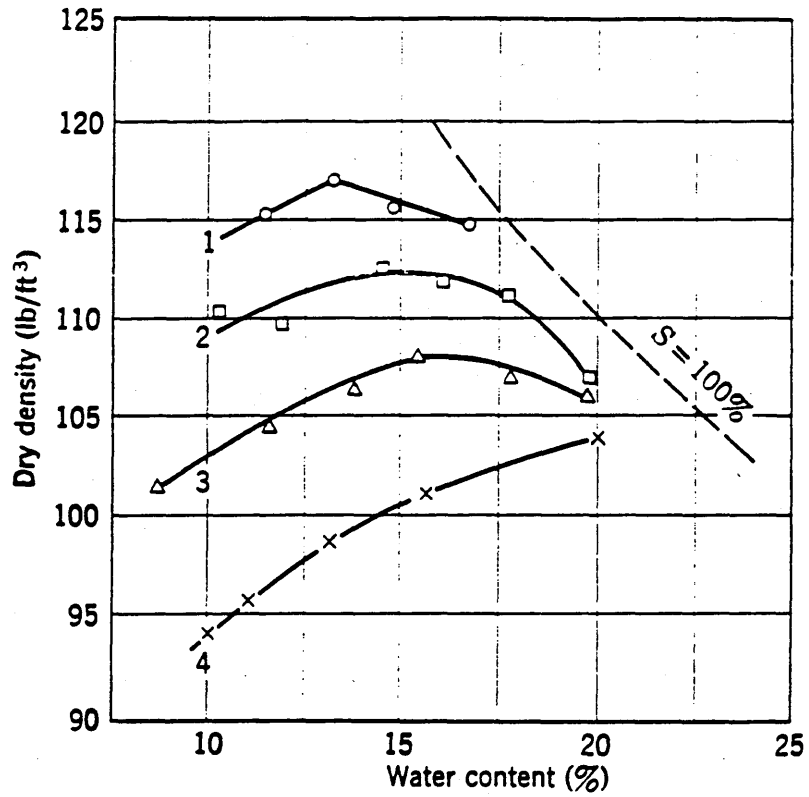


Figure 6.8 Static compaction curves for a silty clay. (1) 13.8MPa static stress. (2) 6.9MPa static stress (3) 3.4MPa static stress. (4) 1.4MPa static stress. (From Turnbull,1950).

From Figure 6.8, if load is plotted against density for a constant initial moisture content, Figure 6.9, is obtained. As stress is increased, maximum dry density for a given load is achieved at progressively lower water contents.

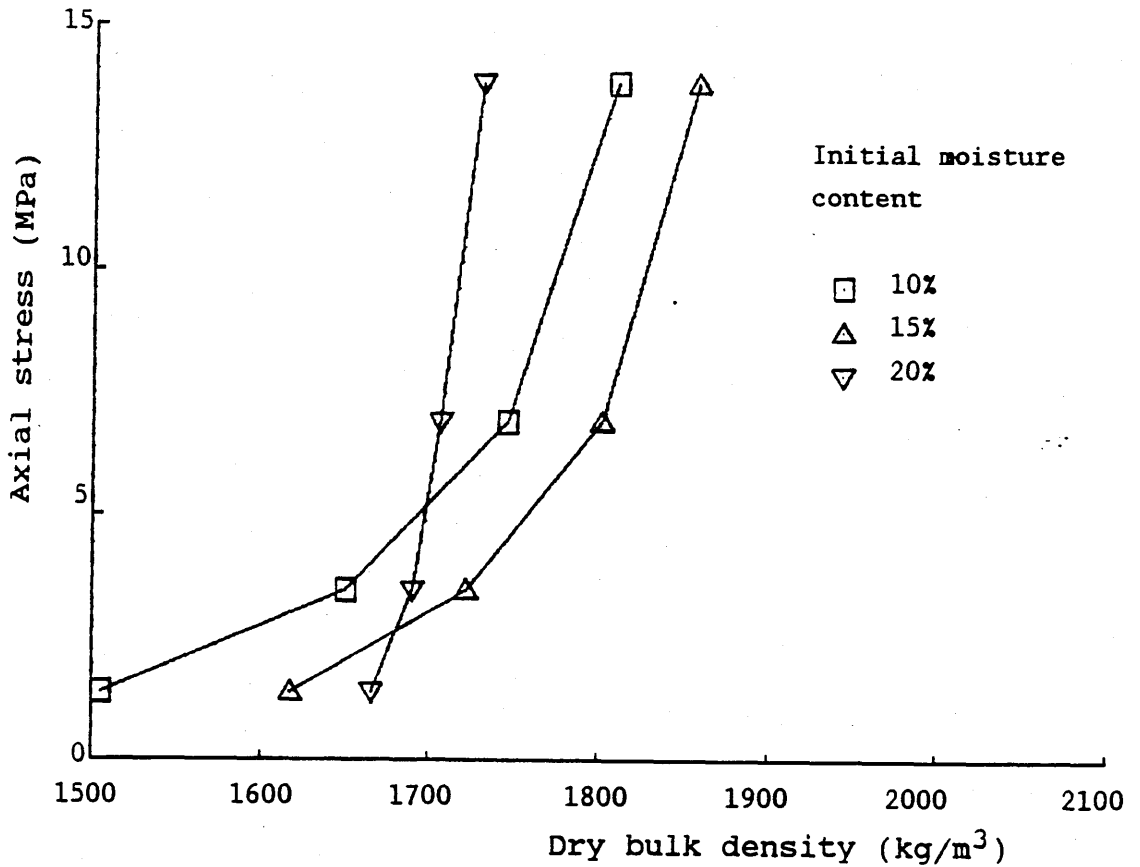


Figure 6.9 The relationship between load and dry bulk density for a silty clay loam.

From Figure 6.9, there appears to be an optimal initial moisture content for achieving the highest dry bulk density, ie the most compaction for a given stress range. For example, for stresses in the range 3 to 15MPa, 15% is optimal. At stresses less than 1MPa, which are applicable to agricultural machinery, 20% becomes optimal. It is accepted that Proctor and static compaction tests are normally performed on disturbed samples with little in the way of bonds between aggregates. If this trend is assumed to apply also to the results of plate sinkage tests on fined grained soils, then there

will be an optimal moisture content, for a given soil subjected to a given stress range, at which maximum compaction occurs. In terms of sinkage curves and CPs, the following form of curves, Figure 6.10, might be expected.

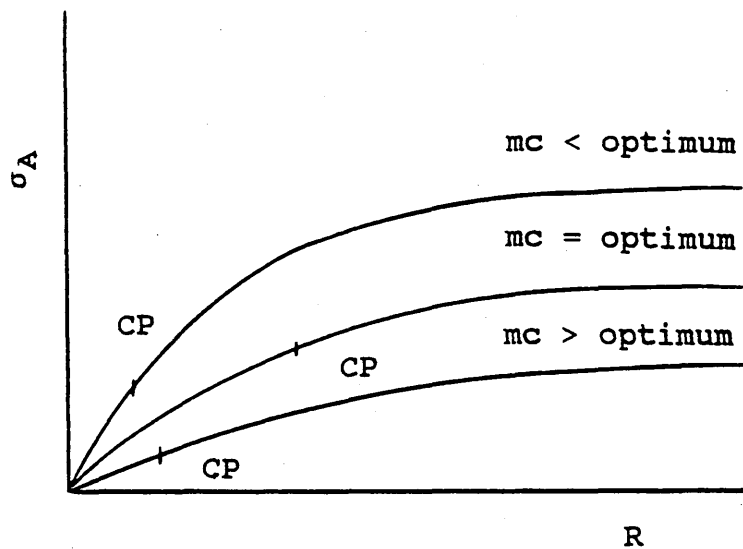


Figure 6.10 Hypothetical relationship between axial stress (σ_A) and sinkage depth (R) for a clay soil at various moisture contents.

From Figure 6.10, if the moisture content is greater than optimal, then less soil air is available for expulsion and so the CP is low and sinkage occurs at lower stresses due to soil displacement. At moisture contents less than optimal, soil strength increases resulting in less sinkage for a given load and a lower CP. It follows from this that there could be a relationship between degree of saturation (S)

and sinkage depth at the CP (R_{CP}) of the form shown in Figure 6.11.

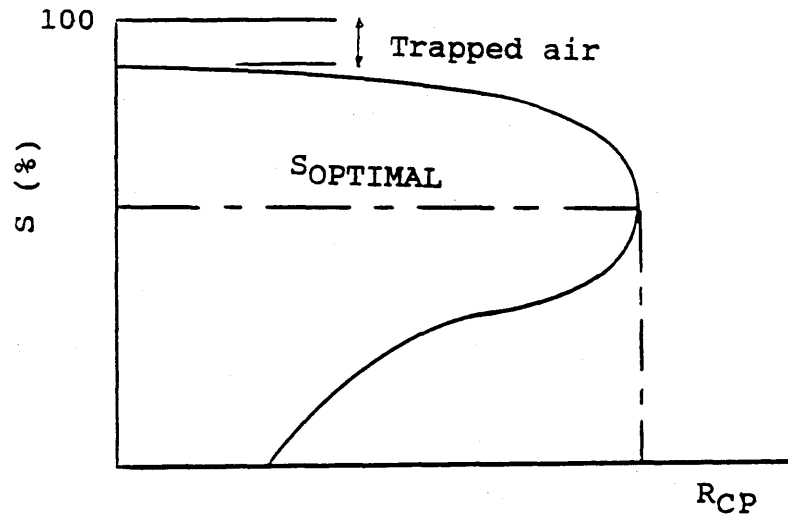


Figure 6.11 Hypothetical relationship between degree of saturation (S) and sinkage depth at the CP (R_{CP}) for the Evesham soil series.

If field data, generated from tests on the Evesham soil series, are plotted in this way, then a similar trend, albeit very speculative, to that of Figure 6.11 is suggested despite the data originating from two different plots and depths - see Figure 6.12.

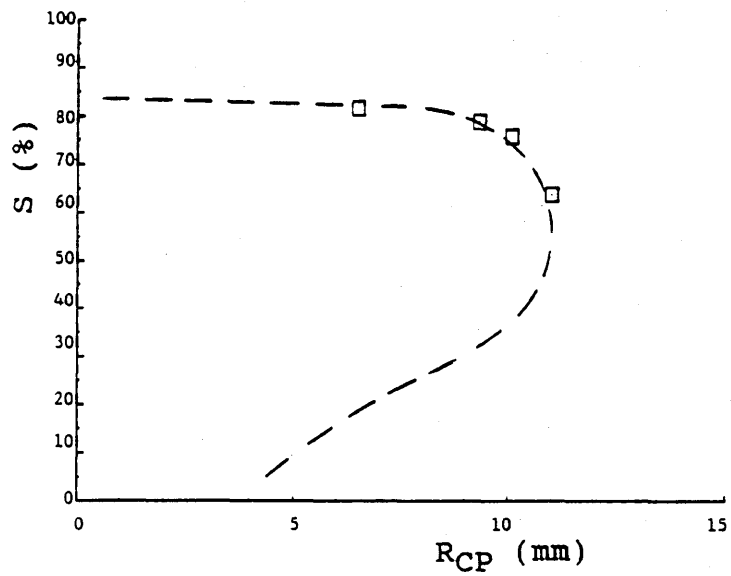


Figure 6.12 The relationship between degree of saturation (S) and sinkage depth at the CP (R_{CP}) for the Evesham series.

If $S - R_{CP}$ curves could be established for a given soil series, then with a knowledge of S , sinkage due to compaction could be predicted.

6.3.2 THE BEARSTED SOIL SERIES

The most obvious difference between the results for the Bearsted soil series and those for the Evesham is that the sinkage curve asymptotes, σ_{ULT} , are very much higher for the sandy soil ie greater loads can be supported without continuous sinkage. The topsoil under grass and the subsoil under wheat both sank significantly further, as a result of compaction, than the other two treatments, however, the majority of compaction occurred in phase (2) ie. with increasing lateral stress.

The mode of compaction for the topsoil under wheat was predominantly phase (1) and occurred at relatively low axial stress. This was as expected because the bulk density was low, compared to the others, following autumn cultivation. After sinking 6mm only, the soil surrounding the sinkage plate could no longer confine the lateral stresses generated from beneath the plate and the mode of deformation changed from one of predominantly compaction to displacement.

The subsoil under grass showed little inclination to compact at all and that which did occur was entirely of the phase (2) type. Comparing the results of the two subsoils, the condition of both, in terms of D_B and S , was initially very similar. Under compression, however, the soil under grass was clearly stronger with an initial modulus of 33.5kPa/mm compared with 20.0kPa/mm under wheat. One explanation for the difference between the two is that the cropping history has affected soil strength. The grass plot had been a permanent grass ley for some years, whereas crops on the arable

plot had been rotated annually. At 300mm depth, the root mass build up under grass may have contributed to the soil strength.

The Bearsted results from Table 6.6 have been rated in terms of magnitude ie. high, medium or low, according to Table 5.2, and are presented in Table 6.9

Table 6.9 Rated soil deformation behaviour parameters for the Bearsted soil series.

Crop	Depth	σ_{ULT}	σ_{CP}	RCP	m_{CP}	m_i	Ko dip	Final Ko
Grass	50mm	H	H	M	H	H	H	M
	300mm	H	L	L	H	H	L	M
Wheat	50mm	M	L	M	M	L	M	M
	300mm	M	H	H	H	M	H	M

From Table 6.9, the Bearsted soil series, at the time of assessment, can be described in the following way:-

The soil is low in compactability, with the exception of the arable topsoil which is rated as having medium compactability.

The soil under grass is of high strength with the topsoil compacting predominantly during phase (1), and the subsoil entirely during phase (2).

Under wheat, the topsoil is of low strength with a significant proportion of compaction occurring in both phases (1) and (2), whereas the subsoil is of medium

strength, the compaction occurring predominantly during phase (1).

Soils of low cohesion, such as the Bearsted series, do not show a consistent response to variations in initial moisture content when under compression. Figure 6.13 shows results from a Proctor test on a sample of Bearsted series subsoil.

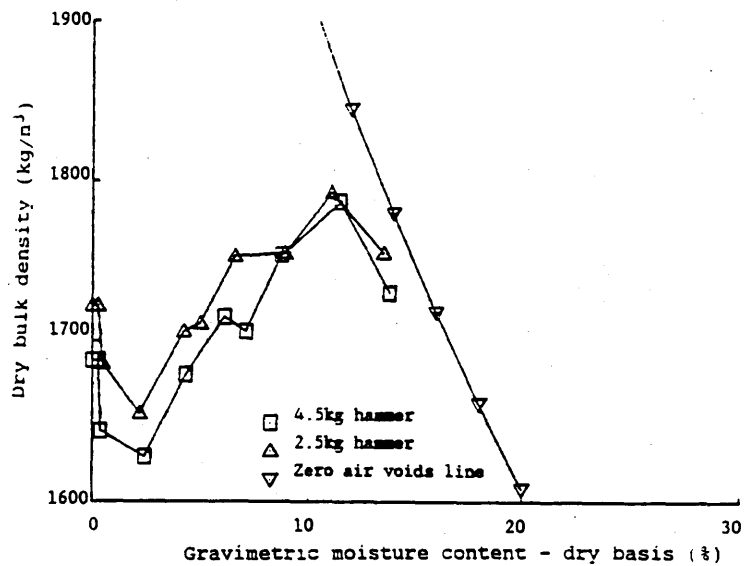


Figure 6.13 The relationship between dry bulk density and gravimetric moisture content obtained from a Proctor compaction test on a clay soil: Bearsted series subsoil.

The shape of the curve is very different to that for the Evesham series (Figure 6.7). Lambe (1969) explains the shape of the curve in terms of capillary forces at low moisture contents resisting the rearrangement of sand grains. Due to this phenomenon, known as "bulking", an unreliable relationship is expected for the Bearsted soil series between initial degree of saturation and the sinkage due to compaction during a plate sinkage test.

6.3.3 THE INTERACTION OF SINKAGE PLATE DIAMETER AND LOAD ON EXTENT OF DISTURBANCE.

In order to examine the implications of varying the load and plate diameter on the extent of soil disturbance, the complex mathematical models developed in 5.2.2.5 have been computerised using "Quattro Pro" to allow rapid determination of solutions. Data from the Evesham series arable plot was used, in conjunction with the computer program, to examine the interaction of plate size and load.

(1) Constant plate diameter, increasing load:-

The effect of increasing load on extent of soil disturbance for a plate of constant area is illustrated in Figure 6.14.

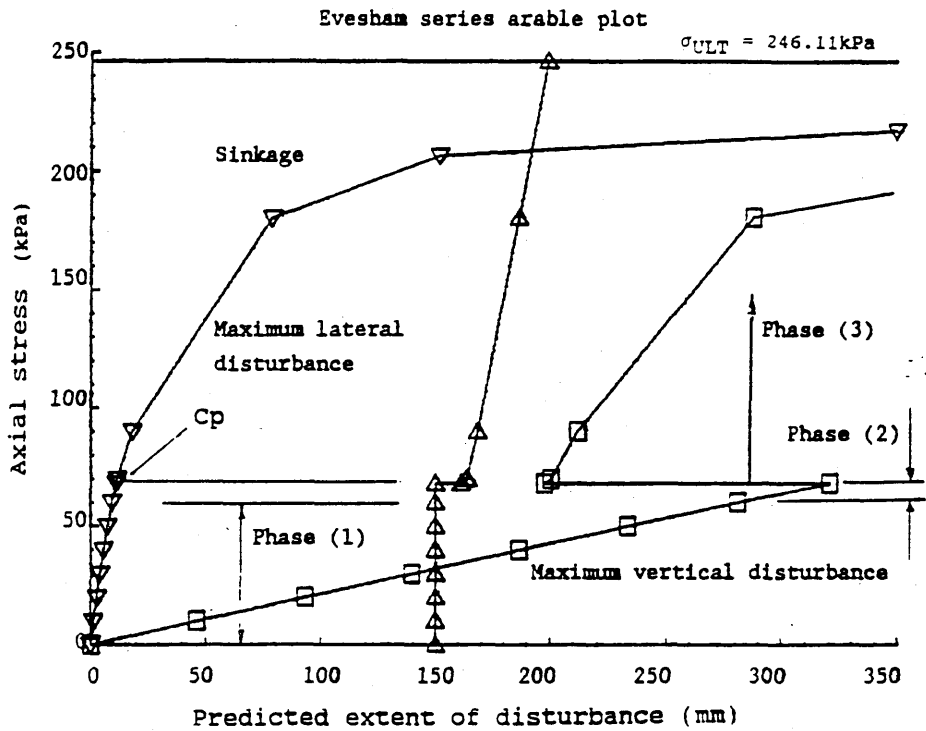


Figure 6.14 Prediction of extent of vertical and lateral disturbance resulting from increasing stress on a sinkage plate.

(a) Sinkage:-

As stress increases, sinkage increases hyperbolically and tends towards an asymptote at the ultimate stress for the soil. No discontinuity is apparent at changes of deformation phase.

(b) Lateral disturbance:-

As stress increases, the extent of lateral disturbance from the plate centre remains constant and equal to plate radius during both phases (1) and (2). When Phase (3) is approached, ie at the compaction point, lateral disturbance increases abruptly as conical failure planes form. During phase (3), lateral soil disturbance increases virtually linearly with load to a maximum (199mm) when stress approaches the ultimate (246.11kPa).

(c) Verical disturbance:-

The extent of vertical disturbance from the soil surface increases linearly with stress during phases (1) and (2). A discontinuity in the curve occurs at the compaction point as the soil cone forms below the plate. Vertical disturbance continues to increase with stress, initially at a lower rate than before, but as stress continues to increase, the curve is strongly influenced by the sinkage curve and tends towards an asymptote at the ultimate stress.

(2) Constant load, decreasing plate diameter:-

A constant load of 3.18kPa was selected for this investigation which is equivalent to a stress of 45kPa from a plate of 0.3m in diameter. The effect of reducing plate the diameter, and hence increasing stress, on disturbance in the Evesham series arable plot is illustrated in Figure 6.15.

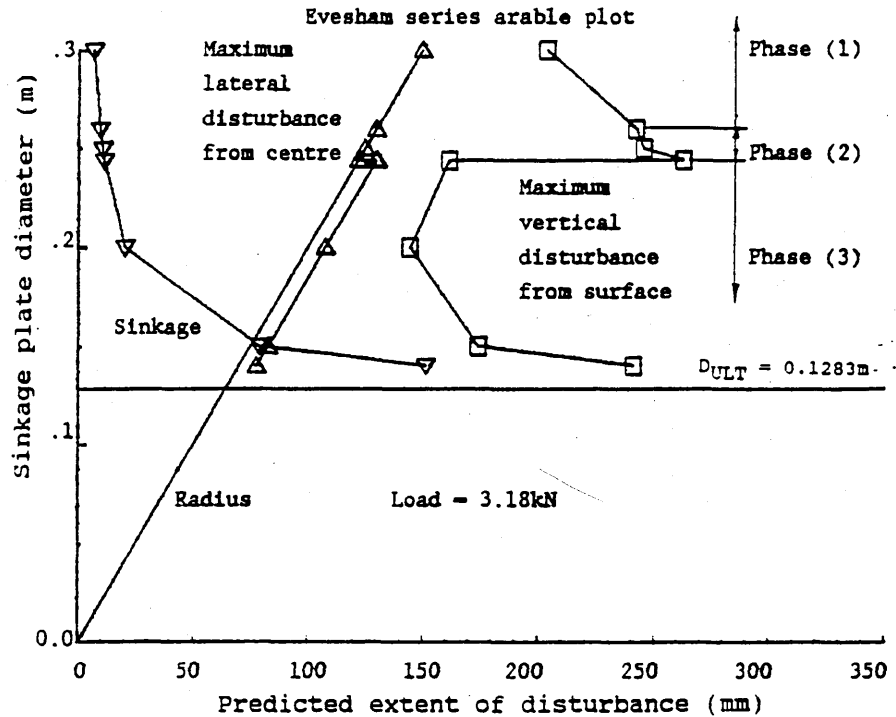


Figure 6.15 Prediction of the effect of reducing plate diameter, for a given load, on extent of soil disturbance.

(a) Sinkage:-

As plate diameter is reduced, stress increases in proportion to the square of the inverse and therefore depth of sinkage increases inversely with diameter, tending towards an asymptote at the ultimate stress.

(b) Lateral disturbance:-

During phases (1) and (2), the extent of lateral disturbance decreases with plate diameter and is equal to the plate radius. The soil deformation mechanism changes from pure compaction to lateral displacement as the compaction point is approached and a soil cone forms below the plate disturbing soil laterally beyond the plate radius. The extent of lateral soil disturbance continues to decrease proportionately with plate diameter, however, the extent of disturbance is greater than the plate radius.

(c) Vertical disturbance:-

The extent of vertical disturbance increases with decrease in plate diameter during phases (1) and (2). A discontinuity occurs at the compaction point as phase (3) deformation takes over causing a reduction in extent of vertical disturbance. Any further decrease in the diameter, and hence increase in stress, results initially in a decrease in extent of disturbance and then an increase which is strongly influenced by sinkage and therefore tends towards an asymptote at the ultimate stress.

(3) Increasing load versus decreasing plate diameter:-

A comparison of the extent of disturbance due to increasing load with that due to decreasing plate diameter is illustrated in Figure 6.16.

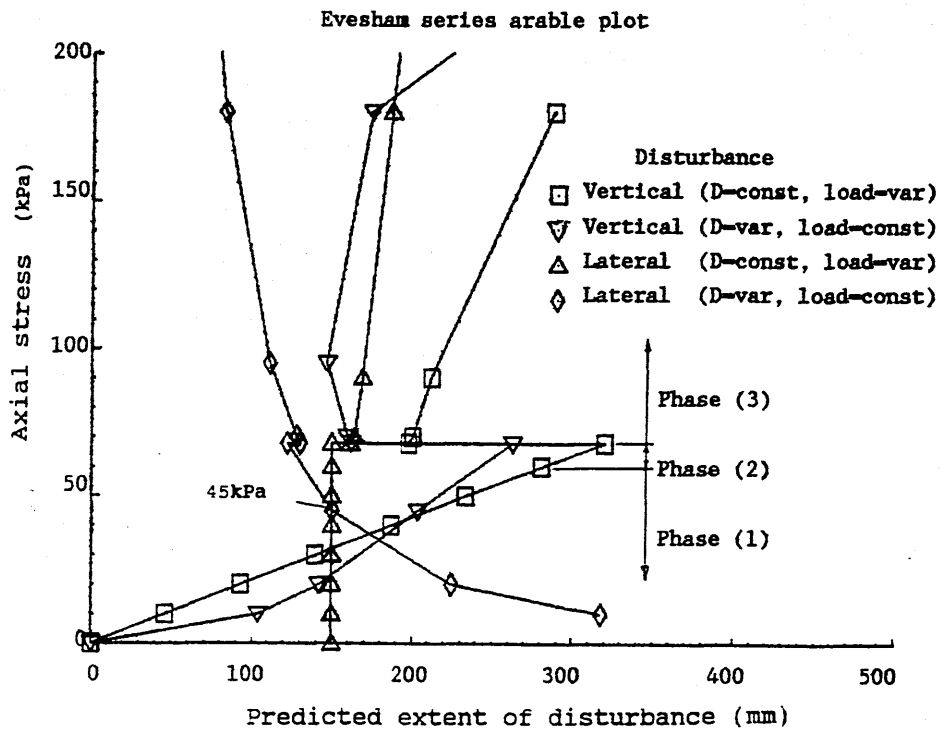


Figure 6.16 Comparison of the extent of soil disturbance below a sinkage plate due to increasing load with that due to decreasing plate diameter.

(a) Lateral disturbance:-

For constant diameter/variable load, as stress increases during phases (1) and (2), the extent of lateral disturbance is equal to the plate radius. During phase (3), disturbance increases proportionately with stress.

For constant load/variable diameter, the extent of lateral disturbance decreases with diameter, and hence increase in stress, throughout all three phases. For stresses greater than 45kPa, disturbance is less than that from constant

diameter/variable load and vice versa. A constant load of 3.18kN was selected which is equivalent to a stress of 45kPa on a plate of 0.3m diameter.

(b) Vertical disturbance:-

A similar effect to that for lateral disturbance is observed for extent of vertical disturbance. Below 45kPa, disturbance due to constant load/variable diameter is less than that due to constant diameter/variable load and vice versa.

Plate sinkage behaviour and potential damage from vehicular traffic are clearly related, however, caution must be exercised in relating the two directly because, for vehicular damage,:-

- (1) contact area is not circular, horizontal or constant,
- (2) stress concentrations occur (particularly below cleats),
- (3) shear damage results from the production of thrust, and
- (4) soil adheres to tyre walls.

Despite these limitations, the prediction techniques developed during this study can be used to assess the relative differences in deformation characteristics for soils in given situations.

6.4 Summary

Soil condition, in terms of compaction and compactability, can be assessed in two ways:-

- 1) Initial condition prior to loading, ie the soil may already have sustained loading.
- 2) Condition during loading, ie the soil's susceptibility to further damage.

The initial condition can be assessed using degree of saturation, packing density and initial gradient of the stress-sinkage curves giving an indication of mode of failure, packing state and soil strength respectively.

Soil damage during loading can be attributed to two distinct processes:-

- 1) Air expulsion with a resultant increase in dry bulk density, termed compaction.
- 2) Deformation due to soil movement with minimal reduction in soil volume, termed displacement.

Confined compression and plate sinkage tests have been found to be useful techniques for assessing the compactive nature of soil. The size of the test equipment was successfully increased from that used by Sieg in 1985 (50mm dia x 90mm height) to 150mm in both diameter and height, allowing a more representative soil sample size to be assessed.

Polyox resin can be used as a lubricant to reduce the angle of soil-metal friction during sampling. Results suggest that if Polyox is used, the angle of soil-metal friction may become independent of the soil texture and values as low as 2 to 3° can be expected.

Stress-sinkage curves, in conjunction with Ko-stress curves, generated from confined compression and plate sinkage tests, can be used to assess the nature of soil damage during loading. The stress-sinkage curves approximate the form of a hyperbola and coefficient of determination values of up to 0.97 can be obtained for both sandy and clayey soils. The curves can be linearised to evaluate the hyperbolic regression parameters.

If the curves from both tests on one soil type are constructed on the same axes, the point at which the two curves diverge denotes a change in the deformation process from one predominantly of compaction to displacement and is termed the Compaction Point (CP). The gradient of the curves initially, and at the CP, is termed the initial and compaction modulus respectively. These moduli give a measure of soil strength and compactability.

Ko-stress curves can be used to assess the level of lateral stress generated during compression. This work has shown that as soil undergoes compression, its behaviour is governed by three distinct deformation phases:-

- (1) Compaction with no increase in lateral stress.
- (2) Compaction with increasing lateral stress.
- (3) Displacement of soil laterally.

Mathematical models, developed during this study, can be used to predict the extent of disturbance below a sinkage plate. The findings of these models can be summarised as:-

- (1) Sinkage depth increases approximately hyperbolically with axial stress and tends towards an asymptote.
- (2) Sinkage increases inversely with contact area.
- (3) For axial stresses below the compaction point for a given soil, lateral soil disturbance does not extend beyond the plate radius.

- (4) For axial stresses in excess of the compaction point, lateral soil disturbance extends beyond the plate radius and increases proportionately with axial stress.
- (5) The extent of vertical disturbance increases proportionately with axial stress during phases (1) and (2).
- (6) A reduction in the extent of vertical disturbance occurs at the compaction point.
- (7) The extent of vertical disturbance increases approximately hyperbolically with axial stress in excess of the compaction point, and tends towards an asymptote at the ultimate stress for the soil.
- (8) When comparing extent of disturbance due to constant load/variable diameter versus constant diameter/variable load, for the same stress, less lateral and vertical disturbance occurs when the plate diameter during the variable diameter test exceeds that of the constant diameter test and vice versa.

The coefficient of earth pressure at rest (K_0) and Poisson's ratio (μ) are often assumed to be constants for a given soil. This study, however, has shown that they both vary considerably during compression. This emphasises the importance of defining the stress-strain conditions under examination before adopting values for these parameters for use in soil behaviour prediction models.

This study had investigated the use of the confined compression test and the plate sinkage test for assessing the compactive nature of soil, however, further research is required in the following areas:-

- (1) To verify the compaction point theory by conducting experiments to assess visually soil failure modes and wedge formation.
- (2) To test the techniques proposed in this Chapter on soil in a wide range of moisture and density conditions.
- (3) To investigate the suitability of degree of saturation as a prediction parameter for sinkage due to compaction.
- (4) To develop and validate the models for predicting the extent of soil disturbance below a sinkage test for layered profiles.
- (5) To amend the phase (3) model to allow predictions of dry bulk density to be made.

CHAPTER 7

OVERALL DISCUSSION, SUMMARY AND CONCLUSIONS.

Introduction

Techniques for predicting trafficability and workability, detailed in Chapters 2 and 3, require critical limits based on soil moisture deficit and soil water suction. In Chapter 7, a procedure for deriving critical limits from readily available soil data is described and applied to the ten most dominant arable soil series in England and Wales. In addition, trafficability and workability predictions, based on findings from Chapters 2 and 3, are compared with compactability and strength assessments, based on findings from Chapters 4, 5 and 6, for two soil types to examine how well the two approaches correlate.

The overall objective of this study was to develop techniques and models for assessing the susceptibility of soil to compaction from agricultural machinery. This was approached by dividing the study into two sections:-

- (1) The prediction of trafficability and workability on a go/no go basis.

- (2) Assessment of the compactive nature of soil during loading.

7.1 Predicting trafficability and workability

Trafficability and workability assessment was considered from two standpoints:-

- (1) Soil condition at a given site on a particular day.
- (2) Prediction of the number of machinery work-days (MWD) for a particular site as an aid to business planning.

7.1.1 PREDICTION AT A GIVEN SITE ON A PARTICULAR DAY.

Strong correlations were found to exist between soil strength and both soil water suction and soil moisture deficit for the upper profile and prediction methodologies for a given soil on a given day, based on critical limits for these two parameters, were proposed in Chapters 2 and 3 respectively.

Soil water suction can be monitored in the field using tensiometers. Tensiometer cups, placed at specific depths in the soil profile, can provide information on the moisture status at those depths. Once installed, septum tensiometers were found to require little maintenance and readings could be taken efficiently using a pressure transducer. One inherent difficulty encountered using all types of tensiometer is the operational limit of approximately 900cm of water, above which, air entry occurs and the instrument

fails. This is, however, not a serious draw back for trafficability and workability assessment as even the most susceptible soil studied during this work was considered to be workable at a suction of 140cm of water.

Soil water deficit can be monitored in the field by the neutron probe or by using an evaporation pan and rain gauge. The correlation between soil moisture deficit for the top 200mm of the soil profile (SMD200) and soil strength is slightly stronger than that between soil water suction (h) and strength. Although SMD200 can be monitored over the full range of soil moisture status encountered throughout a season it is not as convenient as h to monitor as it is calculated from volumetric moisture content and a knowledge of moisture status at field capacity for a given soil. It is, therefore, dependent on the dry bulk density at field capacity which can vary quite considerably from year to year for swelling clay soils.

7.1.2 PREDICTION OF THE NUMBER OF MACHINERY WORK-DAYS FOR A PARTICULAR SITE.

SMD was found to be a useful parameter for predicting the number of days on which a given site would be workable over an entire season. SMD is more practical than h for this application because a large data base of historical SMD data is available from the many weather stations situated throughout the country. These data, termed potential soil moisture deficit (PSMD) have been derived from meteorological data and consideration of a water balance model. They are not, therefore, site-specific but give an overview of SMD for the area in close proximity to the weather station rather than for a particular soil type and crop. Despite this, if average PSMD data for a 15 year period are coupled with critical SMD limits for trafficability and workability for a given site, an indication

of the number of MWD can be derived. Critical SMD limits for workability lie between 20 and 30mm, which is relatively low compared to the range of SMD encountered over an entire season and so site specific discrepancies due to differences in crop and soil type are likely to be small.

A procedure, developed by the Soil Survey and Land Research Centre (SSLRC), can also be used to predict MWD and results from both procedures concur, however, critical SMD limits also enable machinery trafficable days (MTD) to be predicted. This could be of particular interest when planning the purchase of non-soil-engaging machinery for example fertiliser spreaders and agrochemical sprayers.

Critical prediction limits, based on suction, and soil moisture deficit for the top 200mm and 1500mm of the soil profile, have been determined during this study for six soil series under both grass and wheat. In order to extend the predictive models developed from these critical limits to other soils, the relationship between these limits and other soil properties was investigated. Four soil parameters were identified which could be used to estimate the critical limits for other soils. Strong correlations were obtained between the critical limits for the soil series studied and the four parameters when subjected to multi-linear regression analysis.

These parameters, listed below, are available for over 1000 soil profiles in England and Wales from the Soil Survey and Land Research Centre (SSLRC) "LANDIS" data base.

- 1) Retained water capacity ($\theta_{v(0.05)}$) - defined as the volume of water retained in a soil sample at 0.05bar suction as a percentage of sample volume (Hall et al, 1977).
- 2) Organic carbon content (OC) - defined as the percentage, by weight, of organic carbon in a soil sample (Avery and Bascomb, 1982).
- 3) Sand content by weight (SAND).
- 4) Clay content by weight (CLAY).

Other soil properties considered included bulk density and packing density, however, they did not improve the correlations. This concurs with work by Spoor and Godwin (1979) who found the shear strength of clay soil to be more closely related to soil moisture suction than to dry bulk density.

Initially, separate equations were determined for soil under wheat and grass, however, regressions obtained for combined data were not weakened significantly, allowing estimates of critical limits to be made independently of crop cover. Regression equations for the critical limits are presented in Table 7.1

Table 7.1 Regression equations for estimating critical limits for trafficability and workability from soil properties.

Limit	Regression equation	R ²	F	n
Traff h	= -2.36232[$\phi_v(0.05)$]-0.10448[OC]-0.9684[SAND]+0.694093[CLAY]+122.3598	0.73	<0.001	20
Work h	= 6.68449[$\phi_v(0.05)$]+13.1501[OC]+0.9109[SAND]-2.668590[CLAY]-163.8460	0.42	<0.010	20
Traff SMD200	= 1.15429[$\phi_v(0.05)$]-1.07703[OC]+0.2326[SAND]-0.319010[CLAY]-31.88120	0.87	<0.010	10
Work SMD200	= 0.57584[$\phi_v(0.05)$]+0.32771[OC]+0.0567[SAND]-0.168830[CLAY]-6.833333	0.61	<0.050	10
Traff SMD1500	= 2.26592[$\phi_v(0.05)$]+2.87057[OC]+0.4443[SAND]-0.900750[CLAY]-66.16120	0.76	<0.010	10
Work SMD1500	= 1.31049[$\phi_v(0.05)$]+5.37042[OC]+0.1659[SAND]-0.714630[CLAY]-25.56150	0.61	<0.050	10

The regression equations were determined using critical limit data from five soil series under grass and wheat. Data for the Wick soil series were not included in the analyses because, due to a lack of h and SMD field data points for this soil in critical condition, the limits could not be determined precisely enough.

The ten most dominant arable soil series in England and Wales, listed in Table 7.2, were selected for further work to extend the trafficability and workability predictive procedures detailed in Chapter 3.

Table 7.2 The ten most dominant arable soils in England and Wales.

Soil series	Area* (%)	Estimated critical SMD1500 limit (mm)	
		Traff.	Work.
Andover	2.14	20.8	28.5
Bearsted	0.18	20.3	24.3
Curtisden	1.00	27.1	31.1
Cuckney	0.24	24.1	22.3
Denchworth	2.16	15.5	27.5
Evesham	1.86	6.3	16.4
Salop	1.70	21.7	31.4
Wallasea	1.12	18.4	24.1
Whimple	1.18	23.8	25.7
Wick	1.95	5.4	27.5
	<u>13.53</u>		

* Area of England and Wales, from Staff of the Soil Survey of England and Wales, (1983).

From LANDIS, average $\phi_{v(0.05)}$, OC, SAND and CLAY data, for all ten soil series, were substituted into the regression equations in Table 7.1 using a spread sheet to estimate critical SMD1500 limits. These are presented in Table 7.2.

7.1.2.1 Comparison of trafficability and workability predictions with those from LANDIS.

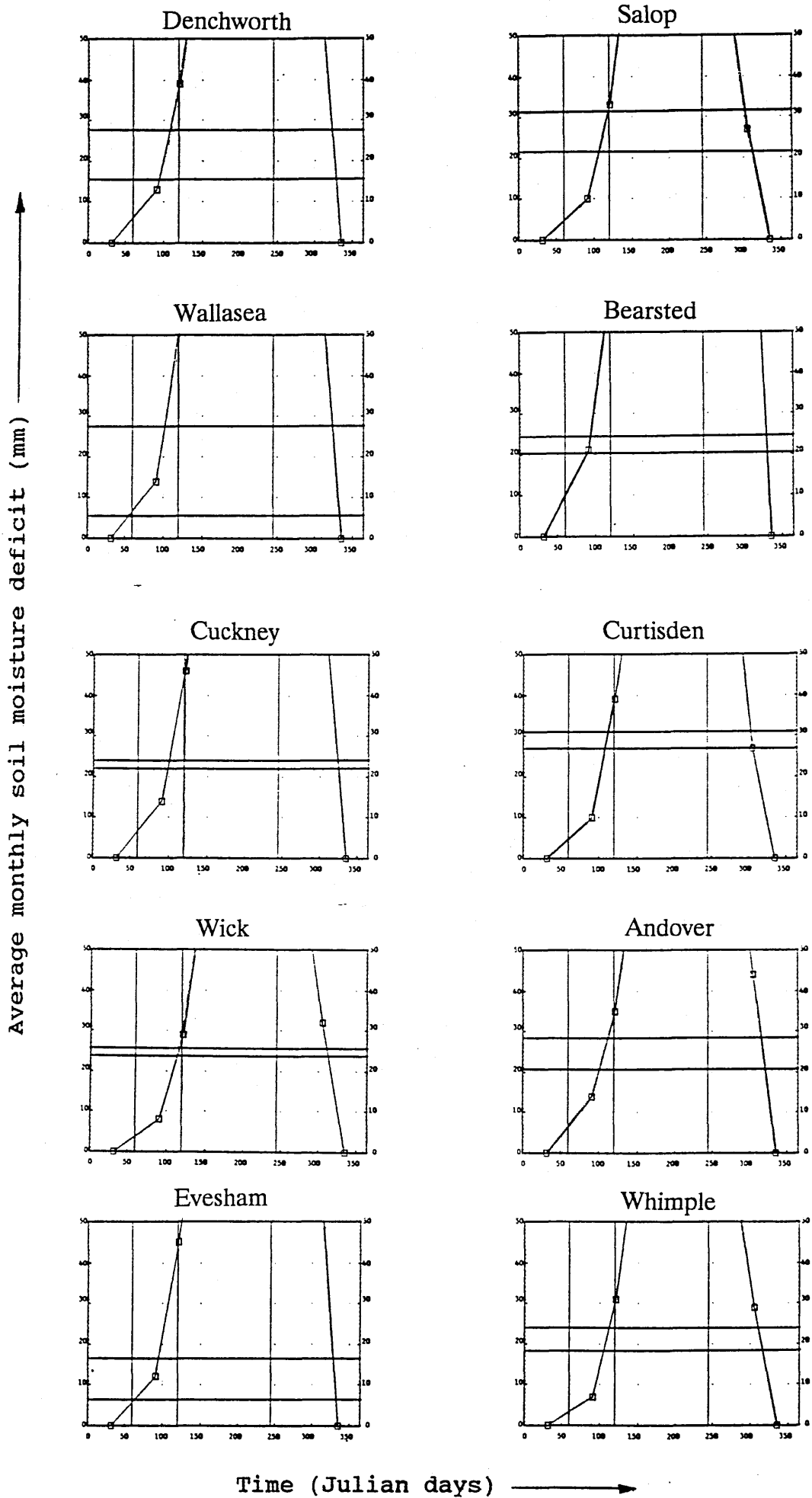
To compare estimates of trafficability and workability for the ten soil series with those from the Soil Survey data base, ten 5km squares, within which one of the ten soil series dominates, were selected from around the country and are listed in Table 7.3.

Table 7.3 5km squares selected for comparative work.

Soil series	Grid reference
Andover	SU 400 750
Bearsted	TL 100 400
Curtisden	TQ 500 200
Cuckney	SK 600 700
Denchworth	SP 450 550
Evesham	SP 850 200
Salop	SJ 400 400
Wallasea	TQ 950 650
Whimble	SK 000 200
Wick	SJ 900 050

From Landis, average monthly SMD was obtained for each square and plotted against time on the graphs presented in Figure 7.1

Figure 7.1 Average monthly soil moisture deficit against time for ten 5km squares in England.



Estimated critical SMD1500 limits, Table 7.2, have been superimposed onto Figure 7.1 enabling the number of workable and trafficable days to be predicted over the Spring and Autumn periods. These results are presented in Table 7.4 alongside predictions of machinery work days from LANDIS for each 5km square.

Table 7.4 Predictions of the number of trafficable and workable days.

Soil series	Traff. days (SMD1500)		Work days (SMD1500)		Work days (LANDIS)	
	Spr	Aut	Spr	Aut	Spr	Aut
Andover	19	76	8	71	22	79
Bearsted	31	86	26	84	45	127
Curtisden	11	61	8	59	12	59
Cuckney	19	79	22	80	42	115
Denchworth	26	84	12	79	5	44
Evesham	57	88	24	83	15	61
Salop	14	67	2	57	2	36
Wallasea	60	88	18	79	28	88
Whimble	14	72	8	65	2	28
Wick	7	68	3	67	21	86

Table 7.4 is presented purely for comparison to be made between LANDIS and the procedures developed during this study and is not a validation.

Predictions of the number of workable days, using both systems, follow similar trends, however, the following observations can be made:-

- 1) The LANDIS Autumn prediction for the Bearsted series is 127 days, however, the total number of days in the Autumn period, defined by SSLRC as from 1st of September to 31st December, is 121 days only.

- 2) A small discrepancy occurs in the Cuckney results predicted from SMD1500 because the number of workable days exceeds the trafficable.

- 3) Predictions from LANDIS are of workability and not trafficability.

In general, the technique looks promising but is difficult to validate without many years of historical trafficability and workability data. The ten most dominant arable soils have been considered here, however, the procedures could be extended to the 710 other soil series and applied at a 5km square level to any arable area in England and Wales.

The SSLRC procedure cannot be applied to a particular year in the past. If this information is required, then either critical h or SMD200 limits can be used as described in Chapters 2 and 3 respectively. Data generated using both procedures, for the Wick soil series under wheat during the 1987-88 growing season, are presented in Table 7.5

Table 7.5 Soil condition prediction for the Wick soil series under wheat over the 1987-88 growing season.

Prediction parameter	Predicted N ^o of trafficable days.		Predicted N ^o of workable days.	
	Aut	Spr	Aut	Spr
h	48	34	47	31
SMD200	51	37	46	24

From Table 7.5, the prediction results, using both procedures, are within a few days of each other with the exception of the workability prediction for Spring 1988 where they differ by seven days. This discrepancy can be explained by examining Figures 2.2A, Appendix 2, and 3.10. A data point is missing in Figure 3.10 due to failure of the neutron probe. Judging from the increase in h which occurred that week compared to the previous one, the effect the missing SMD200 would have had on the prediction would have been to increase it by 4 to 6 days.

Both SMD and h were monitored at six sites over a fifteen month period. The soil type at these different sites ranged from sandy soil through to clay. The relationships derived between these two

parameters and soil strength are therefore specific to soil conditions prevailing at these sites over this period. If conditions were to change, eg. a new crop or a change in dry bulk density following cultivation, then these relationships could be affected. Further work is required to establish what effect changes in site condition has on the relationship between both h and SMD and strength.

7.2 Assessing the compactive nature of soil during loading.

If land is trafficked or worked in unsuitable conditions, soil damage can occur. Assessment techniques are required to investigate the nature of this damage. Indirect measures of soil strength, eg. h or SMD, are not practical options for this application as a more fundamental approach is necessary. A methodology has been developed, and is presented in Chapters 4, 5 and 6, which provides a measure of the susceptibility of soil to compaction and an insight into the modes of deformation occurring in soil during loading. It is based on the results of plate sinkage tests in conjunction with those from confined compression tests.

Although plate sinkage results are insufficient to completely describe the deformation process in the field, for example, under a slipping cleated tractor wheel with oval contact patch, the two are related and provided that the former is considered in this light then the proposed methodology can yield valuable information on the deformation characteristics of field soils in terms of load versus sinkage, lateral stress, compaction and displacement. This information can be used to assess soil behaviour in terms of strength and compactability.

Field testing of this methodology was carried out on a sandy loam and a clay soil under grass and an arable crop. The clay assessment was conducted on Evesham soil series at the same site where the trafficability/workability work was carried out. The Bearsted soil series sandy loam site was not studied in Chapters 2 and 3, however, it was very similar in texture and dry bulk density to the Cuckney series and so comparisons can be made between the trafficability/workability prediction work, Chapters 2 and 3, and the compactability/strength assessment work in Chapters 4, 5 and 6.

7.3 Comparison of trafficability/workability prediction and compactability/strength assessment results.

7.3.1 SOIL WATER SUCTION AND COMPACTABILITY/STRENGTH ASSESSMENT.

The feasibility of using soil water suction (h) as a soil strength prediction parameter has been discussed in Chapter 2. Field sites were monitored over a fifteen month period and a wide range of values of h encountered. The development of a compactability/strength assessment methodology, Chapters 4, 5 and 6 involved the field testing of an assessment procedure at field capacity although it is envisaged that soil in a range of states would be assessed in future. The results for sandy and clayey soils from Chapters 2 and 4, 5 and 6 should therefore be linked. For convenience, trafficability and workability work in Chapter 2, and compactability/strength assessment work in Chapters 4, 5 and 6 will be referred to in the text as (2) and (5) respectively.

The studies in (5) were conducted in the field on soil which had drained for 48 hours following saturation. The soil water suctions persisting in the upper profile at the time of assessment are given in Table 7.6.

Table 7.6 Soil water suction (h) in the Evesham and Bearsted soil series profiles on sampling days.

Soil series	Crop cover	Depth (mm)	h (mmH ₂ O)
Evesham	Grass	50	-150
		150	-100
	Oats	50	-90
		150	-100
Bearsted	Grass	50	-140
		150	-60
	Wheat	50	-150
		150	-40

If critical soil water suction limits in (2) are applied to the results in Table 7.6 the following trafficability and workability predictions, presented in Table 7.7, are obtained.

Table 7.7 Trafficability and workability predictions for the Evesham and Bearsted soil series on sampling days.

Soil series	Crop cover	Depth (mm)	Critical h limits:-		Actual (mm H ₂ O)	Prediction.
			Traff. (cm H ₂ O)	Work. (cm H ₂ O)		
Evesham	Grass	50	-50	-70	-150	Untrafficable
		150	-25	-40	-100	
	Oats	50	-30	-55	-90	Untrafficable
		150	-20	-10	-100	
Bearsted	Grass	50	-5	-35	-140	Trafficable
		150	-5	-30	-60	not workable
	Wheat	50	-5	-30	-150	Untrafficable
		150	-5	-25	-40	

At field capacity, the prediction for the Evesham soil series under grass and oats and the Bearsted under wheat is untrafficable, ie. too weak and susceptible to damage. The prediction for the Bearsted grass plot, however, is trafficable but not workable.

To compare the predictions from (2) in Table 7.7 with the compactability/strength assessment during loading in (5), the results from both are given in Table 7.8.

Table 7.8 Comparison of trafficability and workability predictions with compactability and strength assessments for the Evesham and Bearsted soil series on sampling days.

Soil series	Crop cover	Strength assessment	Compactability assessment	Trafficability prediction
Evesham	Grass	Low to Medium	Low	Untrafficable
	Oats	Low	High	Untrafficable
Bearsted	Grass	High	Low	Trafficable
	Wheat	Low to Medium	Medium	Untrafficable

From Table 7.8, a strong trend exists between the trafficability/workability prediction based on h and the compactability/strength assessment based on σ_{ULT} , σ_{CP} , m_i and final K_o . When the strength assessment is low, or low to medium, the trafficability prediction is untrafficable, regardless of the compactability of the soil. Conversely, when strength is assessed as high, eg. Bearsted under grass, the prediction is trafficable. If soil were to be trafficked in an unsuitable condition, then the compactability assessment describes how the soil will fail, eg. the Evesham under grass is low in compactability and so soil damage will occur predominantly through lateral soil displacement rather than compaction.

Relationships between h and soil strength, expressed as resistance to cone penetration (RP), have been presented in Table 2.4, Chapter 2.

If these regression relationships are applied to the h values from sampling days in Table 6.1 using equation (1) below, the following results, presented in Table 7.9, are obtained.

$$RP = \frac{h}{\frac{1}{m_i} + \frac{h}{RP_{ULT}}} \quad (1)$$

Table 7.9 Predicted resistance to cone penetration (RP) for the Evesham and Bearsted soil series on sampling days.

Soil series	Crop cover	Depth (mm)	Predicted RP (MPa)
Evesham	Grass	50	0.35
		150	0.29
	Oats	50	0.25
		150	0.28
Bearsted	Grass	50	0.84
		150	0.75
	Wheat	50	0.27
		150	0.19

The results in Table 7.9 concur with the assessments and predictions in Table 7.8. The predicted RP for the three untrafficable plots is approximately one third that for the trafficable plot.

In (5), soil susceptibility to compaction was assessed using confined compression and plate sinkage tests. To further compare the strength prediction in (2) with the strength assessment in (5), the initial modulus (m_i) of the plate sinkage curves at 50mm depth, ie. the initial stress-strain gradient, are presented alongside predicted RP at the same depth in Table 7.10.

Table 7.10 Initial modulus (m_i) and predicted resistance to cone penetration (RP) for the Evesham and Bearsted soil series on sampling days.

Soil series	Crop cover	Predicted RP at 50mm depth (MPa)	m_i for plate sinkage (kPa/mm)
Evesham	Grass	0.35	16.5
	Oats	0.25	4.5
Bearsted	Grass	0.84	51.2
	Wheat	0.27	13.3

From Table 7.10, a reasonably strong relationship appears to exist between strength predicted from h at 50mm depth and m_i from plate sinkage tests performed at the same depth. ~~This is further confirmation that h can be used as a convenient parameter to predict the strength of field soils.~~

7.3.2 STRENGTH PREDICTION FROM SOIL MOISTURE DEFICIT AND COMPACTABILITY/STRENGTH ASSESSMENT.

The use of soil moisture deficit in the top 200mm of the soil profile (SMD200) as a strength prediction parameter has been discussed in Chapter 3. During the study, SMD200 at six field sites, was monitored over a fifteen month period and critical SMD200 limits for trafficability and workability were defined. Those for the Evesham and Cuckney soil series are presented in Table 7.11 Compactability/strength assessment work in (5) involved the testing of Evesham and Bearsted soil series at field capacity, ie. SMD200 of zero.

Table 7.11 Critical SMD200 limits for the Evesham and Cuckney soil series, and Trafficability/workability assessment for the Evesham and Bearsted soil series on sampling days.

Soil series	Crop cover	Crit. SMD200 (mm)		Actual SMD200 (mm)	Prediction
		Traff.	Work.		
Evesham	Grass	5	13	0	Untrafficable
	Oats	8	13	0	Untrafficable
Bearsted	Grass	2	5	0	Untrafficable
	Wheat	5	8	0	Untrafficable

From Table 7.11, the soil prediction, in every case, is untrafficable. This contradicts the predictions using h in Section 7.3.1 where the Bearsted series under grass was deemed trafficable but not workable. The critical SMD200 limit for this plot is 2mm and so soil at field capacity is only marginally wetter and hence close to being trafficable. Figure 7.2 shows the typical form of SMD200-RP curves.

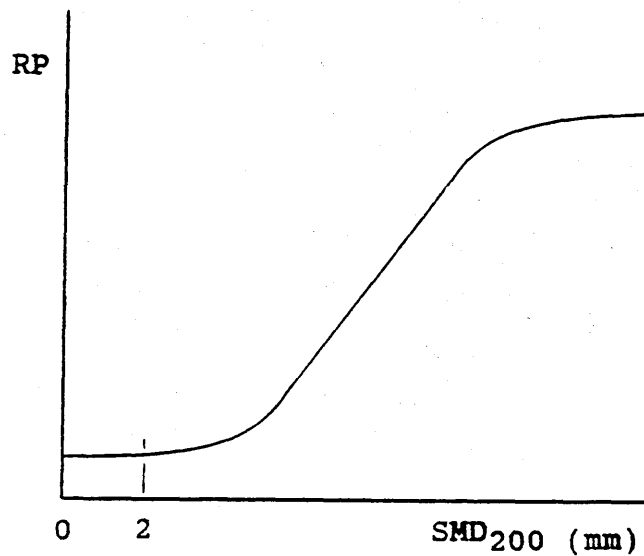


Figure 7.2 Typical form of SMD200 - RP curves.

Because of the S-shaped nature of the curve, the difference in strength at SMD200s of 0 and 2mm is very small - of the order 0.09MPa for the Bearsted soil series. The trafficability predictions of soil used in (5) are therefore similar whether h or SMD200 is used, and these predictions concur with the strength assessments carried out.

The comparisons made between trafficability/workability predictions and compacability/strength assessments provide further confirmation that both h and SMD200 can be used to reliably predict the strength of field soils on a go/no go basis for agricultural machinery planning purposes.

If predictions of the extent of soil disturbance are required for different sized loads, then the trafficability/workability techniques, detailed in Chapters 2 and 3, are inadequate and the more rigorous technique, described in Chapters 4, 5 and 6, is required.

7.4 Summary, conclusions and recommendations

7.4.1 SUMMARY

The findings of this work are summarised below:-

- (1) A strong correlation can be obtained between soil strength, expressed in terms of resistance to cone penetration, and either soil water suction or soil moisture deficit. The relationship is marginally better for soil moisture deficit.
- (2) Critical limits for soil water suction, soil moisture deficit and resistance to cone penetration have been identified for six soil series under grass and cereals. These can be used as a basis for predicting whether a given soil is workable, trafficable or untrafficable on a particular day. A strong correlation was found to exist between these critical limits and organic carbon content, retained water capacity, % sand and % clay contents when subjected to multi-linear regression analysis. These data, for over 1000 different soil profiles, are available from the SSLRC "LANDIS" data base and can be used to estimate critical limits for soils other than the six series investigated during this study.
- (3) A model has been developed, requiring average meteorological soil moisture deficit data from weather stations, which predicts the number of trafficable or workable days at a particular site throughout the year. Data from this model can be used to

predict the number and size of machines required to carry out necessary field work in the time available.

- (4) Tractor-mounted compression equipment, comprising plate sinkage and confined compression test apparatus, can be used to assess the compactive nature of soil.
- (5) The initial condition of soil can be characterised using degree of saturation, packing density and initial modulus - indicating mode of failure, packing state and soil strength respectively.
- (6) The susceptibility of soil to further damage can be assessed from stress-sinkage curves, in conjunction with Ko-stress curves, generated from confined compression and plate sinkage tests.
- (7) Confined compression and plate sinkage test results can be used to separate components of the deformation process of soil under load in terms of compaction and displacement.
- (8) Ko-stress curves, generated during confined compression tests, can be used to assess the level of lateral stress generated during compression of field soils.
- (9) Soil behaviour, during compression under a sinkage plate, is governed by three phases:-

- (a) Compaction with uniform lateral stress.
- (b) Compaction with increasing lateral stress.
- (c) Displacement of soil laterally.

7.4.2 DETAILED CONCLUSIONS.

The following conclusions can be drawn from this work:-

- (1) Soil water suction and soil moisture deficit are both suitable prediction parameters for trafficability and workability of field soils on a go/no-go basis.
- (2) Data from in-field plate sinkage tests, in conjunction with confined compression tests, can be used to assess the compactive nature of given soils in terms of:-
 - (a) the initial condition of the soil, ie. damage already sustained, and
 - (b) the susceptibility to further damage.

7.4.3 OVERALL CONCLUSION

The techniques developed during this study provide a new approach to the selection of, and assessment of damage by, agricultural machinery.

Further work is required in the following areas:-

- (1) To establish what influence differences in dry bulk density of given field soils has on the following relationships and hence the trafficability/workability models:-
 - (a) resistance to cone penetration and soil water suction,
 - (b) resistance to cone penetration and soil moisture deficit, and
 - (c) degree of saturation and sinkage due to compaction.
- (2) To investigate, for a range of soil series, the rate at which soil strength increases during periods of zero rain.

REFERENCES

- ADAMS, W A, TANAVUD, C and SPRINGSGUTH, C T (1985) Factors influencing the stability of sports turf root zones. In: Proc 5th Int Turfgrass Res Conf, Avignon, France, 392-399.
- ANDERSON, G, PIDGEON, J D, SPENCER, H B and PARKS, R (1980) A new hand held recording penetrometer for soil studies. J Soil Sci, 31, 279-296.
- AVERY, B W, BASCOMB, C L, BULLOCK, P, LOVELAND, P J, SMITH, P D and THOMASSON A J (1974) Soil survey laboratory methods, AVERY, B W and BASCOMB, C L (eds.). Soil Survey Technical Monograph No 6, Harpenden.
- AVERY, B W (1980) Soil classification for England and Wales. (Higher categories). Soil survey Technical Monograph No 14, Harpenden.
- AVERY, B W and BASCOMB, C L (1982) Soil survey laboratory methods, Soil Survey Tech mono No 6, Harpenden.
- BEARD, G R (1987) Profile description of of soils at the EC land evaluation project sites: The Wick grass plot. Unpl internal Soil Survey report, Silsoe Beds.
- BEARD, G R (1987) Profile description of of soils at the EC land evaluation project sites: The Wick wheat plot. Unpl internal Soil Survey report, Silsoe Beds.

BEARD, G R and Whitfield, W (1987) Profile description of of soils at the EC land evaluation project sites: The Evesham grass plot. Unpl internal Soil Survey report, Silsoe Beds.

BEARD, G R and Whitfield, W (1987) Profile description of of soils at the EC land evaluation project sites: The Evesham wheat plot. Unpl internal Soil Survey report, Silsoe Beds.

BEARD, G R (1988) Profile description of of soils at the EC land evaluation project sites: The Upton wheat plot. Unpl internal Soil Survey report, Silsoe Beds.

BEARD, G R (1988) Profile description of of soils at the EC land evaluation project sites: The Denchworth grass plot. Unpl internal Soil Survey report, Silsoe Beds.

BEKKER, M G (1960) Off-the-road locomotion. University of Michigan Press, Ann Arbor.

BELL, J P (1976) Neutron probe practice. NERC Institute of Hydrology Report No 19, Wallingford, Oxon.

BERNSTEIN, R (1913) Probleme zur experimentellen Motorpflug-mechanik. Der Motorwagen, Vol 16.

BICKI, J J and SIEMENS, J C (1991) Crop response to wheel traffic soil compaction. Trans ASAE, 34(3) May - June 1991.

BLACKWELL, P S, WARD, M A, LEFEVRE, R N and DOWAN, D J (1985) Compaction of a swelling clay soil by agricultural traffic; effects upon conditions for growth of winter cereals and evidence for some recovery of structure. J Soil Sci, 36, 633-650.

- BRADFORD, J M and GUPTA, S C (1986) Soil compressibility. In: KLUTE, A (ed) Methods of soil analysis, part 1: Agronomy (2nd ed). American Society of Agronomy, Madison, WI, 479-492.
- BRADSHAW, A D and CHADWICK, M J (1980) The restoration of land: the ecology and reclamation of derelict and degraded land. Blackwell Scientific, Oxford.
- CHANCELLOR, W J (1977) Compaction of soil by agricultural equipment. Bulletin 1881, University of California, Davis, California.
- COLLAS, P (1987) A cone penetrometer method for studying trafficability for farming operations. Proc 5th National Drainage Symposium, Chicago, Illinois, Dec 14-15 1987.
- DAVIES, P (1985) Influence of organic matter content, soil moisture status and time after reworking on soil shear strength. J Soil Sci, 36, 299-306.
- DUMBLETON, M J and WEST, G (1970) The suction and strength of remoulded soils as affected by composition. MOT Road Res Lab, LR 306, Crowthorne, Berkshire.
- ERBACH, D C, KINNEY, G R, WILCOX, A P and ABO-ABDA, A E (1991) Strain gauge to measure soil compaction. Trans ASAE, Vol 34(6): November-December.
- GODWIN, R J (1974) An investigation into the mechanics of very narrow tines in frictional soils. Unpl PhD Thesis, University of Reading (NCAE).

- GODWIN, R J, WARNER, N L and SMITH, D L O (1991) The development of a dynamic drop-cone device for the assessment of soil strength and the effects of machinery traffic. J Agric Eng Res, 48, 123-131.
- GOSSAGE S J (1977) A laboratory investigation into the effect of water table depth on soil shear strength. Unpl MSc Thesis, NCAE, Silsoe.
- GUPTA, S C and ALLMARAS, R R (1987) Models to assess the susceptibility of soils to excessive compaction. Adv in Soil Sci, 6, 66-100.
- HAKANSSON, I (1985) Swedish experiments on subsoil compaction by vehicles with high axle load. Soil use and Management, 1(4), 113-116.
- HAKANSSON, I (1988) A method for characterizing the state of compactness of an arable soil. In : Drescher, Horn and De Boodt (editors), Interaction of structured soils with water and external forces, Catena Suppl, 11, 101-105.
- HAKANSSON, I (1990) A method for characterizing the state of compactness of the plough layer. Soil and Tillage Res, 16, 105-120.
- HALL, D G M, REEVE, M J, THOMASSON, A J and WRIGHT, V F (1977) Water retention, porosity and density of field soils. Soil Survey Tech Mono No 9, Harpenden.
- HETTIARACHI, D R P (1992) Unpubl personal communication.
- HOLLIS, J M (1987) Profile description of of soils at the EC land evaluation project sites: The Cuckney wheat plot. Unpl internal Soil Survey report, Silsoe Beds.

- HOLLIS, J M (1987) Profile description of of soils at the EC land evaluation project sites: The Whimple grass plot. Unpl internal Soil Survey report, Silsoe Beds.
- HOLLIS, J M (1988) Profile description of of soils at the EC land evaluation project sites: The Upton grass plot. Unpl internal Soil Survey report, Silsoe Beds.
- HOWSE, K R (1981) A technique for using permanent neutron meter access tubes in cultivated soils. Expl Agric, 17, 265-269.
- KINNEY, G R, ERBACH, D C and BERN, C J (1992) Soil strain under three tractor configurations. Trans ASAE, Vol 35(4): Jult-August.
- KOOLEN, A J (1974) A method for soil compactibility determination. J Agric Eng Res, 19, 271-278.
- KOOLEN, A J and KUIPERS, H (1983) Agricultural soil mechanics. Springer-Verlag.
- KOOLEN, A J (1987) Deformation and compaction of elemental soil volumes and effects on mechanical soil properties. Soil and Tillage Res, 10, 5-19.
- KARAFIATH, L L and NOWATZKI, E A (1978) Soil mechanics for off-road vehicle engineering. Trans Tech Publ.
- LAMBE, T W (1951) Soil testing for engineers, J Wiley and sons, New York.
- LAMBE, T W and WHITMAN, R V (1979) Soil mechanics. J Wiley and sons.

LARSON, W E and GUPTA, S C (1980) Estimating critical stresses in unsaturated soils from changes in pore water pressure during confined compression. Soil Sci Soc Am J, 44(1), 1127-1132.

LARSON, W E, GUPTA, S C and USECHE, R A (1980) Compression of agricultural soils from eight soil orders. Soil Sci Soc Am J, 44(1), 450-457.

LEWIS, W A and ROSS, N F (1955) An investigation of the relationship between the shear strength of remoulded cohesive soil and the soil moisture suction. Road Res Lab, Res note No RN/2389/WAL.NFR, BS249.

MARTHALER, H P, VOGELSANGER, W, RICHARD, F and WIERENGA, P J (1983) A pressure transducer for field tensiometers. Soil Sci Soc Am J, 47, 624-627.

MEYERHOF, G G (1951) The ultimate bearing capacity of foundations. Geotechnique, Vol II, No 4, 301-332.

MEYERHOF, G G (1961) The ultimate bearing capacity of wedged-shaped foundations. Proceedings of fifth Int Conf on soil mechanics and foundation engineering, Paris.

PALMER, R C (1987) Profile description of soils at the EC land evaluation project sites: The Cuckney grass plot. Unpl internal Soil Survey report, Silsoe Beds.

PAUL, C L and DE VRIES, J (1979) Effect of soil water status and strength on trafficability. Can J Soil Sci, 59, 313-324.

- PAYNE, P C J (1956) A field method of measuring soil-metal friction. J Soil Sci, Vol 7, No 2, 235-241
- PRANDTL, L (1920) Uber die harte plastischer korper. (on the hardness of plastic bodies). Nachr kgl Ges Wiss. Gottingen, Math-Phys, kl, 74-85.
- PRANDTL, L (1921) Uber die eindringungsfestigkeit plastischer baustoffe und die festigkeit von schneiden. Zeitschrift fur Angewandte Mathematik, 1, (1), 15-20.
- REEVE, M J (1989) Summary of soils at the EC land evaluation project sites. Unpl internal Soil Survey report, Silsoe, Beds.
- REEVE, M J and EARL, R (1989) The effect of soil strength on agricultural and civil engineering field operations. SSLRC report for MAFF contract 3806, Silsoe, Bedford.
- RENGER, M (1971) Die ermittlung der porengrossenverteilung aus der kornung, dem gehalt an organischer substanz und der lagerungsdichte. Zeitschrift fur pflanzenernahrung und bodenkunde, 130, 53-67.
- SCHAFER, R L, JOHNSON, C E, KOOLEN, A J, GUPTA and S C, HORN, R (1990) Future needs in soil compaction. ASAE Paper No 90-1078, ASAE, St Joseph, MI.
- SCHOLEFIELD, D and HALL, D M (1986) A recording penetrometer to measure the strength of soil in relation to the stresses exerted by a walking cow. J Soil Sci, 37, 165-176.
- SIEG, D A (1985) Soil compactability. PhD thesis, Silsoe College, Silsoe.

- SIMALENGA, T E and HAVE, H (1992) Estimation of soil tillage workdays in semi-arid areas. J Agric Engng Res, 51, 81-89.
- SMITH, D L O (1985) Compaction by wheels: a numerical model for agricultural soils. J Soil Sci, 36, 621-632.
- SMITH, L P and TRAFFORD, B D (1976) Climate and drainage. MAFF Tech Bull, 34, HMSO, London
- SOANE, B D, BLACKWELL, P S, DICKSON, J W and PAINTER D J (1981a) Compaction by agricultural vehicles: a review I Soil and wheel characteristics. Soil and Tillage Res, 1, 207-237.
- SOANE, B D, DICKSON, J W and CAMPBELL, D J (1982) Compaction by agricultural vehicles: a review III Incidence and control of compaction in crop production. Soil and Tillage Res, 2(1), 3-36.
- SOANE, B D (1985) Traction and transport systems as related to cropping systems. Proc. International conference on soil dynamics, 1985, 5, 863-935.
- SOIL SURVEY (1976) Soil survey field handbook. Tech mono 5, Harpenden, England.
- SPOOR, G and GODWIN, R J (1979) Soil deformation and shear strength characteristics of some clay soils at different moisture contents. J Soil Sci, 30, 483-498.
- SOIL SURVEY (1983) Legend for the 1:250000 soil map of England and Wales. Rothamsted, Harpenden.

- STEINHARDT, R and TRAFFORD, B D (1974) Some effects of sub-surface drainage and ploughing on the structure and compactability of a clay soil. J Soil Sci, Vol 25, No2.
- SWAN, J B, MONCRIEF, J F and VOORHEES, W B (1987) Soil compaction - causes, effects and control. University of Minnesota, Agric Bulletin 3115, St Paul.
- TERZAGHI, K (1943) Theoretical soil mechanics. J Wiley, New York.
- TERZAGHI, K (1967) Soil mechanics in engineering practice. J Wiley and sons.
- THOMASSON, A J (1967) The moisture regimes and morphology of some fine textured soils. Unpl MSc Thesis, University of Nottingham.
- THOMASSON, A J (1982) Soil and climatic aspects of workability and trafficability. PROC 9th Conf Int Soil Tillage RES Org, Osijek, Yugoslavia, 551-557.
- TOWNER, G D (1983) Effective stresses in unsaturated soils and their applicability in the theory of critical state soil mechanics. J soil Sci, 34, 429-435.
- TURNBULL, W J (1950) Compaction and strength tests on soil. ASCE meeting (January).
- VAN WIJK, A L M and FEDDES R A (1986) Simulating effects of soil type and drainage on arable crop yield. ICW Tech BULL, 40, ICW, Wageningen, Netherlands.

- VAN WIJK, A L M and BUITENDIJK, J (1988) A method to predict workability of arable soils and its influence on crop yield. In : Drescher, Horn and De Boodt (editors), Interaction of structured soils with water and external forces, Catena Suppl, 11, 129-140.
- VERMA, K F and Bradley, R I (1988) Soil survey of Silsoe College Farm. Internal SSLRC document.
- VOORHEES, W B (1987) Assessment of soil susceptibility to compaction using soil and climatic data bases. Soil and Tillage Res, 10, 29-38.
- WHITFIELD, W (1987) Profile description of of soils at the EC land evaluation project sites: The Whimple wheat plot. Unpl internal Soil Survey report, Silsoe Beds.
- WHITFIELD, W (1988) Profile description of of soils at the EC land evaluation project sites: The Denchworth wheat plot. Unpl internal Soil Survey report, Silsoe Beds.

Appendix 1

SOIL PROFILE DESCRIPTIONS

The soil profile description for each site comprises a general discussion of the soil followed by a more detailed description of the profiles under both the grass and the arable plots. The six soil series are discussed in the following order:-

- (1) Cuckney
- (2) Wick
- (3) Whimple
- (4) Upton
- (5) Evesham
- (6) Denchworth

The Cuckney soil series.

The following description is taken from Reeve (1989).

The soils in both plots are developed in reddish Triassic sandstone (of the Sherwood Sandstone group). They are both very similar with only slight differences in their solum depth and extent of drift contamination. Both plots have a thick Ap horizon extending to about 40cm depth. This overlies a very porous Bw horizon, which in turn, passes into a loose Cu of weathered sandstone. Below about 110cm, the Cu merges into a Cr of soft, weakly consolidated sandstone rock. The Bw horizon is about 35cm thick. The colour and silt content of Ap and Bw horizons suggest some drift influence and a slight lithological discontinuity between 57 and 72cm. In the wheat pit, one face contains a large inclusion of sandy loam material, possibly the disrupted remnant of a Bt horizon developed within a former thick drift cover, now eroded.

The Gleadthorpe profiles are typical of many Cuckney soils throughout England, having very low clay contents that decrease or remain constant with increasing depth and showing no sign of significant clay translocation. As such, they qualify as cambic arenosols in the FAO classification system. Many other Cuckney profiles, however, show a slight increase in clay in their BC or Cu horizons, usually accompanied by a significant increase in fine clay (<0.2 m) and weakly expressed clay lamellae. Such features are sufficient to be diagnostic of luvisc arenosols in the FAO system, although they are not developed enough to be diagnostic of argillic brown sands (Avery 1980).

THE GRASS PLOT

Profile No.: SK57/8807, (Palmer, 1987).

Horizon
depth (cm)
and
notation

Description of horizons

- 0 - 40 Ap Dark brown (10YR 3/3) slightly stony (10%) loamy sand; stones very small to large rounded quartzites and quartz; moist; weak medium and coarse angular blocky fragments; low packing density; extremely porous; moderately weak soil and ped strength; non-sticky, non-plastic; non-calcareous; sharp smooth boundary.
- 40 - 58 Bw1 Strong brown (7.5YR 5/6) slightly stony (5%) medium sand; stones as above; moist; weakly developed medium angular blocky peds; medium packing density; extremely porous; moderately weak soil and ped strength; non-sticky, non-plastic; very few fine fibrous roots; earthworms active and few medium and coarse earthworm burrows filled with dark brown (10YR 3/3) material from above; non-calcareous; abrupt irregular boundary.
- 58 - 79 Bw2 Yellowish red (5YR 5/6) slightly stony (8%) sand; stones as above but mainly large and medium; moist; weakly developed fine angular blocky peds; medium packing density; extremely porous; moderately weak soil and ped strength; non-sticky, non-plastic; few

medium and coarse vertical earthworm burrows filled with dark brown (10YR 3/3) material from above; non-calcareous; abrupt smooth boundary.

79 - 110 Cu Reddish brown (3YR 4/4), yellowish red (5YR 5/6) and reddish brown (5YR 5/4) very slightly stony sand; stones rounded, medium quartzites; moist; apedal, single grain with some evidence of geological bedding picked out by the colour [variations; high packing density; extremely porous; moderately weak, moderately firm in patches, soil strength; non-sticky, non-plastic; few coarse earthworm channels filled with dark brown (7.5YR 3/2).

at 110 Cr Reddish brown (2.5YR 4/4) thinly bedded soft medium Triassic sandstone.

THE WHEAT PLOT

Profile No.: SK57/9005, (Hollis, 1987).

Horizon
depth (cm)
and
notation Description of horizons

- 0 - 40 Ap Dark brown (7.5YR 3/2); slightly stony (7%) very small to large rounded quartzite and quartz pebbles; loamy sand (6%c, 14%z); moist; weakly developed coarse, medium and small subangular blocky fragments, medium packing density; extremely porous; 0.5% very fine macropores; moderately weak soil and ped strength; non-sticky, non-plastic; many fine and very fine fibrous roots; few earthworms present; non-calcareous; sharp wavy boundary.
- 40 - 72 Bw Brown (7.5YR 4/4); loamy sand (5%c, 13%z) with large inclusions of (7.5YR 5/4) and (7.5YR 6/4) sand; slightly stony (5%) as above; very weakly developed coarse subangular blocky peds; medium packing density; extremely porous; no fissures 0.5% very fine macropores; moderately weak soil strength (very weak in sand inclusions) very weak ped strength; non-sticky, non-plastic; few fine and very fine fibrous roots, common large medium and small earthworm channels lined and often completely filled with Ap material; extending vertically throughout the horizon; non-carcareous; abrupt irregular boundary.

(NB. Large inclusion of SL (Bt?) material approximately 20cm x 80cm slanting diagonally throughout horizon on one half of one face of the pit.)

72 - 125 Cu Yellowish red (5YR 5/6); very slightly stony, medium, small and very small as above; medium sand (5%*c*, 9%*z*); moist apedal single grain; medium packing density; extremely porous; no fissures; 0.5% fine and very fine macropores; loose soil strength; non-sticky, non-plastic; few fine and very fine (dead) fibrous roots down earthworm channels; Common medium, coarse and very coarse earthworm channels stretching vertically throughout horizon, lined and often filled with Ap material; clear irregular boundary.

(NB. Small 0.5cm to 4cm diameter marl cores are often included here and in the Cr).

at 125 Cr Soft, thinly current bedded yellowish red (5YR 5/6) sandstone of the Triassic Sherwood Sandstone group.

The Wick soil series.

The following description is taken from Reeve (1989).

These soils typically have sandy loam or sandy silt loam topsoils over brown (usually 7.5YR) unmottled sandy loam permeable subsoils, commonly passing to loamy sand or sand below 0.5m depth. They are variably stony with 2-20% hard stones, usually of quartzite or sandstone, and sometimes overlie gravel below 1m depth. Many Wick soils have a groundwater-table at 2-3m depth which can rise to within 1-1.5m of the surface in wet spells but horizons are permeable and drain freely. Because of this, the soils are easy to work, and are largely in arable use in the drier parts of England and Wales, carrying field crops of cereals, sugar beet and potatoes (the latter often irrigated), and occasional intensive horticultural crops. Pasture is more common in western districts, where the soils are fairly resistant to poaching (treading) by cattle. Wick soils on terrace sites are additionally in demand for building developments. The soil at this experimental site occurs where a river Trent terrace feature, thought to date from the last interglacial period, adjoins valley sides formed in Triassic rocks.

The main soil profile is probably formed in material deposited somewhat later, perhaps in the late Devensian period. The two soil pits show similar profiles. The plough layer thickness is somewhat greater under wheat than under grass and stone content estimates vary randomly in the range 3 to 9% by volume, but otherwise the topsoils are fairly uniform. The Bw1 horizon is a similarly uniform brown to dark brown sandy loam with stone content varying from 10 to 18%. At about 0.5m or slightly deeper the Bw1 passes into

somewhat lighter material, in parts, loamy sand. Stone content is more variable in this layer. Below about 80cm, but undulating within and between the two pits, is a change to a variable deposit showing evidence of clay translocation and accumulation probably originating from an interglacial period of weathering.

THE GRASS PLOT

Profile No.: SK42/7176/1, (Beard, 1987).

Horizon
depth (cm)
and
notation

Description of horizons

0 - 22 Ap Very dark greyish brown (10YR 3/2, rubbed 10YR 3/2, air dry 9YR5/3) medium sandy loam; slightly stony (9%) - medium rounded quartzites and subangular flints; moist; moderate medium and coarse subangular blocky structure; medium packing density; very porous; 3% very fine macro pores; moderately weak soil and ped strength; slightly sticky, slightly plastic; many very fine fibrous roots; non-calcareous; sharp smooth boundary.

22-48 Bw1 Brown to dark brown (7.5YR 4/3, rubbed 7.5YR 4/3, air dry 7.5YR 5/4) medium sandy loam; moderately stony (18%) but very stony in patches - small and medium rounded quartzites and occasional subrounded and subangular flints; moist; moderate fine and medium subangular blocky (with some

angular faces) with dark brown (7.5YR 3/3) ped faces; medium packing density; very porous; 3% very fine and occasional coarse macro pores; moderately weak soil and ped strength; slightly sticky, slightly plastic; common very fine fibrous roots; non-calcareous; earthworm channels lined and filled with topsoil; a few irregular ferri-manganiferous soft concretions; abrupt smooth boundary.

48-72 Bw2 Brown to dark brown (7.5YR 4/4, rubbed 7.5YR 4/4) with patches of (7.5YR 6/4) medium sandy loam (but lighter than above); moderately stony (8-35% in patches) - stones as above; moist; weak coarse subangular blocky with ped faces slightly darker than matrix; extremely porous; 4% very fine and occasional coarse macro pores; moderately weak ped strength; non-sticky, non-plastic; a very few fine fibrous roots; earthworm channels lined with topsoil; a few rounded and irregular ferri-manganiferous concretions and staining of stones; non-calcareous; sharp and, in places, clear irregular boundary.

72-120 Mixed horizon consisting of distinct patches of:

E'b Yellowish red (5YR 4/6, rubbed 5YR 4/4) sandy loam; very slightly stony (3%) - small rounded quartzites, subangular flints and rare tabular siltstones; moist; weak medium and coarse platy with (5YR 4/4) ped faces; high packing density; slightly porous; 2% very fine macro pores; moderately weak ped strength; moderately firm soil strength;

slightly sticky, slightly plastic; no roots; earthworm channels lined with brown to dark brown 7.5YR 4/3 material; a few irregular ferri-manganiferous soft concretions and staining on stones; common continuous distinct clay coats especially around stones and filling some voids; non-calcareous.

B't

Brown to strong brown (7.5YR 5/5, rubbed 7.5YR 5/5) loamy medium sand; moderately stony (16%) - stones as in B't areas; moist; structureless, single grain; medium packing density; very porous; 2% very fine macropores; loose; non-sticky, non-plastic; no roots; a few fine rounded ferri-manganiferous soft concretions; no coats; non-calcareous.

THE WHEAT PLOT

Profile No.: SK42/7176/3, (Beard, 1987).

Horizon
depth (cm)
and
notation Description of horizons

0 - 31 Ap Very dark greyish brown (10YR 3/2, rubbed 10YR 3/2) medium sandy loam; unmottled; slightly stony - small rounded quartzites (7%) and occasional medium stones; extremely porous; very few very fine fissures; very fine macropores (2%); very weak soil and ped strength; non-sticky, non-plastic; common very fine fibrous roots, many probably dead; occasional pieces of dug in potato foliage; non-calcareous; sharp smooth boundary.

31-67 Bw1 Brown to dark brown (7.5YR 4/3, rubbed 7.5YR 3/2) medium sandy loam; unmottled, but occasional faint brown to dark brown colours associated with ferri-manganiferous concentrations; moderately stony (18%) - medium rounded quartzites and some subangular flints; slightly moist; moderate medium subangular blocky structure often with angular facets; medium packing density; extremely porous; very fine macropores (3%); moderately weak ped strength; very weak soil strength; non-sticky, slightly plastic; common very fine fibrous roots; common earthworm channels filled or lined with topsoil; non-calcareous; a few ferri-manganiferous irregular soft concretions, some staining on a few stones; abrupt wavy boundary.

67-87 Bw2 Strong brown (7.5YR 4/6, rubbed 7.5YR 4/4); unmottled medium sandy loam to loamy medium sand; very stony (35%) - medium, and some large, rounded quartzites and subangular flints, slightly moist; weak medium subangular blocky structure; low to medium packing density; extremely porous; very fine pores (2%); very weak soil and ped strength; non-sticky, non-plastic; a few very fine fibrous roots; as few filled earthworm channels; common small (2-4mm) irregular ferri-manganiferous concretions; clear smooth boundary.

87-110 This horizon is variably mixed and contains two distinct parts in about equal proportions. Each is described separately below:-

E'b Brown to dark brown (7.5YR 4/4) and dark yellowish brown (10YR 4/4) medium sand; common fine, distinct clear strong brown (7.5YR 4/6) mottles in discrete patches; moderately stony (18%) - medium rounded quartzites and occasional subangular flints; moist; single grain; medium packing density; extremely porous; very fine macropores (1%); loose (occasional small patches are very weak) soil strength; non-sticky, non-plastic; few very fine fibrous roots; non-calcareous; a few small subrounded ferri-manganiferous soft concretions and some staining on stones.

B't Yellowish red (5YR 4/6, rubbed 5YR 4/4); sandy clay loam; unmottled; slightly stony (15%) - medium rounded quartzites and occasional subangular flints;

moist; weak fine subangular blocky structure with reddish brown (5YR 4/4) ped faces; high packing density; slightly porous; very fine macropores (1%) moderately weak soil strength; moderately stick, moderately plastic; occasional earthworm channels with reddish brown (5YR 4/4) linings; a few small subrounded ferri-manganiferous soft concretions and some staining on stones; common entire distinct clay coats, particularly around stones and in the larger voids.

The Wimple soil series.

The following description is taken from Reeve (1989).

Profiles from both plots are very similar, the only slight variation occurring in the lithology of their parent material which comprises a thin veneer of loamy drift over soft reddish Triassic marl (fine angular blocky calcareous mudstone) containing thin gypsiferous siltstone beds ('skerry bands'). In both profiles the thin loamy drift extends to about 45cm depth. Ap and Eb horizons are developed in the drift and in the pit under wheat a transitional mixed Ap and Eb(g) horizon occurs between about 30 and 40cm. Both of these Ap and Eb(g) horizons and the lower 20cm of their overlying Ap horizons are severely compacted. At about 45cm there is an abrupt lithological and pedological transition to a 2Bt(g) horizon developed in the upper layers of Triassic marl. The 2Bt(g) is dense, coarsely structured and slowly permeable with distinct clay skins on ped and pore faces. Particle size analysis suggests considerable clay translocation has occurred. At about 60 to 70cm the 2Bt(g) horizon merges into little altered Triassic marl, designated 2BCt, which is calcareous or very calcareous with a fine angular block structure. The 2BCt horizons show minor lithological differences between the plots. Work by Thomasson (1967) and Thomasson and Robson (1967) has shown that reddish soil material derived from Triassic marl is, to a great extent, resistant to the process of gleying and the very weak gley fissures in both Eb and Bt horizons, together with their structural morphology suggest that the soils in both plots are of wetness class II.

These soils are typical of most Whimple soils in the country although they have slightly lighter than average topsoils (22% clay as opposed to an average of 25% for 28 profiles) and their 2BCt horizons contain much less clay than is usual. Both profiles qualify as orthic luvisols, as do soils of the Worcesrer series, similar to Whimple soils but with a heavier textured topsoil containing up to 40% clay.

THE GRASS PLOT

Profile No.: SK65/9916/1, (Hollis, 1987).

Horizon
depth (cm)
and
notation Description of horizons

0 - 34 Ap Dark brown (7.5YR 3/3) with common (5%) medium and coarse reddish brown (5YR 5/4) inclusions from the horizon below; clay loam (22%*c*, 30%*z*); very slightly stony (1%), small and very small subangular siltstones; moist; moderately developed medium subangular blocky, breaking into fine angular blocky and granular fragments in the upper 19cm, becoming weakly developed, compact and with coarse subangular block fragments below this depth; medium packing density with patches of high density in the upper 20cm; high packing density below; moderately porous; very few very fine fissures in between some fragments; 0.1% very fine macropores within peds; very firm soil strength in most of horizon; moderately firm in upper 10cm; moderately firm

fragment strength; slightly sticky, very plastic; few very fine fibrous roots mostly dead; common inclusions of chopped and ploughed-in straw; nodules at the base of the horizon; sharp wavy boundary.

34-42 Eb Reddish brown (5YR 5/4); clay loam (21%*c*, 37%*z*) very slightly stony (2%) as above; moist; weakly developed coarse angular blocky peds; high packing density; slightly porous; very few very fine fissures between peds; 0.5% fine and very fine macropores; moderately strong ped strength; very firm soil strength; slightly sticky, moderately plastic; few very fine fibrous roots mainly along structure faces; few coarse earthworm channels filled with Ap material; non-calcareous; common ferri-manganiferous soft concretions and nodules; many continuous faint organic-clay coats on ped faces; abrupt wavy boundary.

42-61 2Bt(g) Reddish brown (2.5YR 4/4) with reddish brown (5YR 4/3) ped faces; stoneless; clay (36%*c*, 55%*z*); moist; moderately developed adherent coarse and very coarse prismatic breaking down to coarse to fine angular blocky; high packing density; very slightly porous; 0.5% fine and very fine macropores; no fissures in situ; very firm soil strength; moderately strong ped strength; moderately sticky, very plastic; few very fine fibrous roots mainly down ped faces; very few earthworm channels in top 10cm filled with Ap and Eb material; few fine ferri-manganiferous soft concretions many continuous distinct clay coats (5YR

4/3 and 5/3) on ped faces and many continuous distinct 5YR 5/4 clay coats on pores. Clear even boundary.

61-104 2BCt Reddish brown (5YR 4/3 and 5/3); moderately stony (20%) (very stony (40%) in places), silty clay loam (30%*c*, 55%*z*); small, medium large angular and tabular (5GR 7/1) greenish grey siltstone and sandstone 'skerries'; moist; moderately developed fine angular block - fine platy in places associated with the skerries; high packing density; slightly porous; 0.1% very fine pores; no visible fissures; very weak soil strength; moderately firm ped strength; slightly sticky, very plastic; no roots; calcareous; very few ferri-manganiferous soft concretions; few discontinuous clay coats on ped faces.

THE WHEAT PLOT

Profile No.: SK654/9916/3, (Whitfield, 1987).

Horizon
depth (cm)
and
notation

Description of horizons

- 0 - 32 Ap Dark brown (7.5YR 3/3 rubbed and moist); stoneless clay loam; moist; moderately developed fine subangular block structure with moderate medium subangular blocks at about 25cm depth; low packing density; moderately porous, medium packing density beneath; slightly porous; many fine pores and fissures; moderately weak soil and ped strength becoming moderately firm below, with some peds exhibiting very firm characteristics due to compaction; slightly sticky, moderately plastic; common fine fibrous roots, occasional medium fleshy roots; much straw incorporated with small patches of rotting muck at the base of the ploughed layer; sharp smooth boundary.
- 32-46 Eb(g) Brown to strong brown(7.5YR 4/5, rubbed 7.5YR 4/4); stoneless clay loam, with layers of dark brown material about 1cm thick incorporated from the horizon above becoming less frequent towards base. Few fine faint and distinct clear brown to dark brown (7.5YR 4/4) mottles; slightly moist; moderately developed medium subangular blocky structure, some peds with brown to dark brown (7.5YR 4/3) faces; high packing density; slightly porous; common fine

pores and fissures; moderately firm soil and ped strength; moderately sticky, moderately plastic; common fine fleshy roots in root channels coated with dark brown (7.5YR 3/3) material, common fibrous roots few large soil filled worm channels; common rounded ferri-manganiferous concretions; sharp smooth boundary.

42-67 2Bt(g) Reddish brown (2.5YR 4/4, rubbed 5YR 4/3) with few fine distinct clear brown to dark brown (7.5YR 4/4) mottles on ped interiors, some thin (40-60mm) greenish grey (5GY 6/1) streaks, especially towards base of horizon; stoneless clay; well developed medium prismatic structure which readily breaks into fine prisms with reddish brown (5YR 4/3) faces, some with dark reddish grey (5YR 4/2) patches on the ped faces; high packing density; very slightly porous; fine fissures between peds; fine pores in ped interiors; very firm ped strength; moderately sticky, moderately plastic; common roots, often through ped interiors, but generally concentrated between structures; common small rounded ferri-manganiferous nodules; abrupt wavy boundary.

67-90 2BCt Reddish brown(5YR 5/4, rubbed 5YR 4/4) with common reddish brown (5YR 4/3) medium and fine, distinct clear mottles; small prominent clear/sharp greenish grey (5GY 6/1) patches associated with weathering siltstone; moderately stony; silty clay loam with medium and large tabular fine sandstone fragments often coated on their surfaces with reddish

brown material (5YR 4/4); moist; generally apedal, massive, but with small patches with weak fine subangular blocky structure; high packing density; very slightly porous; few fine pores; moderately weak soil strength; moderately sticky, moderately plastic; few fine roots; calcareous; sharp wavy boundary.

at 90 Cr Hard greenish grey (5GY 5/1 and 6/1) siltstone.

The Upton soil series.

The following description is taken from Reeve (1989).

Both profiles are very similar, being developed in a thin remnant of loamy drift which overlies, and is partly mixed with, weathered chalk at 25 to 35cm depth. Minor variations across the sites occur in the depth to a coherent, bedded, chalk Cr horizon and the nature of the weathered chalk Cu horizon.

In both profiles the Ap horizons consist of dark brown, clay loam to silty clay loam with about 12 to 14% (by volume) chalk stones and 1 to 2% flints. CaCO₃ contents of the fine earth fraction appear to be very high at 56 to 62% but the brownish colour of the topsoil suggests that they are considerably lower than this and the analysed figures may be misleading if soft chalk stones have been crushed and incorporated within the topsoil fine earth during sample preparation. Below the Ap is a thin mixed horizon with an irregular

lower boundary. It comprises small pockets or inclusions of brown or yellowish brown Bw material within a light yellowish brown extremely calcareous chalk 2Cu or 2BCu matrix containing between 40 and 70% chalk stones. CaCO_3 contents range from 66 to 79% but as in the Ap horizon it is possible that these values may be slightly exaggerated. In both profiles the mixed Bw and 2Cu or 2BCu is underlain by an intermittently occurring, light yellowish brown 2Cu horizon with CaCO_3 content of between 70 and 80%, but considerably less chalk stones than the horizons above and below. This horizon has a very convoluted lower boundary and is often present only as wedge shaped inclusions between the mixed Bw and 2Cu and the underlying 3Cu horizons. The Cr horizon in both plots consists of soft thinly bedded chalk with common vertical or inclined fissures which tend to give very large tabular chalk stones if the horizon is disturbed. Earthworms exploit both profiles down to the Cr.

These Upton soils are, in most respects, typical of Upton soils throughout England but as mentioned above, their topsoils appear to contain a much larger amount of CaCO_3 than is usual (56 to 62%, as opposed to an average of 26% for nine other profiles).

THE GRASS PLOT

Profile No.: TL02/8577/2, (Hollis, 1988).

Horizon
depth (cm)
and
notation Description of horizons

0 - 27 Ap Brown to dark brown (10YR 4/3) slightly stony (14% by volume) clay loam (23%*c*, 60%*z*); medium and small with less common very small and large subangular chalk stones; <1% small subangular flints and medium rounded quartzites; moist; moderately developed medium and fine subangular blocky peds with common fine granular peds often associated with roots; low packing density; very porous, no fissures, macropores difficult to estimate but approx. 0.5% very fine macropores; very weak soil strength (almost loose); moderately weak ped strength; moderately sticky, very plastic; many fine and very fine fibrous roots; common remains of ploughed-in burnt stubble; few earthworms present when pit dug; extremely calcareous; sharp smooth boundary.

27-35 2BCu Brown (7.5YR 5/4); very stony but with variable stone content from 40% to 70%, silty clay loam (as above); medium small and very small subangular and angular chalk stones; moist; structure indeterminate because of stones; low packing density; extremely porous, no fissures, macropores impossible to estimate because of stones; loose soil strength; moderately weak ped strength; moderately sticky,

very plastic; many fine and very fine fibrous roots; common fine inclusions of Ap material from earthworm and other faunal activity; extremely calcareous; abrupt wavy boundary.

35-60 2CU Light yellowish brown (10YR 6/4) with few fine inclusions of 7.5YR 6/4 and common very fine inclusions of white 10YR 8/1; very stony (37%; 45 in places); carbonatic silty clay loam; medium and small with common very small and a few large subangular chalk stones; moist; weak, medium and fine subangular blocky peds in fine earth pockets; low packing density; extremely porous, no fissures, macropores impossible to determine; very weak to loose soil strength; very weak ped strength; slightly sticky, slightly plastic; common fine and very fine fibrous roots; few inclusions and infillings of Ap and Bw material in earthworm channels; extremely calcareous; abrupt wavy boundary.

60-94 3Cu 50% white (10YR 8/1) and 50% light grey (10YR 7/2); extremely stony (80% by volume) carbonatic silty clay loam (chalk flour); medium and large with common small and very small angular and subangular chalk stones; moist; structure indeterminate; low packing density; extremely porous, fissures and macropores impossible to determine; loose soil strength; non-sticky, slightly plastic; common fine and very fine fibrous roots; rare pockets of material with 10YR 5/2 and 4/2 coloured fine earth containing

more roots; extremely calcareous; clear smooth boundary.

94-110 3Cr Soft 2.5Y 8/2 and 7/2 fractured chalk often breaking into tabular stones.

THE WHEAT PLOT

Profile No.: TL02/8577/1, (Beard, 1988).

Horizon
depth (cm)
and
notation Description of horizons

0 - 25 Ap Dark brown (10YR 3/3, rubbed 10YR 3/3); fine distinct strong brown (7.5YR 5/6) sharp mottles derived from small pieces of weathered brick and tile; clay loam, (23%c, 58%z); slightly stony (14%), small and medium subangular (code 31) chalk, rare tabular subrounded flint (code 22); moist; moderately developed fine subangular blocky structure (fragments), some localised patches of medium angular fragments probably as a result of compaction; low packing density; extremely porous; very fine fissures; very fine pores (3%); moderately weak soil and ped strength; moderately sticky, moderately plastic; many fibrous very fine cereal roots; ploughed-in straw stubble common; occasional earthworm channel and earthworm droppings; extremely calcareous (12%); sharp smooth boundary.

- 25-37 2Cu Yellowish brown (10YR 5/4) light yellowish brown (2.5Y 6/4) and white (2.5Y 8/2) clay loam (25%*c*, 50%*z*); very stony (40%) small and medium subrounded tabular chalk (code 31), rare tabular subrounded flint (code 22), interior of some chalk stones have yellowish red pin pricks of colour; slightly moist; structureless, massive with weak very fine subangular structure where less stony; medium packing density; very (to extremely) porous; very fine macropores(2%); sample unobtainable for estimating soil strength; moderately sticky, very plastic; very fine fibrous cereal roots common; occasional earthworm channel lined with surface soil; extremely calcareous; abrupt wavy boundary.
- 37-68 2Cu Pale yellow (2.5Y 7/4, rubbed 2.5Y 7/3) silty clay loam; slightly stony (9%); small and medium rounded and weathered subrounded chalk; slightly moist; structureless, massive; medium packing density (marginal to low, 1.4); moderately (to very) porous; very fine macropores (2%); very weak soil strength; slightly sticky, slightly plastic; few very fine fibrous cereal roots; extremely calcareous; abrupt irregular boundary.
- 68-110 White (5Y 8/1, rubbed 5Y 8/1) extremely stony, medium and large subrounded (code 31) chalk stones; slightly moist; structureless; medium packing

density; few very fine fibrous roots; extremely calcareous; abrupt irregular boundary.

110+ White (5Y 8/1) bedded chalk with local patches of similarly coloured soft weathered ares.

The Evesham soil series.

The following description is taken from Reeve (1989).

Both profiles at the experimental site qualify as Evesham series and are developed in very calcareous Mesozoic (Gault) clay with slight drift contamination in its upper layers. Relatively unweathered, weak fine angular blocky to massive parent material, designated BC(g)k, occurs at about 70 to 80cm depth in both plots, the main variation occurring in the depth of decalcification. In both profiles, the Ap horizon is slightly calcareous, very clayey and compacted. It overlies a slightly mottled, calcareous, weathered angular blocky Bw(g) horizon that has also been badly compacted in its upper parts. Under wheat, the Bw(g) is thick and passes directly into relatively unweathered parent material at about 70cm. There is no intervening BCgk horizon.

Although both profiles qualify as Evesham series, variations in the presence of, or depth to, the BCgk horizon means that there are likely to be slight differences between the water regime of the two plots. Structure and gley morphology suggest that under wheat the soil is of wetness class III and under grass, class II. The main difference between this profile and other Evesham soils is the very

large topsoil clay content (70% clay), the average (of 43 analysed profiles) for the series being 52%.

THE GRASS PLOT

Profile No.: TL03/7741/3, (Beard and Whifield, 1987).

Horizon
depth (cm)
and
notation Description of horizons

0 - 23 Ap Very dark greyish brown (10YR 3/2) moist and rubbed; stoneless clay with occasional small and medium angular flints; moist becoming slightly moist with depth with well developed medium and fine granular structure in top 5cm passing to moderately well developed medium subangular blocky which readily break into fine angular fragments under slight pressure down to 12cm and then strong coarse prisms as a result of compaction and passing structurally into the horizon below; low packing density passing to high packing density below 12cm depth and with moderate and slight porosity respectively; very few fine and very fine pores at base; well fissured in top 12cm becoming very strong ped strength at base of horizon; moderately sticky, very plastic; many fine and very fine fibrous grass roots spreading horizontally across the top of the large prismatic peds at about 12cm depth; leather jackets; slightly calcareous; sharp wavy boundary.

23-70 Bw(g) Dark greyish brown to olive brown (2.5YR 4/3) few medium distinct clear dark yellowish brown (10YR

4/4) mottles on ped interiors; stoneless clay with occasional small rounded quartzites and occasional flint fragments; slightly moist; well developed coarse prismatic peds extending down from the topsoil horizon where compacted and then changing at about 39cm depth to moderately developed medium and coarse prisms which readily break into medium subangular blocky and angular blocky peds, and further into fine angular secondary peds with shiny faces on the major ped faces; high packing density; very slightly porous but less so below 39cm depth; few fine and very fine pores and fissures; there is a sharp break between the compacted material and that below it, and the two zones part from each other with ease; strong ped strength in the upper part of the horizon, becoming moderately firm soil and ped strength below; moderately sticky, very plastic; common fine fibrous roots both through the peds and along the ped faces; common small rounded ferri-manganiferous concretions and irregular hard accumulations of secondary calcium carbonate; abrupt smooth boundary.

70-99 B(g)k Light grey to grey (5Y 6/1) moist with a rubbed colour of (5Y 5/3) with common fine and medium fine distinct clear light olive brown (2.5Y 4/4) mottles; stoneless clay; moist; very weak fine angular blocky structure, mainly structureless; high packing density; very slightly porous; few fine pores; slightly sticky, moderately plastic; moderately firm soil strength; very few fine fibrous roots; very calcareous with accumulations of secondary calcium carbonate;

occasional belemnites and few small soft ferri-manganiferous concretions with few hard manganese nodules.

THE WHEAT PLOT

Profile No.: TL03/7741/1, (Beard and Whifield, 1987).

Horizon
depth (cm)
and
notation Description of horizons

0 - 26 Ap Very dark greyish brown (10YR 3/2 moist and rubbed), with small patches of olive (5Y 5/3) clay ploughed in from the horizon below, stoneless clay with occasional small angular flints and rounded quartzite; moist; moderately weak fine subangular blocky structure passing to weak coarse subangular blocky fragments at about 15cm depth with fine angular blocky weathered fragments in the top 2cm; some distinct laminae due to compaction and there is a tendency for the soil to break along horizontal planes; the bulk of the horizon has a high packing density; slightly porous with some very slightly porous fragments; few fine pores; very fine horizontal fissures; moderately firm soil and ped strength; slightly sticky, moderately plastic; very few fine fibrous roots with thicker fleshy bean roots down to about 4cm depth; patches of ploughed-in straw; slightly calcareous; sharp wavy boundary.

26-38 Bw(g) Olive (5Y 5/3) moist colour, rubbed poor match (4Y 5/3) with common fine light olive brown mottles with

clear boundaries; stoneless clay with occasional small flints and rounded quartzites; very moist; moderately weak fine angular blocky structure with a tendency to apedal massive; high packing density; very slightly porous; few fine pores; deformable; moderately sticky, very plastic; very few fine fleshy and fibrous roots; few small irregular manganiferous concretions/nodules; calcareous; sharp smooth boundary.

38-73 BCgk Olive (5Y 5/3) moist and rubbed colours with many fine distinct clear light olive brown (2.5Y 5/4) and medium olive grey (5Y 5/2) mottles; stoneless clay; moist; moderately developed medium prismatic structure with shiny olive grey (5Y 5/2) faces; high packing density, very slightly porous but slightly lower packing density than the horizon above; few fine pores; moderately firm soil and ped strength; moderately sticky, very plastic; few fine fibrous roots, both within structural fragments and along ped faces; few very small rounded manganiferous concretions/nodules; very calcareous with common nodules and small soft concentrations of calcium carbonate; thin coats around small stones and calcareous nodules; abrupt smooth boundary.

73+ BC(g)k Light grey to grey (5Y 6/1) moist, with a rubbed colour of 5Y 5/4; common medium and fine light olive brown (2.5Y 5/4) distinct clear mottles and medium prominent sharp light olive brown (2.5Y 5/6) mottles; stoneless clay; very weak fine angular blocky

structure, mainly structureless; high packing density; very slightly porous with fine fissures and pores throughout; slightly sticky, moderately plastic; moderately firm soil strength; very few fine fibrous roots; very calcareous with common small (up to 20mm) nodules of secondary calcium carbonate concentrated in specific zones.

The Denchworth soil series.

The following description is taken from Reeve (1989).

The two profiles sampled are remarkably similar in all respects. Topsoils are clays and stoneless except for a few introduced stones. The 25cm thick topsoil under wheat reflects the average cultivation depth for these soils and the rather variable, sometimes massive structures are indicative of cultivations having to be carried out in less than ideal moisture conditions.

The distinctly mottled Bg horizon is slowly permeable throughout. Coarse pores are least in the upper part of the Bg above 40cm depth where structure is only weakly or moderately developed, but below 40cm depth the structure is more strongly developed and the coarse porosity is slightly larger, albeit still small.

On gently sloping sites such as these, unweathered mudstone is not reached until depths of 2 to 3m or more, but there is a transitional

BC horizon which starts below 70 to 90cm depth. This contains common secondary calcareous nodules and concentrations and occasional fossils weathered from the mudstone.

Both profiles are good examples of the Denchworth series as mapped extensively on the Mesozoic mudstones of central England.

Subsoil clay contents vary from 45 to 85%, according to the particular formation on which the Denchworth soils are developed but 55 to 60% is average. Calcium carbonate content of deeper layers varies similarly, calcareous examples such as in these soils being somewhat better structured than in deeply decalcified profiles.

THE GRASS PLOT

Profile No.: SU29/4745/1, (Beard, 1988).

Horizon
depth (cm)
and
notation Description of horizons

0 - 18 Ap Very dark greyish brown (10YR 3/2) and greyish brown to light olive brown (2.5Y 5/3) being patches of the subsoil (rubbed 2.5Y 3/2); few very fine faint sharp dark yellowish brown (10YR 4/6) mottles and few fine dark greyish brown (10YR 4/2) faint diffuse mottles (ped face colours); clay (43%*c*, 30%*z*); stoneless but some small subrounded limestone fragments; moist; moderately developed, medium subangular blocky structure with some angular faces

on most peds; medium packing density; slightly porous; very fine fissures; very fine pores (1%); moderately firm soil and ped strength; moderately sticky, very plastic; abundant fine and very fine fibrous grass roots; non-calcareous; a few large earthworms; abrupt irregular boundary.

18-36 Bg1 Light olive brown (2.5Y 5/4, rubbed 2.5Y 5/3); common fine distinct sharp light olive brown (2.5Y 5/6) and many medium distinct diffuse dark greyish brown (2.5Y 4/2) mottles; clay (60%*c*, 30%*z*); stoneless; moist; weakly developed adherent medium and coarse angular structure with shiny faces locally coated with film of moisture (compacted); high packing density; very slightly porous; few very fine fissures; very fine pores (1%); moderately firm (deformable) soil and ped strength; very sticky, very plastic; many very fine fibrous grass roots; occasional earthworms; non-calcareous; few soft ferri-manganiferous concentrations; many discontinuous distinct stress orientated coats on moist ped faces, possibly accumulations of clay but none visible; clear wavy boundary.

36-61 Bg2 Olive (5Y 4/3, rubbed 5Y 4/3 poor match); many fine distinct sharp light olive brown (2.5Y 5/4) and very many medium and coarse distinct diffuse olive grey (5Y 5/2) mottles; clay; stoneless; very moist; strongly developed very coarse angular blocky structure parting readily to strong fine angular structure; high packing density; very slightly porous; very fine pores

(1%); very weak soil strength, moderately weak ped strength; very sticky, very plastic; few very fine fibrous grass roots; non-calcareous; entire distinct stress orientated coats (slickensides) on ped faces; abrupt wavy boundary.

61-110 BCgk Dark grey (5Y 4/1, rubbed 5Y 4/2); many fine and medium distinct sharp light olive brown (2.5Y 5/6) mottles; clay; stoneless; very moist; strongly developed very coarse prismatic structure parting readily to medium angular structure; high packing density; very slightly porous; very fine pores (2%); weak soil strength, moderately weak ped strength; very sticky, very plastic; few very fine fibrous grass roots; calcareous; common irregular soft calcium carbonate concentrations and nodules (5-10mm in size); many discontinuous stress orientated coats (slickensides) mainly on the faces of the larger structures.

THE WHEAT PLOT

Profile No.: SU29/4745/2, (Whitfield, 1988).

Horizon depth (cm) and notation	Description of horizons
--	-------------------------

0 - 26 Ap	Very dark brown (10YR 3/2) stoneless clay; very moist; very weak medium subangular blocky structured, often massive in parts but with moderately
-----------	--

developed fine angular blocky weathered structures on the top 4cm; high packing density; slightly porous; deformable; very sticky, very plastic; common fine fibrous and fleshy cereal roots; non-calcareous; abrupt smooth boundary.

26-43 Bg Dark greyish brown (2.5Y 4/2) with many small and medium faint clear light olive brown (2.5Y 5/4) and few prominent clear brown to strong brown (7.5YR 4/4) mottles; stoneless clay but with occasional medium and large angular and rounded flints; moist; moderately strong fine angular blocky structure with weak platy peds in the top 5cm along which water is issuing as it percolates through the topsoil; giving shiny faces to most peds; high packing density; very slightly porous; few fine and very fine pores; fine fissures between peds; moderately firm soil and ped strength; very sticky, very plastic; few fine fibrous roots some in yellowish brown (10YR 5/8) clay filled channels; occasional small rounded manganiferous nodules; sharp smooth boundary.

43-91 Bg2 Olive grey (5Y 4/2) with many distinct medium clear light olive brown (2.5Y 5/4) mottles; clay; moist well developed fine and medium angular blocky structure with shiny ped faces of olive grey (5Y 4/2) many of which are inclined; high packing density; very slightly porous; common fine pores; very fine fissures between peds; moderately weak soil and ped strength; very sticky, very plastic; becoming slightly calcareous between 85 and 91cm and with many

distinct clear medium and fine brown (10YR 5/3) mottles; abrupt smooth boundary.

91-110 BCgk Olive grey (5Y 4/2) with many distinct clear medium and large olive (5Y 5/4) mottles; clay; moist; weakly developed medium prismatic structure which readily breaks into fine and medium angular blocky peds; high packing density; very slightly porous; common small and very fine intrapedal pores; common large, but discontinuous shiny ped faces at depth; many very fine fissures; moderately firm soil and ped strength; very sticky, very plastic; common small rounded concretions of secondary calcium carbonate; some large gryphaea at base.

Appendix 2

Figure 2.1A Cuckney series

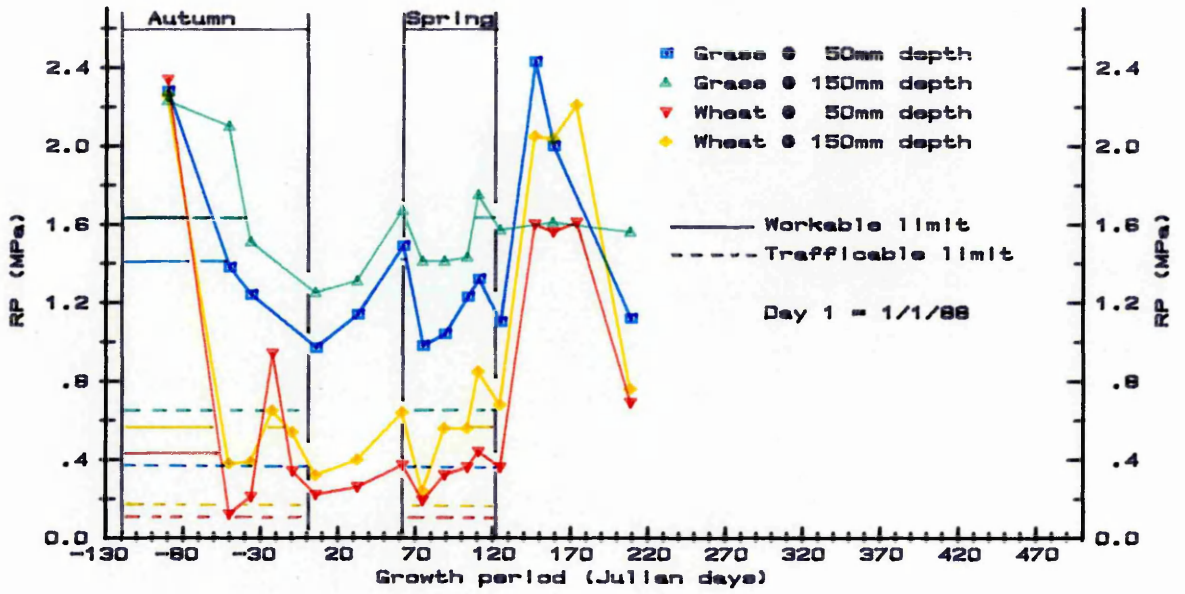


Figure 2.2A Wlok series

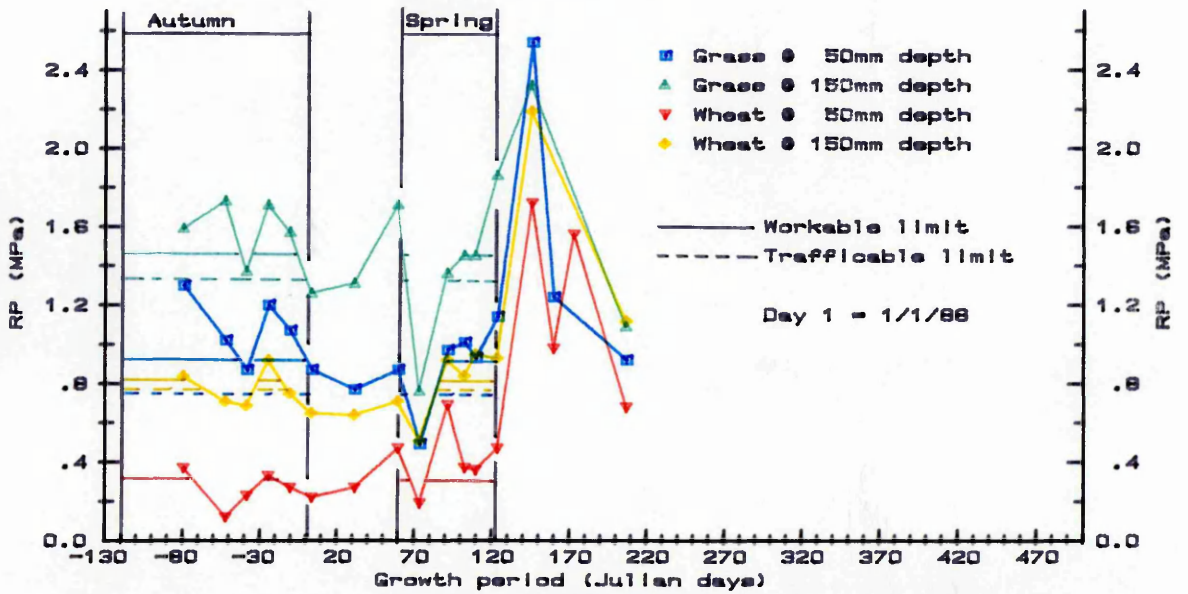


Figure 2.3A Upton series

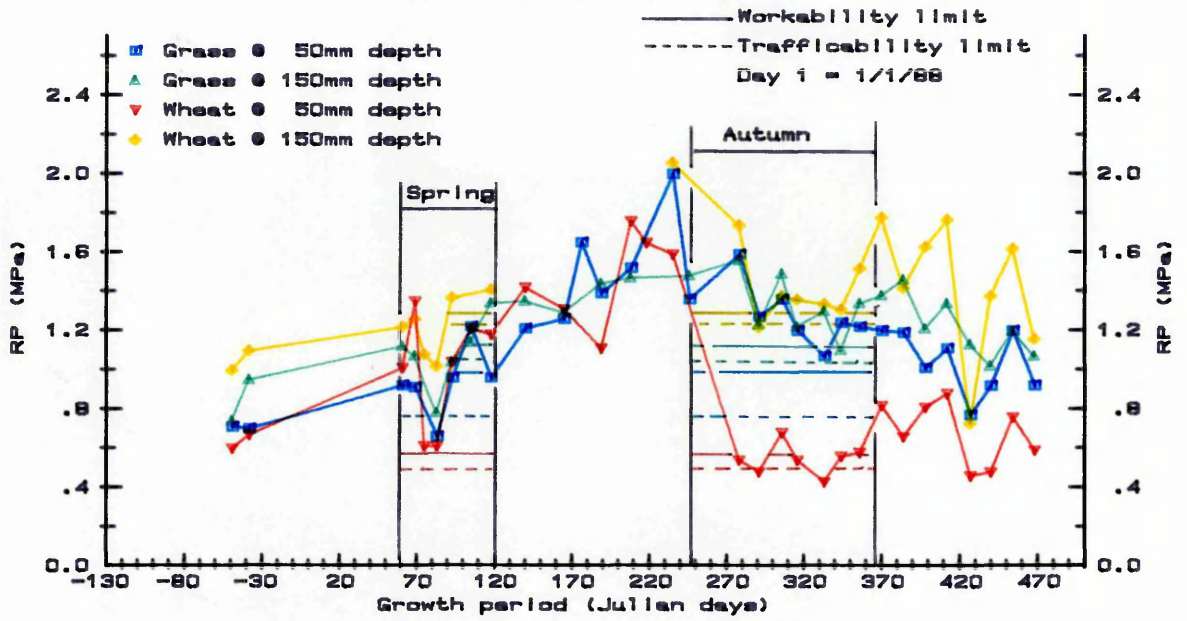


Figure 2.4A Whimble series

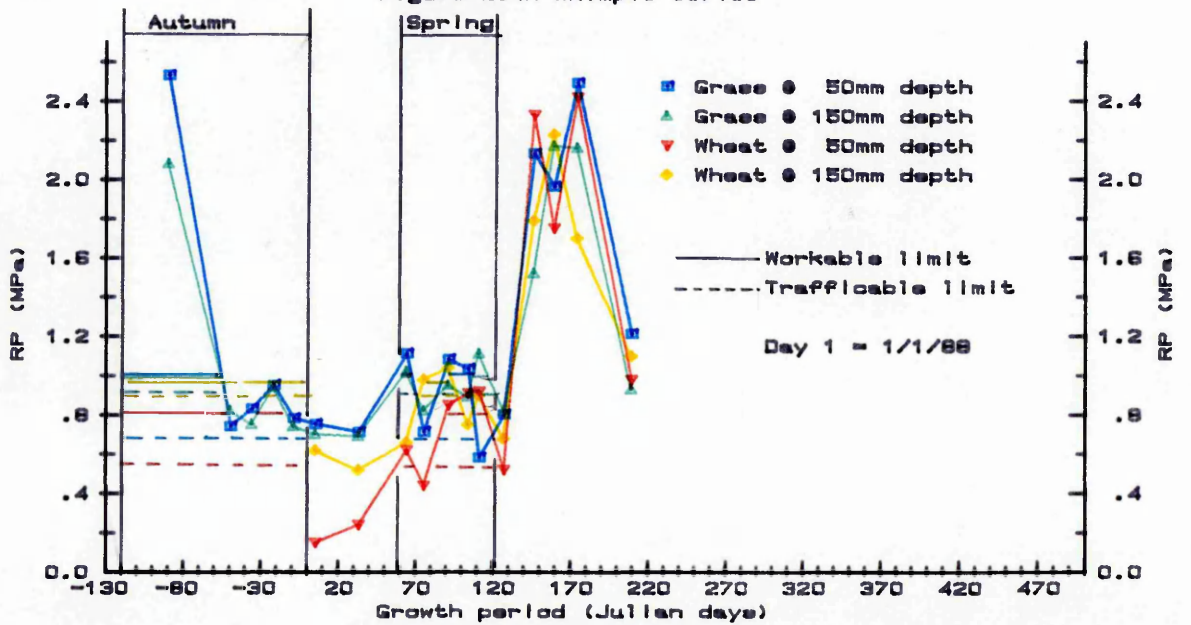


Figure 2.5A Evesham series

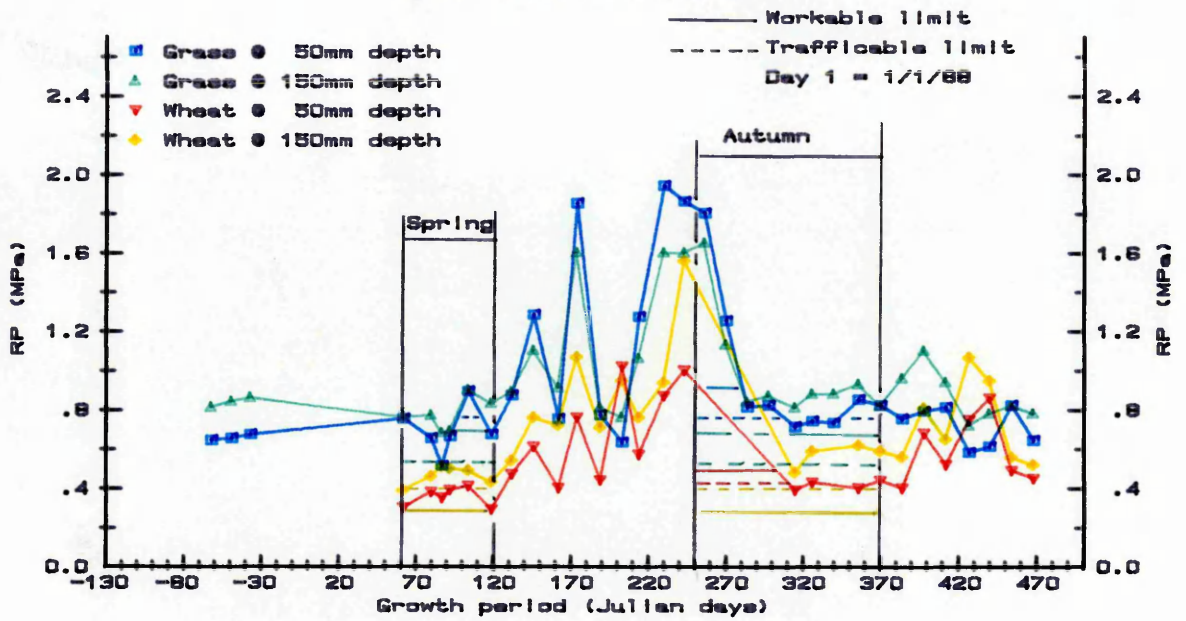


Figure 2.6A Denchworth series

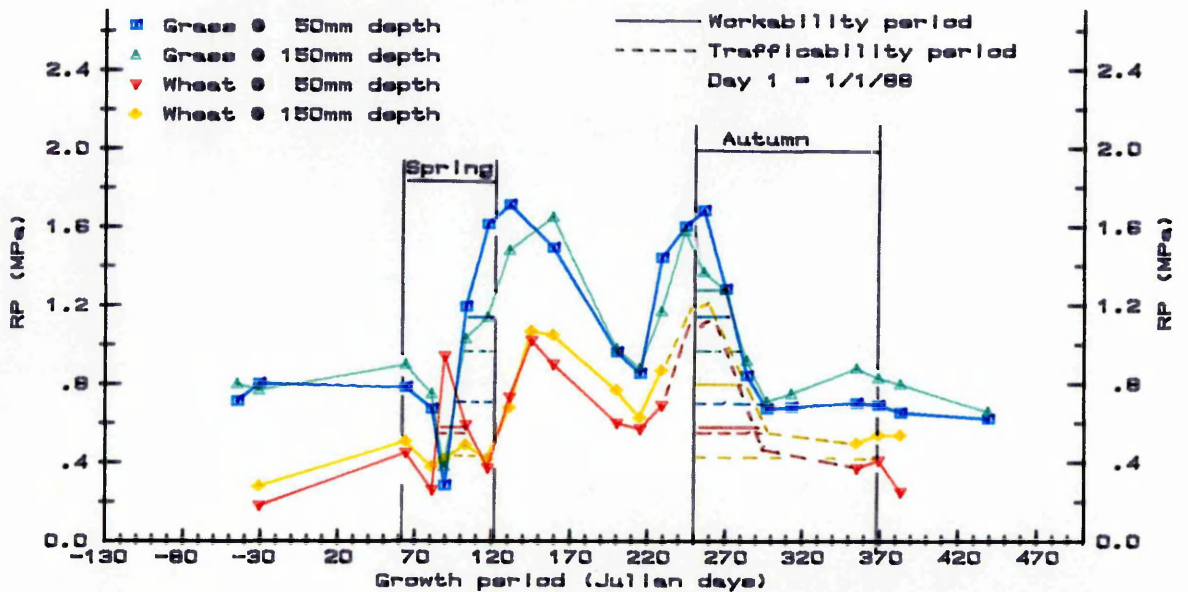


Table 2.1A The number of workable days.

Soil series	Crop	The workable period (Julian days)		No. of days unsuitable for field operations during the workable period due to excess rainfall		No. of workable days	
		Autumn	Spring	Autumn	Spring	Autumn	Spring
Cuckney(1)	Grass	-122 to -50	60 to 67	5	0	58	7
	Wheat	-122 to -51	108 to 117	5	2	57	7
Wick(1)	Grass	-122 to -46	103 to 108	15	0	91	17
		-33 to -5	111 to 121				
	Wheat	-122 to -81	90 to 121	7	1	46	31
		-28 to -18					
Upton(2)	Grass	244 to 344	104 to 117	13	0	106	17
		348 to 365	119 to 121				
	Wheat	264 to 278	93 to 121	6	1	67	28
		300 to 316					
		345 to 365					
Whimple(1)	Grass	-122 to 53	64 to 70	12	0	58	7
	Wheat	-	90 to 97	-	0	-	8
Evesham(2)	Grass	244 to 281	0	5	0	33	0
	Wheat	244 to 304	0	8	0	53	0
Denchworth(2)	Grass	244 to 274	0	5	1	26	0
	Wheat	244 to 287*	0	9	0	35	0

(1) Data for Autumn 1987 and Spring 1988. (2) Data for Spring and Autumn 1988. * Estimated data

Table 2.2A The number of trafficable days.

Soil series	Crop	The trafficable period (Julian days)		No. of days unsuitable for field operations during the trafficable period due to excess rainfall		No. of trafficable days	
		Autumn	Spring	Autumn	Spring	Autumn	Spring
Cuckney(1)	Grass	-122 to 0	60 to 121	19	11	104	51
	Wheat	-122 to 0	60 to 121	19	11	104	51
Wick(1)	Grass	-122 to 0	60 to 64 92 to 121	23	1	100	34
	Wheat	-122 to -72 -27 to -18	87 to 121	14	1	47	34
Upton(2)	Grass	244 to 365	60 to 72 95 to 121	13	2	109	38
	Wheat	244 to 288 297 to 323 340 to 365	91 to 121	9	1	89	30
Whimple(1)	Grass	-122 to -51 -23 to -18	60 to 72 84 to 103 108 to 110 117 to 120	2	6	70	34
	Wheat	-	80 to 98 110 to 112	-	4	-	18
Evesham(2)	Grass	244 to 304 348 to 365	100 to 111	9	0	70	2
	Wheat	244 to 3102	0	8	0	59	0
Denchworth(2)	Grass	244 to 283	102 to 121	8	3	32	17
	Wheat	244 to 293*	87 to 107	9	0	41	21

(1) Data for Autumn 1987 and Spring 1988. (2) Data for Spring and Autumn 1988. * Estimated data

Appendix 3

Calibration of the neutron probe.

Data from the neutron probe was processed using a combination of field calibrations for the top 20cm of the soil profile and standard equations, from Bell (1976), for 30cm+.

The field calibration procedure is outlined in Bell (1976). Triplicate undisturbed soil cores of 222cm³ were taken in close proximity to the access tubes at 2.5 to 7.5cm and 12.5 to 17.5cm using a falling hammer corer (Avery and Bascomb, 1974). The volumetric moisture content of the cores was used to calibrate the neutron probe readings for that particular day. The results are presented in Table 3.1A.

Table 3.1A Calibration results for the neutron probe (top 20cm of the soil profile).

Soil series	Crop	Depth (cm)	Vol. moisture content			Average count	Average std count
			Access tube number 1	2	3		
Cuckney	Grass	10	14.0	21.0	15.9	195	1080
		20	19.0	23.8	20.8	271	1080
	Wheat	10	13.8	14.1	15.8	216	1080
		20	19.6	22.1	21.2	321	1080
Wick	Grass	10	25.6	24.4	25.6		1080
		20	33.3	32.5	35.3	data	1080
	Wheat	10	22.5	21.8	23.7	misplaced	1080
		20	28.5	27.9	30.1		1080
Whimble	Grass	10	29.8	30.3	29.5	386	1080
		20	37.2	35.6	35.1	452	1080
	Wheat	10	31.9	31.3	31.4	411	1080
		20	36.2	35.5	35.5	456	1080
Upton	Grass	10	35.8	29.1	34.5	347	845
		20	32.0	31.8	31.9	369	845
	Wheat	10	36.0	33.8	31.6	286	845
		20	27.9	29.1	28.9	349	845
Evesham	Grass	10	47.4	54.8	49.8	391	845
		20	47.5	45.1	43.8	419	845
	Oats	10	55.1	54.8	53.0	308	845
		20	49.7	54.6	51.3	383	845
Denchworth			Data misplaced				

From Table 3.1A and standard equations in Bell (1976), the following calibration equations, presented in Table 3.2A, were adopted and applied to neutron probe data independently of crop cover.

Table 3.2A Calibration equations for the neutron probe.

Soil series	Depth (cm)	Calibration equation
Cuckney	10	$0.0673 \cdot \text{count} + 3.880$
Wick	20	$0.0786 \cdot \text{count} - 0.077$
Whimple	30	$0.0730 \cdot \text{count} - 0.024$
Upton	10	$0.1022 \cdot \text{count} - 0.016$
	20	$0.0932 \cdot \text{count} - 0.024$
	30	$0.0932 \cdot \text{count} - 0.024$
Evesham	10	$0.0150 \cdot \text{count} + 3.880$
Denchworth	20	$0.1001 \cdot \text{count} - 0.077$
	30	$0.1127 \cdot \text{count} - 0.012$

Appendix 4

Logistic regression analysis results for resistance to cone penetration against soil moisture deficit for the top 200mm of the soil profile at six experimental sites.

The regression curves are of the form: $y = A + \frac{C}{[1 + e^{-B(x-M)}]}$

Soil series	Crop	Depth (mm)	B	M	C	A	Asymptotic		R ²	F
							Min (MPa)	Max (MPa)		
Cuckney	Grass	50	0.2467	9.66	1.916	0.946	0.95	2.86	0.99	<0.001
		150	0.9144	1.37	0.852	1.155	1.16	2.01	0.50	0.196
	Wheat	50	0.3190	14.49	1.437	0.255	0.26	1.69	0.80	0.001
		150	0.3910	15.65	1.838	0.428	0.43	2.27	0.95	<0.001
Wick	Grass	50	0.2158	34.57	53.910	0.928	0.93	54.84	0.82	0.004
		150	0.0434	-66.08	20.760	-17.930	-17.93	2.83	0.77	0.031
	Wheat	50	0.1436	48.52	47.690	0.288	0.29	47.98	0.90	<0.001
		150	0.0590	23.00	4.400	-0.060	-0.06	4.34	0.93	<0.001
Upton	Grass	50	0.0350	-60.85	14.320	-11.710	-11.71	2.61	0.60	0.015
		150	0.6560	-2.99	0.639	0.706	0.71	1.35	0.71	0.014
	Wheat	50	0.3781	5.09	0.849	0.542	0.54	1.39	0.66	0.003
		150	0.2060	12.80	1.730	0.954	0.95	2.68	0.99	0.007
Whimble	Grass	50	0.4850	19.51	1.728	0.816	0.82	2.54	0.97	<0.001
		150	0.6370	21.62	1.329	0.815	0.82	2.14	0.96	<0.001
	Wheat	50	0.2740	14.37	2.080	0.372	0.37	2.45	0.89	0.007
		150	1.5240	12.08	1.197	0.710	0.71	1.91	0.83	0.018
Evesham	Grass	50	0.2080	12.42	1.340	0.612	0.61	1.95	0.89	<0.001
		150	0.2440	14.52	0.851	0.793	0.79	1.64	0.91	<0.001
	Wheat	50	0.0678	109.00	103.500	0.297	0.30	103.80	0.89	<0.001
		150	0.1162	65.07	32.980	0.492	0.49	33.47	0.87	<0.001
Denchworth	Grass	50	0.1910	19.46	1.190	0.522	0.52	1.71	0.77	0.004
		150	0.0395	119.30	42.750	0.200	0.20	42.95	0.75	0.005
	Wheat	50	0.0246	242.00	90.240	0.005	0.01	90.24	0.62	0.032
		150	0.1550	42.27	0.704	0.396	0.40	1.10	0.71	0.008

Appendix 5

The Soil Survey and Land Research Centre procedure for predicting the number of machinery work days, (Thomasson, 1982), is given below.

The soil profile is allocated a workability rating (aa to f) using soil morphology and physical data-sets as shown in Table 5.1A.

Table 5.1A. Soil assessment for workability and trafficability.

Wetness class	Depth to impermeable horizon (cm)	Mineral topsoils			Humose or peaty topsoil
		Retained water capacity Low	Medium	High	
I	>80(sandy)	aa	-	-	-
	>80	a	a	a	a
II	>80	a	ab	b	a
	40-80	b	b	bc	b
III	>80	b	c	c	b
	40-80	c	c	cd	c
	<40	c	cd	d	d
IV	>80	c	d	d	d
	40-80	c	d	de	e
	<40	d	de	e	f
V	All depths	e	f	f	f
VI	All depths	f	f	f	f

Each rating class is given a 'soil weighting' in days to show its relative advantage (+) or disadvantage (-) in terms of opportunity for field traffic and cultivation, see table 5.2A.

Table 5.2A. Soil weightings applied to field capacity data for estimating machinery work days.

Soil assessment	Soil weighting (days)		Total
	Autumn (1Sept-31Dec)	Spring (1March-30April)	
aa	+30	+20	+50
a	+20	+10	+30
ab	+10	+5	+15
b	0	0	0
bc	-10	-3	-13
c	-20	-5	-25
cd	-25	-8	-33
d	-30	-10	-40
de	-35	-13	-48
e	-40	-15	-55
f	-50	-20	-70

Climatic factors are evaluated in terms of meteorological field capacity, defined as zero moisture deficit (Jones and Thomasson, 1985). This is common practice in the UK and uses a simple soil water abstraction model (Smith 1976) to estimate departure from, and return to, field capacity.

From Tables 5.1A and 5.2A, the Wick winter wheat plot is given a soil assessment of 'a', and spring and autumn weightings of +20 and +10 respectively. The 1987 - 1988 season for the Wick site was quite wet and so a 'wet quartile' field capacity period for that area is

selected from the Soil Survey data-base. The meteorological field capacity period extends from 20th October to 1st May.

Autumn machinery work days:-

1st Sept - 20th Oct =	50days
Soil weighting =	+20days

	70days

Spring machinery work days:-

1st May - 30th Apr =	0days
Soil weighting =	+10days

	10days

Appendix 6

Worked examples of the technique, developed in Chapter 5, for predicting the extent of soil disturbance below sinkage plates are presented in this Appendix. Data has been selected from three different plots under specific loading conditions to demonstrate the application of the techniques to phase (1), (2) and (3) situations.

(1) Plot Evesham series arable

Load σ_A = 45kPa, contact width = 0.3m

Soil c = 16kPa

ϕ = 8.6°

γ = 12.939kN/m³

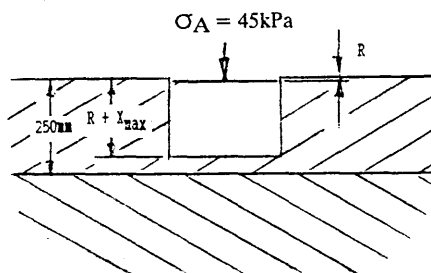


Figure 6.1A Evesham series arable soil profile.

The prediction of the extent of soil disturbance is illustrated in Figure 6.1A. From Table 6.4, 45kPa is below the phase (1) threshold for this soil and so phase (1) deformation is predicted, ie pure compaction with no increase in lateral stress.

To predict sinkage:-

From Figure 5.16:-

$$\sigma_A = \frac{R}{\frac{1}{m_i} + \frac{R}{\sigma_{ULT}}}$$

$$R = \frac{\sigma_A}{m_i \left(1 - \frac{\sigma_A}{\sigma_{ULT}}\right)} \quad [1]$$

Applying equation [1] to data from Table 6.3 for the Evesham arable plot:-

$$R = \frac{45}{8.49254 \left(1 - \frac{45}{246.11}\right)} = \underline{\underline{6.48\text{mm}}}$$

To predict depth of soil disturbance:-

For phase (1) deformation, maximum depth of soil disturbance from the soil surface:-

$$= R + X_{\max}$$

$$= R + \frac{D(\sigma_A - \gamma R)}{4(c + \sigma_p \tan \phi) - \gamma D}$$

$$= 0.00648 + \frac{0.3(45 - 12.939 \times 0.00648)}{4(16 + 10 \tan 8.6^\circ) - 0.3 \times 12.939}$$

$$= \underline{\underline{0.2037\text{m}}}$$

To predict maximum dry bulk density (D_{Bmax}) generated in the disturbed zone:-

$$D_{Bmax} = \frac{D_{Binitial}(2R+X_{max})}{X_{max}}$$

$$= \frac{884(2 \times 0.00648 + 0.2037)}{0.2037} = \underline{\underline{940 \text{ kg/m}^3}}$$

(2) Plot Evesham series grass ley

Load $\sigma_A = 95 \text{ kPa}$, contact width = 0.3m

Soil $c = 16 \text{ kPa}$

$\phi = 8.6^\circ$

$\gamma = 12.939 \text{ kN/m}^3$

$a = 70 \text{ kPa}$

$b = 10 \text{ kPa}$

To predict depth of soil disturbance:-

For phase (2) deformation, maximum depth of soil disturbance below the load (X_{max}) can be determined iteratively from equation [17], section 5.2.2.5:-

$$\sigma_{Amax} = \frac{4X_{max}(a-\sigma_{Amax})}{D(\gamma(R+X_{max})-\sigma_{Amax})} [c+(b-a+K_0\sigma_{Amax})\tan\phi$$

$$+ \frac{K_0(\gamma(R+X_{max})-\sigma_{Amax})}{2} \frac{(a-\sigma_{Amax})\tan\phi}{\gamma(R+X_{max})-\sigma_{Amax}}$$

$$+ \frac{4X_{max}(c+b\tan\phi)}{D} (1 - \frac{a-\sigma_{Amax}}{\gamma(R+X_{max})-\sigma_{Amax}})$$

$$95 = \frac{4X_{\max}(70-95)}{0.3(15.089(0.0037+X_{\max})-95)} [16+(10-70+0.80 \times 95)\tan 8.6^\circ]$$

$$+ \frac{0.80(15.089(0.0037+X_{\max})-95)}{2} \frac{(70-95)\tan 8.6^\circ}{15.089(0.0037+X_{\max})-95}$$

$$+ \frac{4X_{\max}(16+10\tan 8.6^\circ)}{0.3} \left(1 - \frac{70-95}{15.089(0.0037+X_{\max})-95}\right)$$

Try $X_{\max} = 0.411\text{m}$:-

$95 \approx 95.03$

Maximum depth of soil disturbance from soil surface:-

$$= R + X_{\max}$$

$$= 0.0037 + 0.411 = \underline{\underline{0.414\text{m}}}$$

To predict maximum dry bulk density ($D_{B\max}$) generated in the disturbed zone:-

$$D_{B\max} = \frac{D_{B\text{initial}}(2R+X_{\max})}{X_{\max}}$$

$$= \frac{1045(2 \times 0.0037 + 0.411)}{0.411} = \underline{\underline{1064\text{kg/m}^3}}$$

(3) Plot Bearsted series arable

Load $\sigma_A = 95\text{kPa}$, contact width = 0.3m

Soil $c = 10\text{kPa}$

$\phi = 30^\circ$

$\gamma = 17.354\text{kN/m}^3$

From Table 6.6, phase (3) deformation is predicted for a load of 95KPa, ie lateral deformation and compaction.

Applying equation [1] to data from Table 6.3 for the Bearsted arable plot:-

$$R = \frac{95}{18.44186(1 - \frac{95}{404.40})} = \underline{\underline{6.73\text{mm}}}$$

At phase (2) threshold:-

$$R = \frac{87}{18.44186(1 - \frac{87}{404.40})} = \underline{\underline{6.01\text{mm}}}$$

To predict depth of soil disturbance:-

For phase (3) deformation, the extent of soil disturbance can be predicted using the procedure developed in section 5.2.2.5.

Determine r_1 at the phase (2) threshold from equations [29], [30] and [31]:-

$$\begin{aligned}
 & \frac{\pi 0.3^2 87 \cos(45+30) \tan 30^\circ}{4} (0.130 \text{ to } 0.173) \\
 & = -17.354 \left[\frac{0.30 + r_1 \cos(135-30-180 \ln \left[\frac{r_1}{0.3} \right] \cdot \cot 30^\circ)}{2} \right] \{ 0.006 \\
 & + 0.3 e^{(1/2) \ln(r_1/0.3)} \cdot \cos(45-30-180 \ln \left[\frac{r_1}{0.3} \right] \cdot \cot 30^\circ) \} \\
 & \cdot \frac{1}{2} \left(0.3 - \frac{0.30 + r_1 \cos(135-30-180 \ln \left[\frac{r_1}{0.3} \right] \cot 30^\circ)}{2} \right) + \frac{10}{2 \tan 30^\circ} (r_1^2 - 0.3^2) \\
 & + 17.354 \left[\frac{0.30 + r_1 \cos(135-30-180 \ln \left[\frac{r_1}{0.3} \right] \cot 30^\circ)}{2} \right]^2 \\
 & \cdot \left[\frac{0.006}{2} + \frac{0.3 \tan(45+30)}{6} - \frac{r_1 \cos(45-30-\frac{\pi}{2} \frac{\ln \left[\frac{r_1}{0.3} \right] \cdot \cot 30^\circ}{180}}{3} \right] \\
 & + 17.354 \left[\frac{0.30 + r_1 \cos(135-30-180 \ln \left[\frac{r_1}{0.3} \right] \cot 30^\circ)}{2} \right] \\
 & \cdot \left[0.006 + \frac{0.3 \tan(45+30)}{4} - \frac{r_1 \cos(45-30-\frac{\pi}{2} \frac{\ln \left[\frac{r_1}{0.3} \right] \cdot \cot 30^\circ}{180}}{2} \right] \\
 & \cdot \cos(45-30-90 \ln \left[\frac{r_1}{0.3} \right] \cdot \cot 30^\circ) \cdot 0.3 \sin(90 \ln \left[\frac{r_1}{0.3} \right] \cdot \cot 30^\circ) \sin 30^\circ
 \end{aligned}$$

Try $r_1 = 0.355\text{m:-}$

0.231 to 0.307 \approx 0.271

Determine r_2 using the same equation but substituting σ_A at $R_{(3)}$ for that at the phase (2) threshold (ie 95kPa instead of 87kPa).

Try $r_2 = 0.360$:-

0.252 to 0.335 \approx 0.295

β_1 and β_2 can be used to predict the extent of soil disturbance. With reference to Figure 6.2A:-

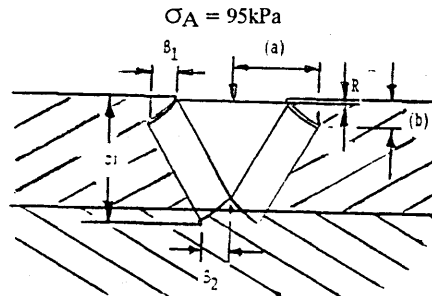


Figure 6.2A Diagram illustrating prediction of the extent of soil disturbance resulting from a 95kPa load on the Bearsted arable plot.